

**This paper has been mechanically scanned. Some errors may have been inadvertently introduced.**

CALIFORNIA PATH PROGRAM  
INSTITUTE OF TRANSPORTATION STUDIES  
UNIVERSITY OF CALIFORNIA, BERKELEY

# **Roadway Powered Electric Vehicle Project Track Construction and Testing Program Phase 3D**

**Systems Control Technology, Inc.  
Palo Alto, California**

**California PATH Research Paper  
UCB-ITS-PRR-94-07**

This work was performed as part of the California PATH Program of the University of California, in cooperation with the State of California Business, Transportation, and Housing Agency, Department of Transportation; and the United States Department Transportation, Federal Highway Administration.

The contents of this report reflect the views of the authors who are responsible for the facts and the accuracy of the data presented herein. The contents do not necessarily reflect the official views or policies of the State of California. This report does not constitute a standard, specification, or regulation.

March 1994

ISSN 10551425

## 2. Systems Engineering and Design

2.1	Objectives and Approach .....	17
2.2	Analysis Tools and Methods .....	18
2.2.1	Electric Vehicle Simulation, EVSIM Program .....	19
2.2.2	Electric Circuit Analysis, PHASE Program .....	20
2.2.3	Magnetic Analysis, POISSON Program .....	20
2.2.4	Hardware Cost Estimates .....	21
2.2.5	Component Loss Estimates .....	23
2.3	System Design .....	24
2.3.1	Goals .....	24
2.3.2	Trade-off Issues .....	24
2.3.3	Baseline .....	28
2.3.4	Sensitivity Analysis .....	32
2.4	Baseline Operating Point .....	35
2.4.1	Goals .....	35
2.4.2	Trade-off Issues .....	35
2.4.3	Baseline .....	36
2.4.4	Sensitivity Analysis .....	39
2.5	Inductor Design .....	45
2.5.1	Core Geometry .....	45
2.5.2	Core Design .....	45
2.5.3	Conductor Selection .....	47
2.6	System Efficiency .....	48
2.6.1	Core Losses .....	48
2.6.2	Roadway Conductor Losses .....	51
2.6.3	Onboard Controller and Pickup Winding Losses .....	54
2.6.4	Power Distribution System Losses .....	55
2.6.5	System Losses .....	55

2.7	Test Facility Layout .....	56
2.8	Conclusions .....	58
<b>3.</b>	<b>Vehicle</b>	
3.1	Pickup .....	61
3.1.1	Design of the Pickup Cores .....	61
3.1.1.1	Geometric .....	63
3.1.1.2	Selection of Core Laminations .....	65
3.1.1.3	Expected Losses .....	67
3.1.2	Conductors .....	68
3.1.2.1	Materials .....	68
3.1.2.2	Mechanical Design .....	69
3.1.2.3	Terminations .....	70
3.1.2.4	Conductor Losses .....	71
3.1.3	Mechanical Design of Pickup .....	71
3.1.3.1	Frame .....	72
3.1.3.2	Cross beams .....	72
3.1.3.3	Coating of Pickup Cores .....	73
3.1.3.4	Acoustic Treatments.....	74
3.1.3.5	Assembly and Mounting Procedure .....	74
3.1.4	Retraction/Suspension System.....	75
3.1.4.1	Hydraulic System .....	77
3.1.4.2	Cabling .....	79
3.1.4.3	Controls .....	79
3.2	Onboard Controller (OBC) .....	80
3.2.1	Description .....	80
3.2.1.1	Electrical .....	81
3.2.1.2	Physical .....	82
3.2.1.3	Expected Losses .....	84
3.2.1.4	Control Algorithms .....	84
3.2.1.5	Safety Systems and Interlocks .....	84

3.3	Steering Assistance System .....	85
3.3.1	Sensors .....	85
3.3.1.1	Loops .....	86
3.3.1.2	Circuit .....	88
3.3.2	Investigation of Existing Automatic Steering Systems .....	88
3.4	Bus Hardware Upgrades .....	89

## 4. Facilities

4.1	Track Configuration .....	91
4.1.1	Physical Constraints and Requirements .....	91
4.1.2	Segments .....	94
4.1.3	Vaults .....	95
4.2	Power Distribution .....	95
4.2.1	Power Conditioner .....	96
4.2.2	Static Switching of Segments .....	96
4.2.3	Dynamic Segment Switching .....	97
4.2.3.1.	Power Hardware .....	97
4.2.3.2	Detection/Communication System Concept .....	97
4.2.3.3	Detection/Communication System Hardware .....	98
4.2.4	Compensation Capacitance .....	102
4.3	Roadway Inductor .....	103
4.3.1	Roadway Core Modules .....	103
4.3.1.1	Magnetic Design .....	103
4.3.1.2	Mechanical Design of Modules .....	105
4.3.2	Conductors .....	106
4.3.2.1	Cables .....	106
4.3.2.2	Bus Bars .....	106
4.3.2.3	Terminations/Crisscross .....	107
4.3.3	Mechanical Design of Roadway Inductor .....	107
4.4	Construction .....	109
4.4.1	Method .....	109

4.4.2 Design .....	110
4.4.3 Roadway Preparation and Grading .....	110
4.4.4 Roadway Inductor Installation .....	114
4.4.4.1 Core Module Installation.....	115
4.4.4.2 Conductor Installation.....	117
4.5 Instrumentation and Control Hardware .....	122
<b>5. Testing</b>	
5.1 Component Testing .....	125
5.1.1 Roadway Cores and Core Modules .....	126
5.1.1.1 Loss and Heating Tests .....	126
5.1.1.2 Mechanical Integrity .....	128
5.1.1.3 Acoustic Noise .....	131
5.1.1.4 Magnetic Flux Levels .....	131
5.1.2 Pickup Cores .....	132
5.1.2.1 Losses and Heating Tests .....	134
5.1.2.2 Reluctance and Fringing.....	134
5.1.2.3 Mechanical Properties .....	141
5.1.2.4 Acoustic Noise .....	141
5.1.2.5 Magnetic Flux Distribution .....	150
5.1.3 Solid-state Switches .....	153
5.1.3.1 Trigger Circuit .....	154
5.1.3.2 Silicon Controller Rectifier .....	159
5.1.4 Onboard Controller Inductors .....	160
5.1.5 Heating of Pickup Frame Materials .....	161
5.2 Inductive Coupling Subsystems .....	163
5.2.1 Pickup Inductor .....	166
5.2.1.1 Current Equalization .....	166
5.2.1.2 Pickup Inductances and Losses..	169
5.2.1.3 Acoustic Noise .....	170
5.2.1.4 Heating .....	173
5.2.2 Roadway Inductor .....	174
5.2.2.1 Current Equalization .....	174

5.2.2.2 Inductance and Losses .....	176
5.2.2.3 Acoustic Noise .....	177
5.2.2.4 Heating .....	179
5.2.2.5 Mechanical Integrity .....	181
5.2.2.6 Magnetic Fields .....	184
5.2.2.7 Electromagnetic Interference .....	189
5.2.3 Power Distribution System .....	190
5.2.3.1 <b>Current Equalization in Transmission Line</b> .....	191
5.2.3.2 Switching and Power Factor Correction Hardware .....	191
5.2.4 Operation of the Onboard Controller .....	194
5.2.4.1 Initial Checkout .....	194
5.2.4.2 Capacitance Steps .....	195
5.2.4.3 Waveforms .....	197
5.2.4.4 Heating/Cooling .....	197
5.2.4.5 Acoustic Noise .....	199
5.3 Accessory Systems .....	199
5.3.1 Signaling Systems .....	200
5.3.2 Pickup Suspension/Retraction .....	206
5.3.3 Steering Assistance System .....	206
5.4 Inductive Coupling System Performance .....	212
5.4.1 Power Coupling Capability .....	213
5.4.1.1 Output Current Available .....	213
5.4.1.2 Sensitivities to Pickup Location .....	214
5.4.1.3 Sensitivity to Roadway Current .....	215
5.4.2 Closed-Loop Control .....	216
5.5 Inductive Coupling System Operation on the Bus .....	217
5.5.1 Mechanical Considerations .....	218
5.5.1.1 Pickup Cabling .....	218
5.5.1.2 OBC Installation .....	218
5.5.1.3 Cooling Systems .....	219
5.5.1.4 Acoustic Noise .....	219
5.5.2 Static Operation .....	220
5.5.2.1 Timing Curve .....	221

5.5.2.2	System Losses and Efficiency .....	222
<b>5.5.3</b>	<b>Dynamic Operation .....</b>	<b>225</b>
5.5.3.1	Power Coupling at Constant Speed .....	225
<b>5.5.3.2</b>	<b>Power Coupling at Variable Speed..</b>	<b>225</b>
5.5.3.3	Controllability .....	227
<b>5.6</b>	<b>Vehicle Operation with Inductive Coupling System .....</b>	<b>229</b>
5.6.1	Range .....	230
5.6.1.1	Driving Cycle .....	230
5.6.1.2	Range Test Results .....	230
5.6.2	Vehicle Performance .....	232
<b>5.7</b>	<b>Testing Conclusions .....</b>	<b>234</b>
5.7.1	System Losses and Efficiency .....	235
<b>5.7.2</b>	<b>Operating Point.....</b>	<b>235</b>
<b>5.7.3</b>	<b>Environmental Impact .....</b>	<b>236</b>
<b>5.7.3.1</b>	<b>Acoustic Noise .....</b>	<b>237</b>
<b>5.7.3.2</b>	<b>Magnetic Fields .....</b>	<b>237</b>

## 6. Related RPEV Research

<b>6.1</b>	<b>Playa Vista Project .....</b>	<b>239</b>
<b>6.1.1</b>	<b>Playa Vista System Overview .....</b>	<b>240</b>
<b>6.1.2</b>	<b>Performance at Nominal Operating Point .....</b>	<b>240</b>
<b>6.1.2.1</b>	<b>Magnetic Fields .....</b>	<b>240</b>
6.1.2.2	Tuning Curves and Frequency Response .....	242
<b>6.1.2.3</b>	<b>Power Testing Methodology .....</b>	<b>243</b>
<b>6.1.2.4</b>	<b>Linearity of System .....</b>	<b>244</b>
<b>6.1.2.5</b>	<b>Power Tests .....</b>	<b>245</b>
<b>6.1.2.6</b>	<b>Rectifier Input Inductance Variations .....</b>	<b>247</b>
<b>6.1.2.7</b>	<b>System Losses and Efficiency .....</b>	<b>247</b>
6.1.2.8	Electra-Magnetic Interference .....	249
<b>6.1.3</b>	<b>Testing at Off-Nominal Conditions .....</b>	<b>250</b>
<b>6.1.3.1</b>	<b>Pickup Turns Variations .....</b>	<b>250</b>
<b>6.1.3.2</b>	<b>Airgap Variations .....</b>	<b>252</b>
<b>6.1.3.3</b>	<b>Field Cancellation Windings .....</b>	<b>255</b>

6.1.4	Alternate Frequency Tests .....	257
6.1.4.1	Acoustic Noise .....	257
6.1.4.2	Power Coupling into Resistive Load .....	258
6.1.4.3	Comparison of Power Coupling at 4000 and 8500 Hz .....	261
6.1.4.4	Losses .....	264
6.1.5	Conclusions .....	265
6.2	Regional Deployment Study .....	266
6.3	Near-Term Deployment on HOV Facility .....	267
<b>7.</b>	<b>Summary of Project Results</b>	
7.1	Systems Engineering .....	269
7.2	Vehicle .....	269
7.3	Facility .....	270
7.4	Testing .....	271
7.5	Related RPEV Research .....	272
<b>Appendices</b>		
A.	Metric Conversions .....	277
B.	POISSON Input .....	285
C.	Control Circuit .....	289
<b>Glossary</b> .....		297
<b>References</b> .....		301

# **list of Figures**

---

## **1. Introduction**

Figure 1.1	Power flow with RPEV system .....	2
Figure 1.2	Roadway and pickup inductor cross section .....	3
Figure 1.3	Predicted magnetic flux lines when coupling power.....	4
Figure 1.4	Prototype roadway power electric bus .....	5
Figure 1.5	Pickup inductor being positioned under bus .....	7
Figure 1.6	Onboard controller mounted in bus .....	7
Figure 1.7	Test track layout.....	8.
Figure 1.8	Placing roadway inductor cores .....	9
Figure 1.9	Roadway and pickup inductor cross sections .....	10
Figure 1.10	Potting of roadway cables .....	11
Figure 1.11	Roadway powered electric bus over bus stop .....	11
Figure 1.12	Power conditioner .....	12

## **2. Systems Engineering and Design**

Figure 2.1 .a	Oscilloscope trace of waveform with a poor value of $di/dt$ inductance .....	21
Figure 2.1.b	Computer-predicted waveform for values of $di/dt$ that produced Figure 2.1.a .....	22
Figure 2.2a	Core loss for 7 mil M-2 at 400 Hz .....	25
Figure 2.2b	Core loss for 7 mil M-2 at at high frequencies .....	26
Figure 2.3	Battery depth of discharge for ten-hour day .....	30
Figure 2.4	Battery discharge as a function of ICS current .....	31
Figure 2.5	Battery DOD as a function of ICS output current for various layover times.....	32

Figure 2.6	Current required for zero net discharge for one roundtrip .....	.33
Figure 2.7	Route electrification required for zero net discharge for one roundtrip .....	34
Figure 2.8	Roadway current for a constant output as a function of frequency for one, two, and three pickup turns .....	40
Figure 2.9	Magnetizing current as a function of frequency for one, two, and three pickup turns .....	41
Figure 2.10	Log-log plot of Figure 2.9 .....	41
Figure 2.11	Losses as a function of number of secondary turns .....	42
Figure 2.12	System losses as a function of frequency .....	43
Figure 2.13	Hypothetical objective function for “optimizing” ICS design .....	44
Figure 2.14	Roadway core lamination geometries.....	46

### 3. Vehicle

Figure 3.1	Coupled flux lines .....	62
Figure 3.2	Cross section of pickup (and roadway) inductor .....	63
Figure 3.3	Three-view drawing of the pickup .....	64
Figure 3.4.a	Clearance from pickup conductors to front axle (raised position). ....	66
Figure 3.4.b	Clearance from pickup conductors to front axle (lowered position) .....	66
Figure 3.5	Design drawing of pickup core .....	68
Figure 3.6	Staggered ends of <b>busbars</b> .....	70
Figure 3.7	Two halves of cross beam .....	72
Figure 3.8	Coating pickup cores.....	73
Figure 3.9	Acoustic treatment of pickup cores.....	74
Figure 3.10.a	<b>Busbar</b> packs in cross beams .....	76
Figure 3.10.b	Partially assembled pickup .....	76
Figure 3.10.c	Pickup being rolled under bus .....	77
Figure 3.11.a	Swing arms in lowered position .....	78
Figure 3.11.b	Swing arms in raised position .....	78
Figure 3.12	Lateral control arm .....	79

Figure 3.13	Schematic of OBC .....	81
Figure 3.14	Front box and radiator on bus .....	83
Figure 3.15	6 x 36 rectangular loops .....	86
Figure 3.16	12 x 36 x 6 trapezoidal loops .....	87
Figure 3.17	Steering assistance motors .....	88

## 4. Facilities

Figure 4.1	Final track layout .....	92
Figure 4.2	Test track site prior to construction. Photo is looking east.....	94
Figure 4.3	Detection/ communication system hardware .....	98
Figure 4.4	High-level circuit diagram that includes various components of the segment switching system .....	100
Figure 4.5	Placing core components into molds .....	103
Figure 4.6	Roadway module being loaded into oven/vacuum chamber.....	104
Figure 4.7	Configuration of the laminations in the core modules (side view.....	104
Figure 4.8	Busbar terminations in vault .....	106
Figure 4.9	Cable terminators in vault .....	108
Figure 4.10	Placement of roadway modules flush with surface .....	108
Figure 4.11	Old pavement sawcut and removed .....	111
Figure 4.12	Excavated roadway trough .....	112
Figure 4.13	Vault wall reinforcement .....	113
Figure 4.14	Vault form with lid frame .....	113
Figure 4.15	Laying the detector loops .....	115
Figure 4.16	Placing roadway cores in the trough .....	116
Figure 4.17	Suspending the cores from the roadway surface .....	116
Figure 4.18	Cores suspended at roadway surface .....	117
Figure 4.19	Grouting cores .....	118
Figure 4.20	Grouting a set of cores .....	119
Figure 4.21	Removing vault lid frame in the way of busbar .....	120
Figure 4.22	Busbars before potting in place .....	120

Figure 4.23	Potting busbars in place .....	121
Figure 4.24	Connecting roadway segments to power conditioner leads at the equipment pad .....	122

## **5. Testing**

Figure 5.1	Calorimetry setup .....	127
Figure 5.2	Roadway core losses at 400 Hz per foot of core .....	128
Figure 5.3	Open roadway lines of flux, full symmetry .....	132
Figure 5.4	Predicted values of flux density .....	133
Figure 5.5	Map of flux density .....	133
Figure 5.6	Pickup core losses .....	135
Figure 5.7	POISSON plot of coupled core flux lines, full symmetry .....	135
Figure 5.8	Normalized output voltage per inch of pickup core .....	136
Figure 5.9	Roadway current required to induce a voltage of 3.0 volts per foot of pickup core .....	137
Figure 5.10	Normalized output voltage .....	138
Figure 5.11	Setup for longitudinal separation fringing tests .....	139
Figure 5.12	National Magnetics core voltage .....	140
Figure 5.13	National Magnetics and Tech-Tran core voltage .....	140
Figure 5.14	Effect of longitudinal separation of cores on induced voltage .....	141
Figure 5.15	Anechoic chamber .....	142
Figure 5.16	Sound pressure level two feet from top of core .....	143
Figure 5.17	Sound pressure level two feet from end of core .....	144
Figure 5.18	Sound pressure level two feet from side of core .....	144
Figure 5.19	Acoustic noise as a function of flux levels and induced voltages .....	146
Figure 5.20	Sound reduction treatment .....	146
Figure 5.21	Sound pressure level to side of Elma pickup core with and without sound treatment .....	147
Figure 5.22	Sound pressure level to side of Elma pickup core with and without sound treatment .....	148
Figure 5.23	National Magnetics core with acoustic treatment.. ....	149

Figure 5.24	National Magnetics core with and without acoustic treatment.....	149
Figure 5.25	POISSON analysis of magnetic flux lines while coupling power .....	151
Figure 5.26	Predicted vertical component of flux while coupling power.....	151
Figure 5.27	Test setup .....	152
Figure 5.28	Measured flux in National Magnetics and Elma cores .....	153
Figure 5.29	Capacitor voltage and current with late SCR triggering .....	156
Figure 5.30	Capacitor voltage and current with bad SCR triigging .....	156
Figure 5.31	Capacitor current and pickup voltage with capacitor hardwired into circuit .....	158
Figure 5.32	Same as Figure 5.31 with an additional branch of capacitance switched into the circuit .....	158
Figure 5.33	Capacitor current in branch 5 with unsymmetric SCR triggering .....	159
Figure 5.34	Correct capacitor current and voltage .....	160
Figure 5.35	L3 inductor with discolored and warped aluminum panel .....	162
Figure 5.36	Panel warped by L3 inductor heating .....	162
Figure 5.37	Heating of aluminum bars in high and low flux regions .....	164
Figure 5.38	Setup for testing pickup frame heating .....	164
Figure 5.39	Heating of aluminum bars when insulated from each other .....	165
Figure 5.40	Heating of aluminum bars when bolted to each other .....	165
Figure 5.41	Current equalization .....	168
Figure 5.42	Current equalization .....	168
Figure 5.43	Analytically determined crisscross method.....	169
Figure 5.44	Pickup acoustic noise measurements (side) .....	171
Figure 5.45	Pickup acoustic noise measurements (end) .....	172
Figure 5.46	First-generation pickup acoustic noise .....	173
Figure 5.47	Acoustic noise at various frequencies with constant roadway current .....	174
Figure 5.48	Current distribution for the cable section using POISSON.....	176
Figure 5.49	Sound pressure measurements outside automobiles .....	178
Figure 5.50	Sound pressure measurements inside automobiles .....	178

Figure 5.51	Interior and exterior Tracer noise levels .....	179
Figure 5.52	Relative parasitic heating of steel and aluminum under unrealistically severe test conditions .....	180
Figure 5.53	Relative parasitic heating of steel and aluminum under realistic test conditions .....	181
Figure 5.54	Cracks in conductor slots .....	183
Figure 5.55	Conductor slot buckling .....	184
Figure 5.56	Open roadway lines of flux .....	185
Figure 5.57	Predicted magnetic flux ten inches above roadway .....	186
Figure 5.58	Predicted total magnetic flux ten inches above roadway.....	186
Figure 5.59	Predicted and measured total magnetic flux two inches above roadway .....	187
Figure 5.60	Predicted and measured total magnetic flux forty inches above roadway .....	187
Figure 5.61	Predicted flux densities at larger lateral offsets .....	188
Figure 5.62	Measured current distribution within the transmission line .....	192
Figure 5.63	Schematic with parallel power factor correction .....	. 192
Figure 5.64	Waveform with unsuccessful parallel power factor correction..	193
Figure 5.65	Schematic of power distribution system—series power factor correction .....	194
Figure 5.66	Capacitor currents with inappropriate $di/dt$ values .....	198
Figure 5.67	Capacitor current with good $di/dt$ value .....	198
Figure 5.68	Temperature of cooling system reservoir, reactor coil, and electrical connector during testing .....	199
Figure 5.69	Location of inductive loops in the roadway .....	201
Figure 5.70	400 Hz induced voltage on 6 x 18 foot inductive loop sensor 3.5 feet from the roadway inductor .....	202
Figure 5.71	400 Hz induced voltage on a 6 x 18 foot inductive loop sensor 12 feet from the roadway inductor .....	203
Figure 5.72	Inductive loop voltage with roadway inductor current .....	. 203
Figure 5.73	Inductive loop voltage without roadway inductor current.....	204

Figure 5.74	Inductive loop voltage with roadway inductor current (poor scope triggering) .....	204
Figure 5.75	Filtered and unfiltered inductive loop voltage.....	205
Figure 5.76	Steering assistance system-driver's view .....	208
Figure 5.77	First set of sensor loops-10 x 30 inches .....	209
Figure 5.78	Predicted and measured voltages as a function of lateral offset .....	209
Figure 5.79	Polarity reference and the primary position signal for one of the intermediate sets of coils .....	210
Figure 5.80	Final trapezoidal steering sensor loops .....	210
Figure 5.81	Test results for three sets of sensor loops .....	211
Figure 5.82	Final sensor design .....	211
Figure 5.83	Final sensor design mounted on bus .....	212
Figure 5.84	Predicted and measured output current as a function of tuning capacitance .....	213
Figure 5.85	Sensitivity to lateral deviation from design location .....	214
Figure 5.86	Sensitivity to vertical deviation from design location .....	215
Figure 5.87	Output current as a function of roadway current .....	216
Figure 5.88	Output current tracking commanded value .....	217
Figure 5.89	OBC mounted onboard the bus .....	219
Figure 5.90	OBC acoustic cover being lowered into place .....	220
Figure 5.91	Tuning curve of output current as a function of capacitance.....	221
Figure 5.92	Tuning curve of output power as a function of capacitance .....	222
Figure 5.93	Output power as a function of input power .....	223
Figure 5.94	Static efficiency as a function of output power .....	224
Figure 5.95	System efficiency as a function of output power- short dynamic tests .....	226
Figure 5.96	System efficiency as a function of output power- driving cycle tests .....	226
Figure 5.97	Output power as a function of lateral offset .....	228
Figure 5.98	Capacitance as a function of lateral offset .....	229
Figure 5.99	Acceleration with and without roadway power .....	233

Figure 5.100	Effects of ICS on vehicle motor controller voltage .....	233
Figure 5.101	Effects of ICS on vehicle motor controller current..	234
Figure 5.102	Power diagram with loss terms and efficiencies.....	236

## 6. Related RPEV Research

Figure 6.1	Predicted and measured fields 10 inches above roadway.....	241
Figure 6.2	Typical measured tuning curve .....	242
Figure 6.3	Measured frequency response with varying capacitance..	243
Figure 6.4	Model and test results of the ICS used in the RPG-Van .....	244
Figure 6.5	System output into a 1.2 ohm load with various roadway currents..	245
Figure 6.6	Maximum system output into various resistive loads .....	246
Figure 6.7	System performance scaled to roadway current of 240 amp-turns .....	246
Figure 6.8	Tuning curves showing the effect of varying L3 inductance .....	248
Figure 6.9	Data for L3 = 16 mH added to Figure 6.7.....	248
Figure 6.10	Measured output voltage, current, and power into a resistive load.....	251
Figure 6.11	Measured results for one and two turns .....	251
Figure 6.12	Predicted tuning curves as a function of lateral offset .....	252
Figure 6.13	Measured mutual inductance as a function of lateral offset and airgap.....	253
Figure 6.14	Measured leakage inductance as a function of lateral offset and airgap.....	254
Figure 6.15	Measured mutual and leakage inductances at a two-inch airgap .....	254
Figure 6.16	Measured mutual and leakage inductances at a three-inch airgap .....	255
Figure 6.17	Effects of field cancellation windings on measured mutual and leakage inductance .....	256
Figure 6.18	Ratio of measured mutual to leakage inductance .....	256
Figure 6.19	Acoustic noise in a passenger car.....	258
Figure 6.20	Output current and power as a function of frequency.....	259
Figure 6.21	Peak output current and power as a function of frequency.....	260

Figure 6.22	Capacitance for peak power as a function of frequency .....	261
Figure 6.23	Data for Figure 6.22 plotted using a semi-log scale .....	262
Figure 6.24	Tuning curves for 4000 and 8500 Hz with a two-inch airgap .....	262
Figure 6.25	Tuning curve for 4000 and 8500 Hz with three-inch airgap.....	263
Figure 6.26	Open roadway losses at various excitation levels .....	264
Figure 6.27	Parasitic losses caused by car parked over the roadway.....	265

### **Appendix C. Control Circuit**

Figure C.1	Solid state switch .....	281
Figure C.1	Capacitor branch circuit.....	282
Figure C.3	Voltage across switch without bleed resistors.....	283
Figure C.4	Oscilloscope traces of switch h current and voltage .....	284
Figure C.5	Oscilloscope traces of switch voltage and pickup voltage .....	284
Figure C.6	Oscilloscope traces of capacitor current and pickup voltage..	286

## List of Tables

---

Table 2.1	Operating Point Trade-offs .....	37
Table 2.2	Core Losses .....	51
Table 2.3	Conductor Losses .....	54
Table 2.4	Total System Losses .....	58
Table 3.1	Onboard Controller Weights .....	83
Table 5.1	Core Specifications .....	129
Table 5.2	Measured and Predicted Inductance .....	170
Table 5.3	Magnetic Flux Levels .....	188
Table 5.4	Capacitance Wired to Every Switch for Each of the Wiring Methods..	196
Table 5.5	Key Parameters of the Design and Test Duty Cycles .....	231
Table 5.6	Summary of Test Results .....	231
Table 6.1	G-Van Component Losses at 6000 Hz .....	249
Table A.1	Metric Conversions .....	277
Table 2.2	Core Losses (metric units) .....	280
Table 3.1	Onboard Controller Weights (metric units) .....	281
Table 5.1	Core Specifications (metric units) .....	282
Table 5.3	Magnetic Flux Levels (metric units) .....	283
Table 5.5	Key Parameters of the Design and Test Duty Cycle (metric units)s .....	283
Table 5.6	Summary of Test Results (metric units) .....	231

## **Acknowledgments**

---

The work reported here has been performed by the staff of Systems Control Technology, Inc. (SCT) under contract to PATH with funding provided by FHWA and Caltrans. Useful advice and guidance has been provided by Caltrans, PATH, and the Richmond Field Station staff.

The test track on which the testing was done has been developed and operated in close collaboration between SCT and PATH.

This report has been prepared by the staff of SCT's Transportation Systems Engineering Department, who performed the work reported here. The SCT project team includes Daniel M. Empey, Edward H. Lechner, Gregory Wyess, Michael Vincent, Jon Garbarino, Robert Moore, Georginia J. Bailie, Jill V. Josselyn, Jeffrey Frenster, and Constance R. Klein, all under the direction of Steven E. Shladover and later Edward H. Lechner.

## **Funding**

---

This work was funded by FHWA and Caltrans. The prime contracts issued from Caltrans to UC Berkeley and from UC Berkeley to SCT.

Subcontracts were issued by SCT to Elma Engineering for \$277,484 to cover the roadway cores for the test track. All other work was performed by SCT, with some very limited consultant assistance, and all other material purchases were accomplished on various purchase orders.

**Roadway Powered Electric Vehicle Project**  
**Track Construction and Testing Program**

**Phase 3D**

**Final Report**

Prepared for

PATH  
University of California  
Richmond Field Station  
1301 South 46th Street  
Richmond, CA 94804

February 1994

# Table of Contents

---

List of Figures .....	ix
List of Tables.. .....	xvii
Acknowledgments .....	.
Funding .....	xxi
 1. Introduction	
1.1 RPEV Technology .....	1
1.2 Inductive Coupling System Description .....	2
1.3 History of Inductive Energy Transfer for Transportation Systems .....	4
1.4 Description of Test Vehicle and Facility.. .....	5
1.4.1 Vehicle .....	5
1.4.2 Vehicle-Mounted Elements of the Inductive Coupling System.. .....	6
1.4.3 Test Track .....	6
1.4.4 Power Distribution System .....	10
1.5 Report Overview.. .....	12
1.6 Project Objectives and Results .....	13
1.6.1 Dynamic Power Coupling .....	13
1.6.2 Range Improvements .....	14
1.6.3 System Efficiency .....	14
1.6.4 Acoustic Noise Level.. .....	15
1.6.5 On-board Weight .....	15
1.6.6 System Costs.. .....	15
1.6.7 Overall Project Goals and Results .....	16

# **1. Introduction**

---

This report covers the construction and testing of a Roadway Powered Electric Vehicle proof-of-concept system by Systems Control Technology, Inc. under the auspices of the University of California, Berkeley, Institute of Transportation Studies, PATH (Program for Advanced Transit and Highways) program. Funding was provided by Caltrans and the Federal Highway Administration.

## **1.1 RPEV Technology**

The Roadway Powered Electric Vehicle (RPEV) technology provides great promise for widespread use of electric vehicles by overcoming the range limitation of battery electric vehicles. The Inductive Coupling System (ICS) transfers energy from a coil buried beneath the road's surface to the vehicle through a magnetic field. This energy can be used immediately by the traction motor or can be stored **onboard** for later use. **Onboard** energy storage requirements change substantially with this technology compared to pure battery vehicles. Total stored energy becomes less important, while power rating, especially charge acceptance of the battery becomes more important for an RPEV compared to a battery-only vehicle. In an urban area with a network of electrified roadways (perhaps one lane in each direction for most freeways), trips could be made with a relatively small amount of **onboard** stored energy, reducing battery sizes dramatically (possibly by as much as a factor of two or three).

The electrified lanes could be shared with **non-RPEVs**, which makes implementation of the system much easier. Similarly, the RPEVs can travel on **non-electrified roads** using their stored energy, resulting in a very flexible system.

The initial test vehicle for this system is a 35-passenger transit bus, but the technology could be applied to any size or type of electric vehicle. Under separate funding, Systems Control Technology, Inc. (SCT) has designed and built a **roadway-powered** version of the G-Van, and preliminary designs have been prepared for passenger cars.

## 1.2 Inductive Coupling System Description

The inductive coupling system is basically a transformer with the primary winding (roadway inductor) buried in the roadway and the secondary winding (pickup inductor) mounted **onboard** the vehicle. Unlike a conventional transformer, there is an airgap in the magnetic circuit linking primary and secondary windings. The power transfer level is controlled by circuits **onboard** the vehicle. In addition to controlling the level of the output current, the **onboard** circuits rectify and filter the ac current from the pickup inductor into smooth dc for use by the motor controller or battery.

Figure 1.1 shows the energy flow in the system. The dashed lines show energy flow during regenerative braking. The power conditioner is a rectifier/inverter that draws three-phase 60 Hz power and puts out single phase at a higher frequency. Power is delivered to one or more segments of the electrified roadway through a distribution system.

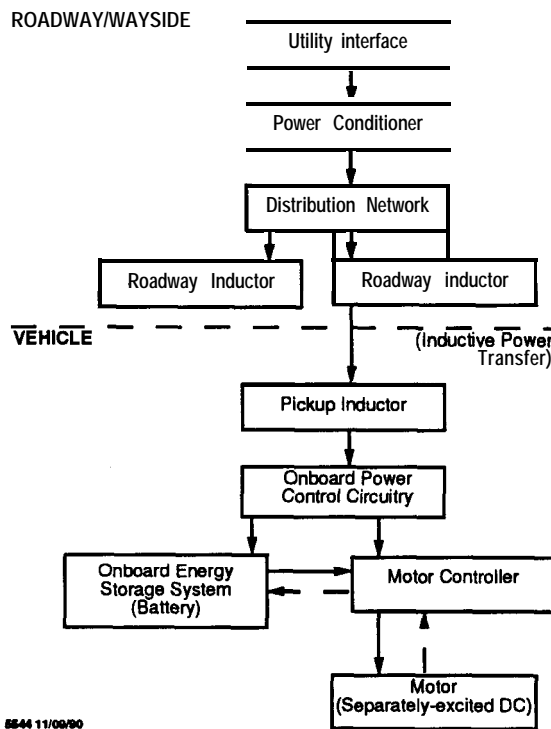
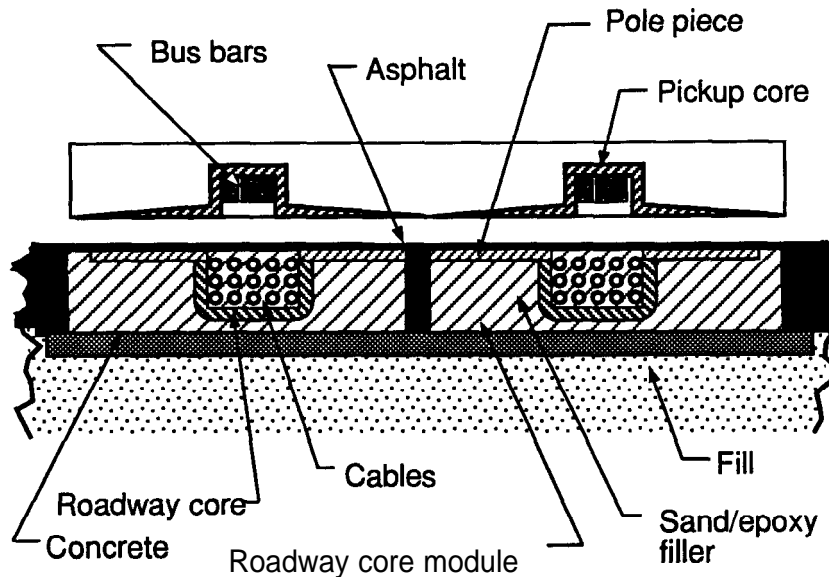


Figure 1.1 Power flow with RPEV system

The roadway inductor is typically three to four feet wide and each of its segments is up to several hundred feet long. In addition to the conductors (cables or busbars), laminated steel cores guide the magnetic flux and reduce the reluctance in the magnetic circuit. The pickup inductor is mounted on the vehicle. It is also about 3 feet wide and 6 – 15 feet long, depending on the vehicle's size and energy requirements. The pickup inductor is suspended within 2 – 4 inches of the road's surface when coupling power, but is retracted to a height of 6 or 8 inches when not in operation. Figure 1.2 shows a cross section of the inductors when energy is being transferred to the vehicle. (Appendix A contains English standard to metric unit conversions and metric (SI) versions of tables appearing in this report.)



5544 09/16/93

Figure 1.2 Roadway and pickup inductor cross section

Electrically and magnetically, the pickup looks very much like the roadway inductor, although the inductors are designed for very different mechanical properties. The roadway inductor is designed to carry full road loads. Price is of primary concern, as the cost of the roadway inductor is the single largest cost within the system, especially in the initial years of application when there is not yet a large fleet of RPEVs. The conductors are rather large as they must carry a large current with low losses to maintain overall system efficiency. The pickup is designed to minimize weight and acoustic noise. The pickup is much shorter than the roadway inductor, so the total energy lost in the pickup is generally less than in the roadway even though the pickup operates at much higher flux levels than the open roadway. Temperature

rise and acoustic noise generation rather than total power loss sets pickup core design criteria. In the roadway inductor, the reverse is true.

The mutual inductance between the roadway and pickup windings is the most important parameter associated with the geometry of the inductors. The mutual inductance indicates the degree of magnetic coupling between the roadway and pickup coils. It measures the magnetic flux lines that link (or couple) the roadway and pickup inductors, as seen in Figure 1.3. The mutual inductance is roughly proportional to the common poleface area and inversely proportional to the airgap height. It is desirable to maximize the mutual inductance (maximize the pickup poleface area and minimize the airgap height) to improve the effectiveness of the inductive coupling system.

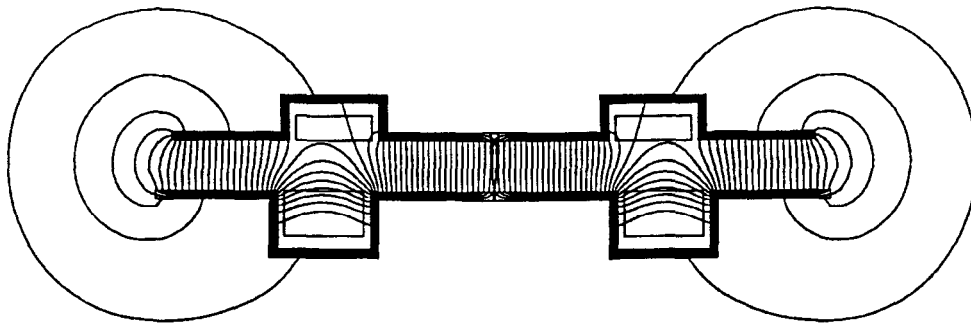


Figure 1.3 Predicted magnetic flux lines when coupling power

### 1.3 History of Inductive Energy Transfer for Transportation Systems

The original patents for inductive energy transfer for transportation applications were issued in the 1890s for railroad use. During the oil crisis of the mid-1970s, interest in this technology was renewed. Work at Lawrence Berkeley and Lawrence Livermore National Laboratories led to fabrication and testing of a 6 kw proof-of-concept system. Neither the vehicle nor roadway were suitable for an operational system. In 1979, the Santa Barbara Electric Bus Project started with a planning/feasibility study, followed by preliminary engineering and prototype development and testing. The project had several, and often contradictory, goals. The first was to provide a clean, quiet transit system for Santa Barbara in a timely manner. A second was to develop and demonstrate a new technology. Despite a break in funding and several changes in project sponsors, the equipment and

facilities described in this report were constructed and tested. The results of this work up to construction of the track and testing of the vehicle are described in great detail in references 1 – 4 and more briefly in references 5 – 7.

#### 1.4 Description of Test Vehicle and Facility

The test track and vehicle described in this report are located at the Richmond Field Station of the University of California, Berkeley. The track is the only operational facility of this kind in the world.

##### 1.4.1 Vehicle

A custom-built 35-passenger electric bus (shown in Figure 1.4) was the test vehicle for most of the work described in this report. Designed for bus routes with frequent stops on city streets, the vehicle has a top speed of about 40 miles per hour. It is 28.5 feet long, weighs 25,400 pounds empty and 31,200 pounds fully loaded. The bus has a conventional dc drive system with a 48 kw separately-excited traction motor



Figure 1.4 Prototype roadway power electric bus

(continuous duty) capable of regenerative braking above the base speed of 12 mph. The energy consumption (dc energy into the motor controller) on a stop-and-go driving cycle is about 2.7 kw-hr/mi. The lead-acid battery is rated at 750 amp-hours (five-hour rate) and weighs 6,000 pounds. The 30-minute rating is about 400 amp-hours. The battery voltage is nominally 128, although it varies between 100 and 155 during the driving cycle. The battery was more than five years old when the testing was performed and had lost a considerable percentage of its original capacity.

#### **1.4.2 Vehicle-Mounted Elements of the Inductive Coupling System**

The pickup and onboard controller (OBC) are the components of the inductive coupling system that are located on the bus. The pickup is 13 feet long, 39 inches wide, and weighs nearly 1200 pounds. Figure 1.5 shows the pickup about to be mounted to the bus. The pickup is made of laminated iron pickup cores and aluminum **busbar** conductors. The **busbar** packs are the main longitudinal beams of the pickup as well as being the secondary winding of the ICS.

The OBC both controls the amount of power coupled from the roadway and rectifies and smoothes the 400 Hz current. The **onboard** controller is shown in Figure 1.6, mounted to the right of the driver's seat. It weighs about 870 pounds. The power circuits in the OBC consist of a switchable ac capacitor bank, a rectifier, several inductors, and a dc filter. There are also sensors and an **onboard** control computer (OBCC). The ac capacitors form part of a resonant circuit. The output current is controlled by switching capacitance into or out of the circuit. This moves the resonant frequency of the ICS closer to or further away from the excitation frequency of 400 Hz. In general, increasing the capacitance increases output current. There are 20 steps of capacitance called control states 0 through 19, which correspond to 383 through 2132 microfarads in approximately equal increments. The capacitors are switched with solid state zero-crossing switches. The capacitors and switches are both liquid cooled, which reduces their size and weight. The **onboard** control computer automatically switches capacitance in or out to maintain the desired ICS output current or the desired battery charging current. The OBC output current flows to the battery, motor controller, or both as conditions dictate.

#### **1.4.3 Test Track**

The facility consists of a 700-foot test track with two 200-foot electrified segments. The layout of the track is shown in Figure 1.7. The electrified segments of the track



Figure 1.5 Pickup inductor being positioned under bus



Figure 1.6 Onboard controller mounted in bus

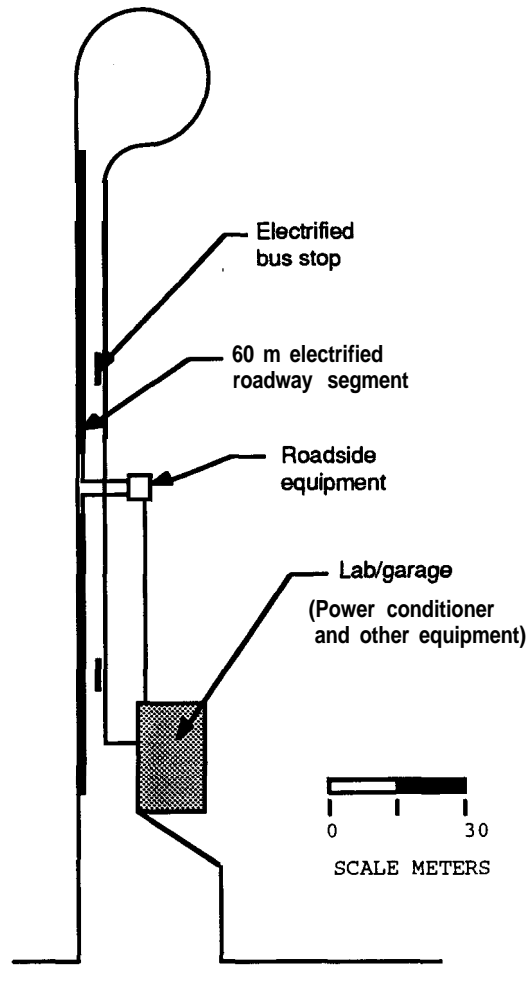


Figure 1.7 Test track layout

consist of roadway inductor core modules and conductors buried just below the road surface. The roadway core modules are made with tape-wound C-cores and laminated iron pole pieces held in an epoxy-sand matrix (see Figure 1.2). The modules installed in Richmond are 9 feet 4 inches long and 18 inches wide and weigh about 900 pounds. Two modules are placed side by side to form the roadway inductor. Figure 1.8 shows the core modules being placed in the test track. The cores were then grouted into place.

One segment uses 350 MCM (0.7 inch diameter) aluminum cable as the conductor and the other uses 0.25 in x 1.5 in aluminum **busbar**. The cables and **busbars** are potted into the conductor slot in a polyester-sand mixture, which, in addition to

## Introduction



Figure 1.8 Placing roadway inductor cores

providing mechanical strength for the loads imposed by vehicles, also provides electrical insulation. Figure 1.9 shows prototypes of the pickup and roadway inductors. This sample display shows both busbars (left) and cables (right) for roadway conductors. Figure 1.10 shows the cable section of the test track as the 350 MCM cables on the left side are being potted into place. Unpotted cables are visible in the slot on the right. The entire roadway was covered with a slurry seal with a thickness of less than 0.2 inches. The slurry seal was not placed over the bus stops, so that on a small portion of the track the construction of the roadway inductors would be visible. Figure 1.11 shows the bus at one end of one of the bus stops. The main track is just to the left of the bus.

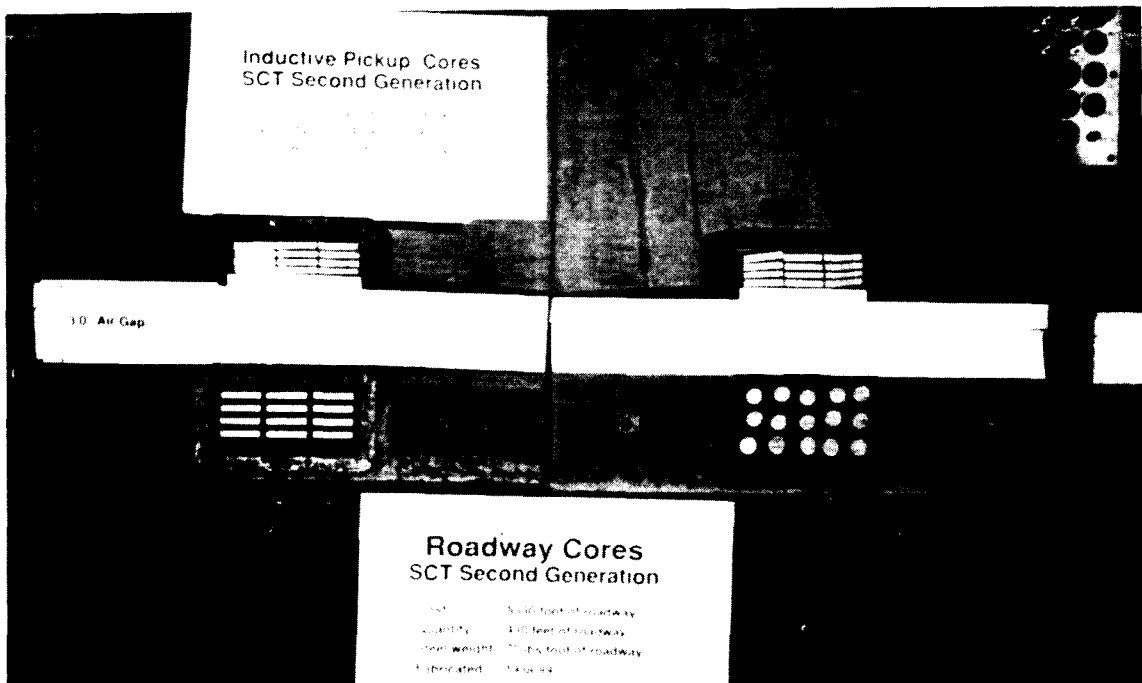


Figure 1.9 Roadway and pickup inductor cross sections

#### 1.4.4 Power Distribution System

The power distribution system consists of a power conditioner and the conductors used to connect it to the roadway inductors. The power conditioner is located in the laboratory building next to the track. Figure 1.12 shows the power conditioner as it arrived on site. This is a rectifier/inverter unit that can supply up to 200 kw at 2000 amps at frequencies from 180 to 400 hertz. The input is three-phase power at 460 volts and 60 Hz. A roadway excitation of 1200 amps at 400 Hz was used for all the work described in this report. Due to skin effect at these currents and frequencies, several conductors are run in parallel. The positions of the cables are carefully selected to ensure all parallel paths have nearly identical inductances and carry essentially equal currents. The output from the power conditioner goes to a patch panel, where the current can be directed to the indoor test stand or to the equipment pad at the center of the track as shown in Figure 1.7. From the equipment pad, current flows to one or both of the segments of the test track.

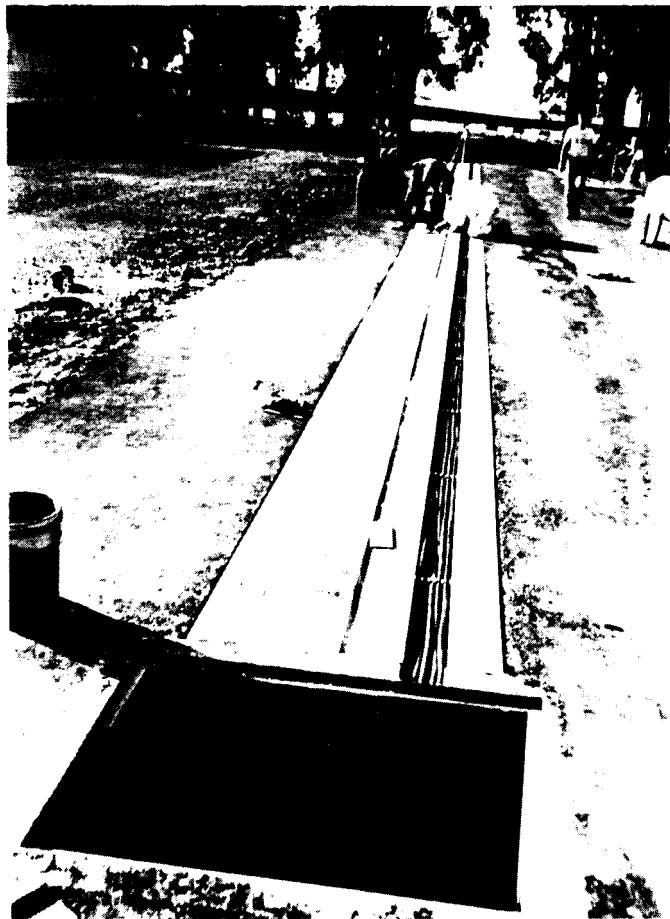


Figure 1.10 Potting of roadway cables

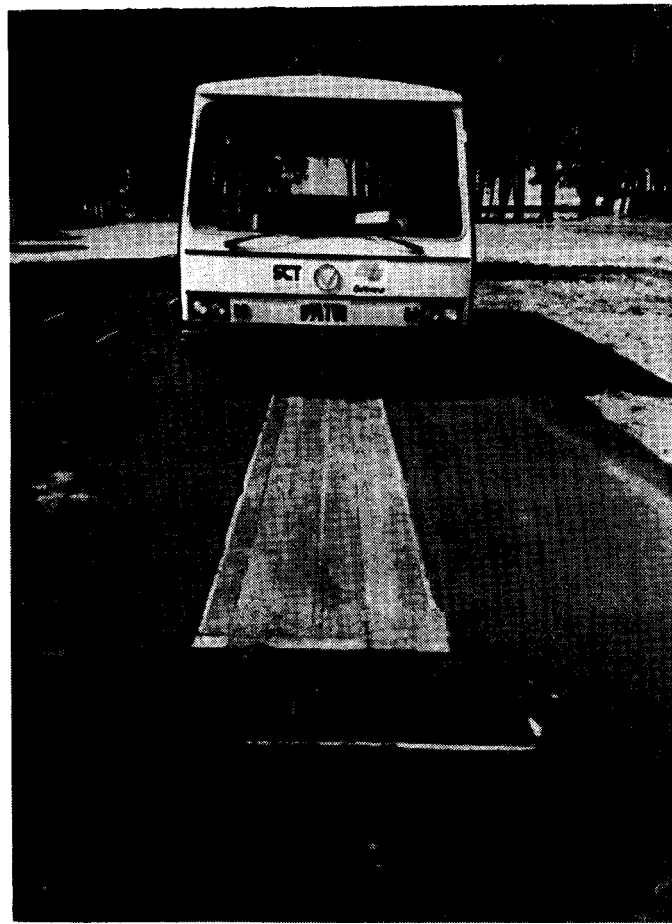


Figure 1.11 Roadway powered electric bus over bus stop

Chapter 4 discusses the design and construction of the test track and installation of the associated equipment, which was one of major undertakings of this project. The facility development had a twofold purpose: to provide a section of powered roadway that could be used to test an RPEV in motion and to learn about and document the construction of the roadway inductor.

Chapter 5 details the system testing that was the most important task in this project. The tests performed would indicate if an RPEV is a viable technology. There were six specific test areas:

- Power transfer ability
- Control of output power
- Efficiency
- Range
- Vehicle performance
- Environmental impacts

Chapter 6 summarizes other RPEV research related to this project, including testing of a system designed for a G-Van using a higher frequency, lower current excitation in the roadway. Two deployment studies are also summarized, one relating to near-term deployment opportunities and the other examining impacts of a full regional RPEV system that would require several decades for deployment.

## **1.6 Project Objectives and Results**

At the conclusion of the previous phase of work there were several aspects of the RPEV technology that required further investigation. These issues-dynamic power coupling, range improvement, system efficiency, acoustic noise level, on-board weight, and system costs-became the objectives of this project.

### **1.6.1 Dynamic Power Coupling**

Testing at the Short Test Facility during the previous phase proved the concept of transferring power across an airgap with a magnetic field, but all testing had to be done with no longitudinal motion. One of the most important goals of this phase of the project was to prove that longitudinal motion of the pickup does not affect the power transfer ability of the ICS. This was to be accomplished by mounting the ICS

pickup on the 35-passenger electric bus and transferring power while the bus was in motion.

Power transfer ability was measured both statically (ICS stationary) and dynamically (ICS mounted to vehicle in motion) and peaked at approximately 400 amps at 150 volts dc. Output current was easily controlled and very low ripple. There was no dynamic interference or interaction between the ICS and the motor controller.

### **1.6.2 Range Improvements**

The main goal of the RPEV technology is to improve the range of electric vehicles but up until this project no operational RPEVs have existed. All computer analyses had shown that an RPEV should have considerably more range than a battery-only EV but no empirical data could be gathered because of the lack of an operational system. A major project goal was to use the hardware built for this project to demonstrate and explicitly measure the range extension of an RPEV.

Range tests showed the vehicle capable of all-day operation while using the ICS but two hours or less on the battery only. These correspond to ranges of 200 miles and 15 miles, respectively.

### **1.6.3 System Efficiency**

Measuring system efficiency was not really possible with the earlier Short Test Facility, because open roadway losses (the losses associated with long unoccupied portions of energized roadway) could not be accurately measured. With the new facility at the Richmond Field Station there would be two 200-foot roadway sections whose losses could be measured and the system efficiency calculated. System efficiency is an important factor in determining the overall feasibility of the RPEV technology because too low an efficiency would increase the cost of electricity to the user.

Efficiency was measured at 60% from ac power into the power conditioner to dc power out of the ICS. The efficiency was the same for static and dynamic energy transfer on a 200-foot roadway segment. When using the indoor static charger efficiency was closer to 80%. Future designs are expected to reduce open roadway losses and increase efficiency by at least 10%, although the system should still be viable at 60% efficiency.

#### **1.6.4 Acoustic Noise level**

The main complaint about the proof-of-concept Inductive Coupling System developed at the Short Test Facility (located at Caltrans' Translab in Sacramento, CA) was the amplitude of the acoustic noise generated by the equipment. While some of the noise could be attributed to factors that would not be present in a actual RPEV system, a significant portion of the 90 dBA noise level was generated by the pickup, onboard controller, and roadway. Redesigning these components for much quieter operation was a goal of this project.

Acoustic noise was reduced to approximately 40 dBA both inside and outside the bus when coupling full rated power. There was some bothersome noise in non-RPEVs operating over the powered roadway, but this was eliminated in later designs by reducing roadway current and increasing operating frequency.

#### **1.6.5 On-board Weight**

The on-board equipment for the first generation (Translab) system met the design goals, but there were indications that some improvement-specifically in pickup weight was both desirable and achievable. Decreasing onboard weight would increase the appeal of the technology when compared with battery-only vehicles. Reduction of the ICS onboard weight was a project goal.

Redesign of the pickup and OBC reduced the onboard weight by approximately 500 pounds compared to the equipment used at Translab. The onboard energy supply equipment represented 26% of the gross vehicle weight, and range tests indicated that further reductions in battery weight are possible.

#### **1.6.6 System Costs**

The proof-of-concept system built for the previous phase of the research had cost more per foot of roadway than would be acceptable for an installation with miles of powered road. This is not surprising as experimental equipment generally costs much more than equipment that is in large-scale (or even small-scale) production. The cost of the experimental equipment was high enough to raise questions about the technology's economic viability. Cost reduction of the next generation of equipment and obtaining realistic cost estimates for an initial application were project objectives.

The prototype system costs remained high but somewhat less than the cost of the short test facility, and we gained important knowledge on the fabrication and installation of the roadway inductor the most costly component in the system. Because of the information and experience gained from this project, further cost reductions of the roadway inductor (and other components) should be achievable in the future. As with the short test facility, economies of scale affected the cost of components as even 400 feet of roadway is not long enough to justify large-scale production of components.

#### 1.6.7      **Overall Project Goals and Results**

The overall goal of the project was to determine the technical viability of the RPEV technology. All key objectives were met; if not completely, then to a significant degree. Areas requiring further work-acoustic noise and electronic engine control interference in **non-RPEVs** and cost of the roadway inductor-were defined and the methods for addressing these issues were identified. Worked funded by other sources demonstrated that the suggested modifications to the design did in fact solve these few remaining problems.

The results of this project were extremely promising and additional work on **third-generation** equipment has been performed making the technology even more attractive. This system should be pursued as the technology has, the capability to make battery electric vehicles viable alternatives to internal combustion engine, trolley wire, or third-rail electric transit vehicles. This technology can also be applied to smaller personal vehicles and may provide the performance necessary to make them attractive to a wider audience.

## **2. Systems Engineering and Design**

---

The Roadway Powered Electric Vehicle system is complicated, and producing an efficient, economical design is very challenging; therefore, SCT adopted a systems engineering approach to the project. At every step, requirements and/or goals were set for various system attributes, such as output current rating, losses, or component costs. Due to the complicated interactions among various system parameters, numerous trade-offs had to be analyzed. The RPEV system is highly non-linear so that when one parameter shifts, much of the previous analysis has to be repeated for the new candidate design point.

### **2.1 Objectives and Approach**

While the basic design of the RPEV bus and roadway was defined in the earlier phases of the project, a significant amount of engineering was required to advance the design to the level warranted for construction of the test track at the Richmond Field Station. Many changes were made to the design, and numerous others were considered, but eventually postponed or discarded.

The objective of these design iterations was to develop a technically and economically viable RPEV technology, realizing that prototype costs would be much higher than costs for a large operational system.

To develop a viable RPEV system, analyses comparing different parameters of the system had to be performed. The goal was to achieve an energy balance **onboard** the vehicle where energy supplied by the RPEV system equals energy consumed by the vehicle, giving an unlimited range. Because of the storage capacity of the battery, an exact energy balance is not required because the battery can make up the deficit to allow a full day (10 or more hours) of operation. The inductive coupling system is highly non-linear, which makes analysis of trade-offs rather difficult. Some of the highest level choices involved the output current rating of the inductive coupling system, length of layovers, and baseline electrification pattern. These all had to be balanced to achieve the energy required **onboard** the vehicle that would allow it to operate for a full day along the design route. The next step in the analysis involved selection of the baseline operating point to obtain the desired output current, which

required specification of parameters such as roadway excitation (current and frequency), number of pickup turns, pickup mutual inductance (with roadway), and onboard capacitance. The next level of detail involved the actual hardware design, such as specification of inductor geometry (both roadway and pickup cores), core material, conductor sizes, and construction techniques for both the pickup cores and roadway modules.

Numerous constraints and goals guided the design process, including targets for infrastructure and operating cost, onboard weight, system efficiency, and environmental impacts. Trade-offs among these parameters were difficult to evaluate, due in part to the complexity of the system and its non-linear nature, as well as lack of crucial information, such as fabricated core costs. Many iterations were required before the final design evolved, and that design cannot be considered optimal, although it was judged adequate to demonstrate the viability and potential of the RPEV technology.

Some consideration was given to alternate power control schemes. The alternate schemes considered have some distinct advantages, such as reduced losses, increased system efficiency, and increased average output current. Some of these changes, such as using non-uniform steps of capacitance to improve the resolution of the output current control were implemented, while others were postponed for future development.

## 2.2 Analysis Tools and Methods

Analysis of the trade-offs involved in designing an RPEV system involves the use of computer simulations, published reference material, discussion with suppliers, and considerable engineering judgment.

We used several computer programs to examine the operation of an RPEV system. The three most important programs are EVSIM, PHASE and POISSON. EVSIM models the operation of an electric vehicle on and off the powered roadway, PHASE simulates the operation of the inductive coupling system, and POISSON predicts the magnetic properties of different core and conductor geometries.

To evaluate trade-offs among various candidate designs, values must be obtained for hardware costs and component losses. This is often difficult, especially for the roadway and pickup cores, which are custom items. These parts cannot be selected from a catalog and engineering judgment and (limited) prior experience must be used to a large extent in estimating component costs and losses.

### 2.2.1 Electric Vehicle Simulation, EVSIM Program

The computer program EVSIM was used to analyze the performance of an electric vehicle, operating on an arbitrary route including segments on or off the powered roadway. The simulation includes models of the battery, motor, vehicle, and route. The inductive coupling system is included as a current source onboard the vehicle while the vehicle is operating over the powered roadway. The current drawn from the roadway is automatically reduced if it would drive the battery above gassing voltage. The route consists of many blocks (we have run routes with more than one hundred) each consisting of acceleration, cruising at a constant velocity, deceleration, and stationary sections. A slope for the entire block is included. The vehicle, battery, and motor models include all parameters normally associated with electric vehicles, including battery voltage and capacity, motor current limit, vehicle mass, rolling resistance, and aerodynamic drag coefficient.

The model was used to determine the net charging/discharging of the vehicle when driven around the baseline design route under various conditions, such as varying the electrification pattern, layover times, initial battery depth of discharge, or inductive coupling system output current. The battery depth of discharge at the end of the simulation was compared with that at the start to determine net battery drain.

A project goal of infinite range while operating on the design route was established. This is somewhat conservative, as the battery could discharge 2–4% per round trip and still meet the design objective of ten hours of operation. Although Santa Barbara has backed away from project sponsorship since the earlier phases of the program, the downtown Santa Barbara route was retained for analysis, both because it was well defined and because it was thought to be reasonably representative of other possible applications.

Several upgrades were made to EVSIM during Phase 3D. The calculation of numerous statistics was added, including integration to obtain amp-hours and kilowatt-hours associated with each energy source and sink. Calculation of RMS (root mean square) currents in the motor was also added. These statistics helped in many ways, including interpretation of simulation runs, correlation of test and model data, and preparation of hardware specifications. A battery specification was prepared during the early part of the project when purchase of a new battery was anticipated. These statistics were also useful when the decision to upgrade the motor controller was made.

Another upgrade involved the addition of a feature allowing for the partial electrification of blocks. For instance, it has been assumed from the project's inception that the roadway inductor would be interrupted through intersections and for mid-block crosswalks, although the simulation previously had the capability only to model a block as fully electrified or fully non-electrified. It is now possible to divide a block into as many as ten pieces, each with or without roadway electrification.

### **2.2.2 Electric Circuit Analysis, PHASE Program**

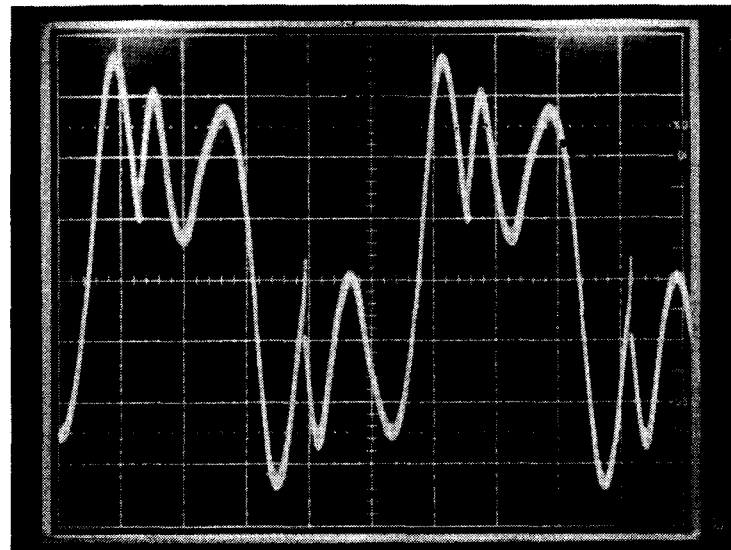
PHASE, the inductive coupling system circuit analysis program, was developed in an earlier stage of the RPEV development and has proven to be a valuable analysis tool. PHASE has worked well and has been modified several times to reflect new insights gained from our increased understanding of the technology. We made three major modifications to this program during the project.

The most important modification is the inclusion of the effects of the current-limiting reactors that are in series with the main AC capacitors of the OBC. Originally the effect was thought to be unimportant and was accounted for by adjusting the capacitor value. Our tests, however, showed that the inductors affected the waveform of the current in the OBC, and lowered the effective capacitance. A poorly chosen inductance value will create badly distorted waveforms in the OBC and affect its operation. We were able to simulate this effect with the modified PHASE program as shown in Figures 2.1.a and 2.1.b, which show an actual oscilloscope trace and a time history generated from the PHASE program output. Clearly the match is very good, adding to our confidence in the simulation.

The other PHASE program modifications concerned alternate control schemes. Two versions of PHASE were created to simulate the effect of separate control and power winding (PHASE-61 and center-tap winding (PHASE-7). Each of these has distinct possibilities and warrants further effort.

### **2.2.3 Magnetic Analysis, POISSON Program**

POISSON was developed by Lawrence-Berkeley Lab and has proved valuable to us in the design of the pickup and roadway inductors. POISSON maps the magnetic field created by various current/magnetic core designs. POISSON outputs are used to calculate the mutual and leakage inductances of the designs. In general, POISSON



time, 0.5 milliseconds/division

Figure 2.1 .a Oscilloscope trace of waveform with a poor value of  $di/dt$  inductance

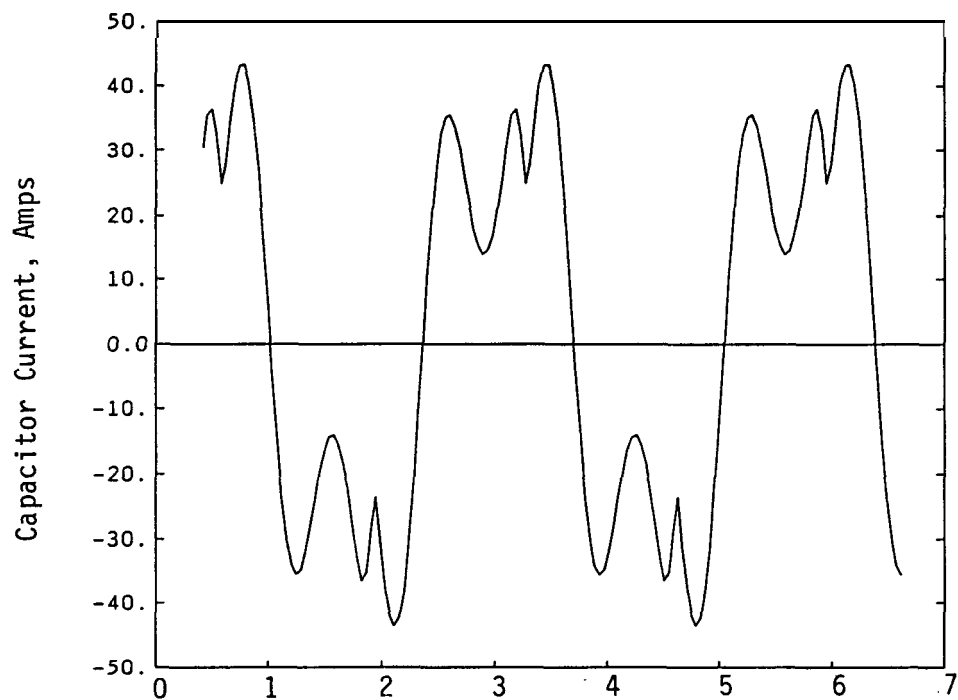


Figure 2.1 .b Computer-predicted waveform for values of  $di/dt$  that produced Figure 2.1 .a

gives results that closely match measurements taken from the hardware. Test results are compared with the POISSON predictions in Chapter 5.

POISSON was used extensively in designing the roadway and pickup cores used in the test track at the Richmond Field Station. Because our experience with core geometries was limited to the single example from the Translab Short Test Facility, we relied heavily on computer predictions when designing the new cores. For instance, the effect of the pole piece thickness on the core performance was unknown when we started this phase of the project. POISSON convinced us that the thickness was of secondary importance compared with the pole face area. Appendix B contains an abridged listing of POISSON inputs used for roadway and pickup core design.

#### 2.2.4 Hardware Cost Estimates

Hardware costs for the various components of the Inductive Coupling System (ICS) were often difficult to obtain. Obtaining firm quotes, or even estimates generally required substantial effort, including visits to potential manufacturers. Because of the unique nature of the roadway and pickup inductor cores used in the ICS, they were not available and, except for the few cores at the Translab Short Test Facility, had never been manufactured. TechTran, the manufacturer of the Translab cores, declined to bid on the cores for the new system so SCT had to locate inductor core manufacturers and educate them about these unique products. The relative complexity and unusual shape of the cores caused consternation among most of the core manufacturers we talked to, and only by working closely with two manufacturers (one of whom did not normally manufacture cores) were we able to produce the pickup and roadway cores required for this project. Because the cores are unusual, it was hard to estimate their cost, and our initial estimates proved to be optimistic. The pickup cores were originally budgeted for \$15,000 and the roadway cores for \$135,000 but they ended up costing \$27,100 and \$277,500, respectively. While this is a large variance, we learned a great deal, and in the case of the pickup cores ended up with a product that was lighter in weight and had better performance than we had originally projected.

Other components of the system, such as the capacitors for the roadway and OBC and the current-limiting reactors for the OBC, were more or less standard. The cost of these components was small compared to the whole system, and they were easily priced and purchased.

The OBC, purchased under Phase 3C, required modifications to the trigger circuits and current limiting reactors. While these parts did not cost very much, engineering time was spent developing a working trigger circuit and determining the correct values for the  $di/dt$  inductors. Additionally the mechanical structure and the wiring of the OBC had to be modified significantly to incorporate the new inductors and to reduce the acoustic noise emanating from the OBC compartment.

#### 2.2.5 Component Loss Estimates

Loss estimates for the various components are determined by numerous methods. Losses for off-the-shelf items, such as the rectifier or capacitors, can be found in catalogs. Losses for the conductors can be calculated in a relatively straightforward manner, as shown in Section 2.6.2. Many of the inductors used in the onboard controller are custom designed for this particular application. Losses can be included in the purchase specification, and manufacturers are able to calculate these losses relatively accurately.

Determining the losses of the cores is the most difficult. Manufacturers of electrical grade steels publish graphs of losses, such as those in Figures 2.2.a and 2.2.b, which are for 0.007-inch M2 steel from Armco, the steel used in the pickup. These plots present ideal, minimum losses, and those in good quality fabricated components tend to run 50 – 100% higher than the published losses, although they can run considerably higher. The increased losses are due to many factors including:

1. Non-uniform flux distribution within core
2. Residual stresses within laminations
3. Flux paths within laminations not parallel to the preferred grain-oriented direction
4. Flux paths with a component perpendicular to the plane of the laminations (flux passing from one lamination to another)
5. Electrical shorts between laminations
6. Joints in the magnetic circuit
7. Non-sinusoidal flux waveforms

**A**s more experience is gained within a particular application, these extra losses should decrease through design refinements. Our assumption during the design process was that real core losses would be approximately twice the book losses. In

reality, the factor turned out to be considerably higher, especially for the roadway cores.

## 2.3 System Design

The highest level of trade-offs involved specification of a system that will provide a full day's operation of the bus on the design route. Numerous combinations of route electrification pattern, bus schedule, and inductive coupling system output current will allow the bus to operate indefinitely along the baseline route in downtown Santa Barbara. Some combinations are rather unattractive, such as those requiring a large percentage of the route length to be electrified (high roadway inductor costs) or those requiring very long layovers (many buses and high driver costs). This section examines these trade-offs, showing trends that apply to all RPEV systems. This analysis resulted in selection of the baseline schedule, electrification pattern and inductive coupling system output current. These served as the basis for the later work, although when more detailed cost information for some of the hardware (particularly roadway core modules) became available, the overall system design was revisited.

### 2.3.1 Goals

The objective of this task was to determine the most effective combination of route electrification, bus schedule (i.e., layover time), and inductive coupling system output current rating. Life-cycle cost is considered the basis for this effort, although during many of the detailed analyses, the trends became clear without carrying out the cost analysis on the system economic model.

### 2.3.2 Trade-off Issues

An inductive coupling system can easily be designed to provide an output current greater than the average current drawn by the motor controller plus accessory loads. This indicates that with full electrification-as with trolley bus systems-the vehicle has infinite range, and an **onboard** energy balance is achieved. Full electrification is not the most cost effective solution, as the capital cost of the roadway inductor would be prohibitive if it were installed over the entire route.

The amount of powered roadway can be kept to an absolute minimum by transferring energy to the vehicle only when the vehicle is stationary, either at bus

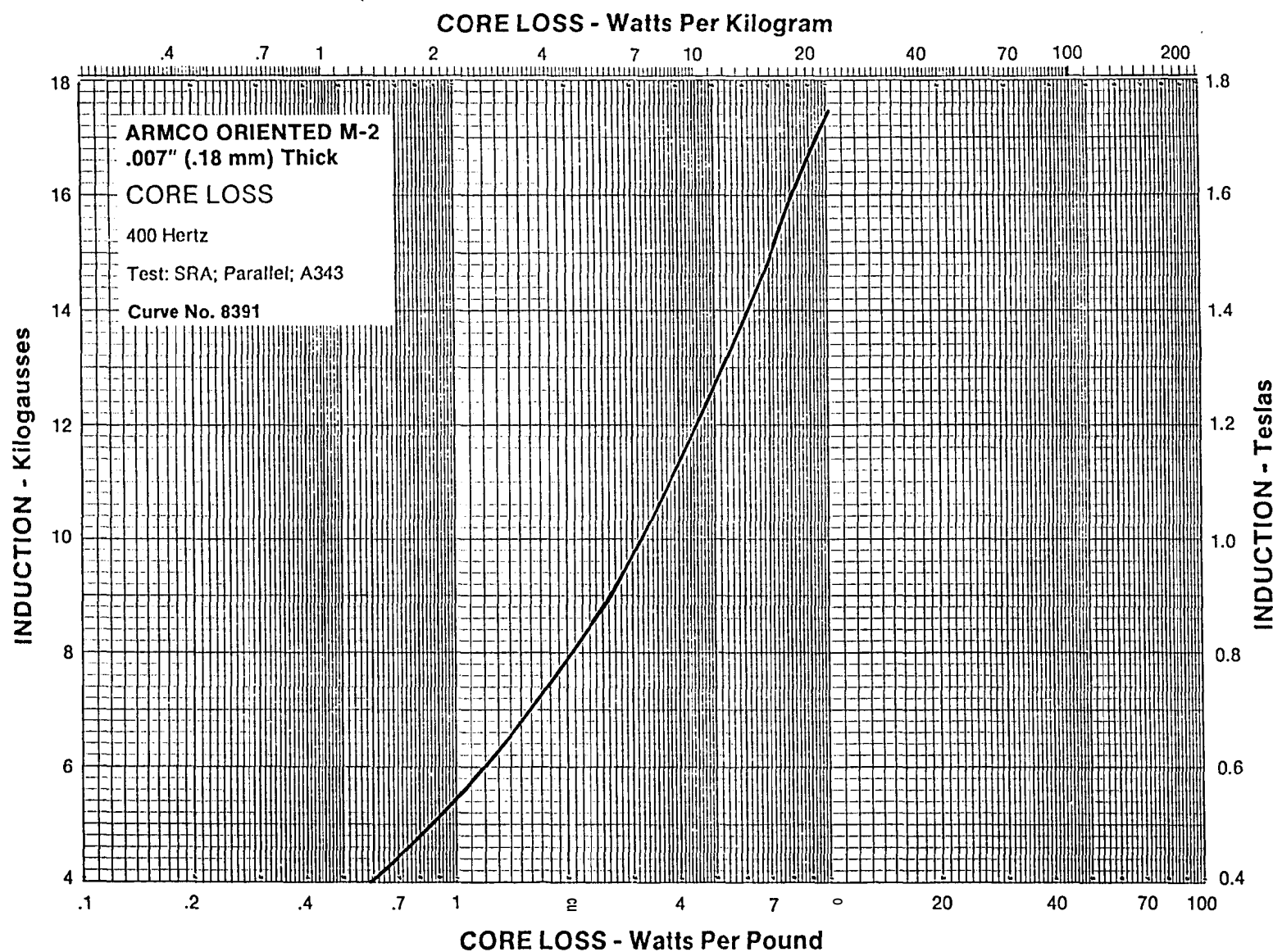


Figure 2.2a Core loss for 7 mil M-2 at 400 Hz

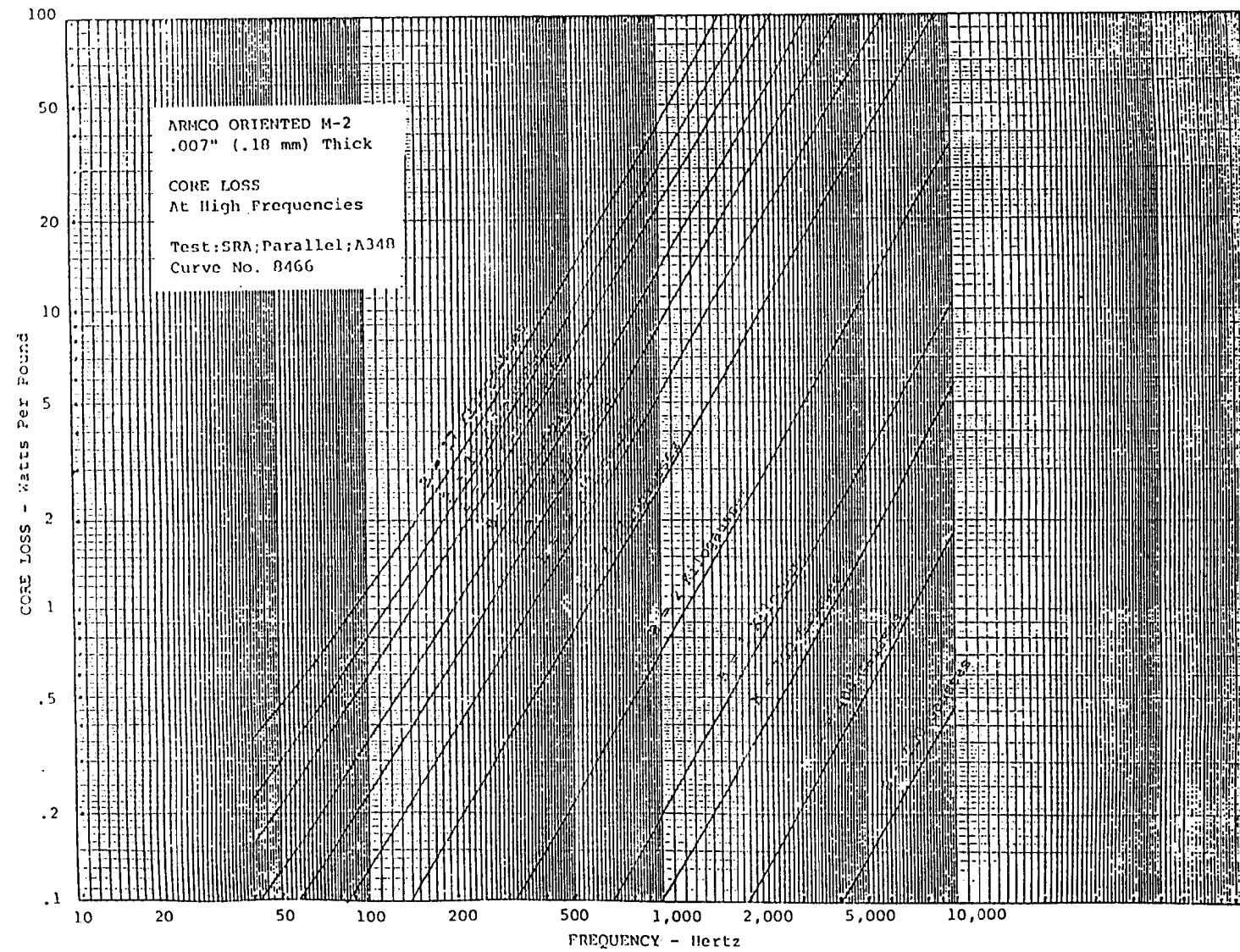


Figure 2.2b Core loss for 7 mil M-2 at high frequencies

stops or layover points. This type of opportunity charging system can provide infinite range if the vehicle spends a substantial portion of its time stopped or if the vehicle's onboard energy storage system has a very high charge acceptance rate considerably higher than the lead-acid batteries on the PATH bus. That vehicle has a very limited autonomous range, especially with the battery currently on the vehicle, which is in poor condition. Even when the battery was new, the operating period in battery-only mode was less than three hours. Achieving unlimited range with opportunity charging would require very long layovers, requiring many more buses to achieve a given headway on the route. While static charging plays an important role in the baseline design, it is not adequate by itself, particularly for the PATH bus. For another vehicle that may have an operating interval of 4 – 6 hours on batteries only, opportunity charging may be all that is required to achieve 10 – 12 hours of operation a day.

The output current rating of the inductive coupling system can be increased through relatively straightforward means, such as increasing the roadway current. There are several drawbacks to increasing rated output current much. First, increasing the current rating of the ICS tends to increase open roadway losses as well as onboard weight. Roadway inductor costs also rise, but their increase is proportionately less than the increase in output current. Another limitation is the ability of the vehicle to accept energy. The ICS output current is limited to the sum of the instantaneous vehicle power draw (motor controller plus accessories) plus the amount of charging current that the battery can accept. When the vehicle is stationary, the motor controller's draw is zero, so ICS output current is limited to slightly more than what the battery can accept.

Similarly, when the battery is fully charged, it can accept little or no charging current, so the ICS output current is limited to the bus's instantaneous power requirements. Lead acid batteries do not have very good charge acceptance, especially when they are at a relatively high state of charge. When an RPEV is operating in a purely static charging mode nearly all energy transferred to the vehicle goes to the battery. Since the battery has an average energy efficiency of 75%, a substantial fraction of the energy is wasted, reducing overall system efficiency (AC kilowatt-hours per vehicle mile). This wasted energy shows up as heat in the battery, which is detrimental to battery life. Limited energy acceptance capability of the vehicle limits the benefit of increases in ICS output current rating. The point of diminishing returns is evident in the analysis presented later.

### 2.3.3 Baseline

The baseline operating point was revised during Phase 3D. There were several reasons for this, including:

- Projected addition of a steering assistance system on the bus
- Higher roadway inductor costs than originally estimated
- More efficient location of the electrified roadway elements

Each of these three factors caused significant shifts in the selection of the final design point.

The addition of a steering assistance system to an RPEV reduces the RMS offset between the vehicle and roadway centerlines, which increases the amount of current available to the vehicle through the inductive coupling system. With a closed loop steering assistance system, as has been postulated as the baseline, the mean lateral offset (error) should go to zero and the standard deviation should be reduced to a low value, probably no more than two inches. This compared to a previously assumed standard deviation of six inches. When the vehicle is within two inches of the roadway inductor centerline, the output current available from the ICS is down less than 10% compared to being perfectly centered. Keeping the vehicle well centered increases the average current available to the vehicle, which will increase the average current actually transferred to the vehicle and decrease the peak-to-average current ratio of the inductive coupling system. With the steering assistance system, the peak-to-average power ratio will depend primarily on the power acceptance of the vehicle rather than the amount of current available at any particular instant from the ICS.

The price quotes for the roadway core modules were considerably higher than expected, which increased the weighting given to minimizing the length of powered roadway to be installed for an operational system. This led to serious study of the most efficient way to utilize the roadway inductor.

The third shift in the route electrification pattern involves a better understanding of the most effective locations in which to install the powered roadway, which began with the realization that while the vehicle is decelerating with regenerative braking, the motor (acting as a generator) is supplying as much energy as the battery can absorb. Clearly, installing the roadway inductor in areas where the bus will be braking-such as immediately before a bus stop-is unnecessary. As described in Section 2.2.1, the EVSIM program has been upgraded to include partial electrification

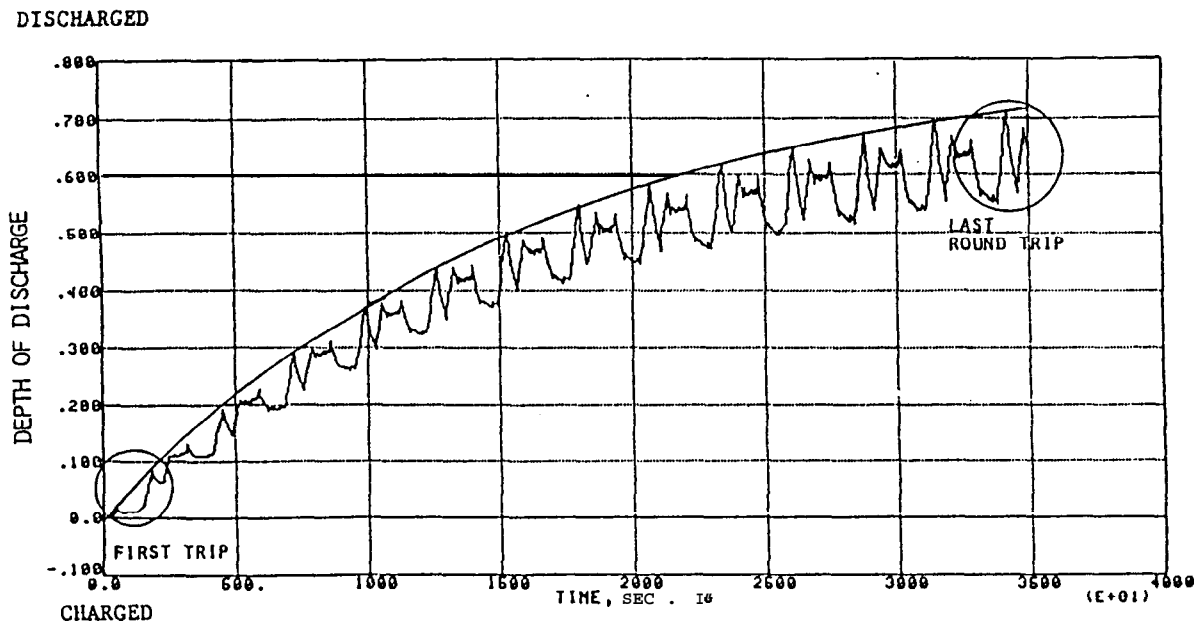
of blocks, allowing the roadway inductor to be eliminated before a bus stop. It is more advantageous to electrify the roadway where the bus is moving slowly and accelerating-longer occupancy time over each foot of roadway and high power acceptance capability of the vehicle-than where the vehicle is cruising at high speed, especially downhill where the motor is drawing very little current and may even be in regenerative braking mode. Partial electrification of blocks allowed the roadway inductor to be located more effectively and reduced the total length of electrified roadway required to achieve infinite range.

The new baseline operating scenario involves many improvements to the baseline system previously defined. Layover points and all bus stops are electrified. All blocks along State Street are electrified, but power is interrupted in three locations. These are:

- during lane change while leaving the bus stop
- through intersections with cross streets
- from the mid-block crosswalks to the bus stops

The third break is the longest and includes the area where the bus is decelerating for the bus stop. The other breaks are included to more accurately represent practical constraints anticipated for urban implementation of the RPEV technology. The new baseline electrification pattern involves electrified segments spread over a wider geographical area than previous designs, making the power distribution system more complicated but this is more than offset by the reduction in the length of powered roadway-31% of the total bus route length compared to 40% in earlier designs.

For the new baseline, the total round-trip time is 40 minutes, with a 3-minute layover at each end of the route. The layovers are 15% of the total round-trip time, which is within the normal range for an urban transit operation. The original design assumed longer layovers and a 45-minute round-trip time. That design contained a 5-minute layover at each end and a 2-minute unpowered wait for crossing Highway 101 in each direction, resulting in fourteen minutes during which the bus was stopped, not including bus stops. Figure 2.3 shows the battery DOD for this scenario. During the early hours, the battery is relatively full (low DOD) and can accept only very small charging currents. This causes the DOD to increase rapidly during the first hours of operation. The curve levels out after several hours of operation to a nearly steady state depth of discharge.



Average Coupled Current = 300 Amps  
 Gross Vehicle Weight = 31,200 pounds  
 State-Cabriilo Route, **45-minute** roundtrip  
 Static charge of 5 minutes at top of Mall  
 Static charge of 5 minutes at Convention Center

Figure 2.3 Battery depth of discharge for ten-hour day

The baseline inductive coupling system is expected to provide an average of 350 amps for the vehicle to meet its range requirements. Figure 2.4 shows the change in battery depth of discharge during a single round trip for various inductive coupling system output currents. The battery DOD was approximately 40% for the computer runs that generated this data. With low inductive coupling system output currents (300 amps or less), the battery discharges significantly on each round trip, and operation of the bus for a full day is doubtful.

At the other **extreme**, with ICS output currents of 450 amps or more, the battery experiences significant net charging, and much of the time (especially when static charging) the bus cannot accept the entire current available. The **curve flattens** out at for higher currents, indicating a point of diminishing returns. The curve in Figure 2.4 crosses through zero at 360 amps, indicating that the vehicle could run indefinitely at this ICS output current and 40% battery DOD.

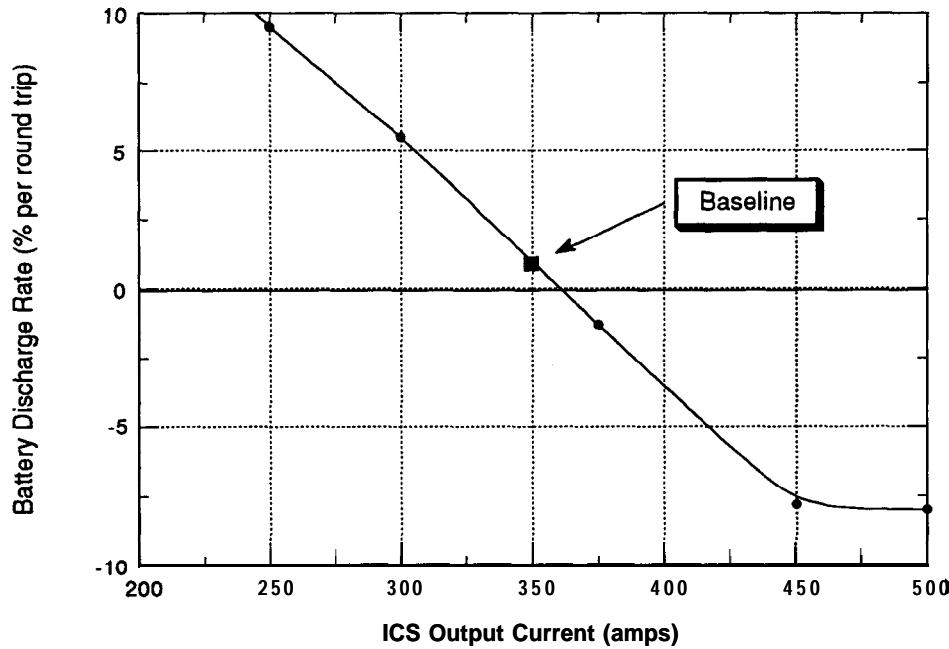


Figure 2.4 Battery discharge as a function of ICS current

The battery DOD for a full day of operation with the baseline design is shown in Figure 2.4. During the early hours, the battery is relatively full (low DOD) and can accept only very small charging currents. This causes the DOD to increase rapidly during the first hours of operation. The curve levels out after several hours of operation to a nearly steady state depth of discharge.

The baseline design has an average available ICS output current of 350 amps. Due to the small variations in the airgap between the roadway and pickup inductors, the current available from the ICS will not always be equal to its full rated output current. Lateral offsets are expected to be small most of the time because of the steering assistance. This keeps the instantaneous current available from the ICS within 10% of its peak value nearly all the time, indicating that a peak current rating of 400 amps would be adequate to provide an average available current of 350 amps. A higher rated output current of 450 or 500 amps would increase the likelihood of achieving the 350 amp available output current at every instant, but is probably not required for successful operation of the bus.

### 2.3.4 Sensitivity Analysis

The trade-offs among baseline electrification pattern, schedule (layover times), and required ICS output current are examined in this section, showing the sensitivity of the operating point to these key parameters.

The data presented in the next three figures are the result of computer simulations with electrification patterns similar to but not identical to the baseline case. Figure 2.5 presents data for four different layover times. These plots were generated with 41% of the route length electrified, but the location of the electrified roadway was not so effective as the baseline design.

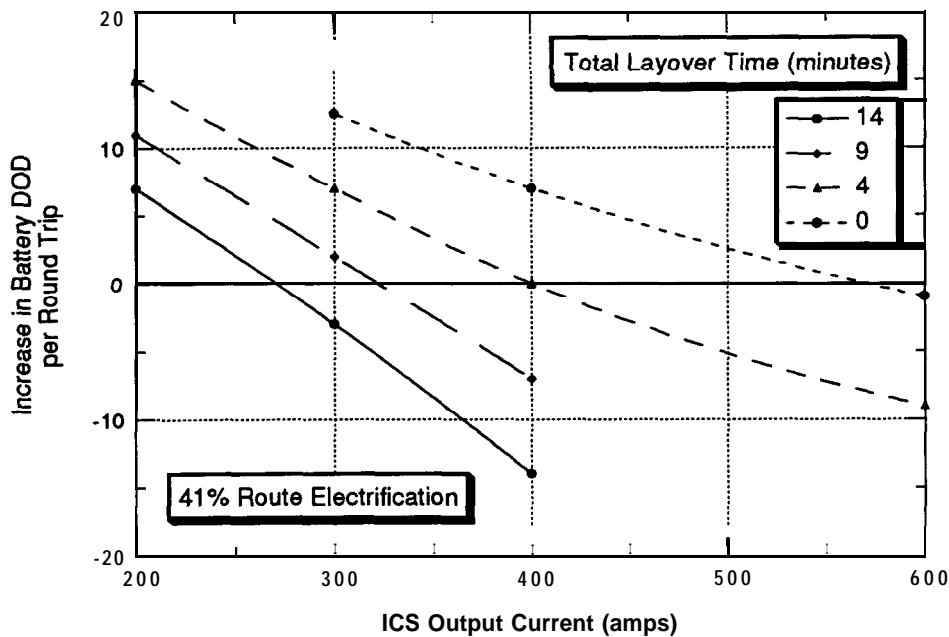


Figure 2.5

Figure 2.5 Battery DOD as a function of ICS output current for various layover times

Neither of the two extreme layover times are very practical. Zero layover time would make it impossible for the vehicles to maintain proper headway, and a 14-minute total layover time would represent 33% of the total route time, which would require more buses and drivers to provide the same headway as designs with shorter layovers. The ICS current required to achieve an energy balance (zero net battery discharge over the entire round trip) is about 275 amps with 14 minutes of layovers. It increases to 325, 400, and 575 amps for layover times of 9, 4, and 0 minutes. Clearly, larger ICS currents are required to achieve steady state operation as the layover times

are reduced. The large increase in required current from 400 to 575 amps (as layover time is reduced from four to zero minutes) indicates that ICS currents above 400 amps are not very effective, as this extra current can only be absorbed a small percentage of the time.

The computer runs that generated the data in Figure 2.5 were repeated for alternate route electrification percentages. Operating points that produced zero net battery discharge were determined by interpolating along these curves. These resulting steady state operating points are plotted in the next two figures.

In Figure 2.6, the ICS current required for various layover times is plotted as a function of the percentage of the roadway electrified. As we previously concluded, higher ICS output currents are required with shorter layover times. For very long layovers, the curves are relatively flat, although the required current does increase slightly as the percentage of the roadway length electrified is decreased. In these cases, most of the energy is transferred to the vehicle during the layover periods and at bus stops, so the required current is a weak function of the percentage of the roadway that is electrified. As the layover time is decreased, the required ICS current is more strongly dependent on the percentage of roadway electrified. An ICS output current

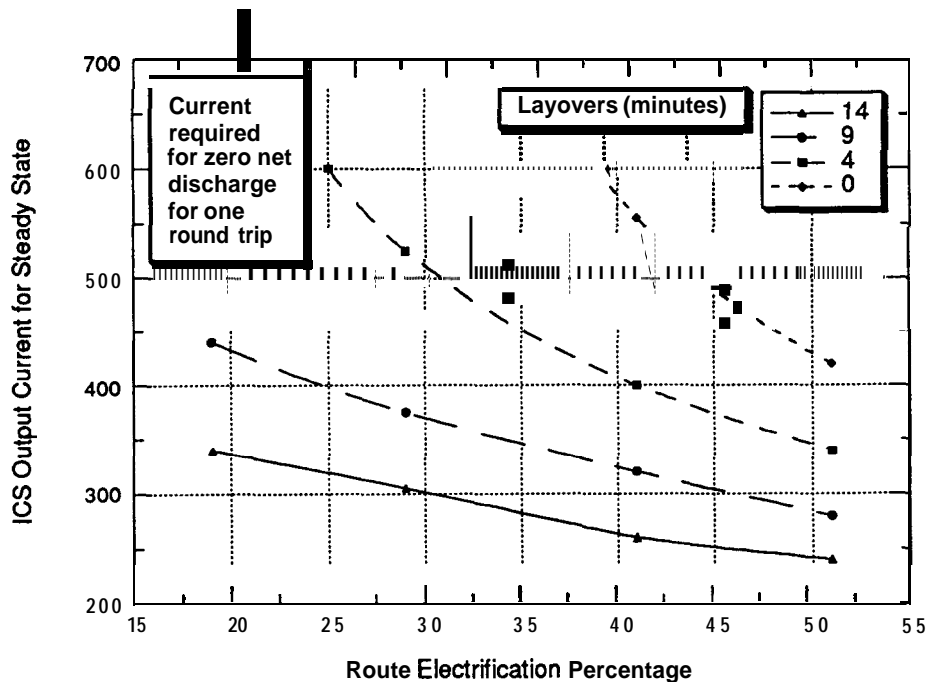


Figure 2.6 Current required for zero net discharge for one roundtrip

of 370 amps is required for 9 minutes' layover time and 31% of the route electrified. The baseline operating point from the previous section is slightly better-360 amps with 6 minutes of layovers and 31% electrified-due to more effective selection of the locations of the powered roadway.

Figure 2.7 presents the same data as Figure 2.6 but with lines of constant ICS current rather than constant layover time. Data for each ICS current plots along a straight line, and all lines are parallel. This presents a very clear trade-off between layover time and length of route electrified. Ten minutes of layover time (two additional buses and drivers at 5-minute headways) corresponds to 35% route length, or 1.9 lane-miles of roadway inductor. This allows trade-offs of capital and operating costs to be examined and quantified very easily. The spacing between the lines is closer for high currents, again indicating the small incremental benefit of increasing the ICS current above 400 – 450 amps.

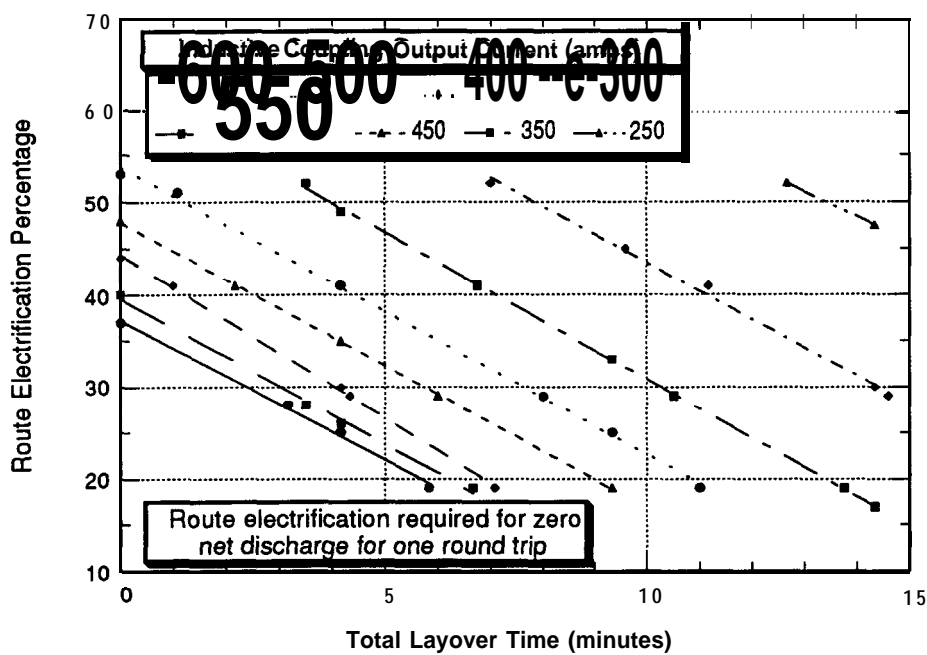


Figure 2.7

Figure 2.7    Route electrification required for zero net discharge for one roundtrip

## 2.4 Baseline Operating Point

The required ICS current was determined in the previous section. The next step in the process is the selection of an appropriate operating point. Selection of the operating point and design of the inductors couple very strongly. It is often necessary to iterate with several cycles of adjustments to both the operating point and inductor design required to formulate a good design. There are many operating points that can produce the desired output current. An operating point was defined in Phase 3C of this project and much hardware was purchased for that operating point, including an **onboard** controller and a power conditioner. At the beginning of Phase 3D, we anticipated that a new power conditioner would be purchased to allow segment switching. With the new power conditioner, it would be possible to change at least some of the system parameters, such as roadway current or frequency. In addition to determining the roadway excitation, many **onboard** features must be specified, including the inductor geometry, number of pickup turns, and **onboard** capacitor and inductor values. There are very strong, non-linear interactions among these parameters, making this task challenging and time consuming.

### 2.4.1 Goals

The primary goal of the inductive coupling system is to transfer energy across the **airgap** between the roadway and pickup inductors, so meeting the target output current is of primary importance. Minimizing cost (primarily capital cost) is the second most important objective, although it is often difficult to translate changes in the system parameters into hardware costs, especially for a technology in its infancy. Several other factors are also important, such as minimizing **onboard** weight and volume, achieving acceptable environmental impacts (primarily acoustic noise and the magnitude of stray magnetic fields), and achieving a high system efficiency.

### 2.4.2 Trade-off Issues

Many goals compete with each other. For instance, system efficiency can be driven close to 100% by selecting grossly oversized components that have very low losses at the design operating point. This choice would be very expensive as well as increase **onboard** weight and volume.

There are trade-offs between wayside and **onboard** equipment, with some operating points reducing component sizes in one location while increasing those in the other. One such trade-off involves the sizing of the **onboard** isolation inductor. A larger

inductor increases the power coupled to the vehicle for a given roadway current and frequency or conversely lowers the roadway current required to deliver a specified output current but at the price of driving the pickup voltage considerably higher than the battery voltage. The magnetic flux levels in the coupled cores must increase to induce a higher voltage in the pickup, which causes the coupled core losses and acoustic noise to increase. There are also higher **onboard** currents (pickup and **onboard** capacitor), causing additional losses unless the size, weight, and cost of these components are increased. In this particular case, the value of this inductance was lowered from the Phase 3C baseline during Phase 3D, primarily to reduce acoustic noise, but at the price of increased roadway current.

Numerous trade-offs among various system parameters are shown in Table 2.1. It is clear from this table how complicated the interactions are among the numerous system variables. At lower frequencies, the maximum output current increases with frequency. In this regime either the frequency or roadway current must be increased to get increased output current (or voltage). At higher frequencies, the maximum output current is independent of frequency, with other variables such as number of pickup turns held constant. The location of the breakpoint or knee in the curve between the low frequency and high frequency regimes is a complicated function of many variables, including number of pickup turns, mutual inductance, output voltage, and roadway current. This issue is investigated in greater depth in the Parametric Studies chapters.

#### 2.4.3 Baseline

The baseline operating point was thoroughly examined during the early portion of Phase 3D. Before construction of the test track, very high confidence had to be established that the operating point selected would adequately fulfill the project's objectives of demonstrating that an inductive coupling system could transfer high power levels across an **airgap** of several inches to a vehicle operating at normal road speeds and at a cost that would be competitive with alternative technologies.

During Phase 3C, static power transfer had been demonstrated at Translab with an output current of approximately 400 amps at 150 volts. That first-generation hardware operated at 400 Hz with 1200 amps in the roadway. Acoustic noise in the **onboard** equipment (pickup and **onboard** controller) was objectionable, but the electrical performance of the system was acceptable. Efficiencies across the **airgap** of more than 90% were recorded with an IS-foot static charger. Several changes were

Table 2.1  
**Operating Point Trade-offs**

Independent System Variable	Variables that Increase (Positive Correlation)	Variables that Decrease (Negative Correlation)
Frequency	Open roadway losses (especially at higher frequencies)	<b>Airgap</b> flux <b>Onboard</b> capacitance <b>Onboard</b> currents (pickup and capacitor) Roadway current (lower frequencies)
Mutual inductance (poleface area divided by <b>airgap</b> height)	System efficiency	<b>Onboard</b> Capacitance <b>Onboard</b> currents
Number of pickup turns	Roadway current Open roadway losses	On board capacitance <b>Onboard</b> currents Coupled core losses <b>Airgap</b> flux Acoustic noise
<b>Onboard</b> isolation inductance	Pickup voltage On board currents Coupled core losses <b>Airgap</b> flux Acoustic noise	Roadway current
<b>Onboard</b> DC voltage	Pickup voltage <b>Onboard</b> currents Coupled core losses Roadway current (lower frequencies) <b>Airgap</b> flux	
Leakage inductance	Roadway current	System efficiency

made to the baseline operating point in Phase 3D, although the more radical changes considered were not implemented.

Reduction of the roadway current was considered to be desirable, primarily to keep open roadway losses as low as possible. Reductions in roadway current also reduce magnetic fields above the open roadway and any adverse environmental impacts associated with them. Two avenues were available to reduce the roadway current. The more radical involves reducing the number of pickup turns from two to one, which would reduce the roadway current by nearly a factor of two and would require a quadrupling of the amount of **onboard** capacitance. The increase in **onboard** capacitance could be at least partially offset by increasing the operating frequency. This approach was not practical since the second-generation **onboard** controller to be used in Phase 3D had already been fabricated in the closing months of Phase 3C and the capacitors in it would not work for such a large change in operating point. The power conditioner, which was retained in Phase 3D, cannot supply the rated ICS output current at substantially reduced roadway currents. The power supply conditioner is also incapable of operating at frequencies much above 400 Hz.

The second change in baseline operating point involved use of a relatively large isolation inductor within the **onboard** controller. Tests at Translab demonstrated that an output current of 400 plus amps was possible with two pickup turns and approximately 1000 amps in the roadway with a large value of isolation inductance. Increasing the isolation inductance increased the pickup voltage approximately 50% from 175 to 250 volts and resulted in increased **onboard** currents, **airgap** magnetic flux, and acoustic noise. The second-generation pickup and **onboard** controller were thought to be able to handle these higher values acceptably, but the power conditioner could not. It runs up against an internal limit (turn-off time in the inverter solid-state devices) and cannot supply the ICS rated output current at roadway currents below 1200 amps. The trick (of running a second coil in parallel with the roadway inductor to get the power conditioner current up to 1200 amps with only 1000 amps in the roadway) that was used at Translab to overcome this problem is not practical at the Richmond Field Station because of the full-length roadway segment. When we decided not to purchase a new power conditioner, the opportunity of reducing the roadway current from 1200 amps to 1000 amps was lost.

One change that was made in Phase 3D involved the roadway and pickup inductors. The roadway inductor cores in Phase 3C were asymmetric to provide better energy transfer with the vehicle at lateral offsets of 2 – 6 inches. With the steering assistance system assumed in Phase 3D, lateral offsets of the vehicle relative to roadway

centerline were presumed to be very small nearly all the time. The roadway core was made symmetric, resulting in a higher but narrower power curve versus lateral offset. The width of both the roadway and pickup cores was increased. The length of the pickup was also increased. These changes increased the mutual inductance between the roadway and pickup by approximately one-third for the Phase 3D hardware compared to 3C designs. The increase from 12 to 16 microhenries decreased the required onboard capacitance and onboard currents.

#### 2.4.4 Sensitivity Analysis

The sensitivity analysis in this section is more quantitative than the trade-offs involved in the selection of the baseline operating point. Plots of specific trade-offs are presented that are typical of the analyses performed. Many of the curves are plotted as a function of frequency, as nearly all system variables change as a function of frequency.

The first sensitivity analyzed is the dependence of the roadway current required to couple a specified current (500 amps) into the bus as a function of the number of pickup turns. This is examined for frequencies from 180 Hz to 1000 Hz, the most common range used during these sensitivity analyses. Figure 2.8 presents these results. The roadway current required to induce 500 amps output current varies proportionately with the number of turns, but is independent of frequency. In the upper frequency range (all data shown), where output current does not vary with frequency, the output current is generally slightly less than the roadway current (amp-turns if there are multiple roadway turns) divided by the number of pickup turns. (The roadway current divided by the number of pickup turns is 540 amps, 585 amps, and 625 amps for three, two, and one pickup turns, respectively.) This is exactly analogous to a conventional transformer, where the output current equals the input current divided by the turns ratio. The fact that the output current is slightly lower than given by the standard transformer equation is due to the leakage inductance in the ICS. While leakage is negligible in a standard transformer, in the ICS it often reduces the output current by 10 – 20% compared to the theoretical input current divided by the turns ratio. At lower frequencies, the output current is much lower than the standard transformer formula values.

In addition to investigating the roadway current as a function of the number of turns and the frequency, examination of the magnetizing current provides several insights. Airgap flux is proportional to the magnetizing current. Pickup voltage per

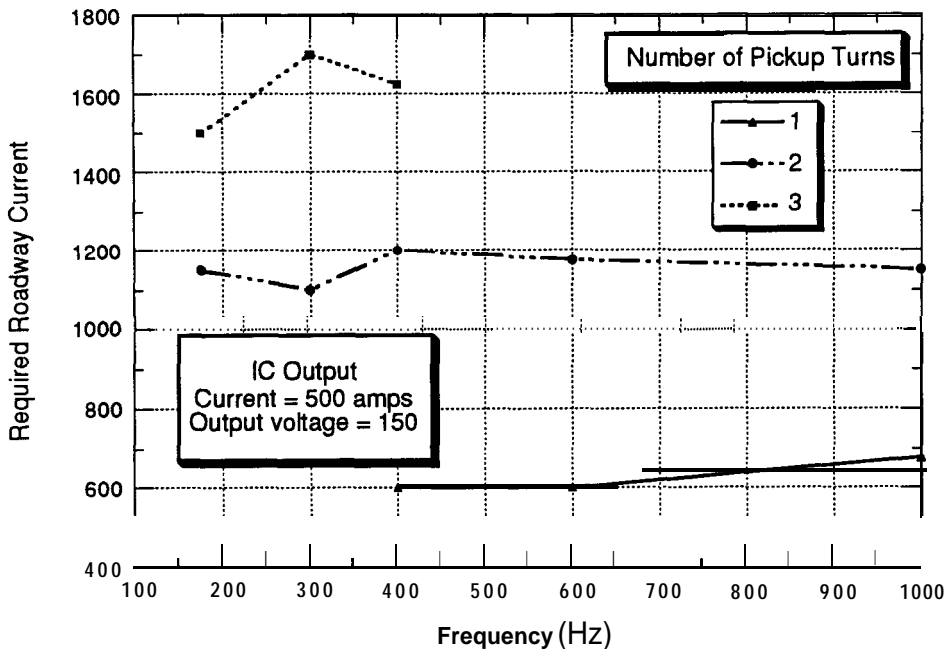


Figure 2.8 Roadway current for a constant output as a function of frequency for one, two, and three pickup turns

turn is proportional to the time rate of change of the magnetic flux. Since the (overall) pickup voltage is approximately constant (especially if a small value is chosen for the isolation inductor), one expects the product of magnetizing current, frequency, and number of pickup turns to be approximately constant. In Figure 2.9 at 400 Hz and two turns the magnetizing current is 2500 amps. With one turn, the magnetizing current is approximately doubled, while for three turns it is approximately one-third less at 1700 amps. Similarly, doubling the frequency from 400 to 800 Hz cuts the magnetizing current from 2500 to 1250 amps.

This data is replotted in Figure 2.10 with log scales on both axes. The data plot as parallel straight lines. When the line for two turns is extended (dotted line), it goes through 10,000 amps magnetizing current at 100 Hz, a factor of ten higher in magnetizing current and a factor of ten lower in frequency than the point at the lower right corner, demonstrating that the product of these two variables is a constant along any line.

As the key system parameters are varied, certain factors become dominant. There are many losses in the system and each will vary as the operating point is shifted to a

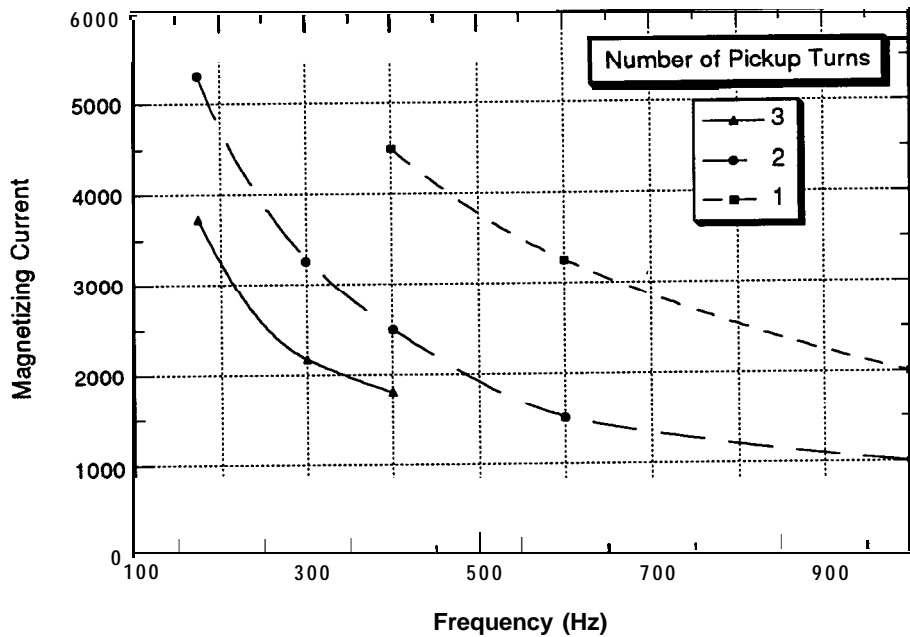


Figure 2.9 Magnetizing current as a function of frequency for one, two, and three pickup turns

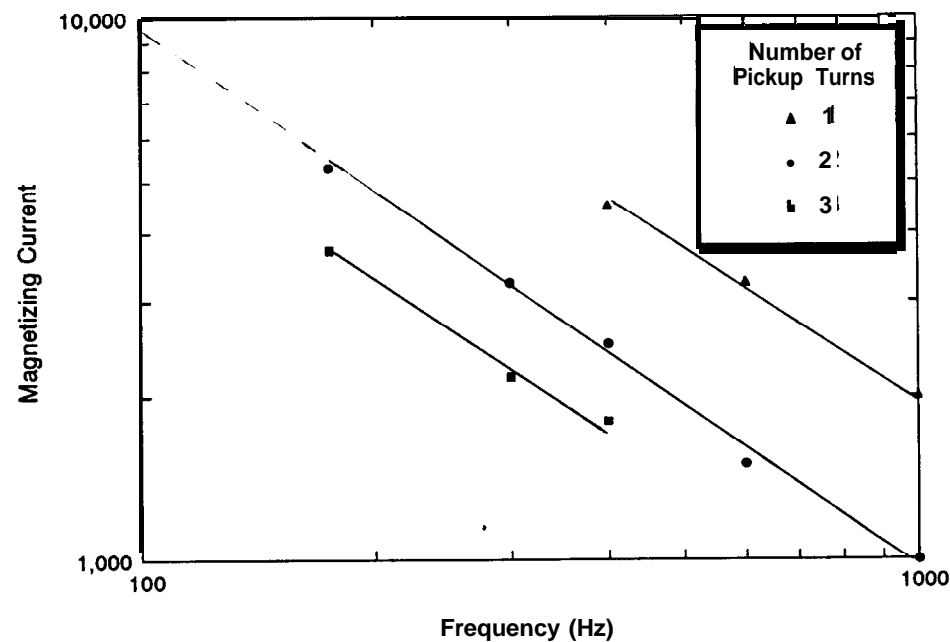


Figure 2.10 Log-log plot of Figure 2.9

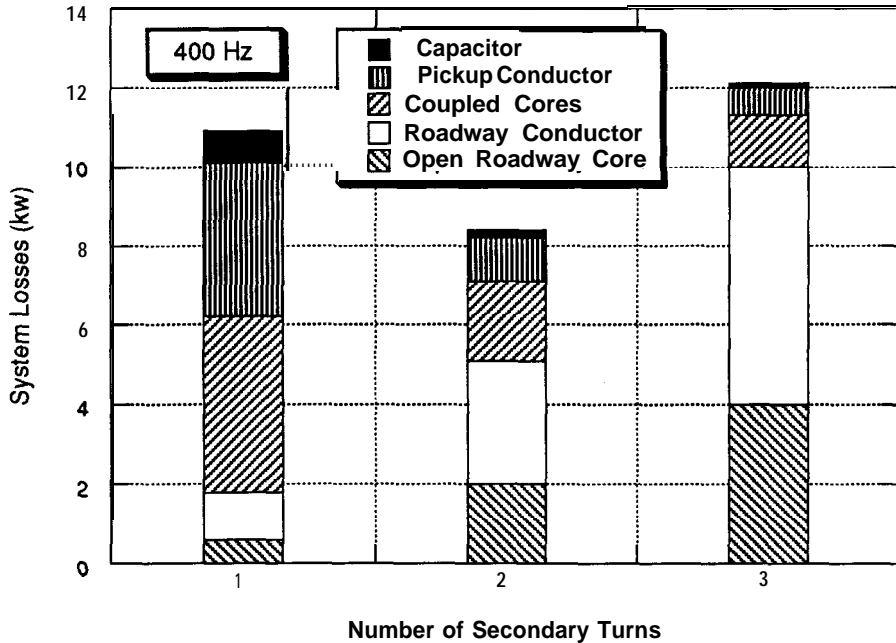


Figure 2.11 Losses as a function of number of secondary turns

new combination of roadway current, frequency, and number of pickup turns. Figure 2.11 shows the calculated values of the various loss terms for the baseline hardware design with one, two, and three pickup turns. The hardware was designed for 400 Hz, two pickup turns, and 1200 amps in the roadway. With one pickup turn, the roadway current is reduced by approximately a factor of two. Open roadway core losses and roadway conductor losses show a corresponding drop. The core losses presented are the theoretical losses and one would expect the actual losses to be higher by a factor of two. The other loss components (primarily **onboard** equipment), show corresponding increases (with a one-turn design), as the flux levels in the coupled cores and **onboard** currents increase very sharply. With three turns, the **onboard** component terms become very small (about two kilowatts), but the roadway terms grow very large. This indicates that at 400 Hz, with **this particular hardware design**, total system losses are minimized with two pickup turns. If three turns were selected for the baseline operating point, the hardware designs would be modified; for instance the cross sectional area of the roadway conductors would be increased, while **onboard** components could be reduced in size.

Figure 2.12 is analogous to Figure 2.11 except that now the number of turns is held constant and the frequency is varied. Roadway current is approximately constant

regardless of frequency; however, the core losses vary with both frequency and amplitude of excitation—thus open roadway core losses increase very dramatically with frequency. The roadway conductor losses are nearly constant, showing a slight increase toward the right side of the plot due to increased skin effect at higher frequencies. The coupled core losses are also approximately constant as well. At the higher frequencies, the magnetic flux density is lower, but the loss per pound at a given flux density is higher. These two effects are approximately equal and opposite—giving little net change with frequency. At the lower frequencies, the

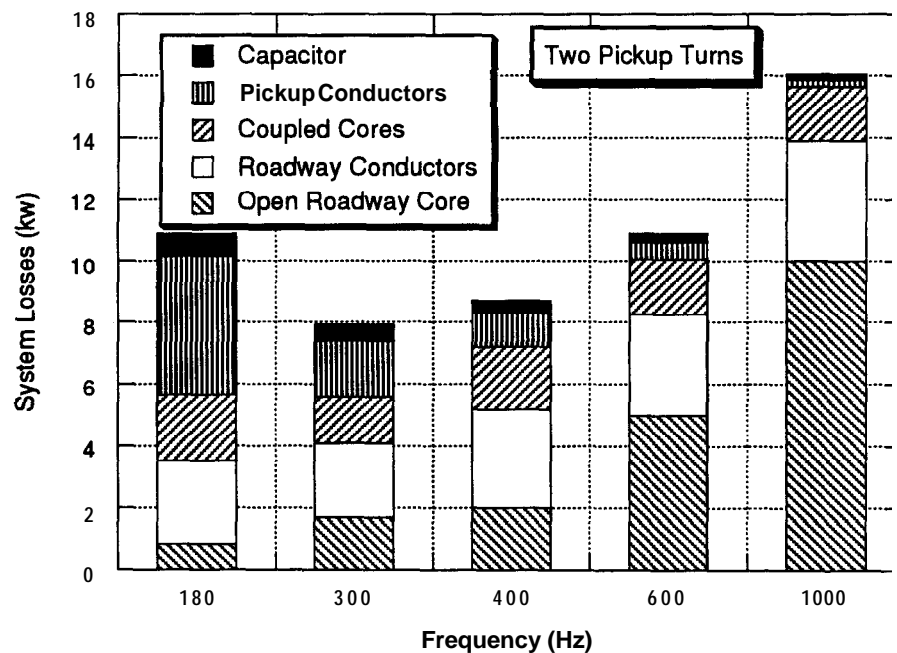


Figure 2.12 System losses as a function of frequency

pickup and capacitor currents are much larger and their losses increase accordingly. Total losses increase if the operating frequency is too low or too high. Figure 2.12 indicates that the minimum losses actually occur at 300 Hz, although the 400 Hz losses are nearly as low.

One might conclude from Figures 2.11 and 2.12 that two turns and 300 – 400 Hz is the best operating point. This is a reasonable, but incorrect, conclusion. Due to the non-linear multi-dimensional nature of the problem, optimizing on one variable at a time does not yield the optimal solution. Figure 2.13 presents contours of some

objective function that must be maximized to find the optimal solution. The curves in Figure 2.13 have the proper shape, but represent an arbitrary guess about actual values of this “yet-to-be-defined” objective function. Specifying this function is presently impossible. A value of 1.0 was chosen for the baseline operating point. Scanning horizontally at two turns, the objective function is maximized in the range of 300 ~ 400 Hz. Similarly, taking a vertical slice at 400 Hz reveals that two turns is the best number of turns. These two conclusions are those reached from Figures 2.11

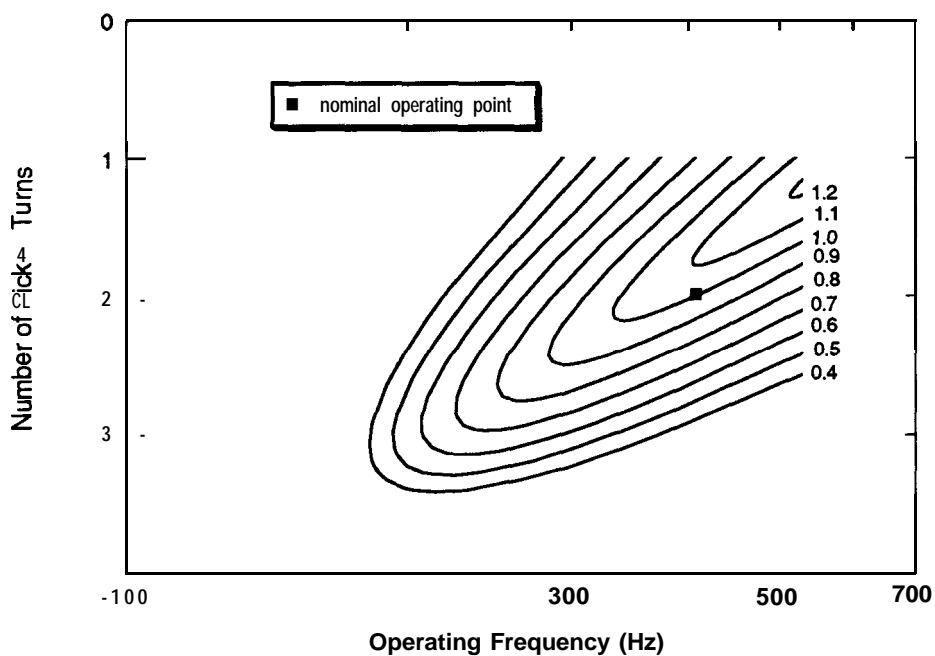


Figure 2.13 Hypothetical objective function for “optimizing” ICS design

and 2.12. Looking at Figure 2.13, it is obvious that by increasing the frequency and decreasing the number of pickup turns to one, a better solution can be found. This figure illustrates the complexities involved in the selection of an operating point, even when many of the parameters, such as output current and voltage, are specified.

## 2.5 Inductor Design

Because of the possibility for high power losses (and high costs), the pickup and roadway inductors had to be carefully engineered. The original designs from the Caltrans Short Test Facility had many drawbacks, and new approaches to the fabrication of these items were developed. The conductors as well as cores had to be studied and costs versus losses considered. Losses in both the cores and conductors are tied to the operating frequency so frequency had to be investigated at **the same** time. Because of the many trade-offs inherent in a system such as **this**, there were **no** clear-cut answers, and we depended on our engineering judgment for **many** of the decisions about final configuration.

### 2.5.1 Core Geometry

In transferring power across **an airgap** through a magnetic field, the pole face area of the gap should be as large as possible. This requires roadway and pickup cores with an unusual geometry-able to provide the large pole face area without using an undue amount of material or exceeding the envelope for the pickup **onboard** the bus. Several different arrangements that provide the desired characteristics can be envisioned. Figure 2.14 shows four possible configurations. While all the geometries shown would work magnetically, practical considerations make some of them infeasible.

After talking with several core manufacturers, the III and IV constructions were chosen as the best compromise for our purposes. The III configuration is made up of two easily fabricated pieces made the same way as conventional transformer cores. The IV configuration is unusual but, by working closely with a transformer core manufacturer, we were able to develop a manufacturing technique that allows fairly easy production of this type of core. The process is **labor** intensive for low production levels, but **has** strong possibilities for automation and cost reduction at moderate to high production volumes.

### 2.5.2 Core Design

Even after running a POISSON simulation, we could not be certain how well a given design would actually work as this code provides information about magnetic flux levels and mutual and leakage inductances, but not core losses. With this uncertainty in mind, we decided to have different sample cores fabricated, which

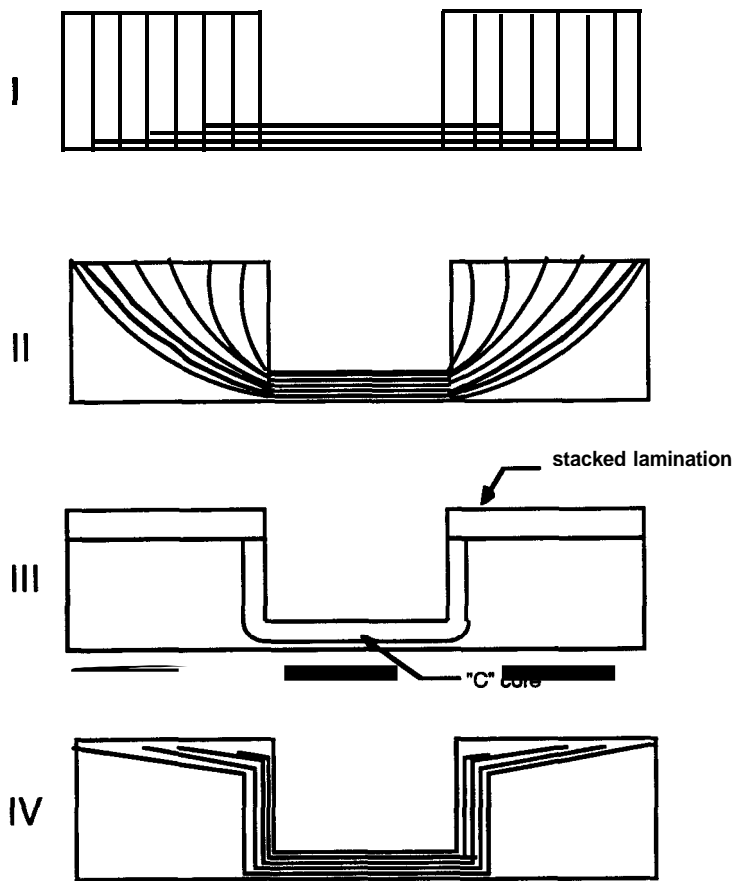


Figure 2.14 Roadway core lamination geometries

allowed us to test several different core designs and helped greatly in developing a core that we had high confidence would work. Several possible core designs were developed using our loss calculations and the POISSON results. These designs all used the three-piece structure because it uses almost the minimum amount of material and is simple to assemble (and expected to be the most cost effective). The designs varied in the type, orientation, and amount of steel used. Chapter 5 discusses the results of testing these cores.

One of the major changes made while studying the inductor design was to widen the pickup to the maximum width that fits under the bus (39 inches) and to make the roadway core an inch wider. This was a big change from the first core designs in which the roadway had asymmetric poles and a total width of 37 inches and the pickup was 32 inches wide. The reason behind these changes was two-fold: first, we assumed that we would use a steering assistance system that would reduce the requirement for off-center power transfer and, second, we wanted to increase the

pole face area as much as possible to improve mutual inductance and so improve system performance. The result is a system with better power transfer capability when centered but with a quicker drop off in power transfer as it is moved off-center.

### 2.53 Conductor Selection

Because of large currents in both the pickup and roadway inductors, losses in the conductors of these components are significant. This situation is exacerbated by the fact that conductors are not as efficient (have a higher effective resistivity) at higher frequencies. Conductor losses are easier to calculate than core losses but do require correction for frequency. Greater resistivity at higher frequency is caused by “skin effect” or the tendency of current to flow near the conductor’s surface at higher frequency. This effect is fairly well understood and tables to find the correction factors are available. Because of skin effect, a larger number of small conductors is better than a small number of large conductors. Since conductor losses are a significant part of overall system losses, the roadway conductors were sized based on total losses rather than on the rated current-carrying capacity of the conductors. In the **Phase 3C** design tested at Translab, the **majority** of the roadway cost was in the cores, while a majority of the losses occurred in the conductors. The conductor cross section area was approximately doubled from **Phase 3C** to **3D**, cutting the roadway conductor losses by a factor of two, while increasing costs 5 – 10%.

Aluminum was chosen as the conductor material for both the pickup and roadway, which made sense for two reasons: aluminum is less expensive than copper of **the** same resistivity and aluminum is lighter than the equivalent copper. Low cost drove the roadway conductor decision, and light weight was of prime importance for the pickup.

Stranded aluminum cable and  $\frac{1}{4} \times 1\frac{1}{2}$ inch solid aluminum **busbar** were used for **the** roadway conductors. In the west roadway segment, the 350 MCM\* aluminum cable was used, and in the east segment  $\frac{1}{4} \times 1\frac{1}{2}$ -inch **busbars** were used. Fifteen cables in a 3 high by 5 wide array were placed in the west segment, and 12 **busbars** in a 4 high by 3 wide array were placed in the east segments. In each design, approximately  $\frac{1}{4}$  inch was left between the conductors. The **busbar** arrangement is

---

\* MCM stands for 1000's of circular **mils**—the area of a circle .001 inch in diameter. This measurement for electrical wire size is generally used when wire gets above 0000 or 4/0. In the AWG (American Wire Gauge) system, 4/0 is approximately 212 MCM.)

more compact than the cable layout, and if this design were chosen, the roadway slot could be made shallower. The losses of the two designs are similar, with the final choice being based on mechanical, not electrical, considerations.

## 2.6 System Efficiency

Efficiency of the RPEV system is very important as the technology is not very attractive if a large portion of the energy drawn from the utility grid ends up as losses. Determining the system efficiency is not a simple problem (especially before the system is built) and involves many parameters. We looked at the following losses when trying to determine the efficiency:

- pickup and roadway cores
- pickup and roadway conductors
- **onboard** control components
- battery
- the power distribution system

Since most of the losses occur in the AC portion of the circuit, losses are tied to the power frequency and change as the frequency changes. Trade-offs concerning many of these loss terms were examined in Section 2.4.4. That analysis showed how the loss terms vary with frequency and number of pickup turns. In this section, we examine system losses and efficiency at the baseline operating point in greater detail.

### 2.6.1 Core Losses

Tables and graphs are available from the producers of electrical grade steels to analytically determine power losses in laminated transformer cores. (See Figure 2.2.a and 2.2.b for an example.) These graphs show power loss per pound of steel versus flux level and excitation frequency for each material type; however, the tables are only accurate for the idealized test case, which is not a realistic situation. Because of the limitations of published loss information, a correction factor of two is usually used to make the loss estimate as realistic as possible.

The relationship among losses, magnetic flux, and frequency is approximately

$$\text{loss} \propto (\text{frequency})^{1.6} * (\text{flux density})^{1.9}$$

Again, real-life considerations render this equation less than accurate and the exponents do vary, both with material type and with operating point. It is useful, however, because it shows that flux level has a greater impact on the losses than the frequency. This is consistent with test results that indicate that for a constant output voltage (constant product of flux and frequency) core losses decrease as the operating frequency is raised.

Specification of the pickup **cores** is easier than the roadway cores as only the coupled condition needs to be considered. When the pickup voltage (generally slightly higher than the battery voltage), number of pickup turns, and length of pickup are determined, the volts per foot of pickup are specified. Dividing volts by the frequency yields the total flux in the cores. Use of a thinner core reduces weight, but increases flux density and losses (both per pound and total losses). The losses can be reduced by selection of a higher grade of material (thinner laminations or alternate chemical composition). Core losses for both roadway and pickup inductors are presented in Table 2.2 for various' material types and core builds (thicknesses). All materials listed are grain-oriented silicon steels, with the principal difference between them being the lamination thickness. The four righthand columns deal with pickup cores. The "thick" pickup cores (0.51-inch steel thickness) have lower flux density than the thin cores (700 vs. 1000 gauss).

The product of thickness and flux density is constant as both designs carry the same total flux and induce the same voltage in the pickup winding. As one goes down the table to the thinner laminations, the losses are reduced. The losses are nearly halved as one goes from M6 (0.014-inch) to M2 (0.007-inch). The losses per pound go up nearly 70% as the core build is reduced from 0.51-inch to 0.38-inch. Since there are fewer pounds of core in the "thin" design, the total pickup core losses only go up about 25%. The design chosen for construction uses M2 steel and the thick build (0.51 inches of steel, about 0.53 inches overall). Thinner laminations cost more than the thicker ones and this was to be factored into the design as well.

The roadway specification is more difficult, as both open roadway and coupled losses must be considered. In addition, a three-piece design was selected, providing the option of using different material types in the C-cores and pole pieces. (See Chapter 4 for a more detailed discussion of the roadway module design.) Table 2.2 presents losses for the C-cores used in the roadway while operating in the uncoupled condition. The voltage per foot is about 2.0 versus 6.0 when coupling power to the vehicle. With a 0.51-inch build, the flux density drops from 3000 gauss to 1000 gauss.

Table 2.2  
Core Losses

Lamination		Roadway C-Cores-Open Roadway Losses				Tapered Pickup Cores-Coupled Losses			
	Thickness	Thick (0.73 Inch)		Thin (0.51 inch)		Thick (0.51 Inch)		Thin (0.38 inch)	
Material	(inches)	Watts/ pound	Watts/ foot	Watts/ pound	Watts/ foot	Watts/ pound	Watts/ foot	Watts/ pound	Watts/ foot
M6	0.014	0.05"	3.1	0.08*	3.3	0.60	30.6	0.96	43.2
M4	0.011	0.035*	2.2	0.065'	2.7	0.47	28.2	0.80	36.0
M3	0.009	0.030"	1.9	0.060*	2.5	0.38	22.8	0.62	27.9
M2	0.007	0.025*	1.6	0.040'	1.7	0.33	19.8	0.58	26.1

Thick Roadway C-cores	0.73-inch build	700 gauss	62.8 pounds/foot of roadway (C-core only)
Thin Roadway C-cores	0.51 -inch build	1000 gauss	41.4 pounds/foot of roadway (C-core only)
Thick Pickup Cores	0.51 -inch build	3000 gauss	60 pounds/foot of pickup
Thin Pickup Cores	0.38-inch build	4000 gauss	45 pounds/foot of pickup

\* Extrapolated value

Note that this build is considered thick for the pickup cores, where weight is an important consideration, but thin for the roadway. The losses per pound drop by nearly an order of magnitude for every material type as the flux density is reduced from 3000 to 1000 gauss. The reduction in (uncoupled) roadway core losses from M6 to M2 is very similar to that displayed by the pickup cores. As with the pickup **cores**, the same losses can be achieved by a large build of a thicker material or a smaller build of thinner laminations.

The cost of the roadway cores represents a major fraction of the entire life cycle cost of the RPEV system. Initial quotes for the roadway cores were considerably higher than budgeted, resulting in a very strong desire to reduce core costs as much as possible. This biased the design toward the thinner build and the less expensive M6 material. The production roadway core modules were specified with 0.50-inch build, using M5 (0.012-inch) material for the C-cores and M6 for the pole pieces. Tests of prototype cores indicated that this combination would perform acceptably, although the losses are higher than they would be with a better grade of material or a thicker build.

#### 2.6.2 Roadway Conductor losses

When the final configuration of the test track was determined and the length of the roadway conductors was known, it was relatively easy to calculate the expected conductor losses. Losses were calculated separately for the two types of conductor used in the roadway. The configuration of the **busbar** conductors was determined very quickly, and at the time we thought these would be the preferred conductors. For 500 feet of **busbar**, the losses are 2000 watts. Since we wanted to make one size roadway core for the two types of conductors, the choice of the aluminum cable was driven by the amount of conductor that would fit in the core slot size required for the **busbars** (5.5 x 2 inches). We decided, however, that the slot could be made deeper (3.25 inches) without compromising the **busbar** design, which would allow more cables to be used. Table 2.3 shows the results of loss calculations for many different conductor configurations. The cost figures are for comparison only and are based on the cost of conductors at the time. Because the costs were all fairly close, the final decision was based on losses and ease of installation. A conductor installation like this had never been done before so we exercised our judgment and came to two conclusions: fewer conductors are easier to install and conductors larger than 350 MCM would be difficult to work with as well as suffer large skin effect losses. With this in mind, the choices were quickly narrowed to Designs 16, 18 and 19. Design 16

**Table 2.3**  
Conductor Losses

Design Number	Aluminum Conductor	$R_{ac}$ 400 Hz $\Omega/500$ ft	Skin Effect $R_{ac}/R_{dc}$ at 400Hz	$P_{loss}$ in 500 ft at 400 Hz, 1000A	Conductor Array			Total Conductor Area (sq in)	$\$/500$ feet of conductor array
					Wide	High	Number		
1	#2	0.1613	1.01	2988	9	6	54	3.62	4725
2				2688	10	6	60	4.02	5250
3	#1	0.1280	1.01	4571	7	4	28	2.44	3500
4				4000	8	4	32	2.78	4000
5				3200	8	5	40	3.48	5000
6	1/0,	0.1020	1.015	3643	7	4	28	3.05	4004
7				3187	8	4	32	3.49	4576
8				2550	8	5	40	4.36	5720
9	2/0	0.0819	1.03	3412	6	4	24	3.31	4008
10				2925	7	4	28	3.86	4676
11				2340	7	5	35	4.83	5845
12	3/0	0.0660	1.04	3667	6	3	18	3.11	3618
13				2750	6	4	24	4.15	4824
14				2357	4	7	28	4.84	5628

Table 2.3, Continued

Design Number	Aluminum Conductor	$R_{ac}$ 400 Hz $\Omega/500$ ft	Skin Effect $R_{ac}/P_{dc}$ at 400Hz	$P_{loss}$ in 500 ft at 400 Hz, 1000A	Conductor Array			Total Conductor Area (sq in)	\$/500 feet of conductor array
					Wide	High	Number		
15	4/0	0.0530	1.06	2944	5	3	15	3.29	4212
16				2208	6	4	24	5.26	5616
17	250 MCM	0.0454	1.07	3028	5	3	15	3.90	4170
18	350 MCM	0.0345	1.14	2876	4	3	12	4.37	4722
19				2301	5	3	15	5.46	5902
20	500 MCM	0.0276	1.24	3450	4	2	8	4.15	4020
21				2300	4	3	12	6.23	6030
22	750 MCM	0.0202	1.43	3372	3	2	6	4.69	4410
23				2529	4	2	8	6.26	5880
24	1,000 MCM	0.0173	1.64	2893	3	2	6	6.24	6375
busbar design	1/4 x 1 1/2 busbar	0.0238	1.25	1985	3	4	12	4.50	4721

has the most cables of the three but the lowest losses, Design 19 has the fewest number of cables but higher losses. Eventually, we chose Design 18 which while it did not have the fewest cables or the lowest losses (or even the lowest price) seemed to be the best compromise and was also most compatible with the geometry requirements of the bus bar design.

#### 2.6.3 **Onboard** Controller and Pickup Winding losses

The onboard control equipment consists of a switched capacitor bank in series with inductors. The switches, capacitors, and inductors are the biggest loss components in the OBC. The power lost in the switch is relatively easy to calculate as it equals the voltage drop across the solid-state switch times the current through the switch. The capacitors and inductors are more complicated. As explained in greater detail in Chapter 5 (Testing), the inductors originally used in the OBC created many problems, including excessive acoustic noise and losses. When these were replaced, the losses of the new inductors were specified (at their rated operating point). They are on the order of several hundred watts per inductor, resulting in less than a kilowatt (or about 1%) loss for all inductors combined. The capacitor losses are also very low. While they become significant in designs in which the capacitor current and pickup current become very large (as is the case in very low frequency designs), they are not a major source of losses in the baseline design (less than 1 kw).

We considered three OBC configurations in detail. The first was the original type OBC that was used at the Caltrans Short Test Facility and was the scheme (with some modifications) eventually chosen for implementation. Two other ideas were seriously considered: one required a two-winding pickup with a different number of windings for the power and control circuits of the OBC, which would allow a higher voltage, lower current control circuit. The control winding would have more turns than the power winding. A lower current control circuit would presumably have lower losses and smaller, less expensive components than a control circuit designed to operate on the power winding. The other control circuit required a center tap arrangement on the pickup windings with the power being tapped out at a lower voltage than the control circuit. This arrangement gives essentially the same benefits as the two winding case but may make the pickup simpler to fabricate and reduce pickup conductor losses.

The conductors in the pickup are  $\frac{1}{4} \times 1\frac{1}{2}$  aluminum bars, identical to the conductors in the east roadway segment. Twelve conductors are used, as in the roadway. The

current density in the pickup busbars is considerably higher than in the roadway. Total losses are not excessive, due to the relatively short length of the pickup.

The one major modification made to the OBC circuit as compared with the original design was to change the capacitance step sizes from five equal steps to five uneven steps. This change produced a much more even control of the power and was fairly simple to implement. Five steps of 150, 150, 300, 383, and 766  $\mu\text{F}$  were chosen to give increments of 83  $\mu\text{F}$  or 67  $\mu\text{F}$  between adjacent control states between 0 and 1749  $\mu\text{F}$ . These five steps provided much smoother control than the five equal steps as discussed in greater detail in Chapter 5 (Table 5.3).

#### 2.6.4 Power Distribution System losses

The losses in the power distribution system are composed of the power conditioner losses and the losses in the conductors that carry the current to the roadway segments (“transmission line”). An estimate of the power conditioner losses was made based on the efficiency specification of the equipment (approximately 96% at its full rated output) In our loss calculations, we assumed the loss would be about 5% of the power output of the device.

When calculating the transmission line losses, we had to consider both the skin effect and the effect of the inductance of the lines caused by the separation of the power and return conductors. Because of the physical configuration of the transmission line conductors, we decided that the inductance effect could be ignored. Four-plex (4 conductors under one jacket) 4/0 copper wire was used as the transmission line with two of the conductors for power and two for return. The inductance was effectively neutralized by this intermixing of the conductors and the natural spiral of the four-conductor cable. Four 4-plex cables were used to carry the power to the roadway segments, which is significantly less conductor than would have been required if the inductance had been a factor. The losses in the transmission line were calculated to be 3.7 kilowatts. These losses were higher than desired but the transmission line selection was based on cost as well as losses and we initially had hoped to be able to use parallel compensation capacitance at the roadway end of the line, which would have reduced the transmission line current to about 400 amps and reduced the transmission line losses by a factor of 9.

### 2.6.5 System losses

The losses for the RPEV system installed at the Richmond Field Station were calculated based on theoretical losses before any components were fabricated. As prototype components became available they were tested for losses and the design changed if the losses were too high. This was especially true of the roadway and pickup cores. After the system was built, we tested for efficiency to see how close the actual system was to our predicted results.

Table 2.4 shows the four sets of losses and that the actual losses are somewhat higher than predicted. The first column presents calculated (or book) losses for the various components. For many components, such as roadway conductor losses, these values are used in all columns, as no corrections are necessary and no test could be performed to accurately measure these terms individually. Expected losses (second column) includes items such as doubling the published core loss numbers. Preliminary results, based on component tests, are presented in the third column. The actual results (fourth columns), based on system tests, involve some manipulation of various test measurements. The total losses, 32.8 kilowatts, are accurate, although individual component values are subject to much larger uncertainty. When the power conditioner losses (about 5 kilowatts at full rated power) are added to the last column, the total system losses are 38 kilowatts, with 60 kilowatts delivered onboard the vehicle. This yields an efficiency just over 60% for the existing hardware. (Test results for the next generation hardware indicate efficiencies will be over 70%. See Chapter 6.)

The core results (both coupled and uncoupled) show considerable growth from the “expected” to “actual” values. Unfortunately, these losses are the most difficult to measure, especially the uncoupled losses. Some of these losses may be due to measurement errors (and properly belong in other rows, such as conductor or OBC losses). Nevertheless, core losses are the largest loss terms, and in future design special efforts must be made to reduce these losses if system efficiency is to increase into the high 70s.

### 2.7 Test Facility Layout

The design of the test facility at the Richmond Field Station required specification of the bus stop locations and the length of each section of powered roadway. A section is defined as several contiguous inductor modules without any transposition of

**Table 2.4**  
**Total System Losses**

---

conductor locations. At the Richmond Field Station, the sections consist of two to twelve modules. Vaults are located between sections, thereby allowing for transposition of the conductors. Many sections are wired together to form a segment. Since all sections in a segment are wired together, they act as a single unit for switching purposes (i.e., segment switching).

The transposition of conductors must be done properly to ensure that the currents flowing in the parallel conductor paths are approximately equal. Transposition schemes could not be verified experimentally before construction of the facility, which imposed a requirement that analysis be used to generate a high degree of confidence that a successful crisscross (transposition) design could be implemented within the various sections of the two segments at Richmond.

There are two segments in the test track, one with cables and one with **busbar** conductors. The maximum length in which **busbars** are readily available is 40 feet. This resulted in 12 sections within the **busbar** segment. With this many sections, there are many possible transposition locations, and one can be virtually guaranteed of finding an acceptable criss-cross pattern. In the cable segment, there are no significant limitations on section length, and longer sections require fewer terminations, reducing cost and increasing reliability.

In the layout of the Richmond Field Station test track, the number of sections into which the cable segment should be split became an area of concern. The segment was to consist of a main roadway approximately 200 feet long and a bus stop, approximately 20 feet long. This layout dictated a minimum of four sections, two 200 feet long (one for each side of the roadway inductor) and two 20 feet long.

Various transposition patterns were analyzed for this configuration. We soon concluded that no acceptable transposition scheme could be developed for sections of these lengths and decided to split the 200-foot section into two sections. Analysis of transposition schemes revealed that splitting the 200-foot section into two sections of lengths 120 feet and 80 feet would allow effective transposition. We decided to attempt symmetric criss-crosses between both sides of the bus stop and both sides of the 80-foot section. This resulted, in effect, in four sections of lengths 120 feet, 40 feet (both sides of the bus stop), 160 feet (both sides of the 80 foot length of track) and 120 feet. A transposition scheme for this layout was determined analytically, and as presented in Chapter 5, it worked very well.

## 2.8 Conclusions

The design of an RPEV system is a very challenging problem. At this point in the development of the technology, there is virtually no hope of finding an “optimal” solution (or even the proper objective function to be optimized), although clearly acceptable or even very good designs can be formulated. The technology is still far from the “cookbook” stage where one defines the inputs, turns the crank, and the solution appears; however, rules of thumb are slowly evolving and our understanding of the technology has advanced significantly during this project. The technical aspects of the RPEV system are no longer the largest unknown relative to implementation of this technology. Economic and institutional issues and uncertainties are at least as important as the technical ones.

## **3. Vehicle**

---

Work relating to the vehicle is described in this chapter. The first two sections are the most important, describing the pickup and **onboard controller**, respectively. The third section discusses the steering assistance system, and the fourth describes other vehicle work, such as the motor controller upgrade, and battery ventilation system modifications. The work described in this chapter includes portions of many contract tasks, including Preparation of Vehicle and Facility for Testing, Vehicle Enhancements, Inductive Pickup Development, **Onboard Controller**, Electronic Guidance, and Extended Electronic Guidance.

### **3.1 Pickup**

The pickup serves as the secondary of an **airgap** transformer, in which the roadway inductor is the primary. The pickup does this by providing a low reluctance path (cores) for magnetic flux created by the roadway current and a set of windings in which a secondary current can flow (conductors). The magnetic field in the **airgap** is maximized when the polefaces of the cores (both roadway and pickup) are large and when the **airgap** is small. Figure 3.1 shows the magnetic flux lines when the inductive coupling system is transferring energy to the vehicle.

The cores and conductors are related both geometrically and structurally, as shown in Figure 3.2. The slot in the cores has to be properly sized so the conductors will fit with minimal gaps. The conductor packs support the cores and provide the primary longitudinal bending stiffness of the pickup (patent pending).

#### **3.1.1 Design of the Pickup Cores**

The energy transfer from the roadway to the vehicle is enhanced by maximizing the mutual inductance (or degree of magnetic coupling) between the roadway and pickup inductors. The mutual inductance is proportional to the **poleface** area divided by the **airgap** height. After this has been maximized (within the other project constraints), the material to be used for the cores must be selected. This selection process includes the material type and thickness of laminated core material as well as overall core build.

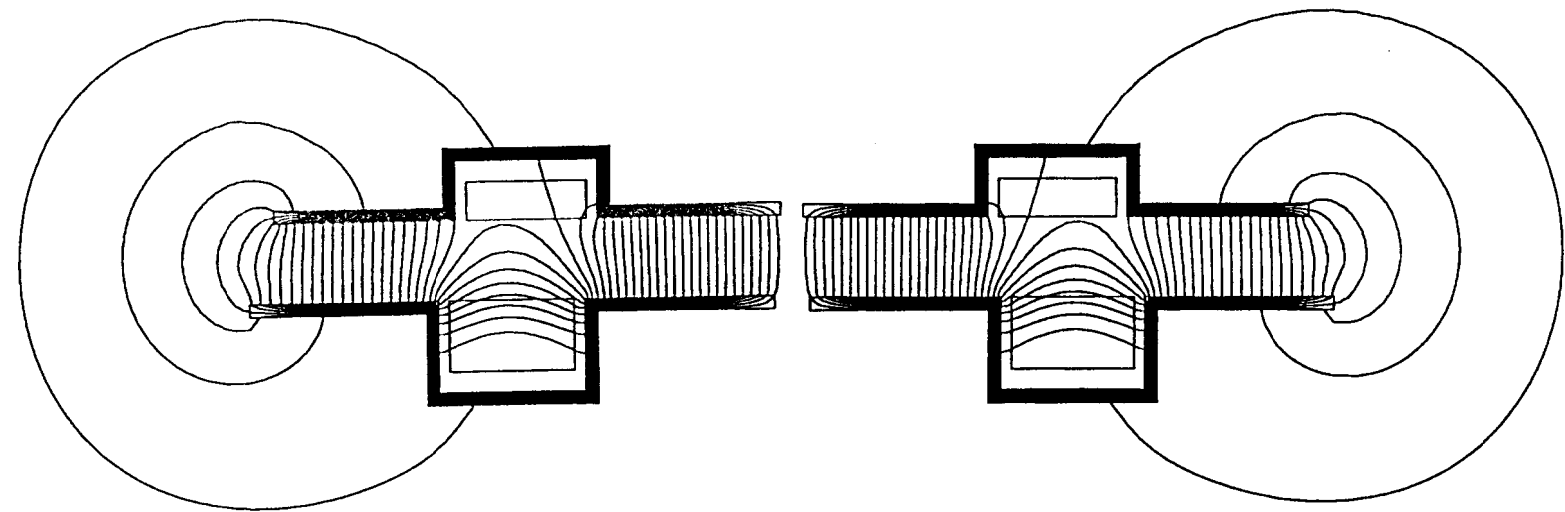
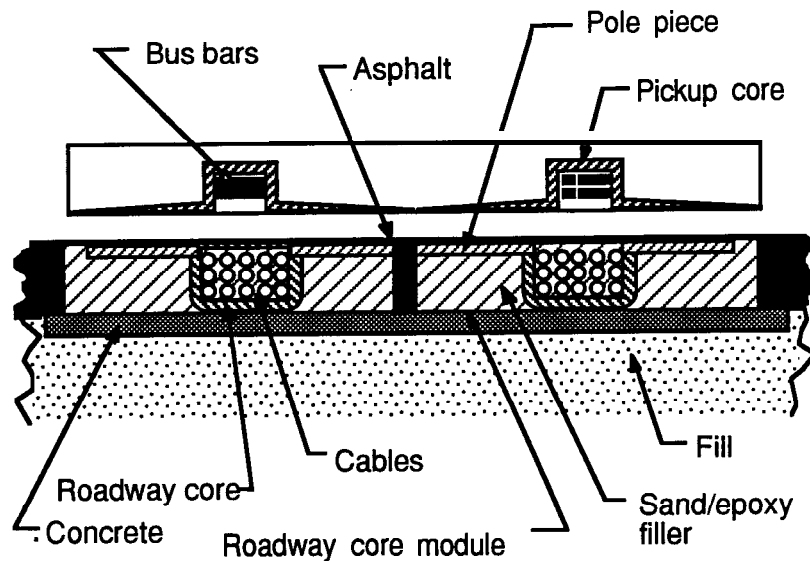


Figure 3.1      Coupled flux lines



5544 04/15/93

**Figure 3.2 Cross section of pickup (and roadway) inductor**

#### 3.1.1.1 Geometric

The geometric design of the pickup cores couples strongly with the design of the roadway cores and the pickup conductors. Adequate space must be allowed for the pickup conductors and the polefaces of the roadway and pickup cores should align relatively well to maximize mutual inductance as well as to minimize leakage inductance. Any flux line that intercepts both the roadway and pickup windings is mutual flux. A flux line that passes through only one of these two windings is leakage flux and contributes to the leakage inductance of the winding it passes through.

The width of the pickup is constrained by the distance between the main frame rails on the bus between which the pickup must retract. The length of the pickup is constrained by the distance between the rear axle and the front axle. The size of the pickup has been significantly increased compared to the first-generation pickup developed in Phase 3C. The width of the pickup has increased from 31 inches to 39 inches, and the length has increased from 162 inches to 172 inches. A three-view drawing of the pickup is shown in Figure 3.3.

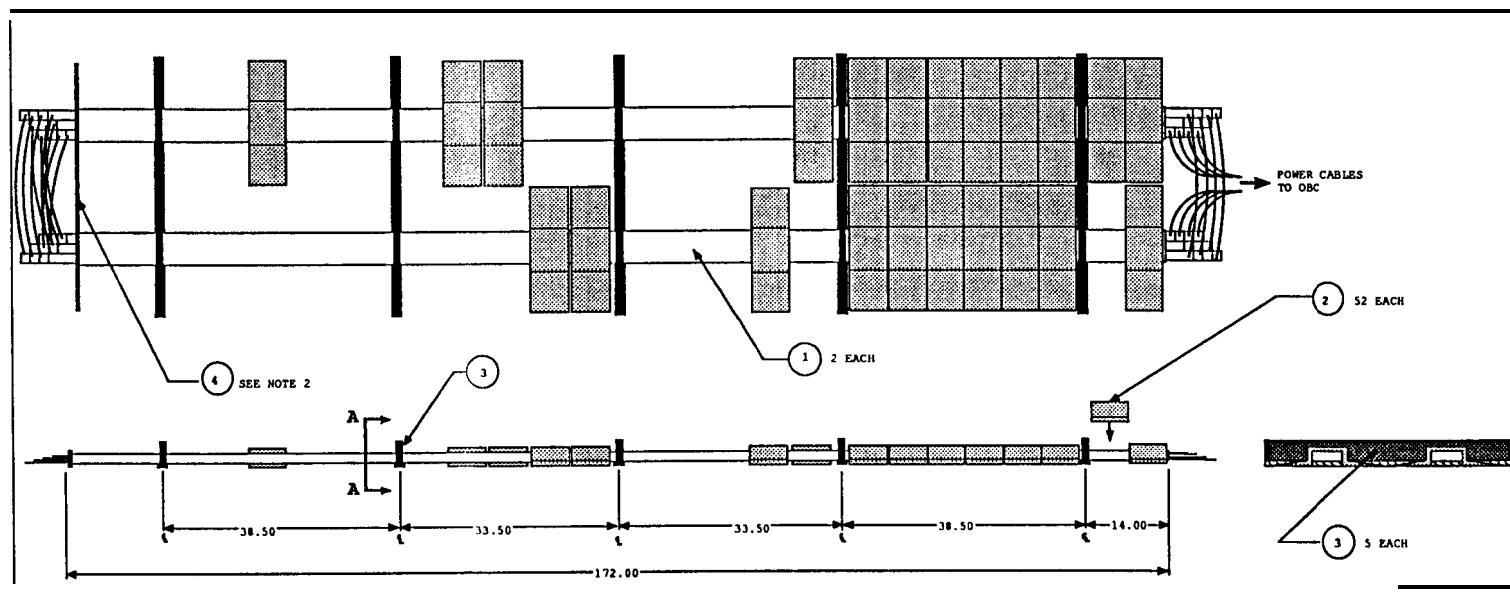


Figure 3.3     Three-view drawing of the pickup

Some of the width increase in pickup width is due to a change in the design of the pickup suspension, which no longer requires space beside the pickup. The new suspension uses a single hydraulic actuator and ten swing arms instead of the ten pneumatic cylinders and system of cables and pulleys in the original suspension. The suspension/retraction system is described in greater detail in Section 3.1.4.

The length of the pickup was carefully determined, based on clearances at both ends while the pickup is in both the raised and lowered positions. A dummy pickup was fabricated before final specification of the operational pickup and used to test the pickup suspension as well as size the actual pickup. Figures 3.4a and 3.4b show the clearance between the dummy pickup and the front axle and steering arm with the pickup in the raised and lowered positions, respectively. A prototype of the conductor pack was attached to the dummy pickup to help determine exact wiring routes for the cables connecting the pickup with the **onboard** controller. Similar checks were made at the rear of the pickup, although there the situation is simpler as the pickup conductors simply connect from one side to the other.

The shape of the cores was chosen to accommodate the pickup conductors, which are aluminum bars, not the copper cables used in the first-generation pickup. The conductor design is discussed in Section 3.1.2.

### 3.1.1.2 Selection of Core laminations

After the geometry of the cores was determined, the design proceeded to the selection of the material for the cores. Factors affecting the choice of material include cost, losses, weight, and durability. Exotic materials such as nickel, cobalt, and amorphous Met-Glass were ruled out because of cost and the inability of many manufacturers to work with them. Laminated silicon steel was eventually chosen due to its relatively low cost, good performance, and ease of fabrication. Solid cores were ruled out due to high losses at the 400 Hz design frequency.

After silicon steel was selected, the choice of using grain-oriented material became virtually automatic, as all the thinner (under 0.025-inch thickness), lower loss materials are grain-oriented. The real choices became material thickness, the number of laminations, and the method of manufacture. As lamination thickness is decreased, the losses per pound go down but the price per pound goes up. Losses decrease due to a reduction in eddy current losses, which dominate over hysteresis losses at high frequencies unless thickness is reduced. Since **onboard** weight is an important consideration, a thinner, more expensive material (0.007 inch) was chosen for the pickup cores than was used for the roadway cores (0.014- and 0.011-inch material).

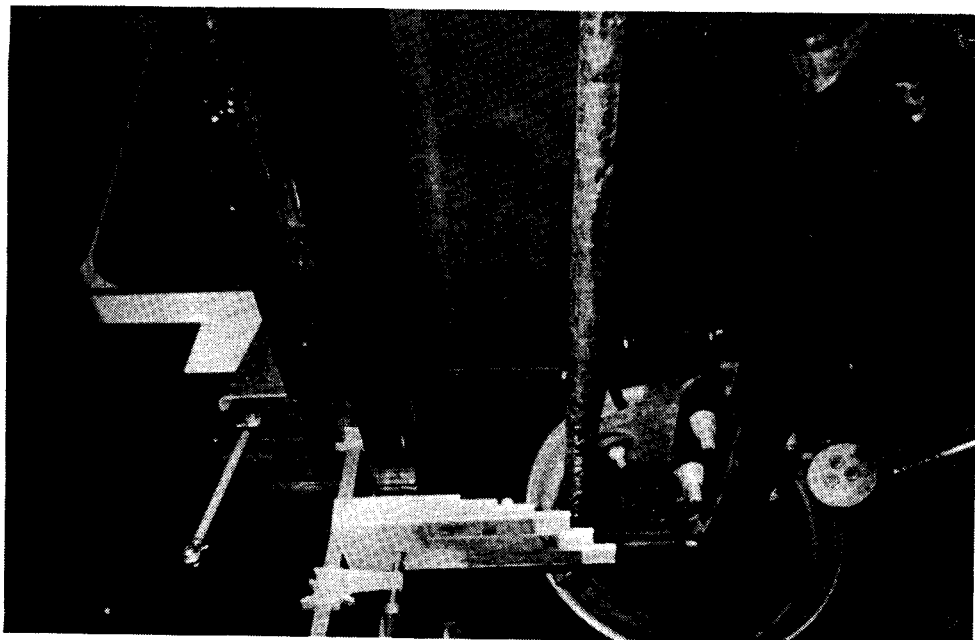


Figure 3.4.a Clearance from pickup conductors to front axle (raised position)

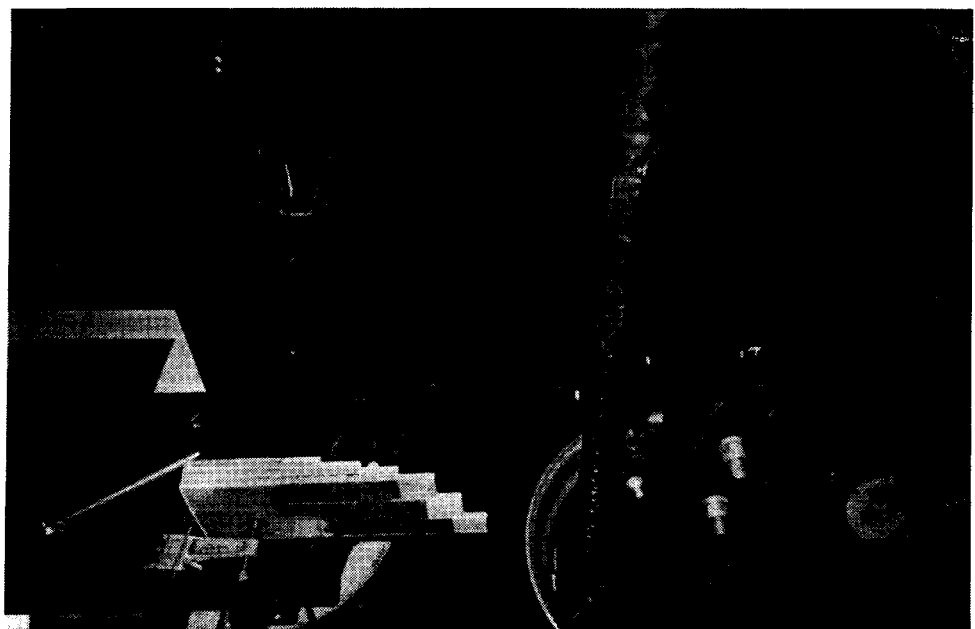


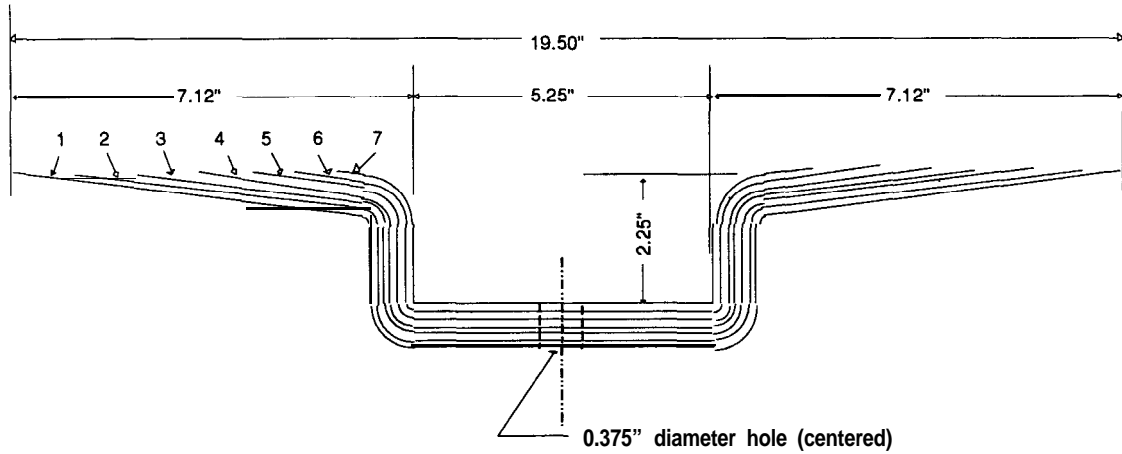
Figure 3.4.b Clearance from pickup conductors to front axle (lowered position)

The final decision involved the number of laminations to be used. The overall thickness of the core is slightly greater than the number of laminations times the lamination thickness, due to small gaps between laminations introduced in the manufacturing process. These gaps are typically 2 – 5% of the total build. Several prototype cores of various designs were fabricated. These were tested for losses as well as acoustic noise. The design finally selected uses 75 laminations of **0.007-inch** M-2 grade transformer steel, resulting in a total build of 0.54 inches. The design is presented in Figure 3.5. The magnetic flux is approximately constant in the **airgap** so that the flux carried by the core increases approximately linearly from the outer edge of the core to the conductor slot. To maintain a uniform flux density in the core, the core tapers in the **poleface** area. The laminations are arranged in groups of ten for ease of manufacture, which is considerably less expensive than 75 different lamination lengths. Tests on the early prototypes showed that fringing caused the outermost bundle of laminations to operate at **flux** densities 50 – 100% higher than the other bundles so the number of laminations in this bundle was increased by 50% from 10 to 15 to compensate.

The pickup has 52 cores, each 6 inches long and 19.5 inches wide. They weigh 15 pounds each, resulting in a total core weight of 780 pounds.

#### 3.1.1.3      Expected losses

The pickup operates at a voltage of 160 – 180 while coupling energy to the bus. Since the pickup has two turns, the voltage per turn is 80-90, or approximately 1.5 – 1.7 volts per core. The cross-sectional area in the throat of the core is 3.15 square inches, requiring an induction level of 3000 gauss at 400 Hz in the core. This compares to a flux density in the **airgap** of about 250 gauss while coupling power. The book losses for **0.007-inch** M-2 steel at this operating point are 0.33 watts per pound, which corresponds to 5 watts per core or 260 watts for the entire pickup. Actual losses tend to be 50 – 100% higher than the book losses, resulting in expected losses in the pickup cores of 400 – 500 watts or less than 1% of the total rated power.



Bundle	Length	No. of Laminations
1	23.5	15±1
2	21.5	10±1
3	19.5"	10±1
4	17.5"	10±1
5	15.5"	10±1
6	13.5"	10±1
7	11.5"	10±1

Notes:

1. Material: 007" M2 oriented silicon-iron transformer steel (super-sil)
2. ±2 laminations on entire core
3. 6" wide laminations

5544 04/19/93

Figure 3.5 Design drawing of pickup core

### 3.1.2 Conductors

The first-generation pickup from Phase 3C was articulated. It was designed in five sections and flexed at each joint, which required cables as the conductors. The second-generation pickup operates at a larger airgap and is rigid, allowing busbars to be used as the conductors.

#### 3.1.2.1 Materials

Aluminum busbars were chosen for the pickup conductors for a number of reasons. For a given resistance, aluminum is less expensive, considerably lighter, and stronger than copper. Aluminum's strength allowed us to design the busbar packs to function as the main longitudinal beams of the pickup as well as the current-carrying members. This cuts down considerably on the weight of the materials that are used purely for structural purposes. A patent is currently pending on this combined use of the busbar packs.

Selection of the alloy and tempering was based almost exclusively on electrical considerations. The pickup is supported at five locations along its length, which keeps

bending moments modest within the pickup. Alloy 6063-T0 was chosen, as it has the lowest resistance of the commonly available alloys. Consideration was given to 6063-T6, which has a tensile strength approximately three times higher, but a resistance 10% higher. The additional mechanical strength was considered unnecessary.

Skin effect (the tendency of current to flow exclusively near the surface of a conductor when operating at high frequencies) can become significant for the operating frequency and size of **busbars** used in the RPEV project. Running several small bars in parallel can minimize the increase in effective resistance caused by skin effect, if the current is equalized among the various parallel paths. Using bars of a high aspect ratio also helps minimize skin effect. The aluminum bars chosen are  $1.5 \times 0.25$  inches, which reduces skin effect 3 -4% relative to square bars of the same cross-section area. The resistance at 400 Hz is still about 1.23 times as high as the dc resistance.

The high aspect ratio is more important for overcoming proximity effect or the tendency of magnetic fields caused by currents flowing in some conductors to push the current toward a particular location within other conductors. In the pickup (and roadway inductors) proximity effect tends to push the current toward the **airgap**. This tendency is overcome by placing the long dimension of the bars in the horizontal plane. Shapes other than rectangular (such as tubes or I-beams) could be used to reduce skin effect even further, but were not seriously considered because of geometric considerations. It is desirable to keep the cross-section of the conductor pack as small as possible, as a large conductor pack area would compromise the core design. If the conductor slot in the cores is too wide, it starts eating away at the **poleface** area. A deep conductor slot increases core weight for the same poleface area and core thickness. It also increases the pickup leakage inductance and makes packaging of the pickup on the vehicle more difficult.

### 3.1.2.2 Mechanical Design

Electrical considerations imposed several requirements on the layout of the pickup **busbars**, including the requirement of many high aspect ratio bars horizontally oriented. We chose to use twelve bars for several reasons. This design gave reasonable resistance at the nominal operating point. Twelve bars also gave considerable flexibility in determining a criss-cross pattern for transposing the conductors at the ends of the pickup to equalize the currents in the various parallel paths. Twelve bars also gave flexibility to change the number of pickup turns, with one, three, or even four turns being easily achieved in addition to the baseline of two turns.

The space under the bus into which the pickup is mounted imposed physical limitations on the pickup height, which was one of the factors leading to the selection of an arrangement of four bars high by three wide. The only other alternative seriously considered was six high by two wide, which would have increased the pickup depth by approximately  $\frac{5}{8}$  inch and increased pickup leakage inductance slightly.

The array of busbars was bonded into a solid pack using fiberglass and epoxy. First, the individual bars were wrapped with an epoxy-impregnated fiberglass tape, and then the entire bundle of bars was wrapped with the same tape. The conductor packs were heated to start the high-temperature curing cycle of the epoxy.

### 3.1.2.3 Terminations

Termination of the busbars was rather challenging due to their very tight packing. The ends of the bars were staggered both vertically and laterally as shown in Figure 3.6, making the overall pickup approximately two feet longer than the length of cores. This is a worthwhile trade-off compared to making the conductor pack larger, especially considering that the envelope for the rear of the pickup tapers as the main vehicle body frame rails bend toward the center of the vehicle to accommodate the rear wheels and suspension. The busbars were tapped and fitted with threaded inserts, allowing connectors to be bolted to the busbars without touching the next lower bar within the

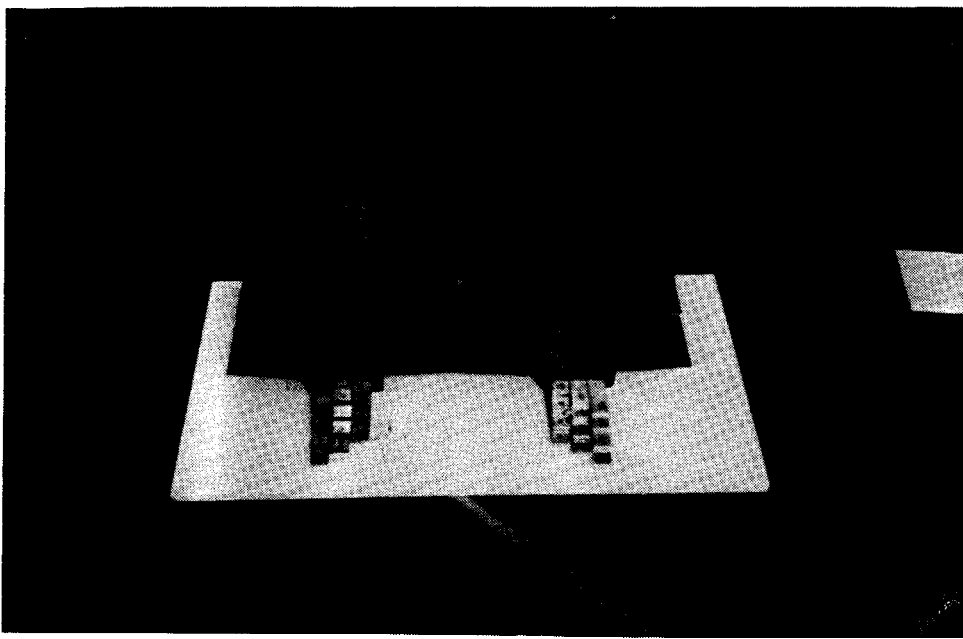


Figure 3.6      Staggered ends of busbars

pack This is important since with two turns, the next bar (vertically or laterally) could easily be at a different voltage. The hole locations and connectors were chosen so that the cables go directly toward the center of the pickup, which allows the overall pickup length to be only an inch longer than the length of the **busbar** packs. The detailed implementation of this wiring is visible in photographs showing assembly of the pickup.

#### 3.1.2.4 Conductor Losses

**Calculation** of conductor losses is straightforward and involves much less uncertainty than the calculation of core losses. The pickup current is about 900 amps at the rated operating point. Two turns gives a total current in the pickup conductor slot of 1800 amps or an average of 150 amps per conductor. After accounting for skin effect, the resistance of each bar is 0.7 milliohms, giving a loss of 16 watts per conductor or 384 watts for both conductor packs. Actual losses will be slightly higher due to losses in the cables connecting both sides of the pickup, non-uniform distribution of current, proximity effect, and higher resistance as the conductors heat up. The combination of these four effects is estimated to be 20%, giving a total loss of just under 500 watts or approximately 1% of the rated output power.

#### 3.1.3 Mechanical Design of Pickup

The mechanical design of the pickup was straightforward after the decision to use the **busbar** packs as the longitudinal beams was made. Cross beams were designed to provide lateral strength and carry the weight of the cores and conductor packs to the suspension attachment points. Brackets were designed to secure the cores to the **busbar** packs and to clamp the outer edges of the cores. The bottom of the pickup is covered with a thin plastic sheet to minimize damage if the pickup strikes an object. A fiberglass frame at the front of the pickup serves the same purpose. Various acoustic treatments were investigated to suppress acoustic noise from the pickup, and the simplest ones were chosen for implementation.

The result of the pickup design task is a pickup that is considerably better than the first-generation pickup. It weighs less, has lower losses, lower acoustic emissions, and is larger, increasing the mutual inductance with the roadway. Assembly is easier than the first-generation pickup, but still required significant effort and there is considerable room for improvement, as was demonstrated with the pickup for the Playa Vista project G-Van.

### 3.1.3.1 Frame

Conductor packs form the two main longitudinal beams of the pickup. There are five lateral beams that tie the conductor packs together and to the pickup suspension. There are also supplemental cross beams at each end to support the cover sheet and the fiberglass frame that boxes in the cables at each end of the pickup.

### 3.1.3.2 Cross beams

The cross beams consist of two parts bolted together. Tests indicated that any metal located below the conductor packs will heat up due to eddy currents, which required a fiberglass bar below the conductor packs to support them. The conductor packs bear against this fiberglass bar, with a thin strip of rubber to absorb vibration. The fiberglass bar is bolted to the aluminum upper half of the cross beam, which carries the loads to the pickup suspension. Figure 3.7 shows the two parts of one of the cross beams while the pickup is being assembled. The conductor packs and cross beams are assembled upside down and then turned over before attaching the cores. Detailed drawings of both parts of the cross beam are included in the appendices.



Figure 3.7 Two halves of cross beam

### 3.1.3.3 Coating of Pickup Cores

The pickup cores are vacuum impregnated with epoxy during the fabrication process, which forms a solid core, but does not provide corrosion protection. After arrival on site, an additional coating of a commercially available plastic was applied. The cores were dipped in the liquid plastic and placed on racks to cure, as shown in Figure 3.8. The primary objective of coating the cores was to provide improved sealing against corrosion, although acoustic noise was also reduced slightly. Two colors were used to coat the cores, which provides better contrast in some of the pictures of the pickup assembly in Section 3.1.3.5.

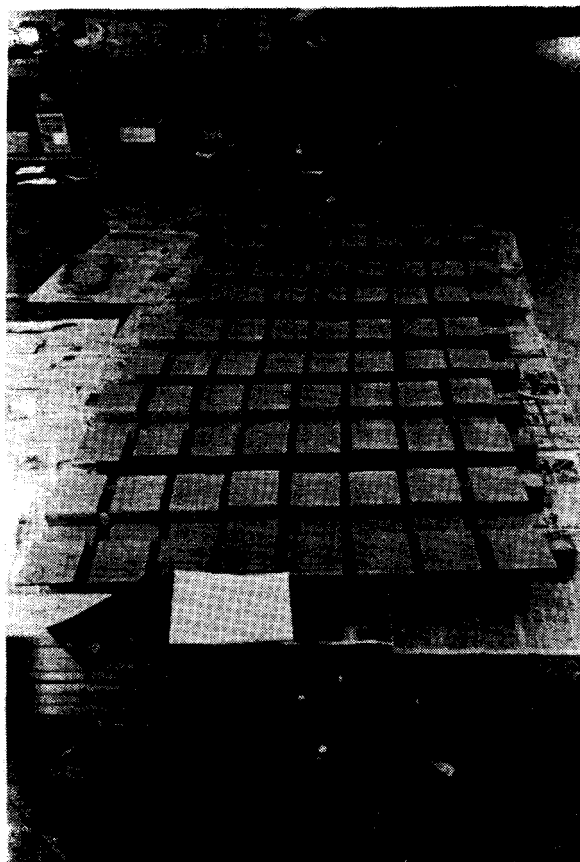


Figure 3.8 Coating pickup cores

### 3.1.3.4 Acoustic Treatments

Acoustic emissions from the pickup were a concern during the Phase 3C testing. A great deal of effort went into noise reduction during Phase 3D. Testing in the anechoic chamber at the Richmond Field Station identified several effective noise reduction treatments, such as the one pictured in Figure 3.9. This treatment reduced acoustic noise more than 10 dB, but was rather cumbersome and impractical. It was available if pickup noise proved to be unacceptable following testing of the pickup while mounted on the bus. A much simpler treatment was devised that proved adequate. A thin layer of soft, sound-absorbing rubber was placed between the cores and the pickup cover sheet, which same material was also used to cover the top of the cores. An L-shaped piece of fiberglass was run along each outer edge of the pickup and attached to the cover sheet with small nylon bolts, effectively clamping the outer edges of the cores. A U-section of fiberglass down the middle of the pickup performed the same function for the inner edge of the cores.

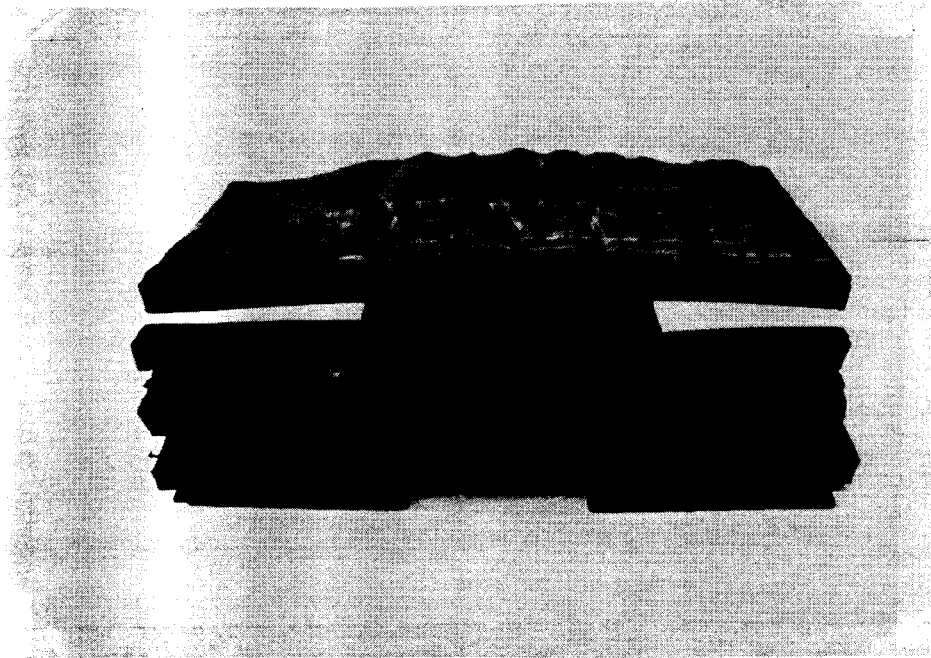


Figure 3.9      Acoustic treatment of pickup cores

### 3.1 • 3.5 Assembly and Mounting Procedure

Assembly of the pickup involves many steps. With the current design, the process takes several man-days. The design developed for the Playa Vista project reduced assembly time an order of magnitude.

The first step in assembling the pickup is laying out the aluminum cross beams (upside down) with the proper spacing. The conductor packs are placed in the notches in the beams and the fiberglass bars secured, as seen in Figure 3.10a. The cover sheet is attached and the pickup frame turned right side up. A thin rubber sheet is placed on top of the cover sheet followed by placing the cores on the conductor packs. (Figure 3.10b). Fiberglass frames are added on both ends. The cores are covered by another sheet of rubber and brackets that secure the cores are added. The primary brackets are made of aluminum channel and run directly above the conductor packs. Supplemental fiberglass brackets are added in the center and outer edges of the pickup, as seen in Figure 3.10c. The cables connecting the **busbar** packs are added before mounting the pickup on the bus. During initial testing, the **busbars** were connected to a patch panel that allowed the crisscross pattern to be easily changed. These cables were replaced with permanent ones before mounting the pickup on the bus. Final assembly of the pickup takes place on a very low cart, which is then rolled under the bus from the front. The pickup is attached to the pickup suspension, and cables connecting the pickup to the **onboard** controller are attached.

#### 3.1.4 Retraction/Suspension System

The purpose of the pickup suspension system is to raise and lower the pickup as required, and to maintain the pickup in the proper position relative to the bus frame in both the raised and lowered positions.

The pickup suspension system was completely redesigned during Phase 3D. The original (partially completed) pneumatic system was replaced by a hydraulic one, which has performed perfectly. The original pickup suspension system had ten pneumatic cylinders that raised and lowered the pickup. The pickup was attached to the cylinders by cables that ran over pulleys. There were two advantages of the original system: raising and lowering the pickup involved no lateral or longitudinal motion and the pneumatic cylinders could be powered from the air supply on the bus that operates the brakes, air bag suspension, and door. The disadvantages far outweighed the advantages. The system had a high parts count and weight and adjusting the cable lengths was likely to be time consuming and require periodic maintenance. Control arms would have to be designed for both the lateral and longitudinal dimensions to prevent the pickup from swinging on the cables. The pneumatic cylinders have more compliance than hydraulic cylinders, which would make a road strike by the pickup more likely when the vehicle hit a bump. Two of the pneumatic cylinders were to be located in the area required for a wheelchair ramp if the vehicle were to meet current accessibility standards.



Figure 3.10.a Busbar packs in crossbeams

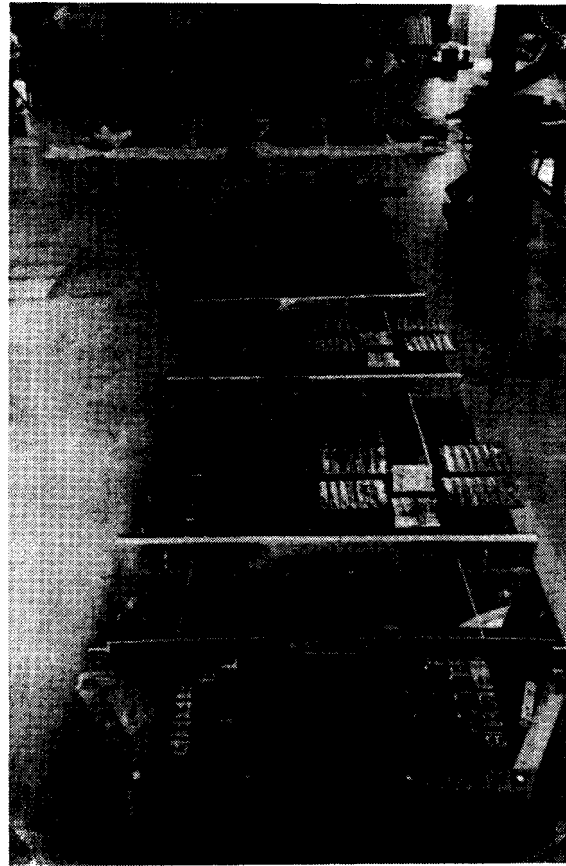


Figure 3.10.b Partially assembled pickup

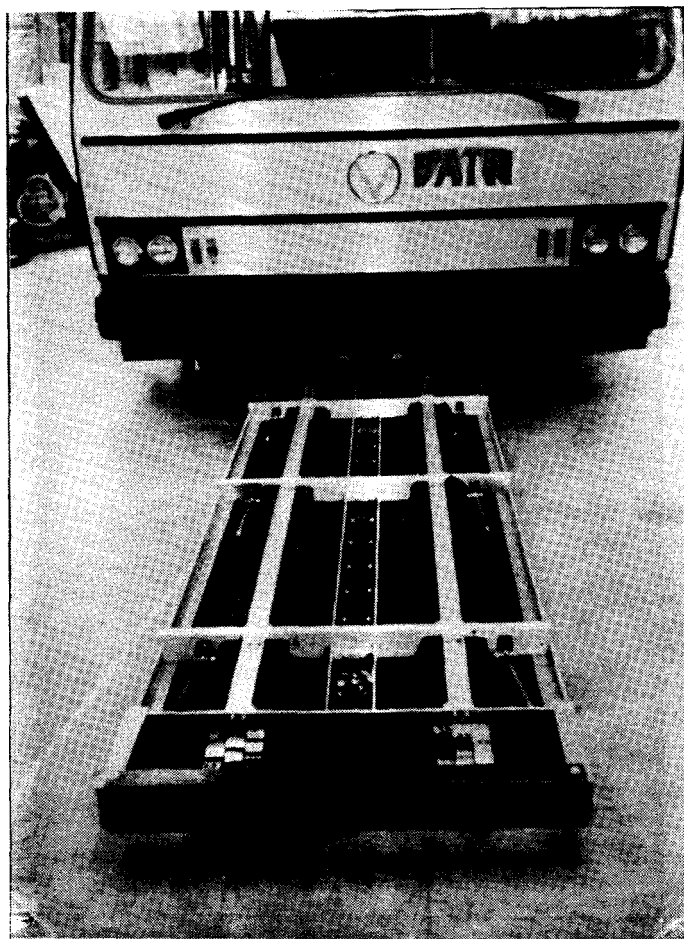


Figure 3.1 0.c Pickup being rolled under bus

#### 3.1.4.1 Hydraulic System

The basic concept of the hydraulic pickup suspension system is that most of the weight of the pickup is carried by ten swing arms, which are attached to each end of the pickup cross beams. A single hydraulic cylinder mounted on the rear of the pickup is used to raise and lower the pickup. The swing arms are attached to the vehicle frame and the pickup cross beams with rod-end bearings. The arms are approximately nine inches long and swing through approximately 60 degrees as the pickup is raised. The length of the swing arms is adjustable. Their positions with the pickup in the lowered and raised positions are visible in Figures 3.11a and 3.11b. The pickup moves approximately six inches toward the rear as it is raised. Lateral control arms (Figure 3.12) are attached to the front and rear of the pickup. They are made as long as possible, allowing them to

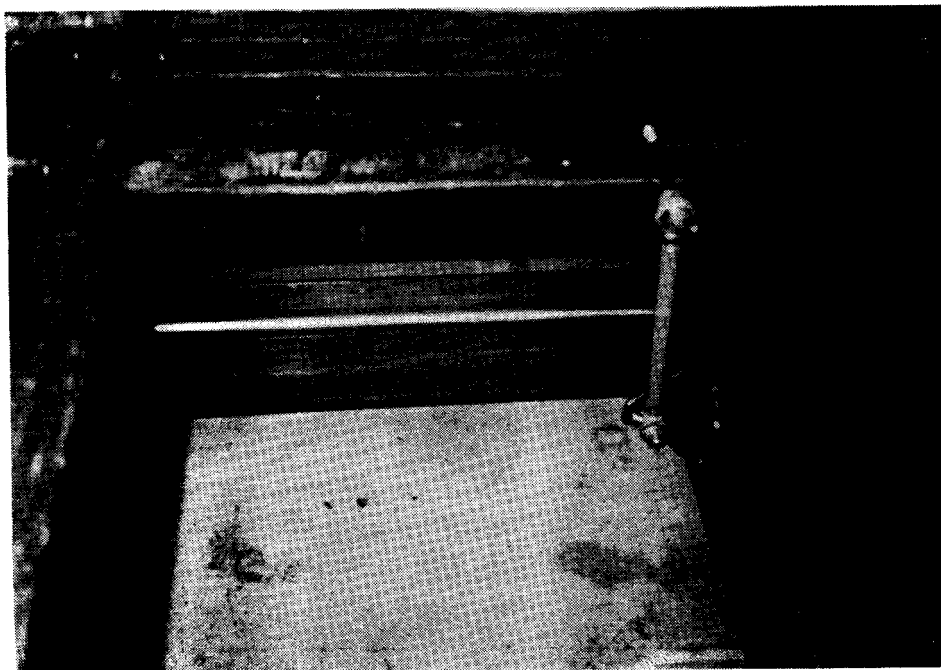


Figure 3.11 .a     Swing arms in lowered position

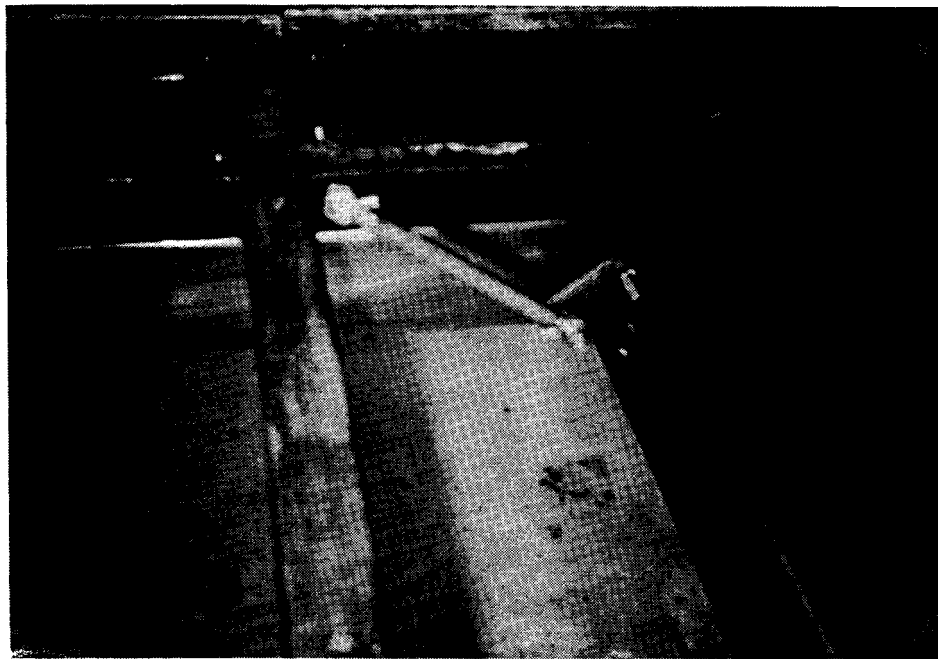


Figure 3.11 .b     Swing arms in raised position

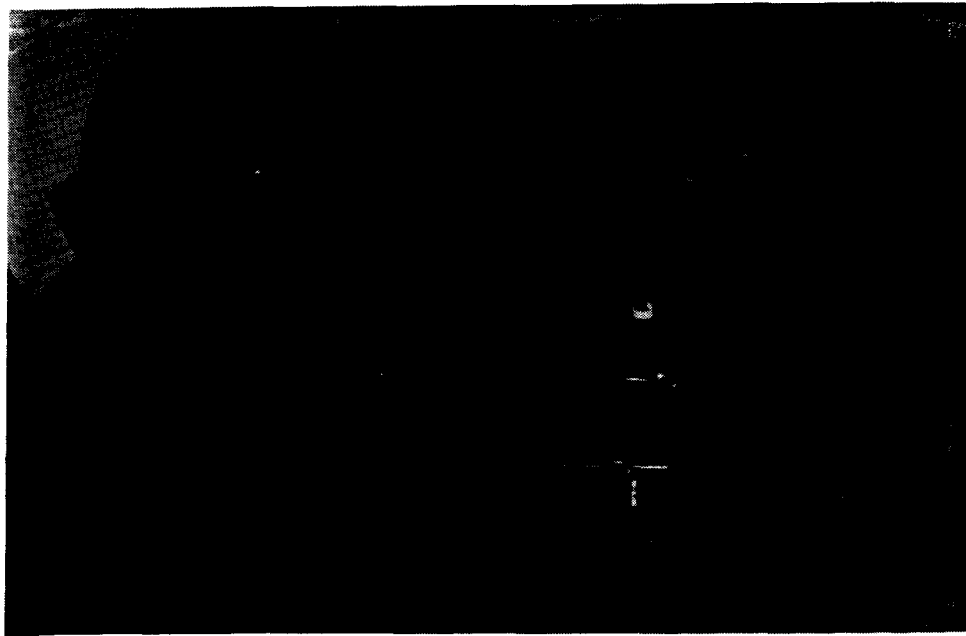


Figure 3.12      Lateral control arm

limit pickup lateral motion to less than 0.25 inch as it is raised and lowered. Hydraulic pressure is supplied by a pump (with integral reservoir) that is driven by the vehicle's 24-volt system.

#### 3.1.4.2      Cabling

The cables connecting the pickup with the **onboard controller** are designed to accommodate the movement of the pickup as it is raised and lowered. The entry point of the cables to the **onboard controller** was chosen to be very near the center of the arc traced by the front of the pickup as it moves up and down, minimizing any stretching or bending of the cables with pickup motion.

#### 3.1 • 4.3      Controls

The motion of the pickup is controlled by the driver through rocker switches mounted on the dashboard. The pickup is lowered by opening a valve, releasing hydraulic pressure in the cylinder. Gravity provides the force to lower the pickup. After five seconds, a timer closes the valve, thus locking the pickup in the lowered position. The exact **airgap** of the pickup in the lowered position is determined by the length of the swing arms. The pickup is raised by starting the hydraulic pump, again from a switch on the dashboard. Either of two microswitches can open the relay when the pickup

reaches the fully raised position. Such switches could be implemented to control the pickup position in the down position if desired, but using the swing arm length to control this works perfectly well.

A system for lowering and raising the pickup automatically as the vehicle entered and left the powered roadway was designed and partially implemented. It involves electronic “signposts” installed at either end of the powered length of the test track. The signpost broadcasts a signal through a conventional presence-detector loop. An antenna **onboard** the vehicle receives this signal and flips a relay as the bus enters or leaves the powered area. The wayside and **onboard** equipment were both installed and fully tested. The only item required to make the pickup rise and lower automatically is connecting the output of the **onboard** relay to the appropriate locations in the control circuit. A more detailed description of the communication system can be found in Section 4.2.3.2.

### 3.2 **Onboard Controller (OBC)**

The **onboard** controller regulates the output current of the inductive coupling system to match the vehicle’s ability to accept current. It also rectifies the ac to dc and provides ripple filtering, resulting in readily controlled, ripple-free dc current **onboard** the vehicle. A second-generation **onboard** controller was built at the end of Phase 3C, but never tested. Considerably more work was required to make the **onboard** controller work properly than had been budgeted. The **onboard** control computer, which has been used successfully with the first-generation **onboard** controller during Phase 3C, continued to function properly through the current phase.

#### 3.2.1 **Description**

The second-generation **onboard** controller is much more compact than the first-generation unit. Most of the components in the first-generation controller were natural convection air-cooled, which resulted in rather large, heavy heat sinks. The second-generation OBC used liquid cooled capacitors and solid-state switches, greatly reducing their volume. Other components have forced-air cooling, again reducing their size and weight. As a result of the many new components, a number of problems were introduced into the OBC, several of which took a great deal of effort to solve.

### 3.2.1 .1 Electrical

The onboard controller uses a switched capacitor bank to control the natural frequency of the resonant circuit formed by the onboard tuning capacitor and the mutual inductance of the airgap. As the natural frequency of this resonant circuit is driven closer to the roadway excitation frequency, the response of the resonant circuit increases, raising the pickup current and voltage and supplying more output current from the OBC to the vehicle.

The switchable capacitor bank and rectifier are connected in parallel across the terminals of the pickup. An inductor is wired in series with the rectifier input, as shown in Figure 3.13, which inductor tends to isolate the non-linearities introduced by the rectifier, minimizing the propagation of non-sinusoidal waveforms into the ac portion of the circuit. It is impossible to do this completely, but a properly selected value of this isolation inductance can play an important role in minimizing distorted waveforms in the ac circuit.

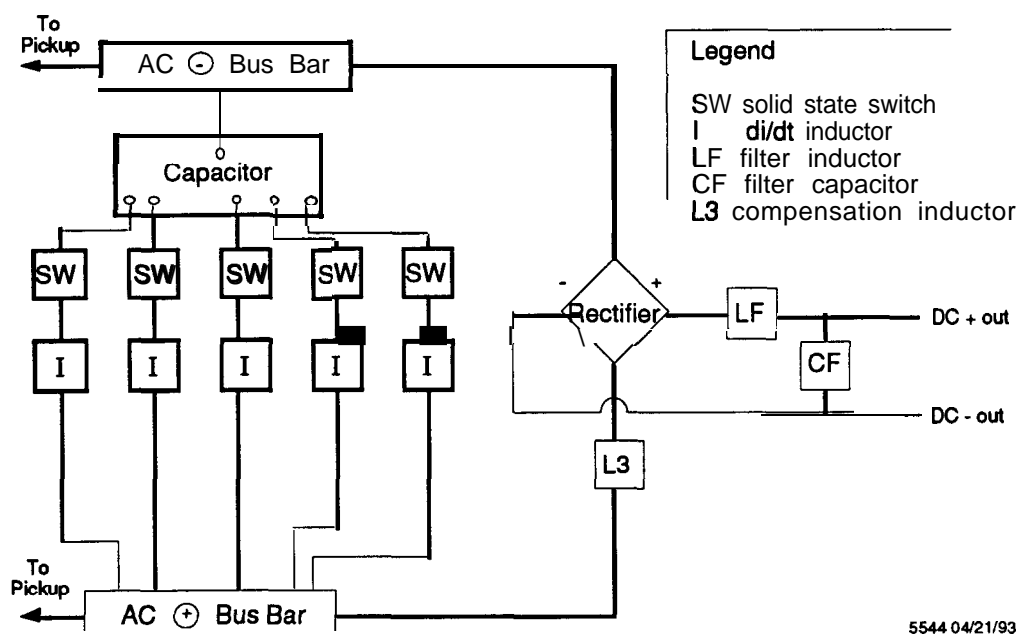


Figure 3.13 Schematic of OBC

Having inductors in series with the solid-state switches also plays an important role in keeping the ac waveforms clean. These inductors were originally introduced to limit the rate of rise of current in the switches if they were triggered at other than zero voltage (across the switch). Since these inductors limit the rate of rise of current, they are

generally referred to as  $di/dt$  inductors. Use of  $di/dt$  inductors was considered necessary as a high rate of rise in current through the solid-state switches can cause premature failure of the switch. The switches are turned on (gated) by a zero-crossing trigger circuit.

When the switch is gated, it conducts until the current drops to zero. The zero current condition corresponds to a maximum charge on the capacitor. When the switch is deactivated, the natural frequency of the resonant circuit moves further away from the driven frequency. Pickup voltage and current drop, as does the inductive coupling system's output current. If the capacitor remained at the high voltage that was on it when it was removed from the circuit, the pickup voltage would always be smaller than the capacitor voltage (even when the pickup voltage was at the peak of its waveform). The voltage across the solid-state switch would never go to zero, and the switch could never be re-energized. Bleed resistors are installed across the capacitors to bleed this charge, allowing the capacitor branches to be re-activated. These bleed resistors also provide a valuable safety function, as the ac capacitor voltage is reduced to zero when the vehicle is removed from the powered roadway. A patent has been applied for the design of the zero-crossing switch/current limiting inductor/bleed resistor branch of the circuit.

### 3.2.1.2 Physical

The **onboard controller** is packaged in three boxes with aluminum frames, side panels, and lids. The lids are strong enough to walk on, as the driver steps on all three of the boxes on the way to the driver's seat. The OBC occupies the space between the front wheels. The weight of the OBC and its components is shown in Table 3.1.

The liquid-cooled components (solid-state switches and capacitors) are located in the front box. The radiator for the liquid cooling system is located ahead of the front box and is visible in Figure 3.14. Fans and the filter for the air cooling are located in this area, as well as the pump for the liquid cooling system. The first box, with the ac capacitors, solid-state switches, and rectifier is the most crowded of the three, as it contains liquid cooling lines as well as cables. Working on any component located in this box is very difficult, which provided motivation for relocating the trigger circuits (originally mounted on the base of the solid-state switches) into the second box.

**Table 3.1**  
**Onboard Controller Weights**

Box	Weight (pounds)	Components
1 (Front)	379	ac Capacitors Rectifier Solid State Switch One Inductor
2 (Middle)	268	Inductors 1 @ 92 = 92 2 @ 37 = 74 1 @ 26 = 26 2 @ 7 = 14 Box, Misc = <u>62</u> 268
3 (Rear)	59	Filter Capacitor Transducers
<b>Total</b>	<b>706</b>	

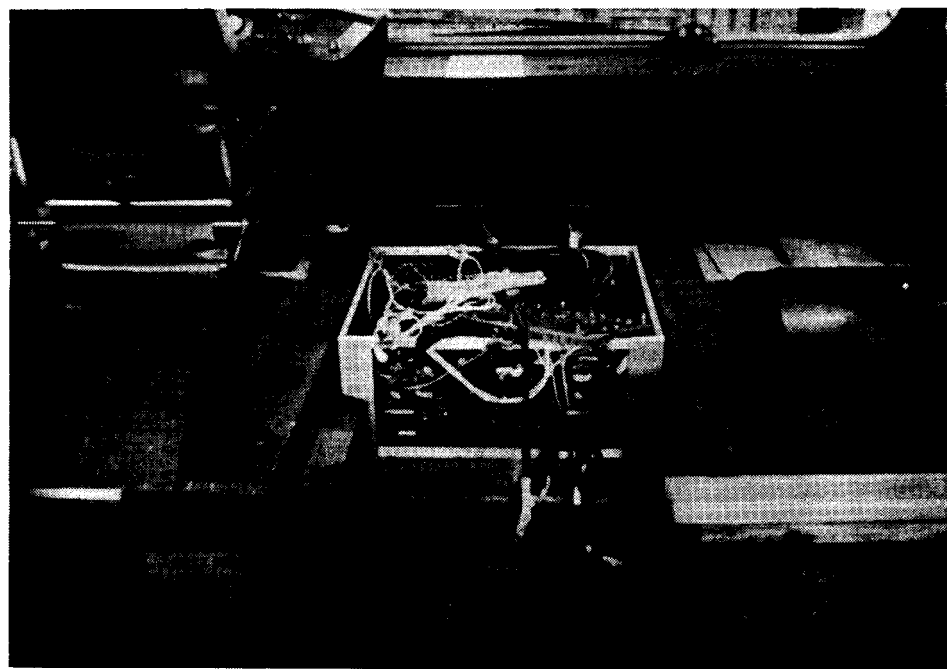


Figure 3.14      Front box and radiator on bus

The middle box is narrower than the other two, as the sides of the volume allocated to the OBC step in to make room for the air-bags of the front suspension. The second box contains six inductors, the output fuse and transducers, and a panel of small electronic components such as the trigger circuits, fuses, and bleed resistors. All components on this panel are connected to devices in the front box. The cables from the pickup enter the OBC through the bottom of the second box.

The third box is only half as high as the others and contains the filter capacitors. The output power cables that run to the rear of the bus exit through the floor of this box.

### **3.2.1.3      Expected losses**

The losses in the onboard controller, like the pickup, amount to only a small percentage of the rated output power. The majority of the losses come from the rectifier (1000 watts), solid-state switches (1000 watts), and inductors (1250 watts total). The capacitor losses amount to only 250 watts. The losses are low enough that the cooling systems (both liquid and air) can easily handle the load.

### **3.2.1.4      Control Algorithms**

The algorithms controlling the OBC output current went through three major changes during the project. The first involved equalizing the time that the various capacitor branches were active. The algorithm was changed from a LIFO (last in first out) to a FIFO (first in first out) scheme for removing branches of capacitance. The second involved improving the resolution of the control steps. Originally, the control system had five steps of switchable capacitance, each with a nominal value of 383 microfarads. One of the ac capacitors in the OBC has taps of 150 microfarads. By connecting one switch to a 150 microfarad tap of capacitance, the alternating steps of 150 and 233 microfarads can be added to the circuit. This is explained in more detail in Chapter 5.

### **3.2.1.5      Safety Systems and Interlocks**

One of the objectives of this project was to move the technology from the laboratory to commercialization and implementation in a real-world setting. Part of this involves determining failure modes and establishing safety systems to deal with those failures. Although a comprehensive fault tree analysis is beyond the scope of the project, several possible faults within the OBC were identified and equipment to diagnose them was procured. The faults identified include:

- capacitor failure (internal over-pressure switch)
- high temperature in liquid cooling system
- low flow in liquid cooling system
- low flow in air cooling system
- high temperature in air cooling system

The heat sinks in the solid-state switches have thermal overload protection, which prevent starting a switch with an over-temperature heat sink. Functional testing of the fault detection sensors was performed, and all sensors worked as specified. Circuitry was designed to interface the fault detection sensors with the onboard control computer, so that a fault condition would trigger a shutdown of the inductive coupling system and record the cause. At this point, work on this task was abandoned so that project resources could be devoted to higher priority tasks.

### 3.3 Steering Assistance System

The inductive coupling system can transfer the maximum current to the vehicle when the vehicle is properly centered above the roadway inductor. The magnetic field created by the roadway inductor is very strong and distinctively shaped. It forms a good position reference for a steering assistance system. Two types of systems were investigated. The first was a high-power system in which the driver would relinquish complete control of the steering function to the automatic steering system. The second was a very low power system that the driver could easily overpower if desired. Such a system will apply only very small inputs into the steering system, small enough that the driver may not even notice that the system was there. It will be powerful enough, however, to keep the vehicle well centered (within 1 – 2 inches) nearly all the time the vehicle is moving.

The system actually installed on the bus did not provide any input to the steering system, but used the reference signal to drive a display that shows the driver how far off center he is. The signal that drives the display can be used as the input to either of the systems mentioned above.

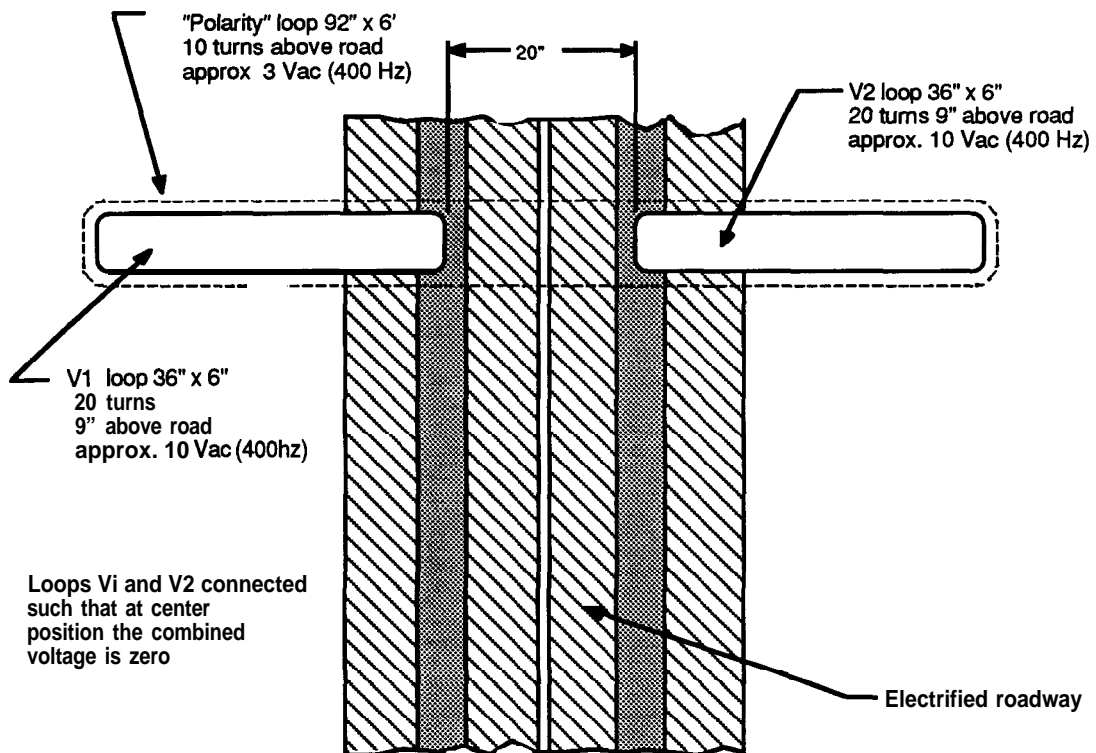
#### 3.3.1 Sensors

The sensors for a steering assistance system using the RPEV roadway inductor as a reference can be as simple as many turns of wire wrapped around a form, such as a piece of plywood or Styrofoam. The loops are connected to a simple analog circuit that

determines the lateral offset and provides an error signal, which can drive a display for the driver (as was done in our case) or as the sensed position input for an automatic steering system.

### 3.3.1 .1 loops

Three sets of loops were fabricated and each worked well. The primary sensor consists of two loops, one on either side of the vehicle. The difference between the two voltages gives a signal proportional to the lateral offset of the vehicle. When the vehicle is centered, the voltages induced on both loops are equal so the difference is zero, indicating zero lateral offset. As the vehicle moves to the side, the difference between the two voltages increases. A third loop is used to obtain a polarity signal. If the difference between the two primary sensor loops is in phase with the reference loop, the vehicle is left of center. When the vehicle is right of center, these two signals are 180 degrees out of phase.



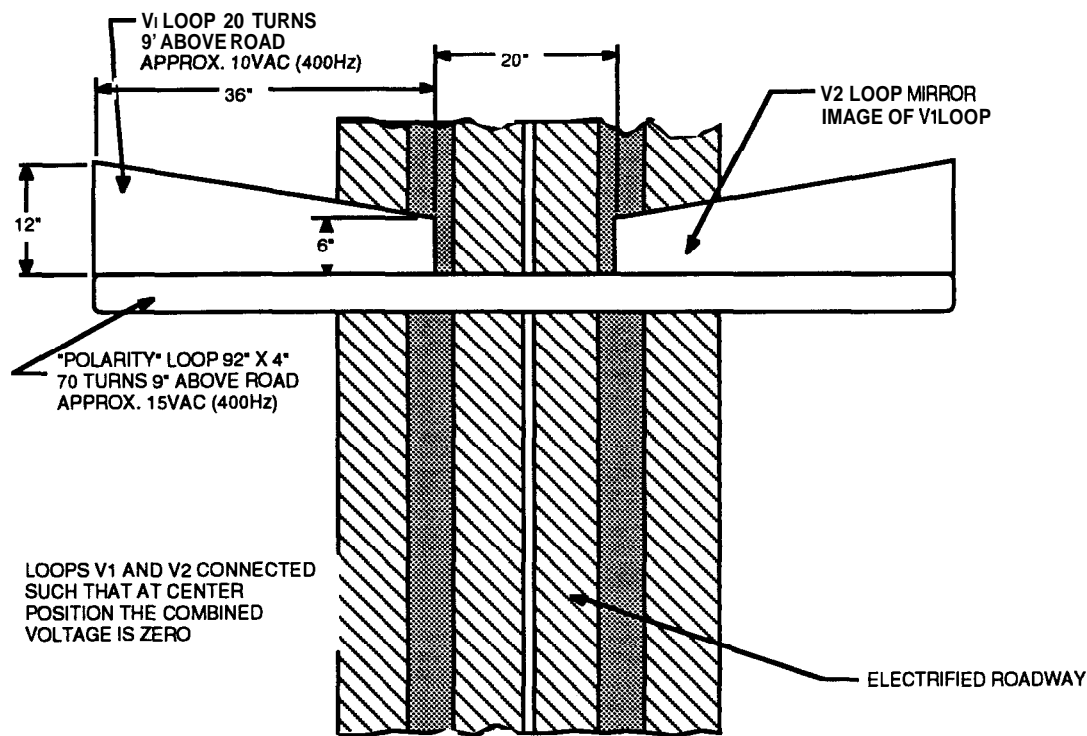
5544 06/15/91

Figure 3.15      6 x 36 rectangular loops

The first set of loops was intended for proof of concept only and was put together in less than an hour. The loops were rectangles approximately 10 x 30 inches. They were used to measure induced voltages. The measured voltage characteristic matched the predicted shape, indicating that the idea was sound.

The second set of loops was intended to serve as operational hardware. Their size was selected more carefully to provide the maximum linear range. A drawing of these loops is shown in Figure 3.15. A polarity/reference loop was built with this second set, and an analog control circuit was designed and fabricated as well, which setup worked very well, giving a linear signal to just beyond 24 inches to either side of center.

A third set of loops, shown in Figure 3.16, was made in an attempt to extend the linear range of the steering assistance system sensor. A trapezoidal shape was used, which did extend the linear range out to approximately 30 inches. This third set of loops was mounted to the vehicle, where it remains, functioning properly.



5544 07/15/91

**Figure 3.16**      **12 x 36 x 6 trapezoidal loops**

### 3.3.1.2 Circuit

The control circuit for the steering assistance sensor is very simple. The inputs from the primary sensor loops (difference of the left and right loops) and the polarity sensor are first amplified. The polarity is checked to determine whether the vehicle is left or right of center. The primary sensor input is rectified and fed out through transistors that apply the proper polarity to the signal. Two meters, shown in Figure 3.17, present this information to the driver. The left meter has a range of  $\pm 30$  inches. The right meter has a much finer scale, with  $\pm 5$  inches full-scale deflection. A more detailed description of the control circuit can be found in Appendix B, and test results appear in Chapter 5.

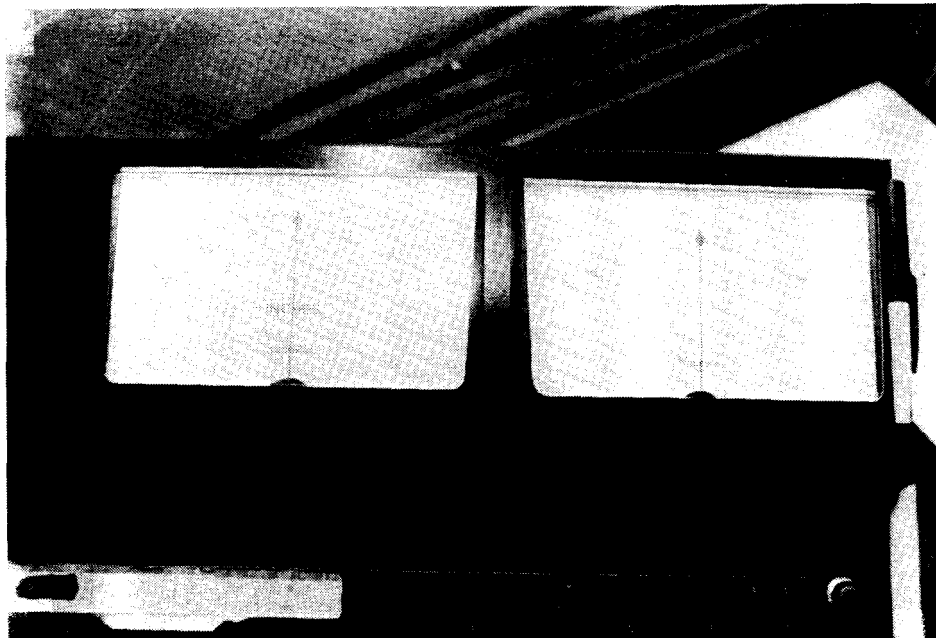


Figure 3.17      Steering assistance motors

### 3.3.2 Investigation of Existing Automatic Steering Systems

Project personnel visited MAN and Daimler-Benz to assess their automatically steered buses. The Daimler-Benz system is more sophisticated, and serious discussions were held concerning their possible cooperation with the PATH automatic steering effort, which effort centered on their equipment, including hydraulic pumps, actuators, and the redundant control system. The initiative never got beyond the talking stage.

On the same trip, a visit was made to Vetter, the manufacturer of the chassis of the RPEV bus. Mr. Siegbert "Teddy" Rosenkranz, chief engineer at Vetter made specific

recommendations concerning retrofitting an automatic steering system on the bus, including a discussion of the various possible attachment points for the actuator. A detailed report of these discussions is included in the above mentioned trip report.

### 3.4 Bus Hardware Upgrades

Bob Davis of Bus Manufacturing USA made upgrades and repairs were made to the bus, including installation of the pickup suspension, fabrication of a dummy pickup, installation of acoustic insulation in various locations, sealing of the battery compartment and equipment hatches, reworking the floor hatches, moving the 24-volt battery and power steering fluid reservoir, installation of cables from the OBC output location to the motor controller compartment, installation of an OBC disconnect switch, and completion of the battery compartment ventilation system.

The motor controller was damaged when the battery ventilation blower relay shorted to the chassis. The controller was shipped back to its manufacturer, Soleq Corporation, for repairs. At the same time the motor controller was upgraded from 600 amps to 850 amps, improving the bus acceleration and hill-climbing ability. The cables from the motor controller to the motor were replaced with larger ones at the same time.

The brushes in the motor for the air compressor wore down very quickly, probably because the inductive coupling system frequently drives the **onboard** voltage to 150 volts or more. Under normal battery operation, the air compressor runs with the **onboard** dc voltage at or below the nominal value (128 volts) except for very brief moments of regenerative braking. If high voltage did in fact cause accelerated wear of the brushes and rotor, it indicates that this must be considered in selection of the traction motor controller and the high voltage accessories (primarily high power motors and the dc-dc converter) to make certain that they can stand the swings of **onboard** voltage. These swings are typically twice as large for an RPEV as for a pure battery vehicle with the same nominal voltage.

A PC-based data acquisition system that records velocity, motor controller current, battery current and voltage, and lateral offset, as well as several inductive coupling system variables, most notably the ICS output current, was installed on the bus. The system runs from a 12-volt inverter that can be switched to draw power from either of the two **12-volt** batteries, which in series comprise the bus's 24-volt battery. The data acquisition system is essentially the same hardware that was used in Phase 3C to test the first-generation inductive coupling system, and while it is somewhat out of date, it worked well. The original Compaq computer used with the data acquisition system

failed early in the project and was replaced by an SCT-supplied PC/AT. The data acquisition system hardware board and software were transferred to the AT and the system worked as before, with two major improvements-a hard disk was installed in the computer, allowing operation without changing floppy disks and a 12-inch monitor was used, making operation of the computer much easier.

## **4. Facilities**

---

Construction of the RPEV test track at the Richmond Field Station was the most costly and time-consuming portion of this RPEV development project. The RFS track is the only large-scale operational RPEV facility in the world and represented the first opportunity to test both the RPEV concept and track construction techniques in the real world. Track construction was a major undertaking and required subcontracts to an A&E firm and a general contractor as well as advice and research from Caltrans engineers. Since this was the first track of its kind-discounting the 20-foot static test track at Translab-many difficulties arose during the course of the construction. Despite these difficulties, the finished track has performed admirably.

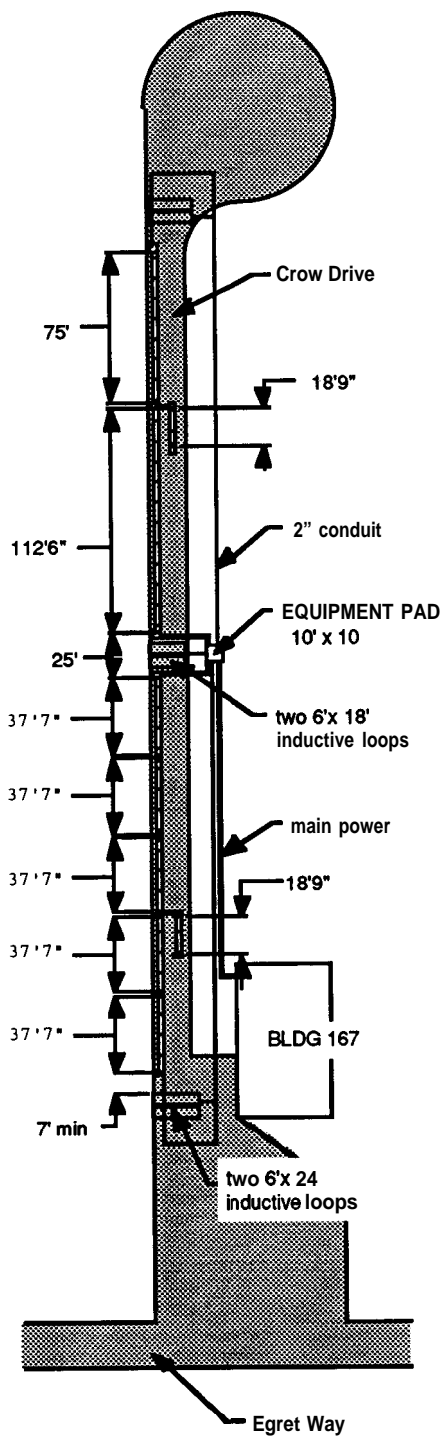
While no one wants to admit to **having** problems, in an R&D project of this scope they are bound to arise. Difficulties encountered during construction included: procurement of the roadway inductor modules, red tape in the bidding process for the construction contract, obtaining the proper vault lids and frames, interference with existing utilities at the track site, choosing the potting compound for the roadway and developing the method for installing the inductor modules-not to mention unanticipated costs on almost all phases of the construction. This list of problems sounds quite daunting, but the amount we learned while solving all of these challenges was immense.

### **4.1 Track Configuration**

Determining the configuration of the test track involved consideration of many factors such as site **constraints**, budget limitations, conductor type, roadway inductor module size, and type of electrical connections. The final track layout (700 feet long with 440 feet of buried inductor) is shown in Figure 4.1.

#### **4.1.1 Physical Constraints and Requirements**

The University of California Richmond Field Station was chosen as the site for the RPEV test track because of the large open areas available for construction (and the



5544 1 0/26/90

Figure 4.1 Final track layout

fact that the use of existing University property would reduce costs). Restricted access avoided the need for a comprehensive environmental review. The initial location chosen for the track was near Building 280, a 1000-foot fog chamber originally used for testing cockpit configurations for landing aircraft in foggy conditions. The track itself went through an open field and ended at an existing road. This location had the advantage that the bus could use the existing road (Crow Drive) to leave the test track for unpowered tests and as an acceleration strip for higher speed tests. An undesirable feature was the poor quality of the ground in the field, which the A & E contractor (Sverdrup Corporation) advised us would be costly to improve to support the test track.

After preliminary work, including preparation of Building 280 to house the bus and an engineering layout by Sverdrup, RFS administration decided to move the track to a new location because of plans to develop RFS into a commercial research park. The move negated most of the work that had been done, with the exception of some track construction details, but had the advantage of a better building (Building 167) and solid ground for the track, which would now run down Crow Drive. Since the track was being placed in an existing road, the construction process more closely followed the process that will be used when an RPEV system is installed in a public facility. Two disadvantages of the new location were that the bus could no longer leave or enter the test track at a high speed and the track would have to go through a line of trees. Figure 4.2 is a photo of the track site taken from the tree line looking east before construction began.

After the final site had been determined, the track design could proceed in earnest. This process took longer than anticipated due to the complexity of the design. Sverdrup's construction documents had to be reviewed by SCT several times, and SCT had to supply particulars to Sverdrup concerning conduit size and location, vault spacing, and electrical conductor size and type. The result was a fairly complete set of construction plans. The final plan called for the track to have two segments: one using aluminum bus bar conductors and the other using 350 MCM aluminum cable. Both would use the same type of inductor module, but because the maximum available length of bus bar was 40 feet that segment required more in-ground connections and thus more vaults than the cable segment.

#### 4.1.2 Segments

To better simulate a complete RPEV system, the RFS test track was designed with two separate segments that can be powered individually or together. The original



Figure 4.2 Test track site prior to construction. Photo is looking east

plan was to be able to switch one segment off and the other on as the bus moved from one to the next. Two powered “bus stops” were also included with one stop powered from each segment. As mentioned above, different conductors were used in each segment, and this created slight differences in the configuration of each segment.

The bus bar segment, because of the length of the bus bars, was made up of five separate sections, each 37.5 feet long with an in-ground vault between sections. The vault provided access to the electrical connections between each section.

The cable segment had no length limitations imposed by the conductors, but one connection point near the midpoint of the track was left for conductor transposition and connection to the bus stop. This resulted in a segment with two sections with nominal lengths of 80 and 120 feet.

#### 4.1.3      Vaults

The **inground** vaults used for electrical connections between sections of a segment, bus stops, and the power distribution system were cast in place and were different sizes for the cable section and the bus bar section. Because of the location and size of the openings required in the vault walls and the limited number of vaults being used (thirteen overall) cast-in-place vaults seemed to be a more economical solution than having vaults precast. At the time the specifications were made, we thought that two vault sizes were needed due to the different connection requirements of the cables and bus bars. Hindsight showed that a single size precast vault would have been a more prudent solution, both financially and physically.

One of the earliest issues encountered with the vaults was induction heating of the vault lid by the roadway cables. Lab tests had shown that steel lids might not be acceptable, so we decided to use aluminum. This posed a problem because standard vault lids are not made in aluminum (and the lids had to be quite strong to carry the **20,000-pound** loads imposed by the rear axle of the bus). Sverdrup thought they had located a foundry that was willing to cast aluminum lids to match standard vault dimensions and thus specified the two vault sizes used at **RFS**.

When it was time to order the frames and lids, two problems emerged. The foundry backed out, and the cast iron lid frames turned out to be quite bulky and expensive. Because construction of the track had already begun, it was not feasible to change the vault sizes to take advantage of other vault lid alternatives and we decided to fabricate lids and frames ourselves. This process turned out to be fairly simple and cost less than any other alternative, but in a few vaults, the frames were warped so the lids rocked and were hard to seal.

The frames that were cast into the vaults were welded from **1 1/2 x 1 1/2 x 1/4-inch** steel angle by the welder on the RFS facilities staff and the lids were pieces of **1 1/4** inch thick **6061-T6** Aluminum Alloy ordered cut to size from a metal distributor. The only modification needed to the lids was a **1/2-13** threaded hole in the center of the lid to allow a screw eye to be inserted when the lid was removed from a vault. These simple lids and frames have proved durable and easy to remove and install.

### 4.2    Power Distribution

The power distribution system for the RFS test track consists of a power conditioner, transmission lines, and wayside equipment (compensation capacitors, capacitor cooling system, junction box, and instrumentation). There is additional equipment

associated with the segment switching system-high current solid-state switches and vehicle detection hardware.

#### 4.2.1 Power Conditioner

The initial plan for the RPEV track at RFS was to purchase a new power conditioner that would be capable of segment switching and would operate at a single frequency of 400 Hz. Due to budget constraints, this idea was shelved and the variable frequency (160 – 440 Hz) power conditioner from Translab continued in service. This power conditioner is a versatile machine with plenty of power for the RFS installation, but was not designed to accommodate segment switching. A design for the power distribution network was formulated that offered a possibility of segment switching with the old power conditioner. The concept was a long shot, but required minimal incremental cost, so we implemented it. Due to the harmonic content of the power conditioner output, this plan did not work and segment switching was abandoned for the current phase of work.

#### 4.2.2 Static Switching of Segments

To provide maximum flexibility during testing, the ability to power any segment (cable segment, **busbar** segment, or indoor static charger) is required. In addition, it must be possible to power both segments of the test track simultaneously. Hardware that achieved these requirements was designed, fabricated, and installed successfully.

The first junction for splitting power was constructed at the power conditioner output. Five aluminum bus bars were drilled and tapped to accept the 2-hole connectors used on the conductors. The positive and negative sides of the power conditioner, the indoor track, and the outdoor track were each connected to a separate bar. Using jumper bus bars to connect the power conditioner bus bars to either the indoor or outdoor track, it was possible to power either track and to switch between them fairly quickly.

At the equipment pad, the power was again split to the east and west segments. A system of bus bars closely resembling the indoor junction was constructed with additional space to bolt on conductors **leading** to capacitors that can be connected in parallel or series with either or both test track segments.

### 4.2.3 Dynamic Segment Switching

Losses in the open roadway are the single largest component of total system losses and must be minimized. The best way of doing this is to de-energize every segment unless there is a vehicle drawing power from that particular segment. This switching of segments, while the system is energized is referred to as dynamic segment switching or simply segment switching.

#### 4.2.3.1. Power Hardware

It was possible to connect the segments to the power conditioner by using jumper bus bars, as described above, or by solid-state switches that were triggered by the detection loops.

Unfortunately, due to a resonance between the power conditioner and the roadway, it was impossible to use the switches. The connections were then made so the east and west segments were wired in series with the capacitance. The series connection compensated the voltage across the segments and allowed the power conditioner to power both segments without hitting voltage limits on either the power conditioner or the transmission line cables.

Also included in the power cabinet was a fluid cooling system that pumped ethylene glycol through the capacitors and switches to prevent their overheating. Safety switches on the capacitors triggered by overheating were connected to an emergency cutoff switch for the power conditioner.

#### 4.2.3.2. Detection/Communication System Concept

Segment switching or supplying power to a roadway segment only when there is an RPEV on that segment is highly desirable in an operational system. Segment switching reduces the system's environmental impact because each segment of roadway is powered for a relatively small fraction of time and greatly improves system efficiency by eliminating the conductor and core losses in unused roadway segments.

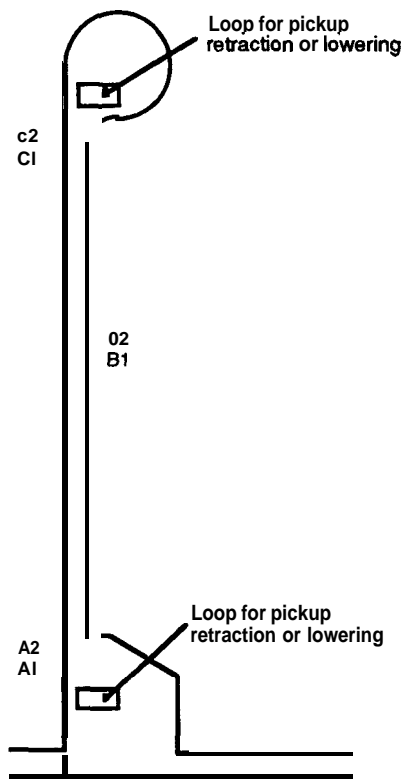
The vehicle should also be able to automatically lower the pickup inductor when it enters the electrified portion of the roadway and retract the pickup inductor when it leaves. The higher clearance minimizes the risk of hitting an obstacle.

Automatic segment switching and pickup lowering/retraction require communication between the roadway and the RPEV. The segment-switching system should respond to the vehicles' presence near the ends of an electrified roadway

segment. A vehicle-mounted transmitter or transponder transmits the vehicle signature (code) to a wayside receiver. A simple and inexpensive logic system can be used to convert the signals received at the detection points to appropriate roadway segment-switching commands. A transmitter or transponder transmits the appropriate signals for lowering or retracting the pickup to the vehicle at the ends of the electrified roadway segments. Methods of transmitting a signal from the roadway to the vehicle or vice versa, include optical, infrared, radio-frequency (RF), and magnetic sensors. The need for a clean transceiver surface limits the utility of infrared and optical scanning systems.

#### 4.2.3.3 Detection/Communication System Hardware

The presence and travel direction of the vehicle is detected at three locations on the test track (see Figure 4.3). At locations A and C, the vehicle turns the west and east segments on or off depending on the direction of travel. At location B, the vehicle simultaneously turns on the segment ahead of it and turns off the segment behind it.



5544 05/03/93

Figure 4.3 Detection/ communication system hardware

Figure 4.4 shows a high-level circuit diagram that includes various components of the segment switching system. Here we describe the role of each component in the system. Detector Systems, Inc. supplied all of the following components except the segment switching logic system.

Preformed inductive loops. Inductive loops are commonly used for automatic control and coordinating of traffic lights. These loops are permanently installed two to six inches below the road surface. When a vehicle passes over the loop, the loop inductance changes. The inductance change is used for detecting the vehicle's presence. An inductive loop consists of a number of turns of insulated stranded copper wire laid on top of each other in a loop slot. The number of turns and the area of the loop are dependent on the width of the traffic lane and the type of detection equipment accommodated.

The inductive loops we used for segment switching are functionally identical to those used for traffic applications. Eight loops were installed beneath the surface of the test track, six of which were used for segment switching. These loops are all preformed, that is, the wire turns are fully enclosed in PVC pipes, which makes installation much easier. As shown in Figure 4.3, the segment switching loops are installed beneath the detection areas A, B, and C. As the vehicle passes over the loops in each area, the vehicle changes the inductance of one loop before it affects the inductance of the other. The travel direction is determined by the sequence of inductance shifts. This function is performed by the directional logic units. One of the inductive loops serves as the receiving antenna for the identification signal of the vehicle in addition to its detection function. The identification signal is detected by the **pre-empt** detector. The identification signal is continuously transmitted from a transmitter mounted beneath the RPEV.

loop detectors. One of the adjacent loops in each detection area is connected to a loop detector. The other loop is connected to a **pre-empt** detector. The loop detector digitally measures changes in the resonant frequency of the loop network, which changes with the loop inductance. This is accomplished by providing an excitation voltage to the loop and then continuously monitoring for changes. The excitation frequency is switch selectable in the range of 25 to 65 KHz. Based on successive measurements of the loop frequency and its sensitivity setting, the loop detector makes decisions on whether or not to generate a "call signal." The sensitivity can be adjusted by a knob located inside the unit. When adjusted for highest sensitivity, a call signal is generated when the inductance changes by 0.04 percent or more. At the

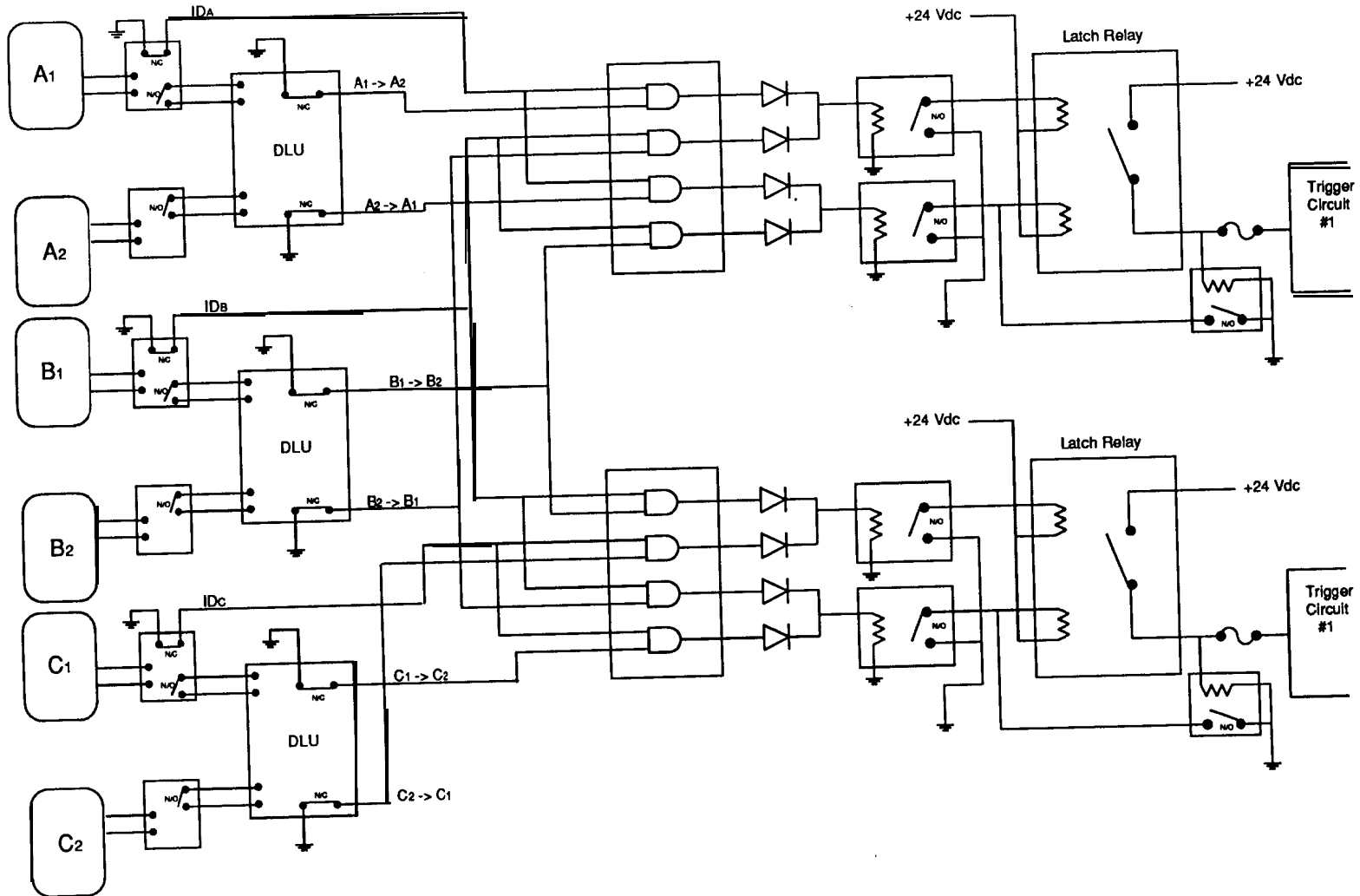


Figure 4.4 High-level circuit diagram that includes various components of the segment switching system

call signal is generated when the inductance changes by 0.04 percent or more. At the lowest sensitivity setting, a call signal is generated when the shift in inductance is 0.64 percent or more.

**Pre-empt detector.** In addition to the inductance signature, a pre-empt detector detects the identification (ID) signal of the vehicle. The ID signal is transmitted continuously from a vehicle-mounted transmitter. This signal is received through the inductive loop connected to the pre-empt detector. As shown in Figure 4.4 a pre-empt detector provides two output signals (relay closures). The contactors of one of its output relays close in response to inductance change. The contactors of the other output relay close when the transmitted code matches with the preset code of the detector.

**Directional logic units.** The directional logic units (DLUs) are used for identifying the vehicle's travel direction. As shown in Figure 4.4, the inputs to a DLU are the presence signals (relay switch closures) of two presence detectors, in our case generally a standard loop detector, and a pre-empt detector. One input occurs before the other as the vehicle passes over the adjacent inductive loops. The DLU determines the input that occurs first and identifies the travel direction by activating one of its two output relays.

**Switching logic unit.** The switching logic unit (SLU) is the only component of the segment switching system that was completely designed and built by SCT. As the vehicle enters the east segment, the direction signal A1-A2 and the identification signal IDA are applied to the SLU. These inputs are converted to a command signal that applies a triggering voltage (24 Vdc) to a power contactor intended to turn the east segment on. As the vehicle leaves the east segment the direction signal B1-B2 and the identification signal IDB are applied to the SLU. These inputs are converted to an off signal that commands the east segment off. The same inputs are converted to an on signal that commands the west segment on. As the vehicle leaves the west segment, the IDC signal and the C1-C2 direction signal are converted to an off signal that commands the west segment off. The logic is executed in a reverse sequence as the vehicle travels west to east.

The system includes two identical circuit modules. the output of circuit module 1 is the appropriate command for switching the east segment on or off. Circuit module 2 provides the appropriate commands for switching the west segment. In each circuit module, a solid-state timer eliminates the possibility of failing to de-energize a segment after the RPEV has departed. This unit starts timing when a segment is energized. It resets when the segment is turned off. If the segment does not de-

energize at the end of the pre-set period (perhaps one minute), the timer sends an off signal and the roadway segment is commanded off, and the timer resets.

**Vehicle-mounted transmitter.** This transmitter is mounted on the underside of the vehicle forward of the front wheels and behind the front bumper. The mounting height is about 10 inches above the pavement. The transmitted signal is pulse code modulated and the radiated power complies with FCC regulations for unlicensed operation. The transmitted code includes 9 bits. It is preset by the manufacturer and can not be altered. The carrier frequency is 375 KHz. The transmitter draws about 100 mA at 12 VDC.

#### 4.2.4 Compensation Capacitance

Power factor correction capacitance can be used to adjust the power factor of the roadway (either open or when coupling power) from highly inductive to near unity if desired. Since the power conditioner is designed to drive into a highly inductive load, it is not always desirable to have unity power factor. When two segments are energized, use of power factor correction capacitance offers the opportunity to reduce the transmission line (and power conditioner) current and/or voltage.

Adding series capacitance reduces the system voltage. This is normally done when both segments are connected in series. The capacitance effectively compensated for the voltage of one segment, keeping the power conditioner voltage to 500 volts instead of 1000 volts.

Parallel capacitance reduces the current drawn through the transmission line, although the voltage remains at the nominal value. The unsuccessful attempt at segment switching involved using parallel compensation capacitance to reduce the current drawn by a segment to about 200 – 250 amps instead of 1200 amps. This brings the current down to the level of economically available solid-state switches. Unfortunately this scheme did not work as the parallel combination of a roadway segment and the power factor correction capacitance forms a resonant circuit of its own. Since the power conditioner output voltage waveform has a small glitch, it excites a wide range of frequencies, and the roadway/capacitor oscillated at its own resonant frequency rather than the driven (power conditioner) frequency.

### 4.3 Roadway Inductor

The roadway inductor consists of two basic components: the inductor modules and the conductors. They are designed to withstand full road loads and require little, if any, maintenance. There are approximately 440 feet of inductor in the test track at the Richmond Field Station.

#### 4.3.1 Roadway Core Modules

The inductor modules used in the roadway at Richmond were manufactured to SCT design by Elma Engineering of Palo Alto, California. These modules are 112 inches long, 20 inches wide, 4.5 inches thick, and weigh about 900 pounds. Approximately 420 pounds of the weight is in the silicon-iron laminations that make up the operational part of the core, while the other 480 pounds come from the epoxy/sand mixture protecting and supporting the laminations. Figures 4.5 and 4.6 show the cores under fabrication.

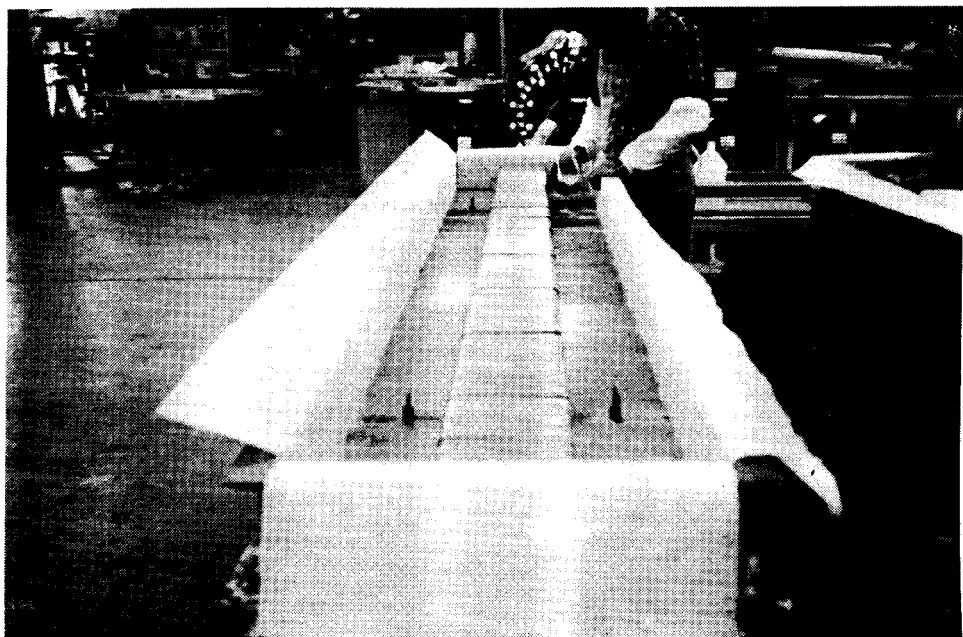


Figure 4.5 Placing core components into molds

##### 4.3.1.1 Magnetic Design

The configuration of the laminations in the core modules is shown in Figure 4.7. The poleface laminations are oriented vertically and run parallel to the short side of

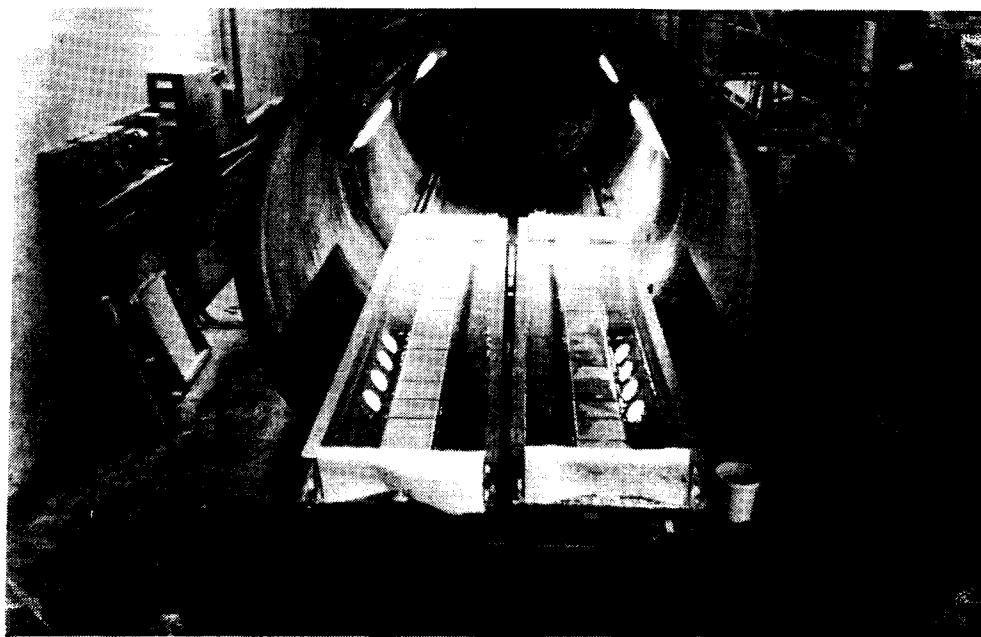
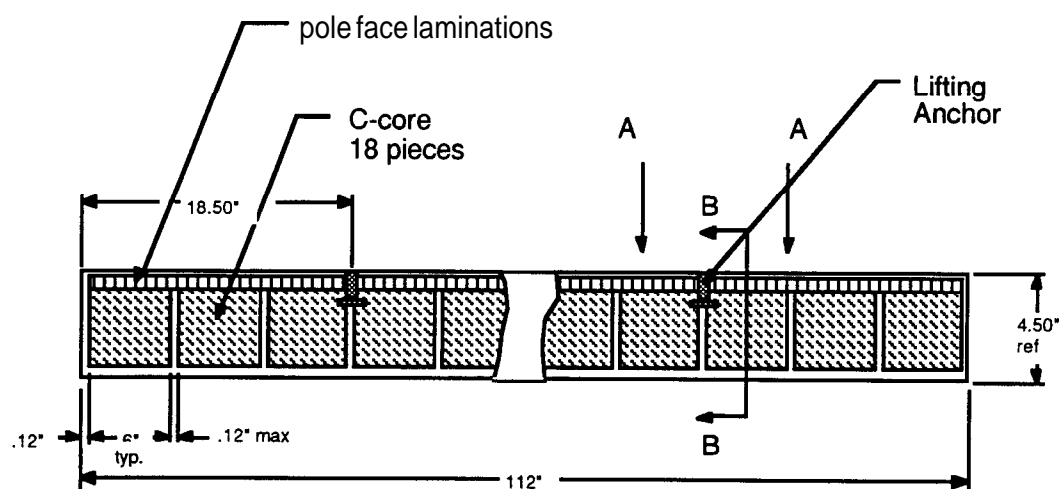


Figure 4.6 Roadway module being loaded into oven/vacuum chamber



5544 10/24/91

Figure 4.7 Configuration of the laminations in the core modules (side view; not to scale or proportion)

the module. The C-core is one-half of a standard tape wound transformer core and is wound from .012 inch thick (12 mil) grain oriented silicon-iron transformer steel. The polefaces are made of a similar material 14 mils thick and have the grain oriented perpendicular to the conductor slot. This design uses two standard transformer laminations and minimizes cost of the cores. It is also quite effective at shaping the magnetic field.

#### 4.3.1.2 Mechanical Design of Modules

The roadway core modules were designed with several, often conflicting, objectives in mind. They must hold the cores and conductors in the proper locations with the appropriate tolerances. They must be able to withstand various mechanical loads, including both vehicular traffic and thermal cycling. The modules must be sealed well enough that these mechanical loads will not create cracks which would allow the steel laminations in the cores to corrode. Cost of both manufacture and installation of the modules is very important, as the cost of the roadway inductor is the single biggest cost in the system.

To ease installation, the core modules are flat on the bottom and have provisions for lifting and supporting them from above. To fabricate these core modules two identical molds were built. The molds were expensive (\$25,000 for both) as they are machined to very tight tolerances, as required for the vacuum impregnation process. The molds were lined with fiberglass mat and the loose poleface laminations were loaded in by hand, the C-core was placed in next, and finally the entire assembly was filled with the sand/epoxy filler and an additional layer of fiberglass mat. The modules were placed in a vacuum chamber to insure penetration of the epoxy to all of the laminations and then oven cured for a strong product. Concrete was considered instead of the sand/epoxy mixture, but it would not have provided as much protection for the cores as the epoxy/sand/fiberglass approach, even though the cost **would** be considerably lower.

The slot in the roadway core module was designed to accept either cable or **busbar** conductors. The electrical resistance of both the cable and **busbar** designs are very similar, although the bus bars are more compact. The slot could be approximately one inch shallower if the cables were not used. (A single module design was used for both types of conductors to minimize cost.)

#### 4.3.2 Conductors

Two different conductors were used in the two segments to compare performance and ease of construction. In actual construction only one type would be used. The total current in each bundle was designed to be the same. After comparing the construction and performance of the two conductors and considering other factors, cable conductors were deemed superior to bus bars.

##### 4.3.2.1 Cables

The cable conductors consisted of 350 MCM aluminum cable (approximately 0.63 inch conductor diameter and 0.77 inch overall diameter) placed in three rows of five cables for a total of fifteen conductors. There was no practical limit to the length of these conductors, but vaults for terminating the segments were constructed to allow for transposing conductors as described in Section 4.3.2.3.

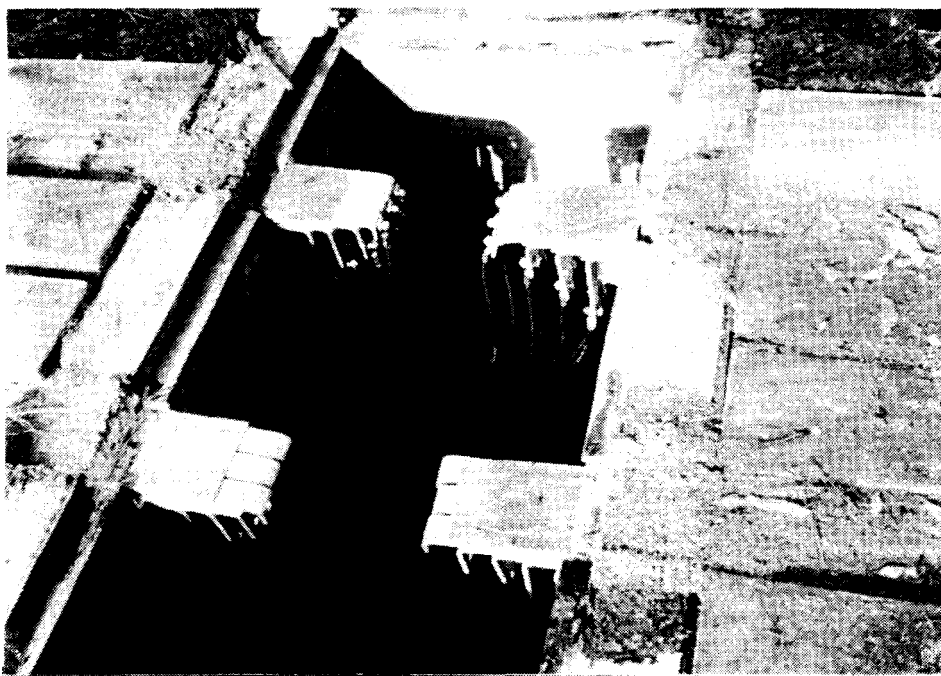


Figure 4.8 Busbar terminations in vault

##### 4.3.2.2 Bus Bars

Aluminum (Alloy 6063-T5) bus bars of  $1\frac{1}{4} \times 1\frac{1}{2}$  inches were used in the east segment of the test track. They were placed in four rows of three for a total of twelve conductors. The bars were bent 90 degrees at the ends, and the bars in each row were bent 2 inches further from the end than the row above, creating a staircase effect

(Figure 4.8) in the vaults. This enabled simple connections between each segment. Each of the five sections was 37.5 feet as the maximum bar length was only 40 feet including bends.

The bars were pre-bent by the supplier, but several bars had to be rebent. Also, because the bars could not be rolled onto a reel like the cables, they had to be delivered in a 40-foot long steel cage on a flatbed truck.

#### **4.3.2.3 Terminations/Crisscross**

Each section of roadway terminated in a vault that allowed connections to be made between adjacent sections or between the segments and the power cabinet at the equipment pad. The vaults also allowed testing of various crisscross patterns for equalizing conductor currents, which is discussed further in Section 5.2.3.3.

The terminations in the cable section required crimping large two-bolt connectors to each cable and fastening them to a fiberglass panel attached to the vault wall. (Figure 4.9). The jumper cables, also with two-bolt connectors, were then bolted to the same panel in direct contact with the other connectors. The jumper cables crisscrossed the connections to create the best current distribution. In vaults #1 and #4 (see Figure 4.1), the cables made a 180-degree turn and went into the other slot without terminating. Ample cable was left in these vaults to add a crisscross if needed, but this proved unnecessary.

The crisscross on the bus bar sections was made by bolting jumper cables directly to the bars, which allowed the vaults of the bus bar segment to be narrower than those in the cable segment as there was no need for panels or for as many connections.

In future projects these connection panels and vaults may be unnecessary. Using cables, it should be possible to **hardwire** the crisscross by actually crossing the conductors-in effect, braiding them-which will create a bulge that can be accommodated in a much shallower, narrow vault.

#### **4.3.3 Mechanical Design of Roadway Inductor**

The roadway inductor consists of modules (nominally 10 feet in length) placed end to end in trenches just deep enough for the top of the core modules to be at the surface of the roadway with a one-half inch layer of grout beneath them (Figure 4.10). Each module represents only one side of the inductive loop so two modules are placed side by side. Expansion joints, consisting of 0.5-inch thick polyurethane foam

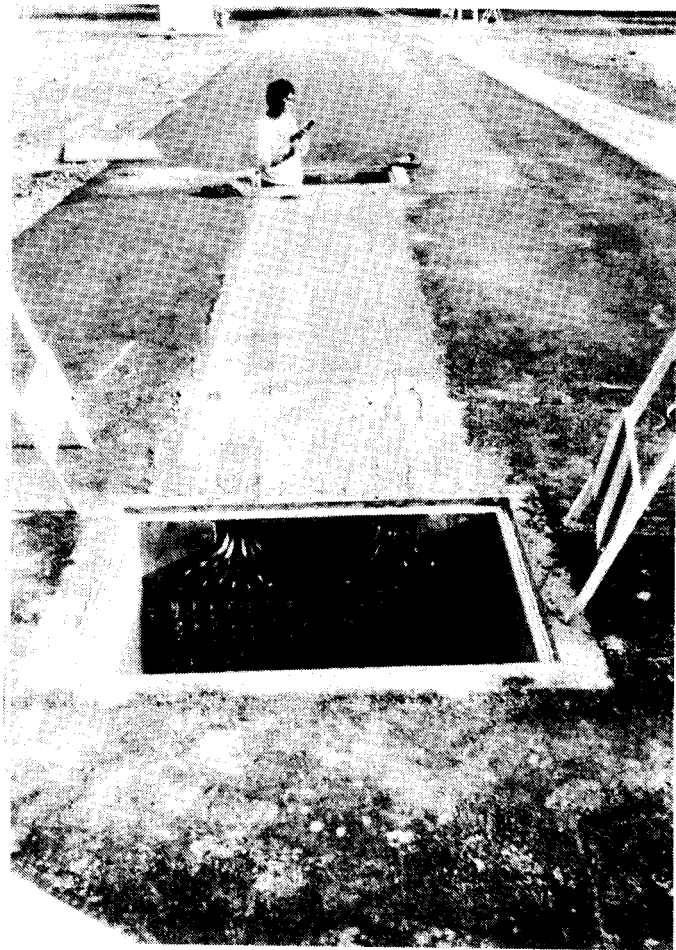


Figure 4.9     Cable terminators in vault



Figure 4.10    Placement of roadway modules flush  
with surface

were placed crosswise between each pair of modules, while the longitudinal gap between them was filled with the same grout that was poured below the module. The conductors were placed into the modules and then potted into place using a mixture of sand and polyester. Considerable time and effort went into the selection of the conductors and the method used to hold them in place while supporting traffic loads. The two primary objectives were to withstand both mechanical and thermal loads, with cost being a secondary (although still important) factor. It was felt that the **busbars** would withstand road loads better than the cables, unless the cables were placed inside conduits, which would increase the size of the slot and also the installation costs. Placing the cables in conduits would clearly resolve the thermal expansion issue, but it was not clear that there would be either thermal expansion or mechanical loading problems with the cables potted directly. Since the strands within the cable spiral, thermal expansion of the cable can be manifested as increase in both length and diameter of the cable. It was a tough decision, but eventually we decided not to use conduits, saving both installation cost and space within the slot. This was a known risk, but the benefit of learning if the minimum cost solution would prove technically feasible was considered worth the risk.

The final step in the installation of the roadway inductor is covering the entire roadway inductor with a slurry seal, approximately  $\frac{1}{8}$ -inch thick. This entire design and installation process (except for application of the slurry seal) was developed and executed by SCT. Caltrans provided technical assistance in the selection of the materials used for potting the inductors, the surface coating, and the expansion joints. Extensive trial and error was necessary to develop efficient techniques for many of the steps in the installation process. Future projects will be constructed much more rapidly at considerably lower cost.

## 4.4 Construction

Construction of the test track at the RFS was the most costly and time-consuming aspect of this RPEV project. The construction process took approximately five months. There was design beforehand and testing and refinement during and after completion.

### 4.4.1 Method

Construction was essentially a three-phase project. Initially, the design and plans were produced by the A&E contractor (Sverdrup). Next, the general contractor

(Overaa) constructed the roadway including trenches for the core modules, and the vaults. Finally, SCT installed the core modules and conductors.

Originally, the entire project, including installation of the core modules, conductors and accompanying power wiring was put out to bid. Because of the unique nature of this project, the bids were all too high (two to three times higher than anticipated). SCT decided to install the core modules and conductors, which reduced the portion put out to bid to essentially a conventional regrading job. Even so, the general contractor encountered difficulties.

#### **4.4.2 Design**

The test track facility design was carried out by Sverdrup Corporation, an A&E firm with experience in the design of automotive test tracks. Because of the unique nature of the RPEV technology SCT had to provide Sverdrup with guidance in some areas, such as transmission line selection, inductor installation, and vault and equipment pad configuration. In addition, the RFS engineer had to be consulted extensively to determine the location of existing facilities, which in many cases were not well documented. This caused some problems as discussed later. Sverdrup's design called for substantial sub-grade work to support the bus axle weight and meet Caltrans standards. In retrospect, these requirements need not have been so strict for a limited-use test track that is not generally accessible to the public. These tight specifications caused some delays and the track was probably over-designed and over-built.

#### **4.4.3 Roadway Preparation and Grading**

The general contractor for this portion of construction was Overaa, who was responsible for removing portions of the existing road surface, removing trees and abandoned telephone poles in conflict with new pavement, constructing the concrete troughs for the core modules, building subsurface vaults, digging trenches to and constructing the equipment pad, burying conduit for instrumentation and power conductors and burying quadruplex cable (power transmission line) between Building 167 and the equipment pad, laying a new drainage pipe under the roadway, and grading and paving the new roadway. Much of this work was performed by subcontractors. The work performed by Overaa was usually executed by one to three workers. One week was spent surveying, sawcutting, and removing the old pavement (Figure 4.11). Several trees and abandoned telephone poles were also removed.

Construction of the concrete troughs and vaults proceeded simultaneously (as did many elements of construction). In total, approximately seven weeks was needed to complete them because of several setbacks.

The first and most persistent difficulty arose during excavation (Figure 4.12) when conduits were discovered at the location of two vaults in the east segment. Sverdrup had overlooked this interference, possibly due to poor documentation. These two vaults had to be redesigned and specially constructed. They were not complete for seven weeks.

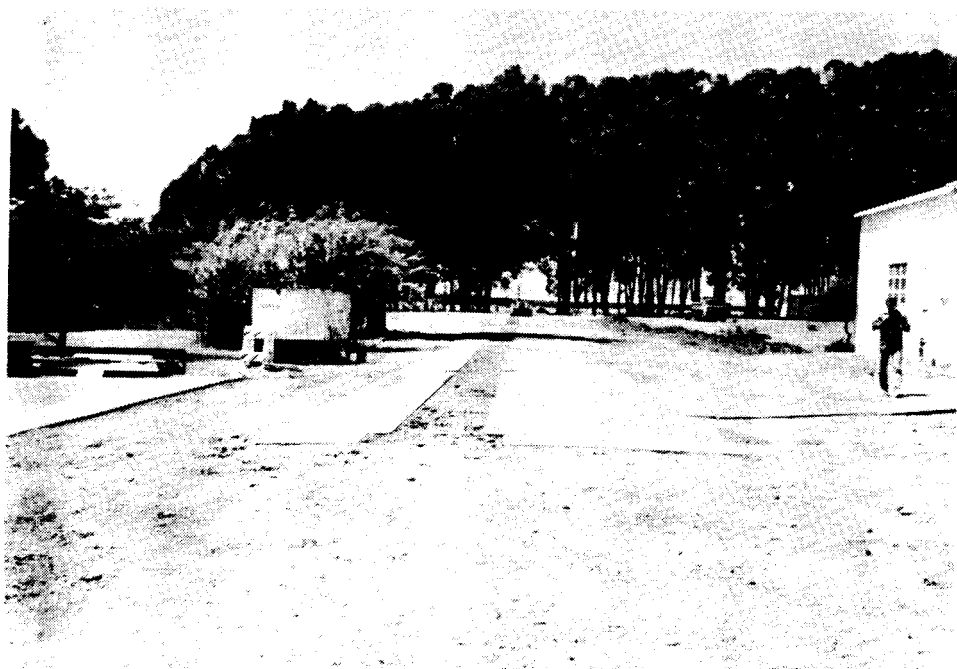


Figure 4.11 Old pavement sawcut and removed

Initially the fill in the bottom of the troughs and vaults failed the 95% compaction test specified in the plans. They had to be deepened, an engineered fill added, and recompacted. Then it was possible to pour concrete for the bottom slabs in the trenches and vaults. Reinforcing bar cages were built by a subcontractor and poured in place with the vaults Figure 4.13.

Building forms for the vaults was a time-consuming process (one week) because one was custom made for each vault. These forms were used once and then demolished. It might have been better to have used precast vaults and lid frames. The frames later caused some problems with sealing the vaults. Figure 4.14 shows a vault form with lid frame.



Figure 4.12 Excavated roadway trough

Setting the forms for pouring the sides of the vaults proceeded when the forms and slabs were complete. After the forms were accurately placed with respect to the future road grade, the concrete was poured, and then the forms removed.

Digging trenches for all the subsurface conduit and conductors slowed when the excavation crew hit water mains on several occasions, (probably due to poor records of existing RFS facilities) and time was needed to repair these. Approximately two weeks were needed to dig the trenches, place the conduit, and backfill. Electrical subcontractors placed the conduit and quadruplex cable.

Excavation, forming, and pouring the equipment pad took several days. Later, the equipment pad had to be raised by adding six inches of concrete because it was under water during the rains. This work was performed by RFS employees. We found after

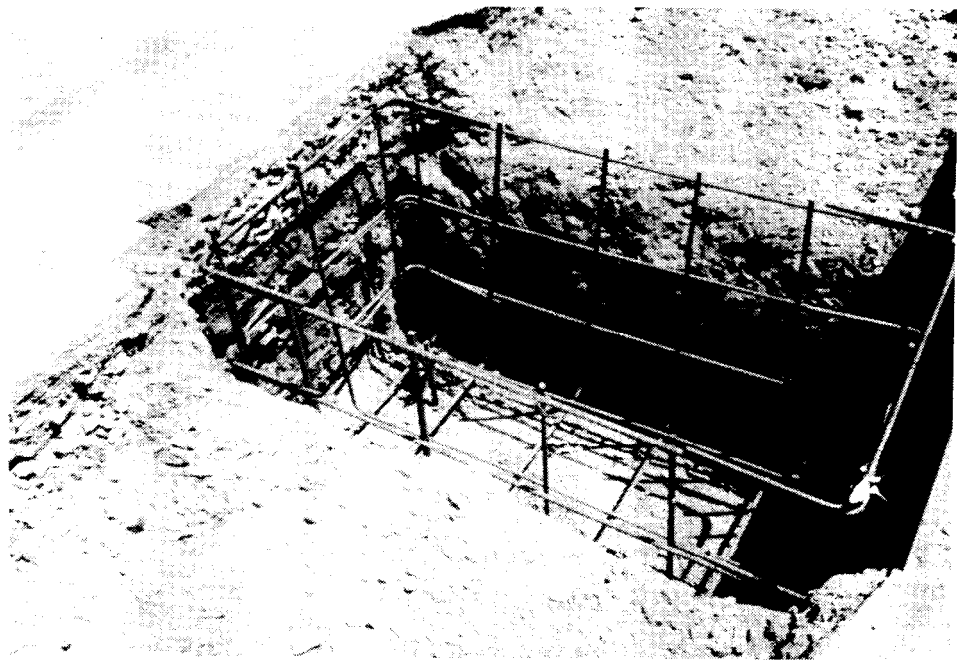


Figure 4.13 Vault wall reinforcement

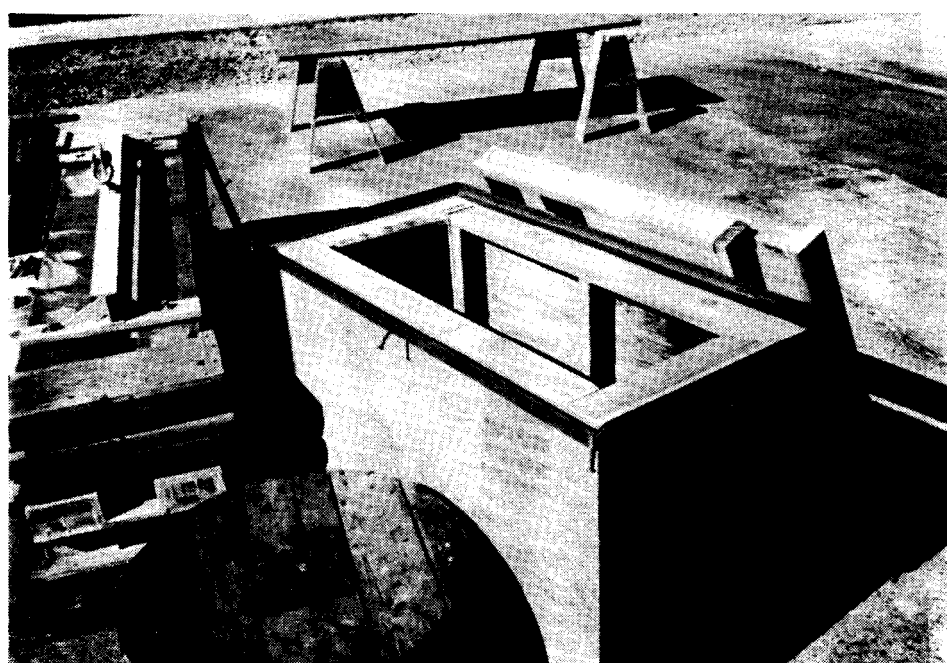


Figure 4.14 Vault form with lid frame. This form goes inside the reinforcements shown in Figure 4.13 and the ground is the outside of the concrete form.

the original pouring of the pad that the conduits, which ran from the equipment pad to the roadway segments, had shifted and had to be cut in order to install the power cabinet.

Placing the new drainage pipe took a week. This involved removing the old, larger diameter pipe and replacing it with two longer, smaller diameter pipes to allow enough cover to support the bus. Also, a precast drain was installed in the road and two concrete headwalls were formed and poured.

Forms were built along the inside edge of the troughs for paving. The pavement and **subgrade** became the sides of the troughs. These forms were also built to be used once and demolished. In a large-scale project, reusable forms would be cheaper and quicker. Forming took several days.

Grading and paving was done by a subcontractor. This involved grading turnarounds at the east and west ends of the track, placing engineered fill for areas that failed the 95% compaction test, and laying asphalt. One section along the troughs had to be removed and repaved because the asphalt was too thick. We thought that the core modules might be too far below the road surface to perform correctly. In retrospect, it seems that this would not have been the case and the module could have been adjusted during installation to account for the deeper slot. This portion of construction took approximately four weeks.

Before the asphalt was laid, the eight PVC detector loops had to be buried in the subgrade. Originally, Sverdrup planned to have the loops placed on the **subgrade** and asphalt laid directly over them. Overaa was concerned that the high temperature asphalt might melt the loops or the roller might crush them. Several workers dug shallow trenches in the rolled aggregate base by hand and buried the pre-formed loops in sand (Figure 4.15). Additional PVC was placed between the loops and the junction box as conduit for the leads.

Paving was finally complete by the middle of the ‘thirteenth week of construction, when the third phase of construction began.

#### **4.4.4 Roadway Inductor Installation**

This phase of the project involved placing the core modules into the roadway, positioning them relative to the road’s surface, grouting them in place, placing and potting the conductors, and terminating all roadway conductors and jumper cables.



Figure 4.15 Laying the detector loops

#### 4.4.4.1 Core Module Installation

Core module placement was a relatively simple procedure involving a crane to lift the modules and two people to guide them into proper alignment. The supplier of the modules provided a special lifting frame that bolted to anchors cast in the module. It took three days to lay all the cores (Figure 4.16).

Originally, we considered placing the cores on shims and pouring grout around them to secure them and evenly bear road loads. After several trial runs, we decided that the shims might continue to bear weight (depending on the shrinkage of the grout during curing), possibly leading to core deformation and cracking under loading. We then developed a technique for suspending the cores from the road surface with 4 x 4s (Figures 4.17 and 4.18).

First, we screwed studs into the anchors in the cores that were lying in the trough. Wood 4 x 4s with predrilled holes were placed over the studs, and the cores were lifted by tightening nuts threaded on the studs. This process allows the modules to be positioned very accurately relative to the road surface, typically within less than  $\frac{1}{16}$  inch. Generally, the disturbances in the road surface were much greater than the positioning accuracy of the modules. A low-viscosity grout was poured between the

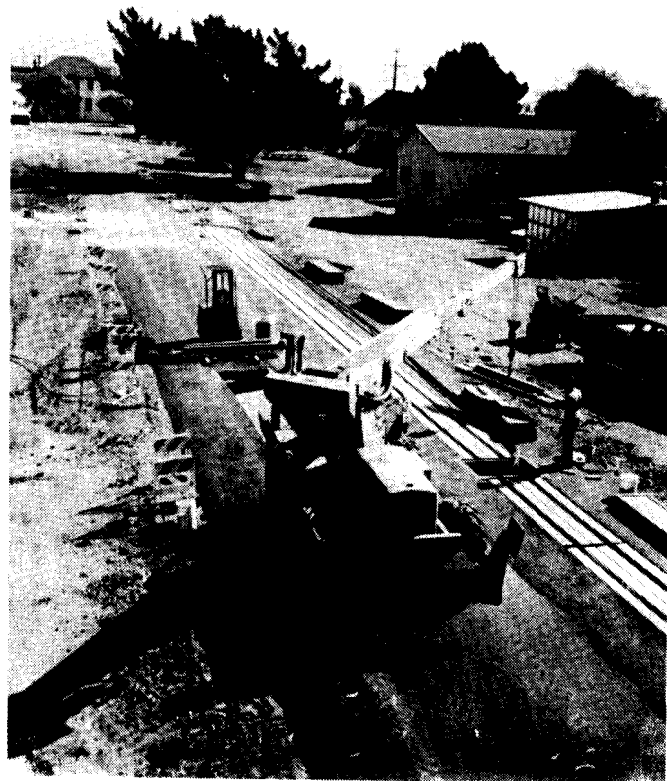


Figure 4.16 Placing roadway cores in the trough



Figure 4.17 Suspending  $\approx$  cores from the roadway surface

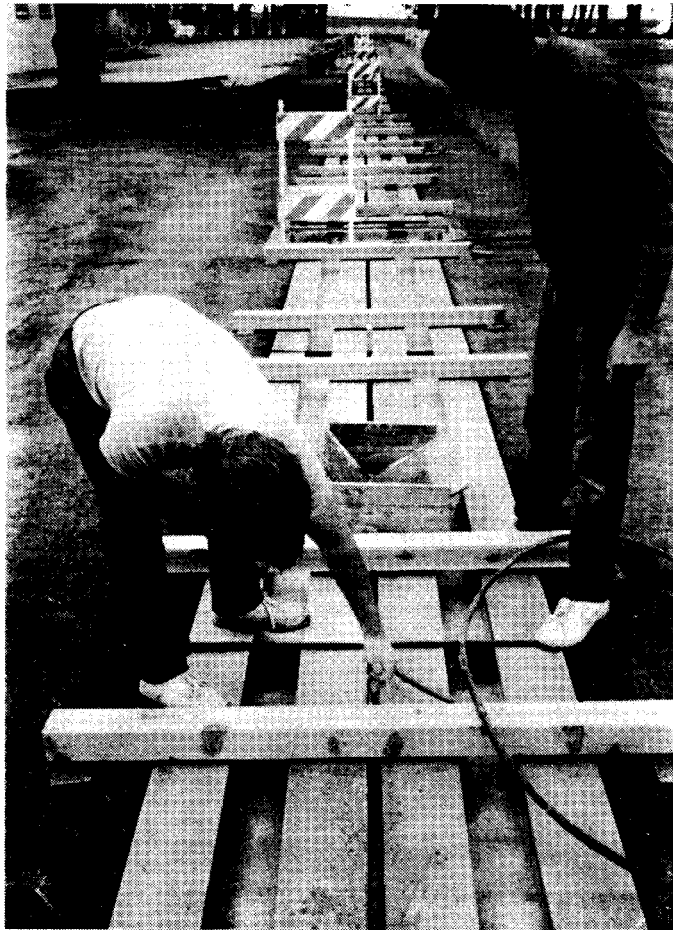


Figure 4.18     Cores suspended at roadway surface

cores (Figure 4.19) and agitated to break up air pockets. Approximately one hour after pouring the grout, the 4 x 4s were removed, ensuring that the grout bore all the load. Expansion joints (made of 0.5-inch foam) placed between sets of cores acted as dams allowing completion of one set of cores before moving on to the next. (Figure 4.20). This portion of the project took five days.

#### **4.4.4.2     Conductor Installation**

Installation of the cables and busbars were similar, but did involve slight differences in the details. For instance before the busbars could be installed, the steel frames of the vaults had to be slotted. (Figure 4.21).



Figure 4.19 Grouting cores

Placing the conductors into the slots involved layering the conductors with fiberglass spacers (chosen for their non-conductance). Several hundred spacers were cut beforehand. The bus bar required fewer vertical spacers than the cables because of their rigidity in the horizontal plane. It was critical to ensure complete isolation of the bus bars because they lacked insulation (Figure 4.22). Later, we found that despite our best efforts, some of the bus bars touched each other, although this did not cause any problems, as it could be accommodated during the transposition of the conductors.

After the conductors were placed, the next step was potting them in with a polyester/sand mixture, which was chosen for its insulation properties and strength. Epoxy was considered because of its lower thermal expansion coefficient but was rejected due to higher material cost.

Before the polyester/sand mixture was poured, the ends of the slots where the conductors enter the vaults had to be sealed, which was difficult. Clay, silicone, and other caulking failed to consistently and completely seal around the conductors. Consequently, when the mixture was poured, some of the polyester drained into the vaults. This left voids in the conductor slots immediately adjacent to some of the vaults. These areas are weaker than other locations in the conductor slot and some started breaking up after several months of use.

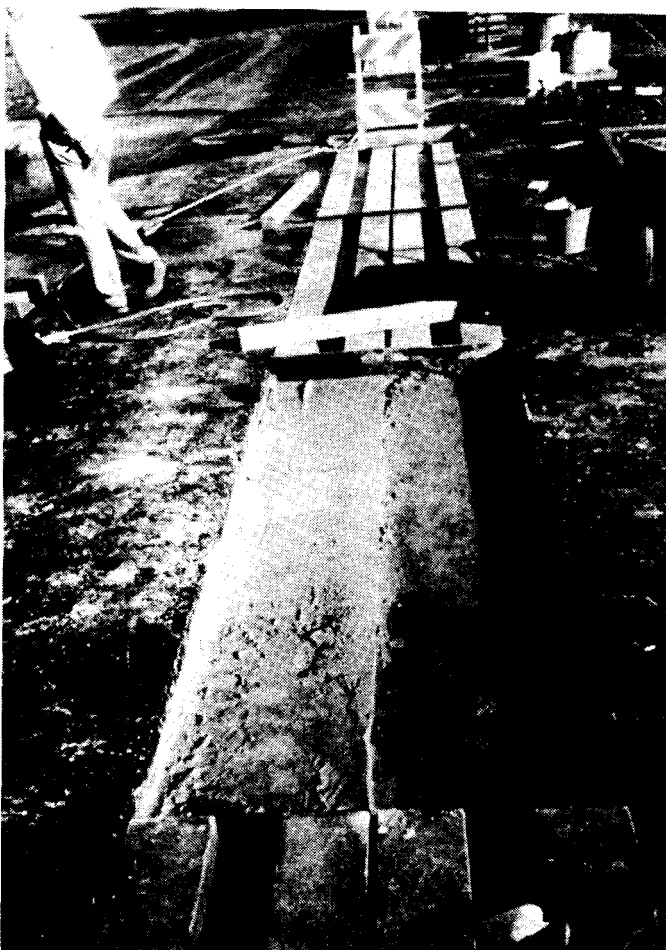


Figure 4.20     Grouting a set of cores

The polyester and sand were mixed in wheelbarrow-sized batches, then poured by buckets into the conductor slots. The mixture was agitated to ensure that it flowed around all the conductors. The sand does not flow nearly as well as the polyester, so there are locations directly beneath the center of most **busbars** which are solid polyester. The polyester shrinks during curing, but not enough to create any cracking in these areas. A one foot section in one of the bus stops was potted with pure polyester to allow the cables to be viewed by visitors. In this area large cracks appeared in the polyester as a result of shrinkage while the polyester cured. Because of the toxicity of the polyester, protective clothing and respirators were worn while the polyester was being mixed and poured (Figure 4.23).



Figure 4.21 Removing vault lid frame in the way of busbar

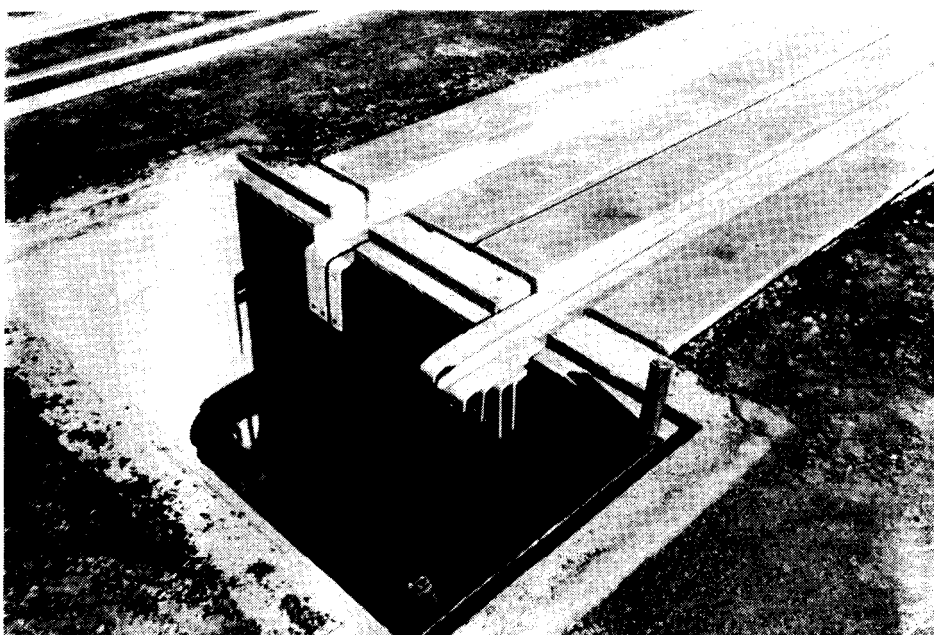


Figure 4.22 Busbars before potting in place (Left slot buses are not completed)



Figure 4.23 Potting busbars in place

In two locations the polyester failed to harden. Polyester is sensitive to proper mixing of the hardener/catalyst (methylethyl ketone peroxide or MEKP), and before proper mixing and quality control techniques were developed, two batches of improperly mixed polyester were made. These two areas were successfully repaired, although the repairs were time-consuming, primarily because of the thoroughly cured potting mixture directly adjacent to (and occasionally directly above) the soft areas.

Eventually, the conductors were all securely potted in. The final step involved wiring together all the sections in each segment and connecting power from the power conditioner to the equipment pad to the segment. (Figure 4.24).

Sealing of some vaults was difficult because their lid frames were not completely flat. This required that the vaults be checked for standing water after rains. The fact that the vaults have solid concrete bottoms prevents any water that runs into the vaults from escaping into the ground. Sverdrup designed the vaults with solid bottoms to prevent ground water from entering the vaults, but this decision should be re-examined on future projects.

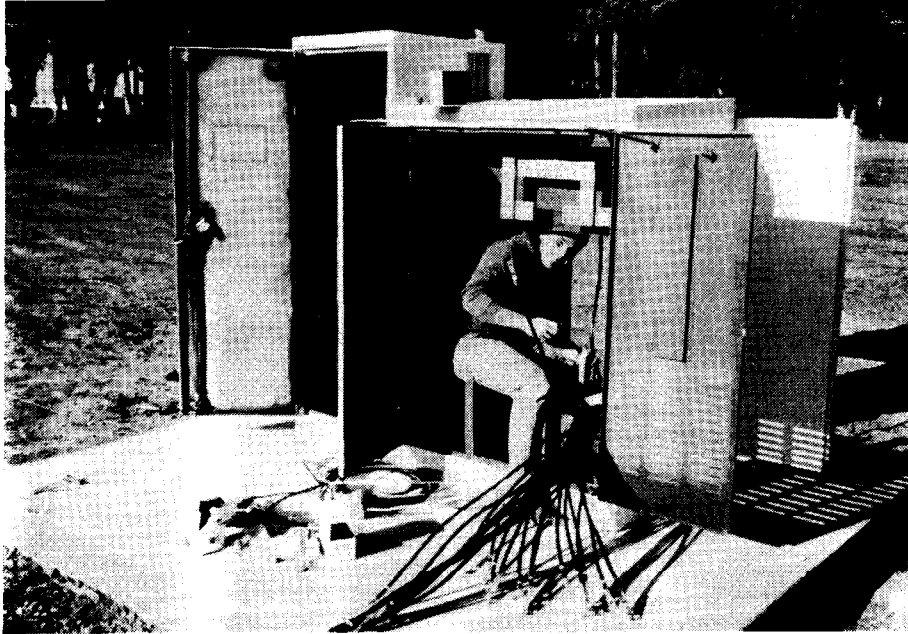


Figure 4.24 Connecting roadway segments to power conditioner leads at the equipment pad

#### 4.5 Instrumentation and Control Hardware

This phase of RPEV development required extensive instrumentation and control hardware to allow for measuring a wide range of variables and to allow for powering various segments independently of one another.

Inside Building 167 an instrument panel was constructed containing meters indicating frequency, power into and out of various sections of the system, and current and voltages in various sections of the system. When we determined that the segments had to be run in series rather than parallel, the meters for measuring current in some sections became redundant and it would have been useful to have voltage meters at these locations.

The meters are powered by transducers that also feed into a data acquisition system run by a 286 personal computer, which enables gathering large quantities of data rapidly to be analyzed later in conjunction with data from the acquisition system onboard the vehicle.

There is also instrumentation in one of the cabinets at the equipment pad. These are duplicates of most of the meters inside Building 167, which enables checking levels

while working outdoors, as the equipment pad is a fair distance from Building 167. The instrument cabinet also houses a cutoff switch for the power conditioner, hardware for operating segment switching, and a pump, radiator, and fan for the cooling system in the power cabinet.

## **5. Testing**

---

This chapter discusses the methods for and the results of testing the inductive coupling system (ICS) and its components. Testing took place on three levels: component, subsystem, and overall system. Component testing allows faulty pieces of hardware to be identified and replaced in a timely and cost-effective manner. Subsystem testing verifies the first level of integration, and system testing provides the best measure of the overall performance and viability of the concept. Testing at all levels provides input to the design process.

The first section of this chapter deals with testing of individual components, such as pickup cores, solid-state switches, and inductors. The next section covers testing of power transfer subsystems, including pickup inductor, roadway inductor, **onboard** controller, and power distribution hardware. The third section deals with accessory sub-systems, such as the steering assistance system and signaling hardware, followed by sections on static testing of the inductive coupling system, dynamic testing of the ICS (**onboard** the vehicle), and vehicle performance with and without use of the ICS. The final section deals with overall performance of the technology.

Testing was generally done at the nominal values of system parameters-frequency of 400 Hz, roadway current of 1200 amps, and coupled excitation of 3.0 volts per foot of core-although sensitivities were measured as well. Data presented in this chapter are at the nominal values unless otherwise specified.

### **5.1 Component Testing**

Testing was performed on most components, especially prototype items, such as roadway and pickup cores. The first objective of component testing is to determine the overall practicality of the part being tested-Will it work? The next step is to determine how well the part works-Do losses match predictions or specifications? Is the acoustic noise generated acceptable? The final aspect of component testing, acceptance testing, is a quality control function to determine if the specific part being tested is on a par with other parts from the same manufacturer. Our acceptance process relied heavily on visual inspection, with spot-testing.

### **5.1.1 Roadway Cores and Core Modules**

Test results for roadway cores were used extensively in the selection of the design ultimately used. Several parameters were tested, including the acoustic noise, losses, reluctance, and mechanical integrity.

Several prototype roadway core modules were built, incorporating variations in lamination orientation, material type and thickness, total build, and filler material. All core types were tested to determine their relative advantages and disadvantages. The objective of building and testing these prototypes was to determine the lowest cost fabrication method while maintaining adequate technical performance. One design was selected for production, and testing of the production modules verified that their performance matched the prototype's

#### **5.1.1.1 Loss and Heating Tests**

Roadway cores losses are a significant contributor to total system losses as many feet of core are excited at any given time. Losses in cores (pickup as well as roadway) are a function of both magnetic induction (flux level) and frequency. In general, losses increase with flux level squared and with frequency to a power of approximately 1.6. Losses can be measured either electrically or through calorimetry.

To measure losses electrically, the total power into a test section of roadway is measured and the conductor losses are deducted. The electrical power is the product of the voltage, current, and the cosine of the phase angle between them. For a highly reactive load, such as the roadway inductor, the phase angle is near 90°. The cosine of an angle near 90° is sensitive to errors in the measurement of the angle. The power conditioner output has a small glitch and is not a pure sine wave, making this method inaccurate even with an extremely accurate phase angle meter.

Calorimetry proved easier and more reliable, although it took substantially longer to conduct experiments. The test core was placed in a thermally isolated container with water to cover the core. A polypropylene or Styrofoam ice chest was used with good results. The core was excited at the desired flux level with a second core and cables that were outside the ice chest as shown in Figure 5.1. All energy lost in the cores appears as heat and is measured by the temperature change of the water and core module itself. This method gave repeatable measurements when the cores were excited at the coupled flux level.

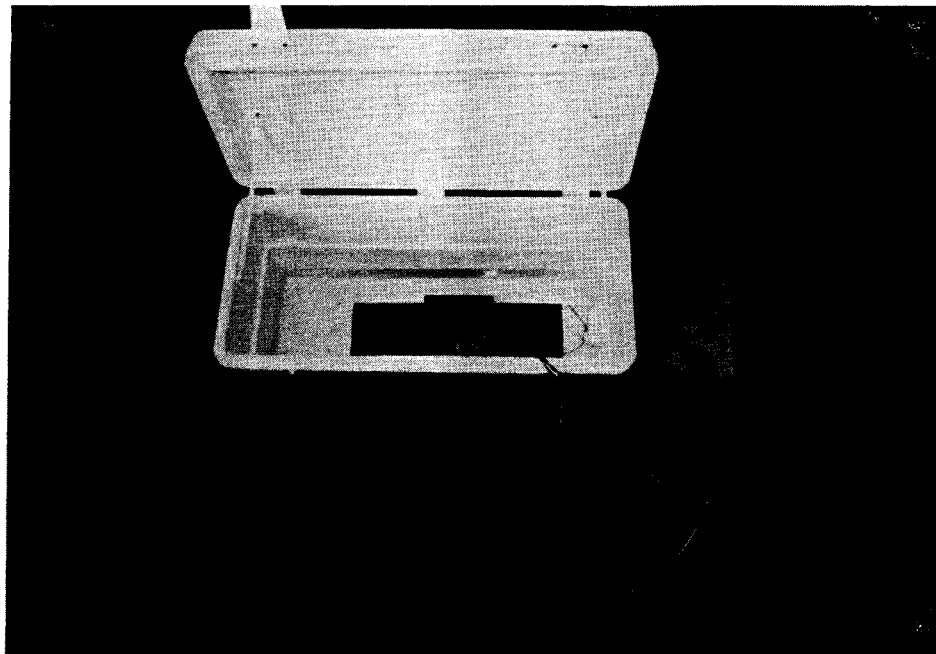


Figure 5.1 Calorimetry setup

Calorimetry tests must run for considerable time to generate enough heat to cause a temperature rise that is large compared to the resolution of the temperature-measuring equipment, which was the major limitation of this test method. Because of the time required for each test, we collected less data than desired.

Measuring open-roadway losses with this method was not feasible because of the extremely long time needed to heat the cores at the low open roadway flux levels. Losses vary with flux level in a known manner, so open-roadway losses can be estimated relatively accurately from coupled core loss data. As shown in Section 5.1.1.4, the flux distribution in the open roadway cores is not nearly so uniform as in the coupled cores, which adds some uncertainty to this calculation.

Losses for five prototype cores are shown in Figure 5.2. Table 5.1 gives the core specifications. All data in Figure 5.2 are per foot of core and should be doubled to find losses per foot of roadway. For all cores, losses increase with excitation voltage as expected. Losses are highest for the National Magnetics core and lowest for SCT's IR&D core, with losses for the three Elma Engineering cores in the middle. The variation in losses can be attributed to the amount and type of material used in the cores, with thinner laminations and thicker sections producing lower losses. The D5 design has the lowest losses of the Elma cores and was selected for the full production run for the Richmond Field Station test track.

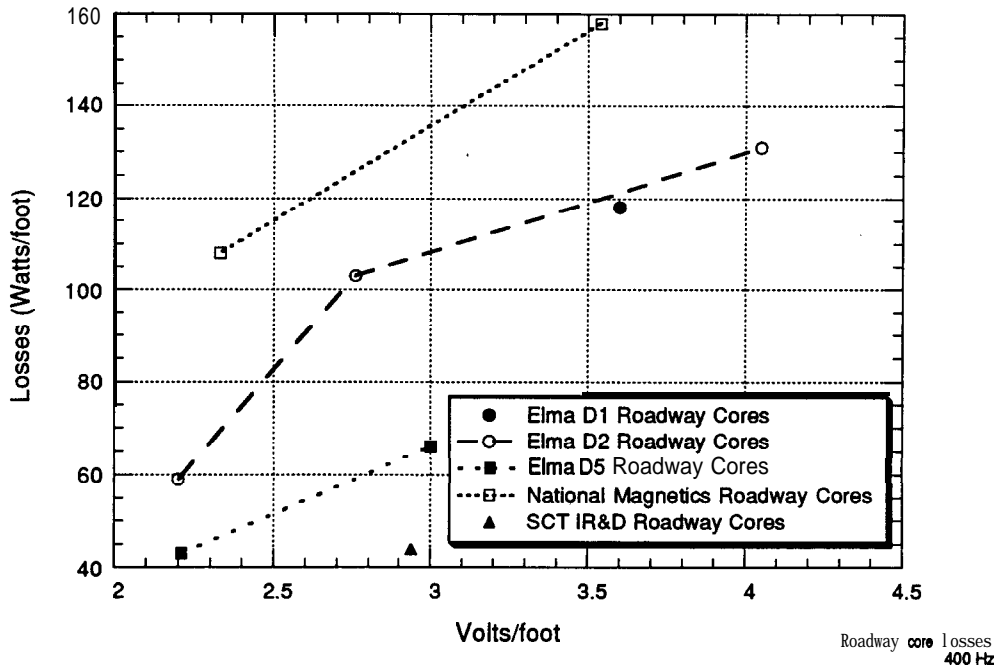


Figure 5.2 Roadway core losses at 400 Hz per foot of core

One prototype core was made with the pole piece laminations oriented in the horizontal rather than the vertical plane, which is much less expensive to manufacture, although the flux in the pole pieces flows from one lamination to the next, resulting in higher (worse) reluctance and higher core losses due to eddy currents. The losses of this core measured at 350 watts/foot at 2.4 volts/foot of core and do not appear in Figure 5.2.

### 5.1.1.2 Mechanical Integrity

It has been assumed that a roadway inductor could be built that will require virtually no maintenance and will last approximately thirty years. To achieve this, the core modules must be completely sealed so that the steel inside the module does not rust. Electrical grade steels have poor corrosion resistance, and sealing the steel from the environment is important.

SCT investigated core modules with epoxy or concrete as the material supporting the steel cores. Concrete is less expensive than epoxy, both for the material and for the casting. Casting epoxy core modules costs more as they are vacuum impregnated and

**Table 5.1**  
**Core Specifications**

	C-Core Build (Inches)	Lamination Thickness (Inches)	Pole Pieces Height (Inches)	Lamination Thickness (Inches)	Tapered Core Build (Inches)	Lamination Thickness (Inches)	Steel Weight (pounds per foot of core)
Elma D1	0.4	0.014	10.0	0.012			57
Elma D2	0.25	0.014	0.5	0.012			36
Elma D5*	0.5	0.012	0.5	0.014			47
SCT IR&D	0.5	0.007	0.75	0.014			59
National Magnetics 3					0.5	0.014	40

\*Prototype for RFS roadway core

require more expensive molds and a long curing period, generally at elevated temperatures. Sand is used as a filler, reducing material costs and warpage that can occur as the epoxy shrinks while curing.

Two aspects of mechanical integrity were checked: module sealing and lifting inserts' pullout strength. The prototype epoxy modules were well sealed, and no voids or cracks were discovered. When the prototypes were scaled up from 12 inches to 112 inches for the production modules, many cores had voids that the epoxy did not completely fill. These tended to be on the upper surface of the cores (bottom surface as cast) and are apparently the result of longer flow paths on the larger modules. Extra care during the final finishing process eliminated the voids. The production modules also had a tendency to warp slightly during curing. On nearly all modules, the center of the module is approximately  $\frac{1}{8}$  inch below a straight line connecting the ends of the module, which is out of the production specification, but was determined to be acceptable. A more significant defect on several of the production modules was a vertical crack along one side, generally near the middle due to epoxy shrinkage during curing. These cracks were patched and apparently were not deep enough to cause structural weakening as no additional cracking was detected during installation.

We were concerned about the pullout strength of the inserts for attaching a frame used while handling the modules. Testing at Translab showed that the pullout strength was 3000 pounds for the 0.375-inch insert used on the prototypes. The production modules were fitted with 0.5-inch inserts that have substantially higher strength, even though the static loading on the inserts is only several hundred pounds each when the module is being lifted. The load can be significantly higher during lifting due to dynamic effects.

Effective sealing against corrosion is the mechanical issue of most concern for the concrete modules. Unlike the epoxy modules, the steel in the concrete modules is not covered with fiberglass during casting. The cores have a coating of polyester or epoxy a few thousandths of an inch thick when delivered from the factory, which is not adequate protection. Two concrete modules were made. One was placed in the test track after a fiberglass-reinforced polyester coating was added to part of the exposed surfaces. This module has no corrosion in the protected area approximately two years after installation, even though the slurry seal was not applied to the bus stop where it is located. The second core module was not coated, and surface rust appeared within several months, although this module is not exposed to traffic.

Lifting inserts in the concrete modules are attached to rebar, so they will not pull out of the module.

#### **5.1.1.3 Acoustic Noise**

Acoustic noise is one of the potential drawbacks documented at Translab during a earlier phase of the project. Acoustic noise is affected by numerous factors, but primarily by the component's mounting. Roadway cores are literally cast in concrete when they are installed in the road, which tends to minimize any noise they may create. Nonetheless, acoustic tests were performed on the prototype roadway core modules. Acoustic testing in the breezeway at Translab was complicated by the proximity of the test area to the power conditioner and series reactor, which were located 15 – 20 feet away. To minimize interference from the power conditioner and coil, a small acoustic isolation chamber was constructed within the Translab breezeway that was relatively effective in preventing ambient noise from influencing the test results.

Another potential noise source was vibration of the roadway cables. A one-foot section of roadway was built to address the issues associated with proper attachment of the roadway cores to the road itself as well as cable vibration. The prototype core module was grouted and sealed into the roadway slot within the breezeway. The cables were potted into the core module with epoxy. When the roadway was excited with the nominal excitation current, sound levels within the acoustic isolation chamber were extremely low and appeared to be noise from the power conditioner. The core's noise was faintly but distinctly audible at a height of less than six inches above the road surface and had a different character from the noise within the isolation chamber at greater heights.

These tests provided convincing evidence that the roadway cores and cables would not create unacceptable acoustic noise.

#### **5.1.1.4 Magnetic Flux levels**

The magnetic aspects of the RPEV system were modeled using the POISSON analysis program, which is used to predict open roadway, mutual, and leakage inductances as well as magnetic flux levels in both the open and coupled conditions. This program has proved valuable in earlier phases of the project. Figure 5.3 shows flux lines for the open roadway. Regions where the lines are close together, such as near the conductor slot, indicate areas of high flux density. Clearly, flux densities drop off

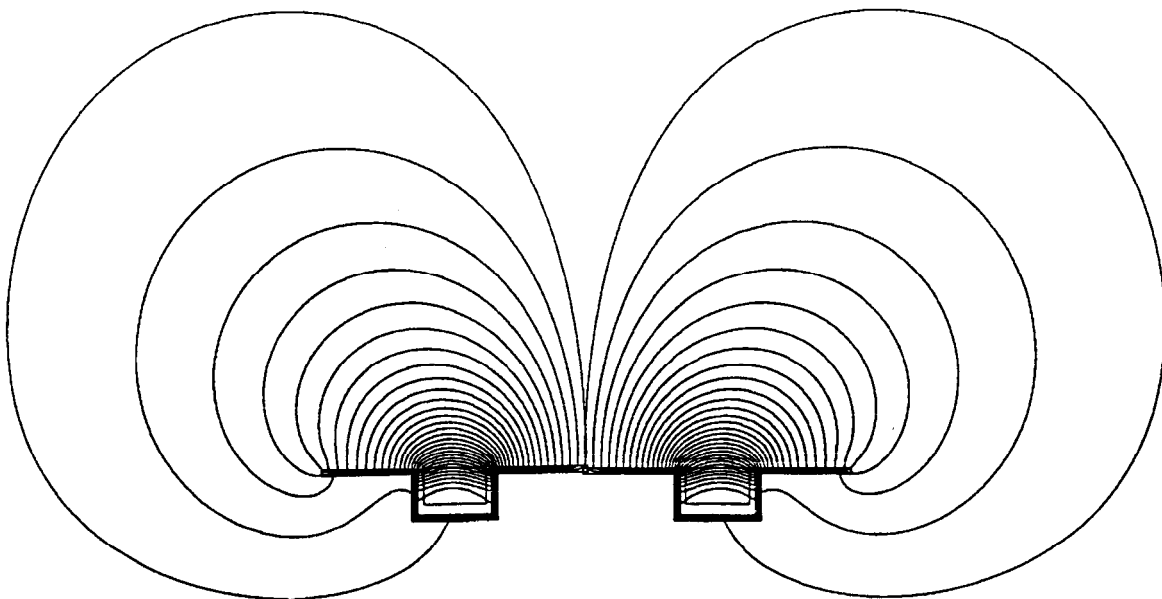
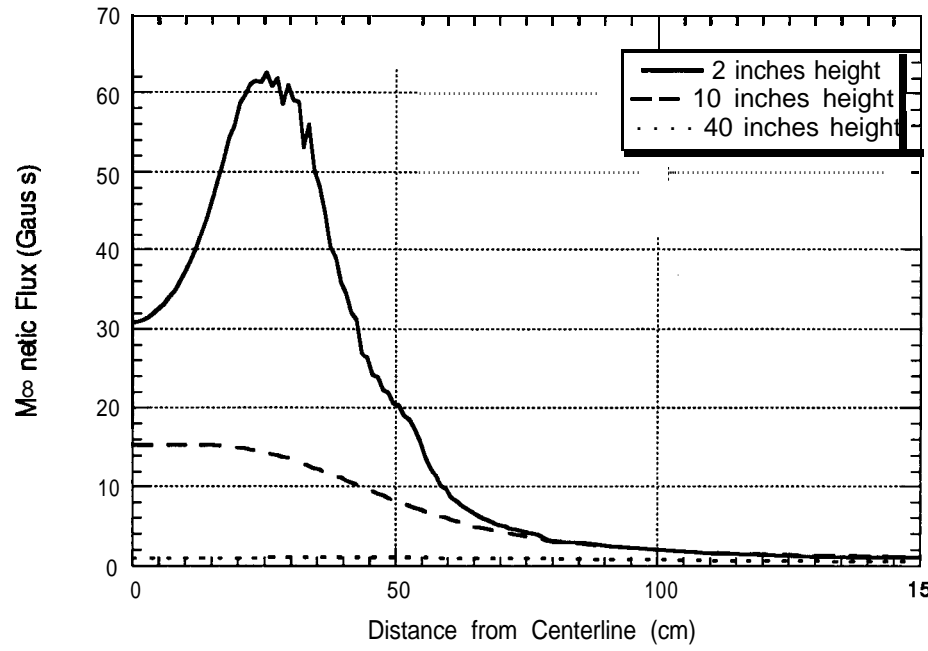


**Figure 5.3** Open roadway lines of flux, full symmetry

with distance from the roadway centerline, both vertically and laterally. Figure 5.4 shows predicted values of flux density at heights of 2, 10, and 40 inches above the roadway. Figure 5.5 is a detailed map of the flux density as measured 0.5 inch above a 12-inch long prototype roadway core module. Each line presents flux density versus lateral offset with measurements taken at a constant distance from the end of the core module. All curves drop as the distance from the slot increases. Near the outer edge of the cores (7 inches), fringing creates a flux concentration. Flux densities are highest for the lines with solid dots at 0.5 inch from either end of the core due to fringing at the ends. The fields drop off moving toward the longitudinal center of the core until the curve for 6.5 inches, which is near the center.

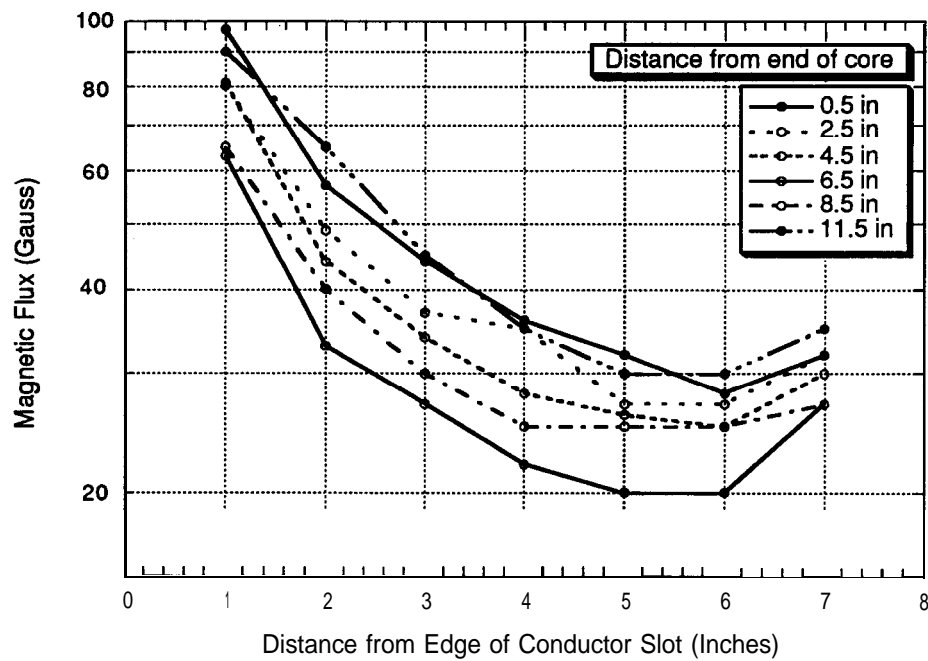
### 5.1.2 Pickup Cores

Results of tests on the prototype pickup cores guided specification of the production cores. Tests were conducted to determine losses, reluctance and fringing, mechanical properties, acoustic noise, and magnetic flux distribution.



B24-Gee

Figure 5.4 Predicted values of flux density



RFS0-046

Figure 5.5 Map of flux density

### 5.1.2.1 Losses and Heating Tests

Three prototype cores were made: two by National Magnetics and one by Elma Engineering. A fourth core, made of spare pieces of SCT's IR&D roadway core, was included in some tests. The National Magnetics cores are a single-piece design made of 0.014-inch M6 steel one with a total thickness of 0.5 inch and the second with a total thickness of 0.7 inch and taper uniformly along the length of the pole face. The Elma Engineering core is a three-piece design and cast in epoxy. This design makes less efficient use of the steel and is heavier for the same losses or, conversely, has higher losses for the same weight. In roadway modules, a weight penalty is of no concern, but on the vehicle the extra weight is undesirable.

Calorimetry was used to determine the pickup core losses. The process was somewhat faster than with roadway modules since pickup cores do not have the substantial mass of filler material that the roadway modules do, which reduces both the heat capacity and thermal time constant.

Pickup core losses are shown in Figure 5.6. The Elma core has the highest losses. Losses in the two prototype National Magnetics cores are similar, with the thicker one having slightly lower losses, approximately inversely proportional to the amount of material. Two changes were made for the production pickup cores: using 0.007-inch M2 steel instead of 0.014-inch M6, which reduces losses approximately 30%, and modifying the taper. Fringing caused the outer edges of the pickup cores to heat up more than the rest of the core because the edges operated at a higher flux density as seen in Figure 5.7. Twenty percent more laminations were placed in the outermost bundle to handle this extra flux and to impart more rigidity to the tips of the pole face. These changes reduced losses and resulted in more uniform heating of the pickup cores. Total weight remained the same as the 0.5-inch prototype core.

### 5.1.2.2 Reluctance and Fringing

Reluctance, or magnetic resistance, is an important characteristic for any magnetic circuit, although it is less important for the RPEV inductors than for most other applications. A large airgap (in the magnetic sense) between the roadway and pickup inductors accounts for most of the overall circuit reluctance. Induced voltages were measured for a variety of cores, airgap heights, and roadway excitations. The frequency was held near 400 Hz for all tests, but the amplitude of the current was decreased at the lower airgap heights to keep the induced voltage near the nominal pickup voltage of 3.0 volts per foot. Measurements were taken for both the 0.5-inch

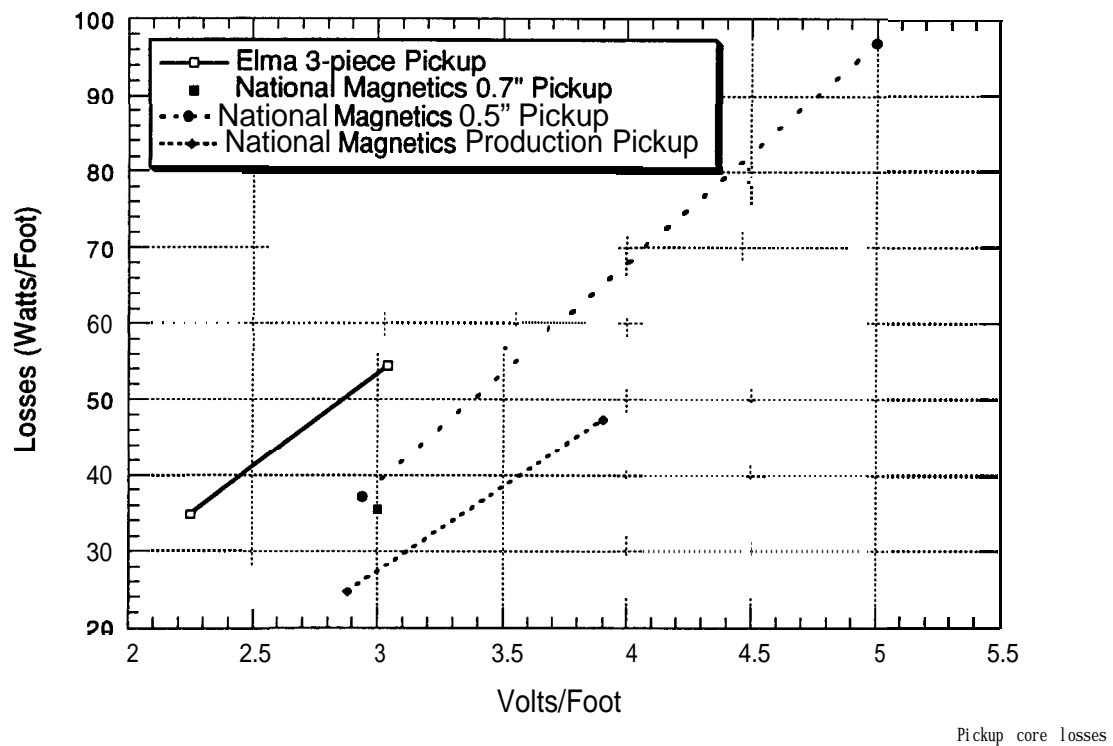


Figure 5.6 Pickup core losses

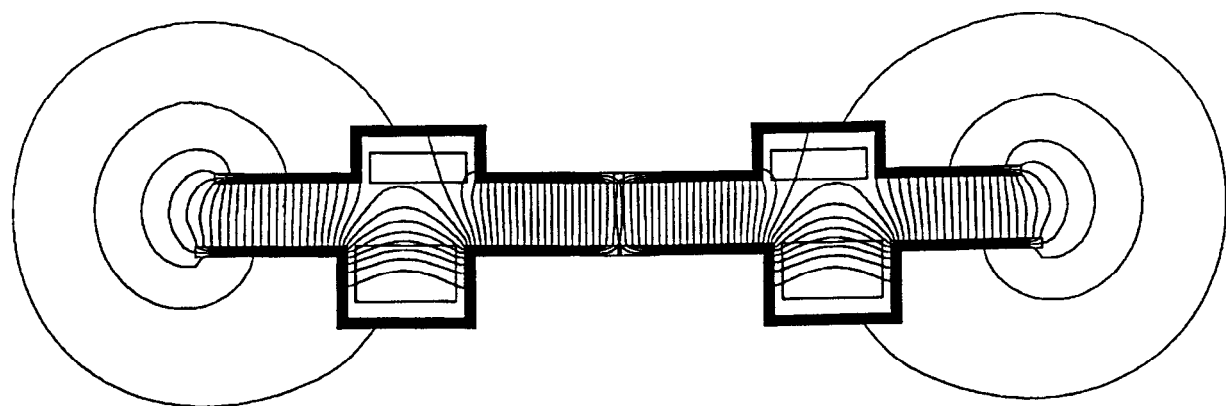


Figure 5.7 POISSON plot of coupled core flux lines, full symmetry

and 0.7-inch National Magnetics cores as well as the Elma Engineering pickup core and a core from the first-generation pickup (manufactured by Tech-Tran in 1985). The cores' length varied, so the induced voltages were normalized for core length as well as roadway current and frequency. Fringing at the ends of the cores can make a substantial contribution to the induced voltage, so a fifth set of data was taken using both National Mag-netics cores placed end to end. This setup has an overall length of 12 inches, the same as the Elma core, making fringing for these two cases equal. The cross-section of the steel in the Elma and National cores is also the same.

Normalized output voltage per inch of pickup core is shown in Figure 5.8. Log scales are used on both axes to convert what would normally be hyperbolas to straight lines, indicating that the voltage varies inversely with airgap height. The voltages for the 0.5-inch and 0.7-inch National Magnetics cores are virtually identical, showing that the extra thickness has no effect on reluctance, although it reduces losses as shown in the previous section. Normalized voltage for the pair of National Magnetics cores is 10% lower than for either core individually. The pole faces on the Tech-Tran core are approximately 30% narrower than those on the National Magnetics or Elma cores. Since reluctance is roughly proportional to airgap height divided by pole face area, one would expect the Tech-Tran core to have a higher

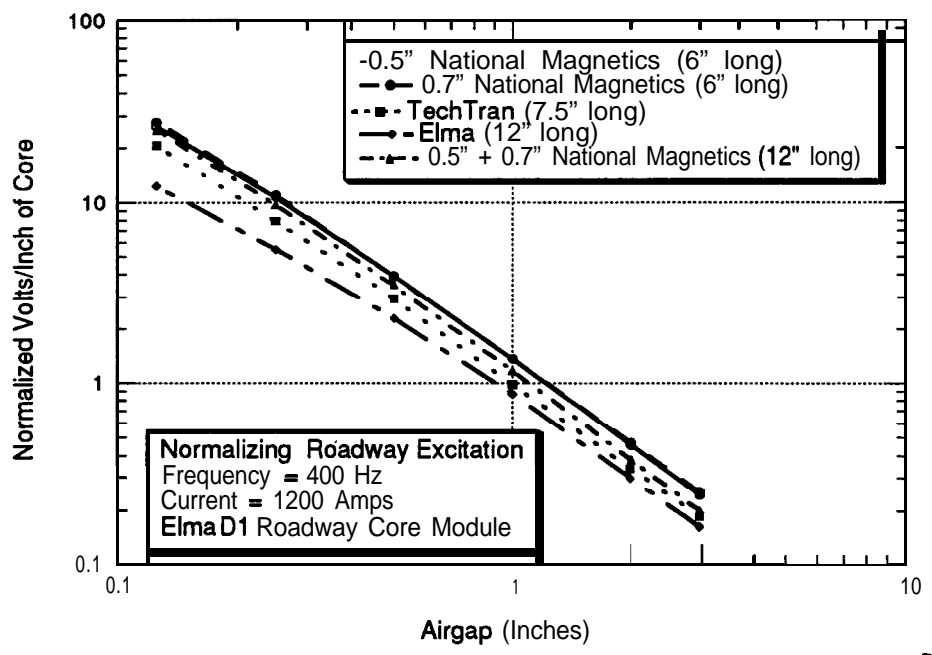


Figure 5.8 Normalized output voltage per inch of pickup core

reluctance and lower induced voltage than the National Magnetics cores, and this is exactly what is seen. Because of increased fringing with the narrower pole face, the induced voltage of the Tech-Tran core is 20 -25% less than the National Magnetics cores instead of the 30% that would be expected based on the difference in pole face area.

The National Magnetics and Tech-Tran cores have a continuous steel path for the flux between the two pole faces. The three-piece Elma core has two gaps in the flux path. If these gaps are several thousandths of an inch, they do not contribute significantly to reluctance. If the gaps are larger, they cause reluctance to increase significantly and induced voltage to drop, which is apparently the case with the Elma pickup core. Its induced voltage is lower than any of the other cores, even the Tech-Tran core that has much narrower pole faces. At the 3-inch airgap, the Elma core's voltage is 20% lower than the voltage for the combined National Magnetics cores.

The higher reluctance (or lower mutual inductance) of the Elma core requires either an increase in magnetizing current (and therefore roadway current) or a smaller airgap to give performance comparable to the National Magnetics cores'. Figure 5.9

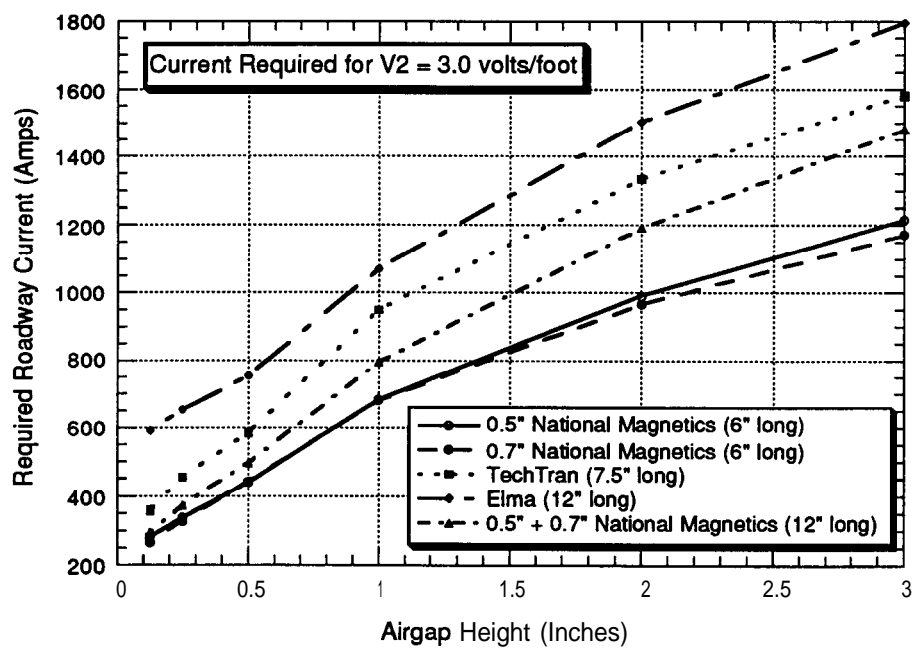


Figure 5.9 Roadway current required to induce a voltage of 3.0 volts per foot of pickup core

RFS1-036b

shows the roadway current required to induce a voltage of 3.0 volts per foot in the various pickup cores while open circuited. The actual roadway current for an operating system could be lower as the magnetizing current is often larger than the roadway current. The currents in Figure 5.9 are intended to show the relative performance of the pickup cores. At the nominal 3-inch airgap height, the Elma core requires 22% more current than the two National Magnetics cores to induce the same voltage, and the combined National Magnetics cores require 22% more current than the single cores, demonstrating how important fringing can be.

The data from Figure 5.8 can be replotted with a linear scale for the airgap height, allowing relative gap heights to be determined more easily as seen in Figure 5.10. For small airgaps, the air-gap for the Elma core must be one-half the gap for the combined National Magnetics cores to produce the same voltage (0.125 inch versus 0.25 inch) to induce a voltage of 15 volts per foot. This difference in airgap height increases in absolute terms but decreases when expressed as a percentage at larger airgap heights. For the nominal airgap height of three inches, the airgap for the Elma core has to be reduced 0.375 inch or 12% to match the performance of the National core.

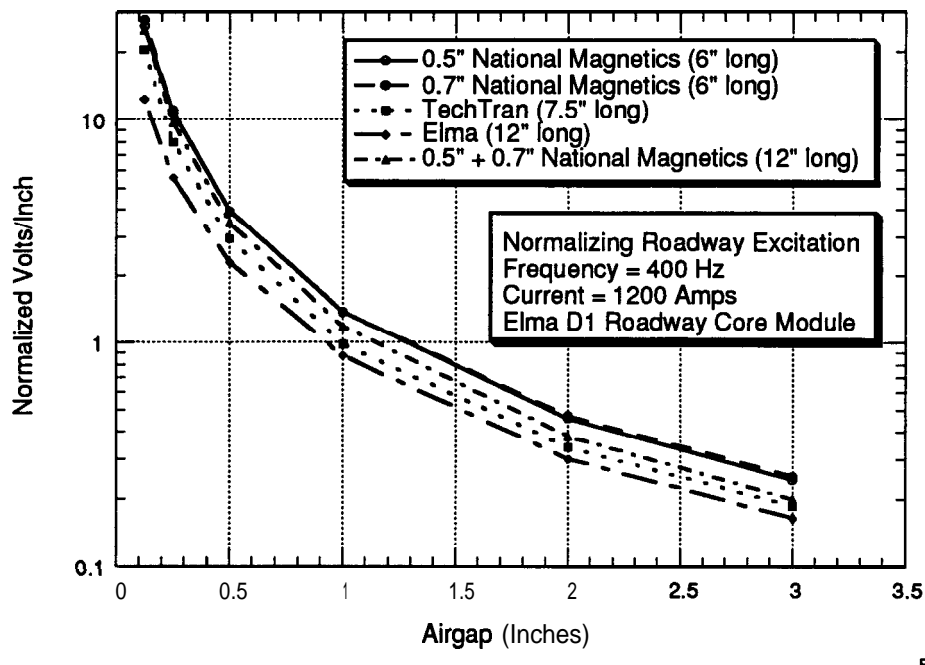


Figure 5.10 Normalized output voltage

The difference in performance between a single National Magnetics core and a pair of National Magnetics cores indicates that fringing is important in the pickup's design. Small separations are left between the pickup cores as the pickup is assembled. Examining the induced voltage as a function of core separation allows the spacing to be determined intelligently. Figure 5.11 shows the setup for the longitudinal separation fringing tests. The voltage in the center pickup core is measured as a function of the longitudinal separation between it and the other two cores, which are moved outward symmetrically.

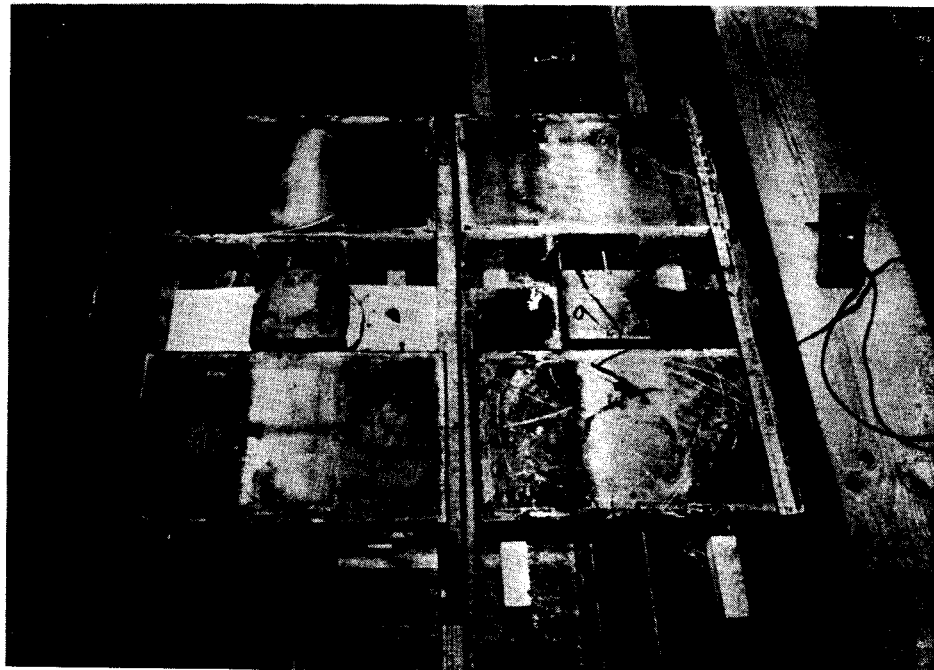
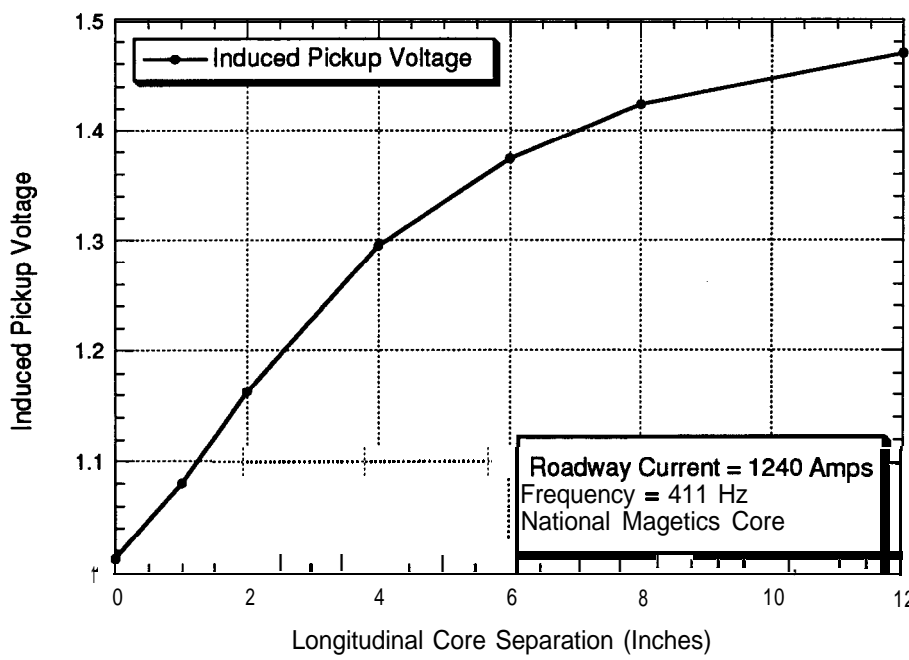


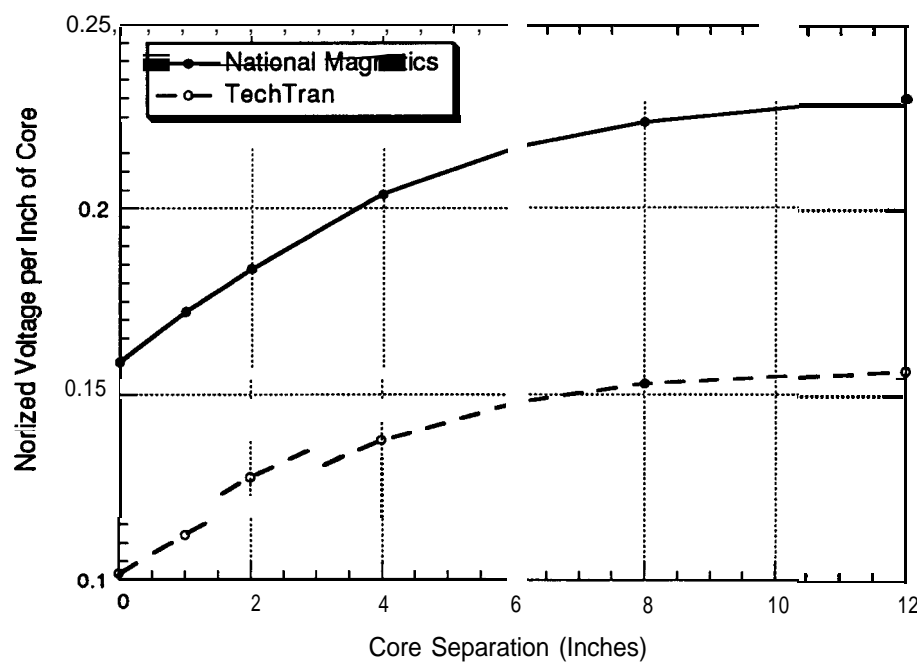
Figure 5.11 Setup for longitudinal separation fringing tests

The voltage of a National Magnetics core is shown in Figure 5.12. Induced voltage rises as the longitudinal separation increases and levels out when the separation is two to three times the airgap height. This test was repeated using a Tech-Tran core as shown in Figure 5.13. Induced voltage in the Tech-Tran core is lower, but follows the same trends. These two figures indicate that mutual inductance is increasing (resulting in higher induced voltage) as the gap between the cores increases. Figure 5.14 shows the effect of longitudinal separation of cores on the induced voltage, both per inch of pickup as well as per inch of core. The induced voltage per inch of pickup decreases as core separation is increased and, unlike voltage per inch of core, does not flatten out at higher separations. To maximize induced voltage for a given



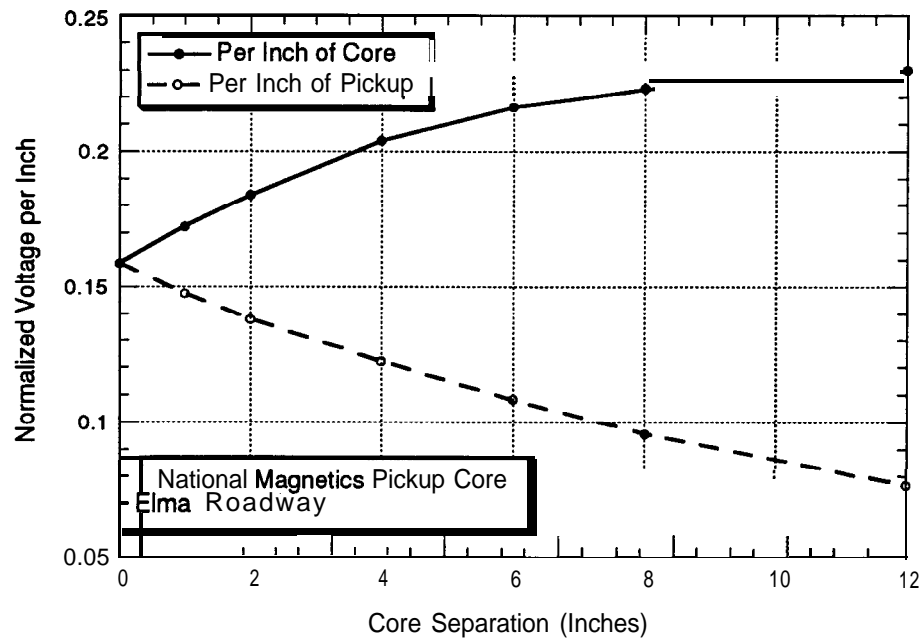
RFS1-053

Figure 5.12 National Magnetics core voltage



RFS1-053a

Figure 5.13 National Magnetics and Tech-Tran core voltage



RFS1-053b

Figure 5.14 Effect of longitudinal separation of cores on induced voltage

pickup length, core separation should be reduced to the minimum practical value, resulting in the maximum number of cores. The spacing required for mechanical installation, overall pickup length, and core length determines the core separation. The maximum number of cores is generally used and the extra length split uniformly among the gaps.

#### 5.1.2.3 Mechanical Properties

Lower mechanical stresses imposed during normal operation meant that the pickup cores did not require the same degree of scrutiny of their mechanical properties as the roadway core modules. Pickup cores were exposed to water during the calorimetry tests to determine core losses. Surface rust was noticed in isolated locations, which indicated that additional sealing would be desirable. Acoustic noise tests indicated that reducing noise would also be desirable. The cores were coated with a pliable plastic that achieves both objectives.

#### 5.1.2.4 Acoustic Noise

The first-generation inductive coupling system (built in 1985) generated objectionable acoustic noise. Due to the poor acoustic environment in the Translab

breezeway, it was impossible to determine whether the pickup or onboard controller was the dominant noise source, but it was clear that both had to be quieted before the technology could be considered practical for public demonstration. With this background in mind, minimizing acoustic noise became a primary objective during the design of the second-generation pickup. The facility assigned to the project at the Richmond Field Station (Building 167) had previously been used as an acoustics laboratory, and an anechoic chamber ( $8 \times 10 \times 12$  feet) was available, which allowed much better acoustic measurements than had been possible at Translab. Initial acoustics tests of the bare pickup cores raised questions about their suitability without a sound-reduction treatment.

Initial testing in the anechoic chamber was frustrating because results had poor repeatability and often disagreed with the experimenters' perceptions. Data did not plot as smooth curves and was obviously not of high quality. Gradually we improved our experimental techniques. The sound level meter was mounted on a tripod, and readings were taken from a distance of several feet, which avoided reflections from the operator's body. Figure 5.15 shows the anechoic chamber as it appeared for most of the testing. Standard measurement locations were defined and markings made to ensure repeatability of these locations. The most important

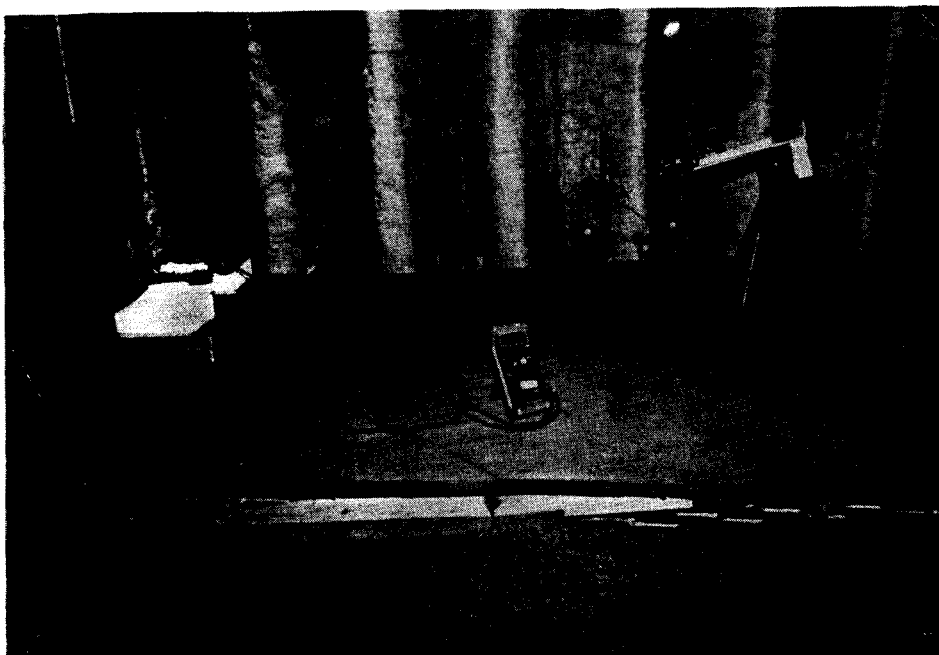


Figure 5.15 Anechoic chamber

change involved taking measurements at a variety of distances. Plotting this data revealed that measurements were in the free field, influenced neither by the near field (within a few feet of the sound source) nor the reverberant field (within a foot or so of the chamber walls where sound bounces off the walls or ceiling). Thousands of measurements were taken, from which many clear trends are observable.

One of the first acoustic tests determined the effect of excitation frequency on noise of the pickup cores. This test was done at Translab, before the experimental technique and quality of results were improved. Four different cores were excited to a voltage of 3.0 volts per foot: two single-piece cores (National Magnetics and Tech-Tran) and two three-piece cores. One Elma three-piece cores was a candidate for use on the bus. The other was made of spares from SCT's IR&D roadway core module and was not being considered for use as pickup cores. It was used for comparison as was the Tech-Tran core (from the first-generation pickup). Eight different excitation frequencies were used, varying from 263 to 434 Hz. Measurements were taken at the top, end, and side of the cores as shown in Figures 5.16, 5.17, and 5.18. All acoustic noise figures show A-weighted sound pressure levels.

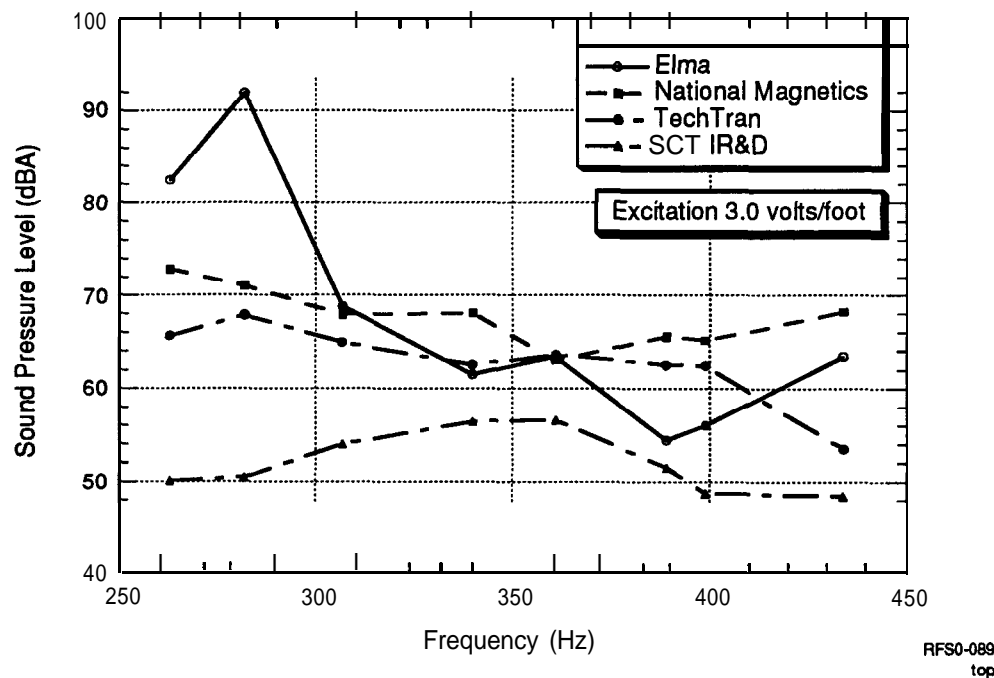


Figure 5.16 Sound pressure level two feet from top of core

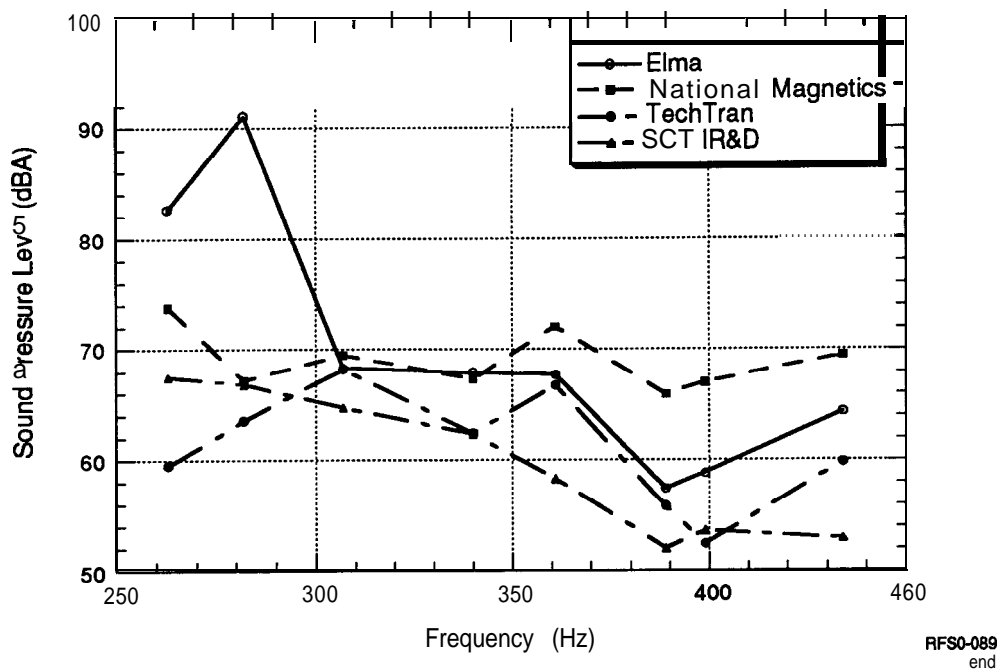


Figure 5.17 Sound pressure level two feet from end of core

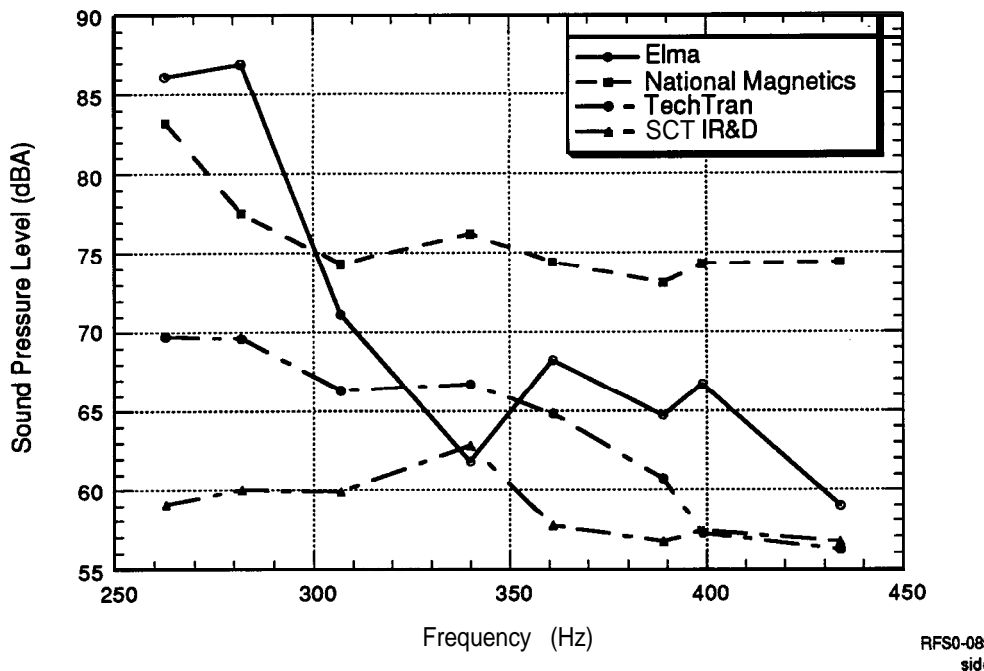


Figure 5.18 Sound pressure level two feet from side of core

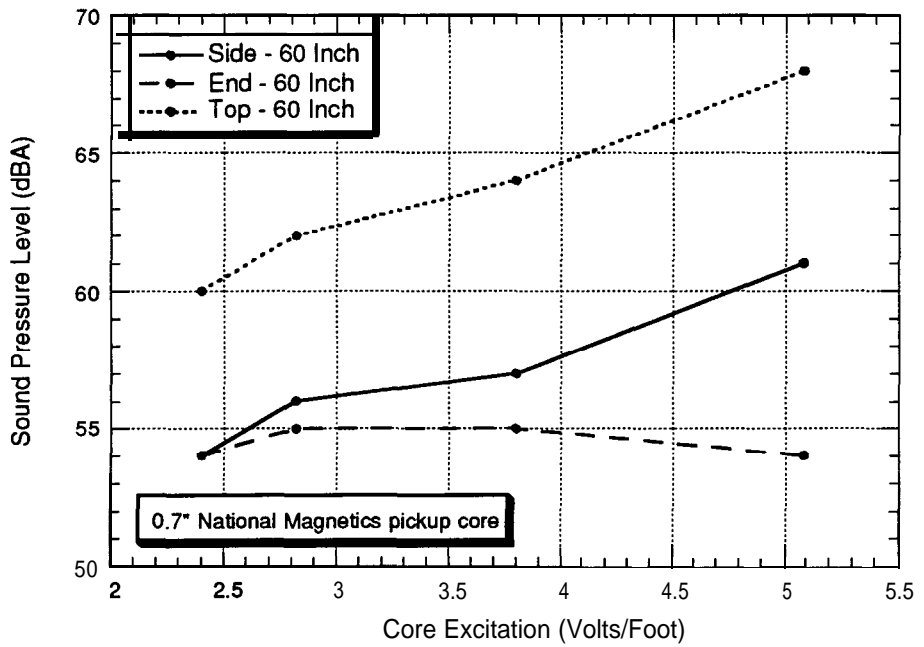
The Elma core apparently has a structural resonance near 282 Hz as this case results in the highest readings in all three dimensions. Other than the Elma resonance, no trends as a function of frequency are clear for the first two plots. Figure 5.18 (side of the cores), shows a general decrease in acoustic noise at higher frequencies although this is not monotonic. Given the uncertainty of the data, it is not even clear that this is statistically meaningful. We found no evidence that pickup noise could be reduced by choosing a frequency lower than 400 Hz, the baseline operating frequency.

The National Magnetics core chosen for production was approximately as loud as the Tech-Tran core that was previously demonstrated to be too loud without noise-suppression treatment, which led SCT to research pickup noise-reduction treatments. It was disappointing that the core made from SCT's IR&D roadway spares, the only one not considered for use as a pickup core due to weight and mechanical considerations, was consistently the quietest.

The next set of tests measured how acoustic noise varied with the voltage induced in the cores. These tests were conducted at that Richmond Field Station before the experimental procedures had been perfected. A single measurement was taken and used directly, rather than calculating the average of a number of readings but, the results are believed to be reasonably accurate. As shown in Figure 5.19, acoustic noise increases as the induced voltages and therefore flux levels in the cores increase. The measurements above the core do not follow this trend. They were taken near the ceiling of the chamber and quite possibly were affected by the reverberant field. That position was chosen so that all measurements could be taken at the same distance from the core. On average, the noise increases by 6 dBA (a doubling of the sound pressure) as the voltage doubles from 2.5 to 5.0 volts per foot, which seems perfectly reasonable.

The next set of tests deals with the effectiveness of sound-reduction treatments. Data are presented for a range of distances from the cores. In the free field, where measurements are most reliable, sound pressure falls 6 dBA as the distance from the source is doubled, making it desirable to plot distance on a log scale so that the standard roll-off curve is a straight line. The theoretical slope of -6 dBA per doubling of distance is shown as a solid line on each plot.

Many materials can be used to suppress acoustic emissions, including various foams and thin sheets of dense materials, such as lead or some plastics. More than a dozen combinations were tried to discover an effective sound-suppression technique. One



RFS1-006

Figure 5.19 Acoustic noise as a function of flux levels and induced voltages

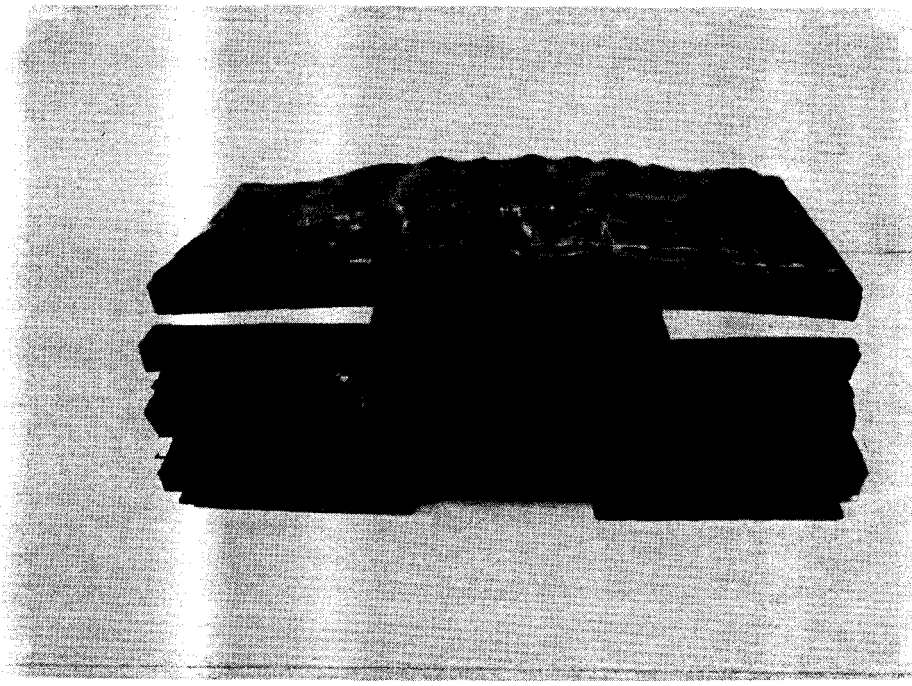


Figure 5.20 Sound reduction treatment

combination, consisting of several layers of foam and thin lead and vinyl sheets, reduced noise reasonably well, was not excessively heavy, and fits in the space between the pickup and the bus floor. Figure 5.20 shows a cutaway of this treatment.

The sound pressure level to the side of the Elma pickup core with and without sound treatment is shown in Figure 5.21. Data are shown over the entire range of distances for which measurements were taken even though the extremes are not in the free field region. Data below 30 or 40 inches and data for the last 10 inches should not be counted heavily during interpretation of results for this or any of the other figures showing a range of distances. The sound treatment reduces acoustic noise 5 – 10 dBA. The plots of the data drop slightly faster than the theoretical curve. The sound treatment certainly helps, but still does not reduce acoustic emissions so they are clearly not an issue.

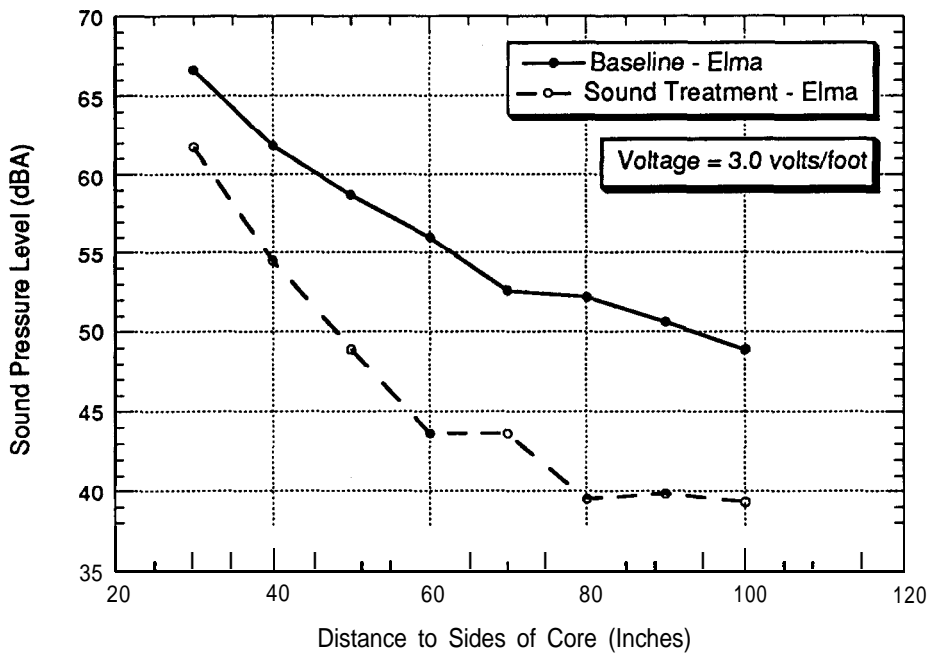


Figure 5.21 Sound pressure level to side of Elma pickup core with and without sound treatment

Figure 5.22 shows sound pressure levels above the pickup cores. In addition to the two sets of data shown in the previous figure, a third curve has been added representing the National Magnetics core with the sound-suppression treatment. Again the treatment reduces the noise of the Elma core by 7 – 10 dBA; however, the National Magnetics core is approximately 10 dBA quieter than the Elma core when

both have the sound treatment. The decibel measurements of the National core are in the mid forties to low fifties, which is in an acceptable range. Each of the curves rolls off at a slope matching the theoretical reference. The bump at 50 – 55 inches is caused by the reverberant field.

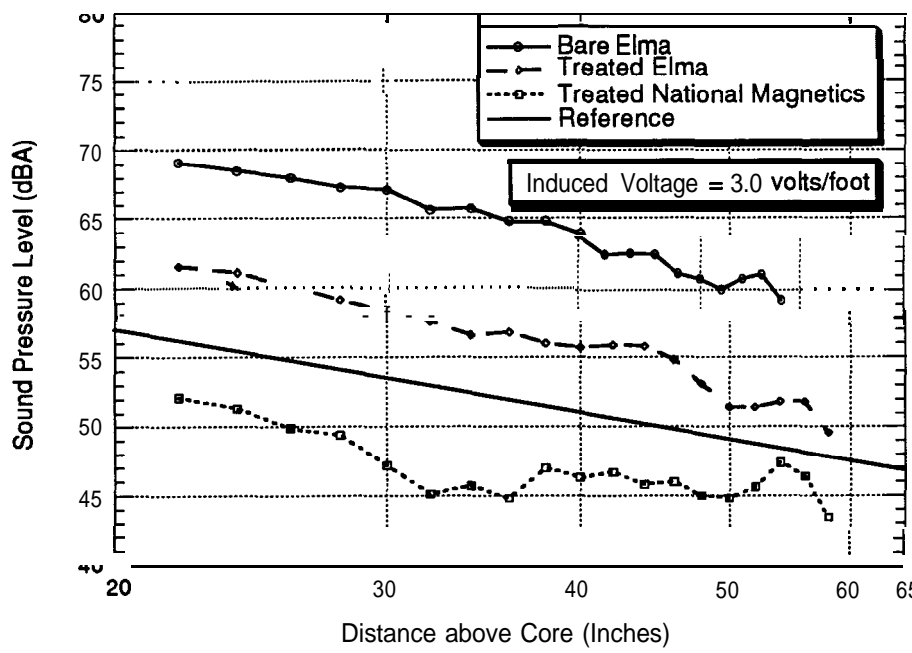
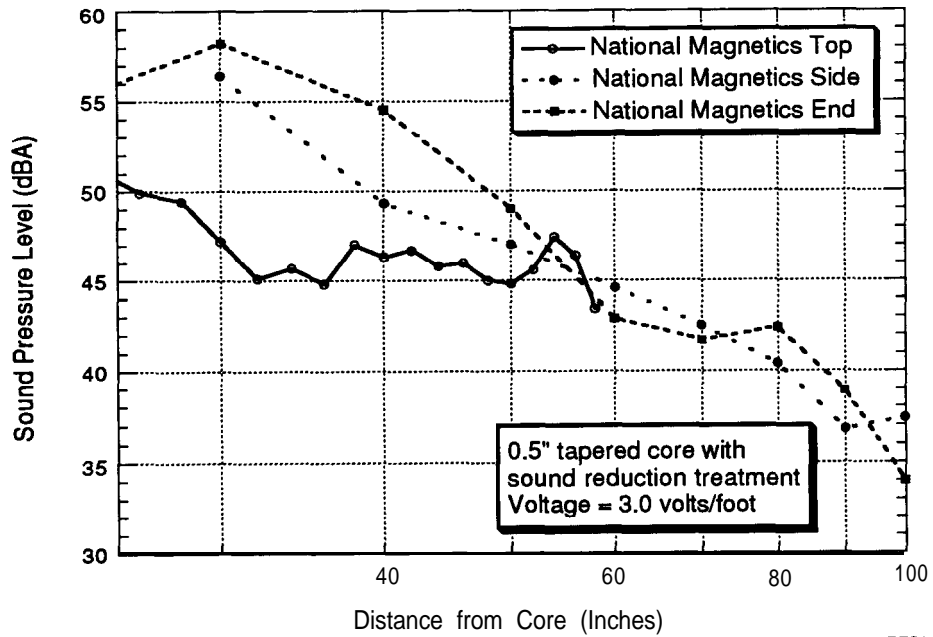


Figure 5.22 Sound pressure level to side of **Elma** pickup core with and without sound treatment

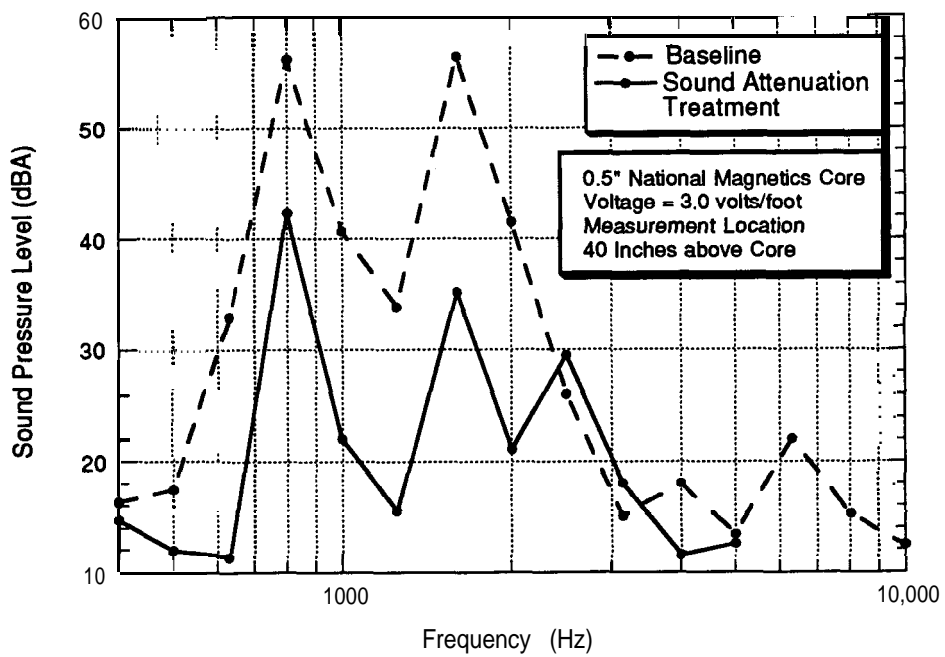
Test results for the National Magnetics core with acoustic treatment are shown in Figure 5.23 for all three dimensions. The data for the side and end are not quite so low as for the top; however, they still are acceptable, especially if one discounts the data for the near field (below 30 or 40 inches). These data convinced us that it would be possible to suppress pickup noise to an acceptable level **onboard** the vehicle. Although cumbersome, the noise-suppression treatment presented in the previous three figures was effective and workable. Simpler methods were discovered later that proved effective, so this treatment was not used on the bus.

The final acoustic data presented in this section deal with the spectral breakdown of the acoustic noise generated by the pickup cores. In theory, the dominant frequency of acoustic noise is twice the electrical frequency because a peak in acoustic noise is generated for both the positive and negative halves of the 400 Hz sine wave.



RFS1-033, 034

Figure 5.23 National Magnetics core with acoustic treatment



RFS1-033

Figure 5.24 National Magnetics core with and without acoustic treatment

Acoustic noise was measured in one-third octave bands for the 0.5-inch National Magnetics pickup core, both with and without the acoustic treatment. The results are shown in Figure 5.24.

As expected, the band with the highest sound pressure level is 800 Hz, with 1600 Hz nearly as high, which is true both with and without the sound treatment. These two peaks are attenuated 15 and 20 dBA, clearly indicating that the treatment is effective. The one-third octave band centered at 400 Hz has a reading under 20 dBA regardless of the acoustic suppression treatment and all bands, except those centered at 800 and 1600 Hz, are below 30 dBA.

The fact that the acoustic energy is concentrated in one or two bands has negative as well as positive implications. If suppression of pickup (or OBC) noise is necessary, it is easier to build a system that blocks a single frequency than one that is effective at all frequencies, in effect a mechanical band-stop filter. On the other hand, pure tones are more perceptible and irritating than broadband noise. Pure tones can be audible even when they are 10 dBA below ambient noise levels.

The acoustic testing of the pickup cores was a long and difficult task, requiring considerably more time and effort than originally estimated. The effort was well worth it, however as it demonstrated that the most significant known problem was solvable.

#### 5.1.2.5 Magnetic Flux Distribution

The POISSON magnetic analysis program was used to predict coupled as well as open roadway magnetic properties, such as flux levels and stored energies (which are used to calculate inductances). The program proved useful, and after the first-generation hardware was built and tested in 1984 – 1985 was considered fully validated for application to the RPEV technology. Figure 5.25 shows the POISSON analysis of the magnetic flux lines for one side of the roadway and pickup inductors while coupling power. The numbers indicate the distance along the surface of the core measured from the outer edge of the pickup. Nearly all the flux enters the pickup through the flat pole area of the pickup, although an occasional line enters the sides or top of the slot. These can be from either the inside or outside the slot. Flux that passes through the slot does not couple all the turns of the pickup (or roadway) winding and contributes to leakage flux. Figure 5.26 shows the predicted vertical component of the flux in the airgap when coupling power. It is at a high and nearly constant level for areas directly between roadway and pickup pole faces and drops off significantly between the slots and beyond the outer edges of the cores.

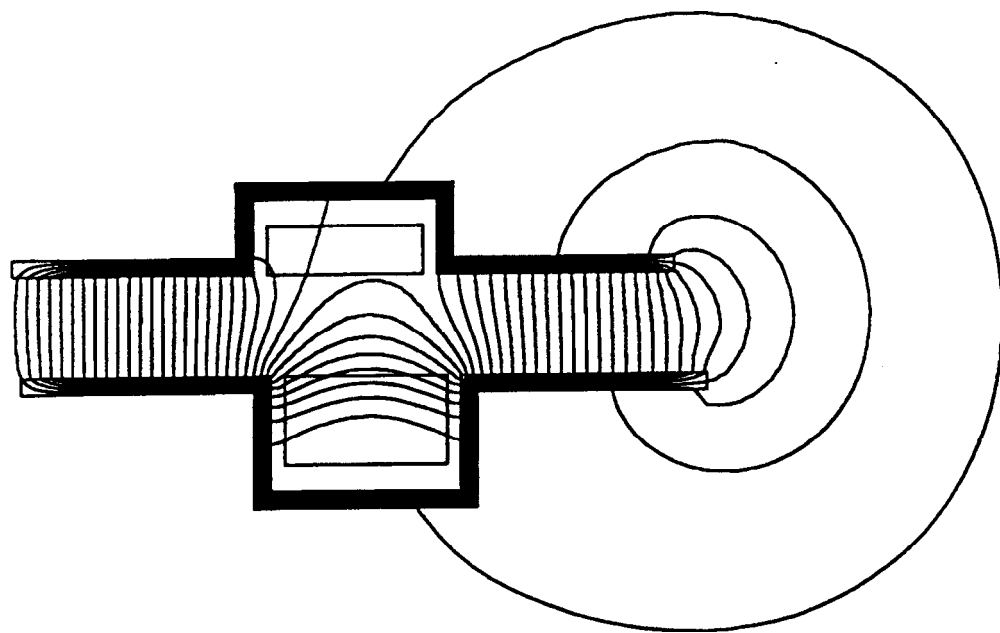


Figure 5.25 POISSON analysis of magnetic flux lines while coupling power

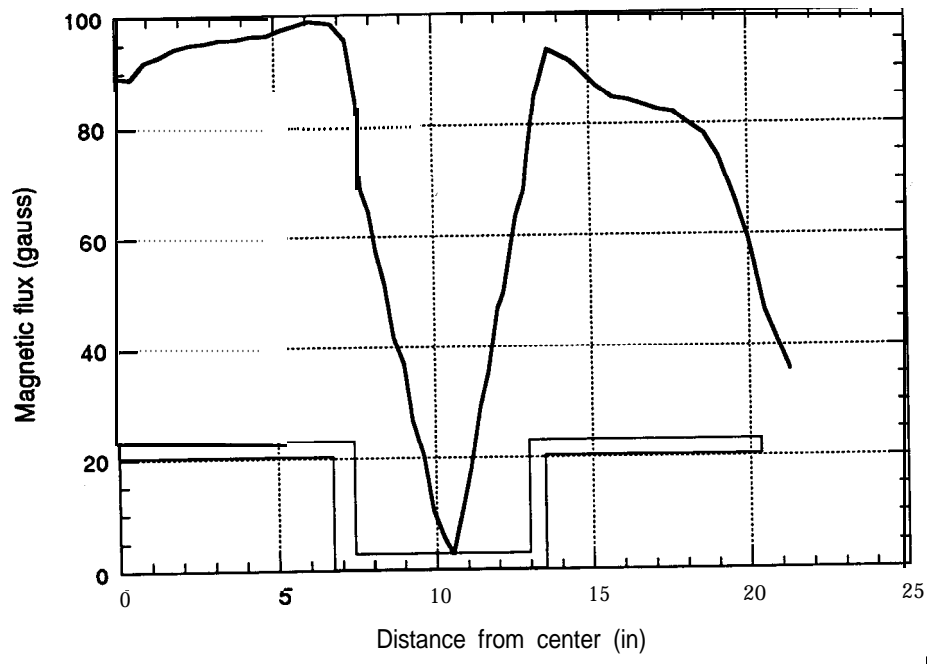


Figure 5.26 Predicted vertical component of flux while coupling power

An experiment was performed in which loops of wire were placed around the core at several locations, the core was placed over the roadway inductor, and the voltage induced in each loop was measured. Figure 5.27 shows the test setup with wire loops at some of the measurement locations. These readings indicate the total flux within the core at that location, approximately proportional to the integral of the flux entering the core from the outer edge to the loop location. These voltages are plotted in Figure 5.28. Curves for the National Magnetics and Elma Engineering cores have a similar shape, with voltage rising rapidly over the first 7 or 8 inches (the pole face area), leveling out around the perimeter of the slot (8 to 16 inches from the outer edge of the core, measured along the surface of the core), and falling back to zero linearly across the inner pole face. This matches the trends in predicted flux of the previous two figures. The National Magnetics core has induced voltages approximately 30% higher than the Elma core, which is consistent with the conclusions of Section 5.1.2.2 regarding their relative reluctance and mutual inductance.

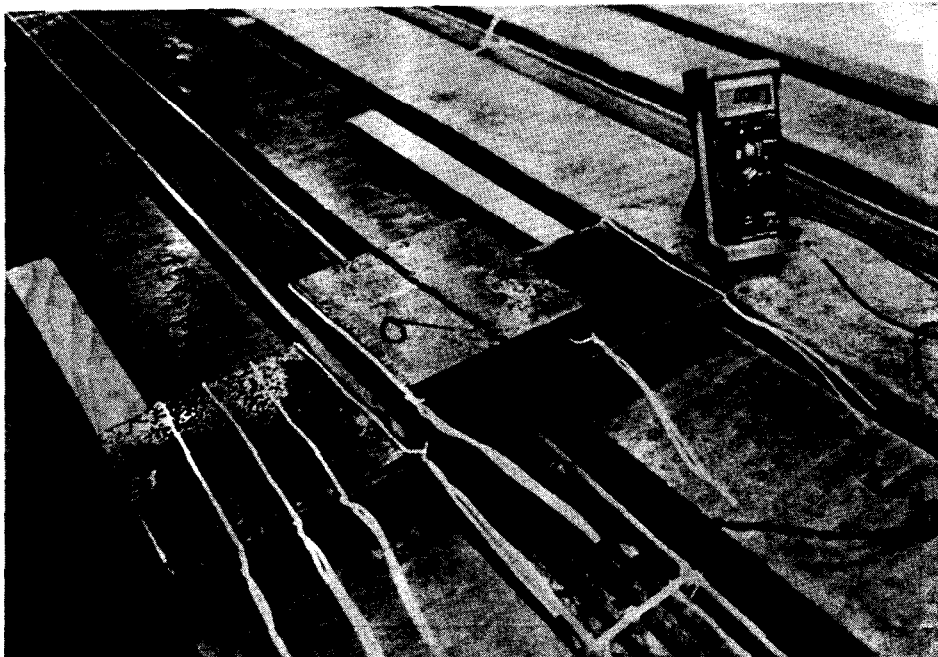
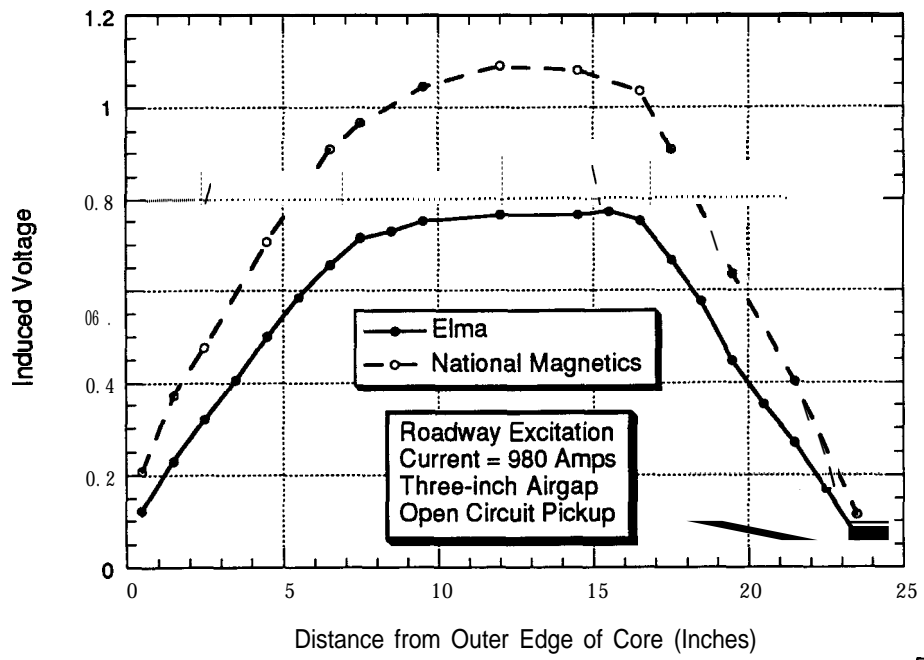


Figure 5.27 Test setup



RFS1-065

Figure 5.28 Measured flux in National Magnetics and Elma cores

### 5.1.3 Solid-state Switches

Solid-state switches in the onboard controller are used to switch steps of capacitance into and out of the circuit to control output current. These solid-state switches are sometimes referred to as contactors, a reference to the mechanical switches they often replace. They have consistently been the most troubling electronic component in the inductive coupling system and have malfunctions that were quite difficult to diagnose. The switches consist of two Silicon Controlled Rectifiers (SCR), one conducting in each direction, and a trigger circuit to gate (turn on) the SCRs at the appropriate time. The SCRs must be activated within approximately one degree of the voltage zero-crossing to prevent waveform distortion and creation of high frequency harmonics. Malfunctions have included:

1. Not turning on at low voltage
2. Turning on late (more than a few degrees after zero-crossing)
3. Not turning off
4. Component failures

These failures can be caused by either the trigger circuit or the SCR, but in this case the problems have been traced to the trigger circuit exclusively. The trigger circuit accepts a low-level dc command (0 – 10 volts or 4 – 20 milliamps) from the onboard control computer or manual toggle switches and generates signals that gate or activate the SCRs. The trigger circuits generally receive their power from the ac circuit. The dc input is optically isolated from the remainder of the trigger circuit so that a fault in the switch cannot damage the computer. The SCRs carry a large ac current (up to several hundred amps) and each switch has two mounted back-to-back, one carrying current in the positive half of the sine wave and the other in the negative half. The SCRs conduct when a bias voltage is applied to the gate supplied by the trigger circuit. The trigger circuit creates this signal (a pulse or continuous signal) as the voltage across the switch goes through zero so that the SCR starts conducting forward current as soon as there is forward voltage. If the trigger signal is too small or late, the SCR does not start conducting immediately. This causes a short period when no current is flowing, followed by a sharp rise in current, which creates higher harmonics, an undesirable result. When current starts flowing in the SCR, it will continue to flow, even if the gate signal is removed, until the forward voltage goes to zero.

After the forward voltage and gate signal disappear, a short time is required (reverse recovery) before the SCR should again be exposed to forward voltage. If reverse recovery time is insufficient, the forward current can punch through the junction within the SCR, causing an immediate failure of the device or the SCR will continue to conduct, even when the gate signal has been removed, causing the SCR to latch up.

Malfunctions with the switches manifested themselves in many ways. Failure to turn on or off was easily detected, but late or erratic triggering was more difficult to detect, because it was masked by the improper sizing of the current-limiting ( $di/dt$ ) reactors, which tended to generate similar symptoms, primarily the presence of higher harmonics, especially in the capacitor current. These two phenomena can interact if the high-frequency oscillations caused by the  $di/dt$  reactors are so severe that they cause the voltage to dip low enough that the SCR shuts off part way through the sine wave, complicating the diagnosis and solution of both problems.

#### 5.1.3.1 Trigger Circuit

The function of the trigger circuit is to supply a gate signal to each SCR at the appropriate time (immediately after the voltage across the switch passes through

zero) whenever the dc control voltage is present. During the development of the RPEV technology, trigger circuits of several designs, supplied by several companies, were used.

Trigger circuits generally draw their power from the ac circuit they are controlling. This voltage is stepped down, often through a set of resistors acting as a voltage divider, from approximately 175 volts to less than 10. The dc input is optically isolated, which prevents the **onboard** control computer from being damaged by a failure in the trigger circuit or ac power circuit. The stepped-down ac voltage and optically isolated dc output feed into a **triac**, which generates the gate signal. A fuse and a thermal switch in the SCR **heatsink** protect the switch components. When the ac voltage is positive (and the dc input voltage is present) the gate on the SCR for the positive half of the waveform is activated. Similarly, the gate signal for the negative SCR is generated during the negative half of the ac waveform.

Initial testing of the second-generation OBC revealed that the trigger circuits were not functioning properly. Although some current was passing through them, the **SCRs** were not being properly triggered and the current through the capacitor had a badly distorted waveform as shown in the oscilloscope traces in Figures 5.29 and 5.30. In the first of these, the SCR is being triggered late as indicated by the flat portion of the current (lower trace) upon going through zero. The flat spot lasts for about 0.3 **msec** or approximately 50°. A step change in voltage (upper trace) occurs at both the beginning and end of the period of zero current. This test was conducted with a resistive load, which tends to improve current waveform. With a capacitive load, the waveform of the current would be much worse as the current through a capacitor is equal to the derivative of the voltage. The contactor started to conduct late because the ac voltage was lower than nominal by approximately a factor of three, reducing the voltage out of the trigger circuit by a factor of three. However, a factor of three improvement is not adequate in this case. The same late gating occurred with this trigger circuit at nominal voltage. The problem was corrected by changing the voltage divider ratio, causing the SCR to activate sooner after **zero-crossing**.

Figure 5.30 shows the current into a capacitive load with a trigger circuit (from another manufacturer) that was not functioning properly. The high-frequency oscillation of the current, which is excited on each zero crossing, is lightly damped, with three cycles clearly visible before the next zero crossing. The high-frequency oscillations are barely visible on the voltage waveform. In a capacitive load, the

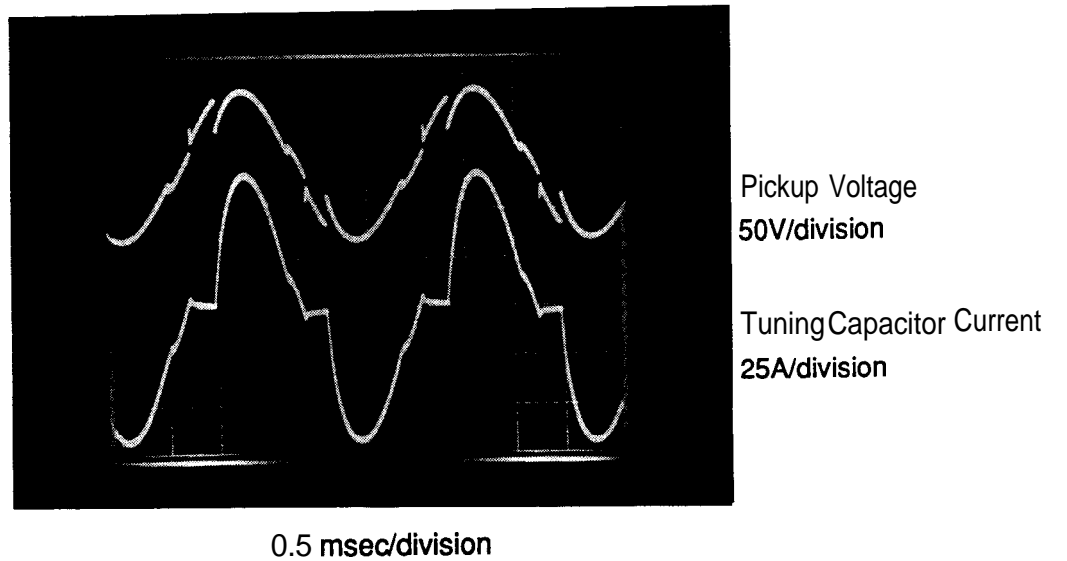


Figure 5.29 Capacitor voltage and current with late S&I triggering

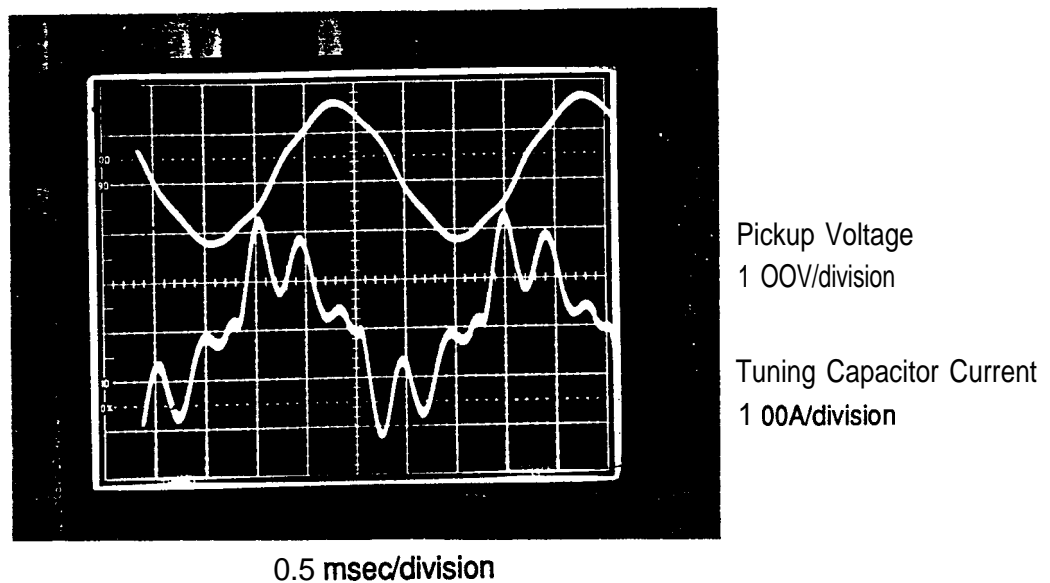


Figure 5.30 Capacitor voltage and current with bad SCR triggering

voltage goes through its minimum). On the oscilloscope trace, the current does not start flowing until approximately one half division (0.25 msec) after the peak of the voltage, which corresponds to a lag of 30 -40" and is the source of the high-frequency oscillations. Changes in the voltage dividing circuit caused the ac threshold voltage for triggering to drop from 50 volts to less than 5, cutting the delay by more than a factor of ten. This cut the turn-on lag to about 2".

Another phenomenon observed occasionally involved unsymmetrical triggering of the switches. (See Figures 5.31, 5.32, and 5.33). In this case, the load was the bus battery combined with a resistor. This non-linear load (like the battery alone in an operational case) tends to be more sensitive to poor triggering. Figure 5.31 shows the current into a capacitor that is hard-wired into the circuit (upper trace) and the pickup voltage. The inductor in series with this capacitor branch is slightly mismatched, causing ripples in the current waveform. Figure 5.32 shows the current in the same branch when the switch in another branch (number five) was turned on. The ripples changed, especially on the negative half of the waveform. Figure 5.33 shows the current through branch number five. The current is clearly unsymmetrical, with a flat spot just before the negative half cycle, resulting in much larger ripples on the negative half cycle for all capacitor branches. The disturbance is propagated through the pickup voltage. It is difficult to distinguish, but the ripples on the downward-sloping portion of the voltage waveform (the portion that corresponds to the negative half cycle of the capacitor current) are larger than those on the upward-sloping half of the curve. This phenomenon was traced to an asymmetry in the voltage divider portion of the trigger circuit, which was corrected.

Sometimes the switch did not turn off when commanded to do so. We traced this latching-up to the output triac of the opto-coupler that was unable to hold the peak back voltage experienced when operating at high power levels, typically when pickup voltage exceeded 180 volts. Initially opto-isolators with a higher voltage rating were tried but with limited success. We modified the circuit with two output triacs connected in series so that each one would have to hold half of the total back voltage, eliminating the latching-up as well as the failures in the opto-isolator.

The trigger circuits were originally located on the mounting plate of the switch assemblies where they were virtually inaccessible, making all work on them—even replacing a simple fuse—a major undertaking. Additionally EMI from the power wiring was thought to be causing the trigger circuits to operate erratically. Both of these issues were solved by relocating the trigger circuits. They were remounted in

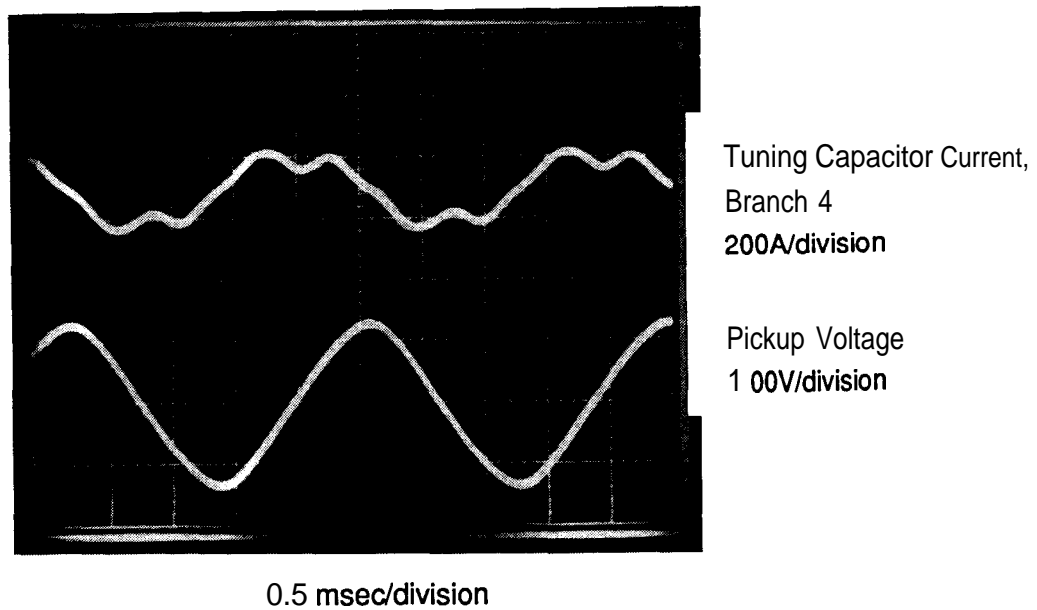


Figure 5.31 Capacitor current and pickup voltage with capacitor hardwired into circuit

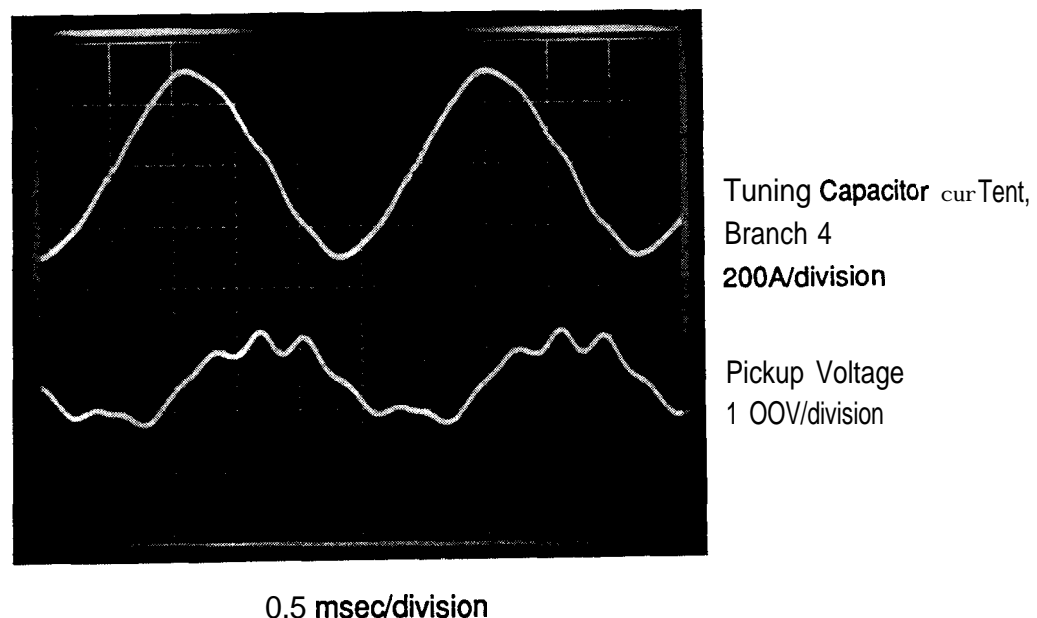


Figure 5.32 Same as Figure 5.31 with an additional branch of capacitance switched into the circuit

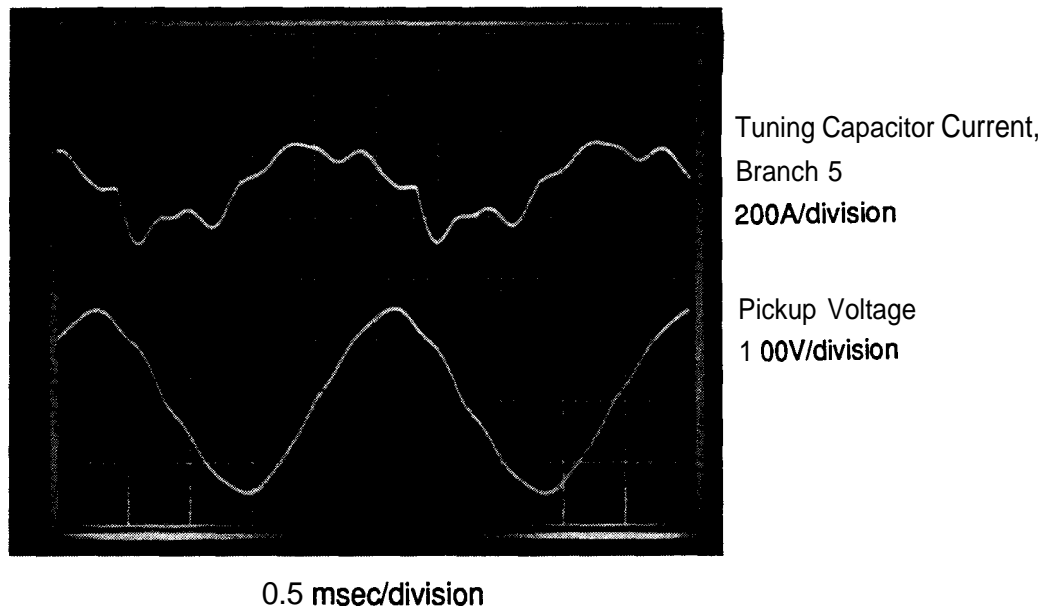


Figure 5.33 Capacitor current in branch 5 with unsymmetric SCR triggering

an aluminum box to provide shielding, but we discovered that this was unnecessary. The final location of the trigger circuits was on an easily accessible fiberglass panel with all other small electronic components, including capacitor discharge resistors and fuses.

Eventually all problems with the trigger circuits were solved. It was a time-consuming and occasionally frustrating process, but the results were satisfying as depicted in the waveforms shown in Figure 5.34.

#### 5.1.3.2 Silicon Controller Rectifier

In contrast to the trigger circuits, the Silicon Controlled Rectifiers (SCRs) themselves functioned well, duplicating the first-generation OBC experience. The SCRs are mounted on liquid-cooled heatsinks with a thermal switch that disables the input to the trigger circuit if the SCR overheats. The thermal switches activated on a few occasions, proving their worth. The heatsinks themselves are compact although the mounting hardware and coolant lines take up some space, but not nearly so much as the natural convection cooled heatsinks of the first-generation OBC. Forced-air-cooled components may minimize onboard size and weight and should be given serious consideration for future work.

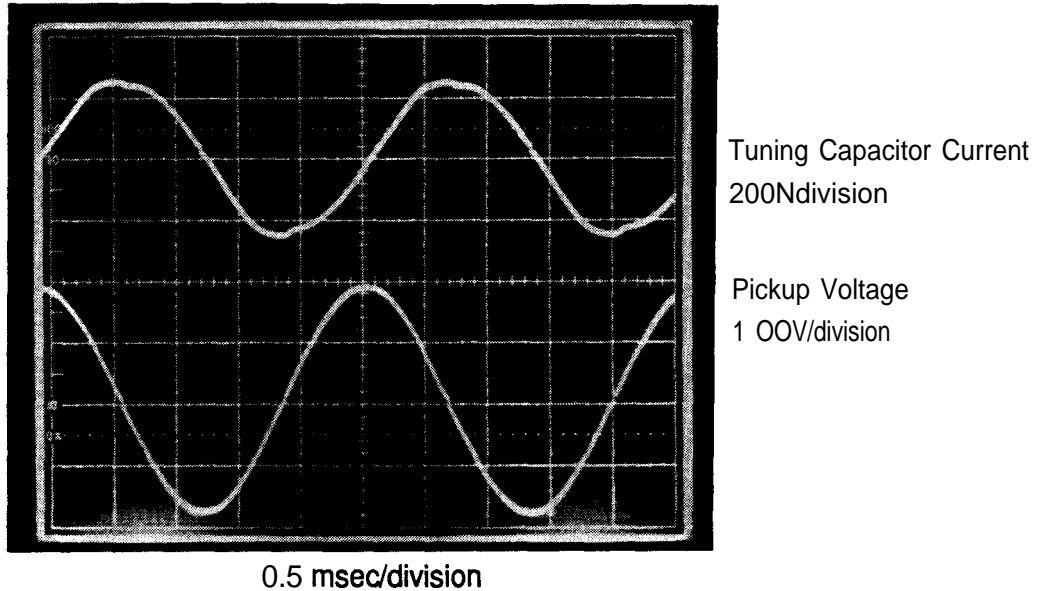


Figure 5.34 Correct capacitor current and voltage

#### 5.1.4 Onboard Controller Inductors

Several problems arose concerning the inductors used in the OBC. The values initially chosen for the  $di/dt$  (current) limiting inductors in each branch of capacitance resulted in poor capacitor current waveforms, much the same as those shown in the previous section due to bad trigger circuits. These inductors produced unacceptable heat and acoustic noise as well. Selection of the proper inductance value is addressed in Section 5.2.4.3 regarding performance of the onboard controller. This section deals with the heating and noise issues, for both the original and replacement inductors.

The original inductors (both the  $di/dt$  and ac isolation) were specified to be toroidally wound air core inductors. Although the project staff members did not know it at the time, the onboard controller was supplied with Brooks coil inductors. (A Brooks coil is a short coil with windings placed concentrically. The total width and thickness of the windings are usually equal, often with six or so layers of windings. They are heavy and have high leakage flux.) Toroidally wound inductors use material efficiently and tend to be lighter than other designs. They also have low leakage flux compared to Brooks coil type air core inductors. Flux containment is desirable as leakage flux can cause vibration, noise, and heating of metallic objects.

Initial operation of the OBC revealed more acoustic noise than desirable. The components were packaged tightly in the boxes housing the equipment, making

diagnosis difficult. After about 15 minutes of full-power operation, traces of smoke were discovered emanating from two of the  $di/dt$  inductors, and they were hot to the touch.

We decided to change the wiring scheme of the OBC to allow smaller steps of capacitance value to provide smoother control. The number of steps was changed from 6 to 10 and then to 20. This required different current ratings on the  $di/dt$  inductors, and there was increasing evidence it would be desirable to change the inductance of the isolation inductor as well. During these tests, some of the inductors were removed from the OBC boxes to allow alternate inductors (individually or in series and/or parallel combinations) to be tried. As some inductors were removed (particularly the isolation inductor), the acoustic noise characteristics of the OBC changed noticeably. We observed that the aluminum wall of the OBC box directly adjacent to the isolation inductor had discolored in a circular pattern that matched the size and location of the isolation inductor. (See Figure 5.35.) When this side wall was removed, we discovered that inductor heating had warped it as shown in Figure 5.36. It was clear that the panel had been heated by eddy currents induced in the panel by magnetic flux leaking from the Brooks coil.

Several quick tests determined the extent of the problems caused by the Brooks coil inductors. They had been heating up to approximately 200°F, which was considered high but not completely unacceptable. A coil was run up to its nominal operating point inside the anechoic chamber and did not emit any noticeable noise. The test was repeated with an aluminum panel placed several inches away from the side of the inductor. The panel buzzed in a loud and annoying fashion. Even before the heating and acoustic noise of the ac inductors were discovered, we had planned to replace them to change their electrical properties. Air core toroidal inductors were included as a possible technology to be used for the replacement parts, but conventionally wound iron core reactors were purchased and performed well.

#### 5.1.5 Heating of Pickup Frame Materials

The mechanical design of the pickup is limited by the choice of materials that can be used near the pickup pole face. Steel and other ferrous materials are ruled out because they heat up too much in this high flux area. Fiberglass is clearly acceptable, although not so convenient to work with as various metals. Aluminum was chosen for the pickup conductors as it is lighter and less expensive than copper for the same resistance. Aluminum bus bars were bonded into a single pack with fiberglass-

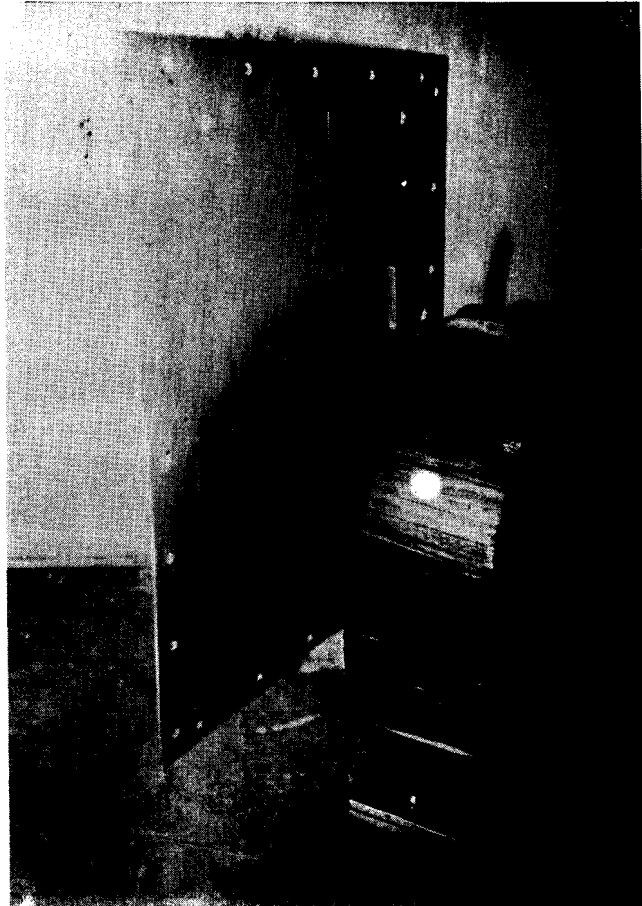


Figure 5.35  $L_3$  inductor with discolored and warped aluminum panel

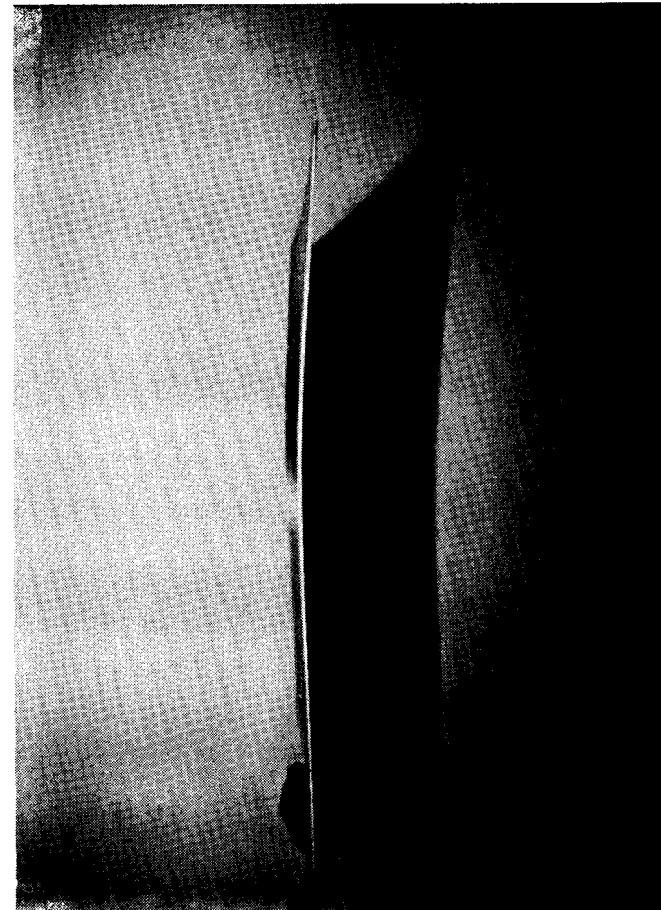


Figure 5.36 Panel warped by  $L_3$  inductor heating

reinforced epoxy. These packs form the main longitudinal structures of the pickup as well as being the electrical conductors. The question of whether aluminum could be used for the cross beams as well was raised. No analytical approach seemed adequate to resolve this issue. As a result, testing aluminum bars in the high flux regions of the pickup cores was determined to be necessary. The feasibility of aluminum needed to be determined for both the area below the bus bar packs (within 0.5 inch of the pole face surface and an area of high fringing flux) and the area even with or above the bottom of the bus bar packs.

Several tests were conducted to determine if aluminum was feasible. In previous phases, steel and aluminum bars were placed at various locations above the pickup (one to two feet above the road surface), and no heating was observed. During this phase of the project, tests were conducted to determine heating of aluminum within 0.125 inch of the pickup cores and conductors. Test samples were placed near the roadway cores and conductors, and pickup cores were placed above the test samples to drive the flux levels to those experienced during system operation.

In the first test, one aluminum bar was placed in the **airgap** between the cores and a second one was placed against the conductor pack on the side away from the **airgap**. As expected, the bar in the **airgap** region of high flux heated up considerably more than the other bar as shown in Figure 5.37. Over 20 minutes, the temperature rises were 24°F and 4°F, indicating that high flux location required further investigation.

Given the difference in heating at these two locations, we decided that testing should also be done at intermediate points to the side of the conductor pack. An aluminum test piece was machined and tested as shown in Figure 5.38. Two tests were run, one with the two pieces insulated from each other and the other with them bolted together. The results are shown in Figures 5.39 and 5.40. The material on the side of the conductor pack does not seem to heat up excessively as was subsequently verified with the full-scale pickup. The material in the high flux region posed enough of a risk that fiberglass was used on the operational pickup rather than aluminum.

## 5.2 Inductive Coupling Subsystems

Subsystem test results are discussed for the roadway inductor, the pickup inductor, the power distribution system and the **onboard** controller.

As components are assembled into subsystems, many characteristics become measurable in a meaningful way. For example fringing is very significant for a single

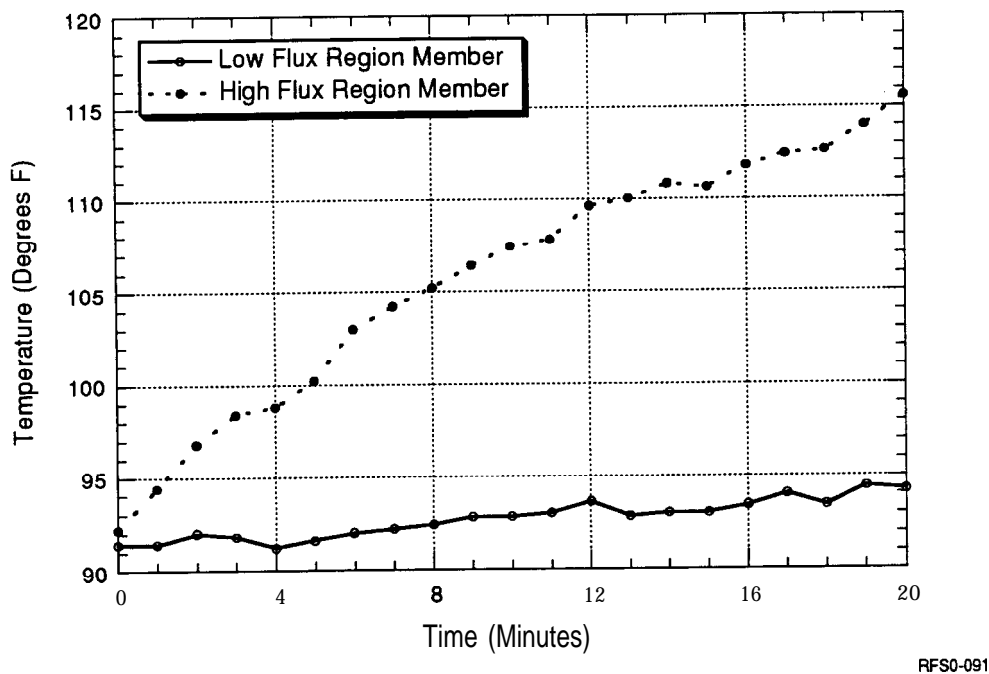


Figure 5.37 Heating of aluminum bars in high and low flux regions

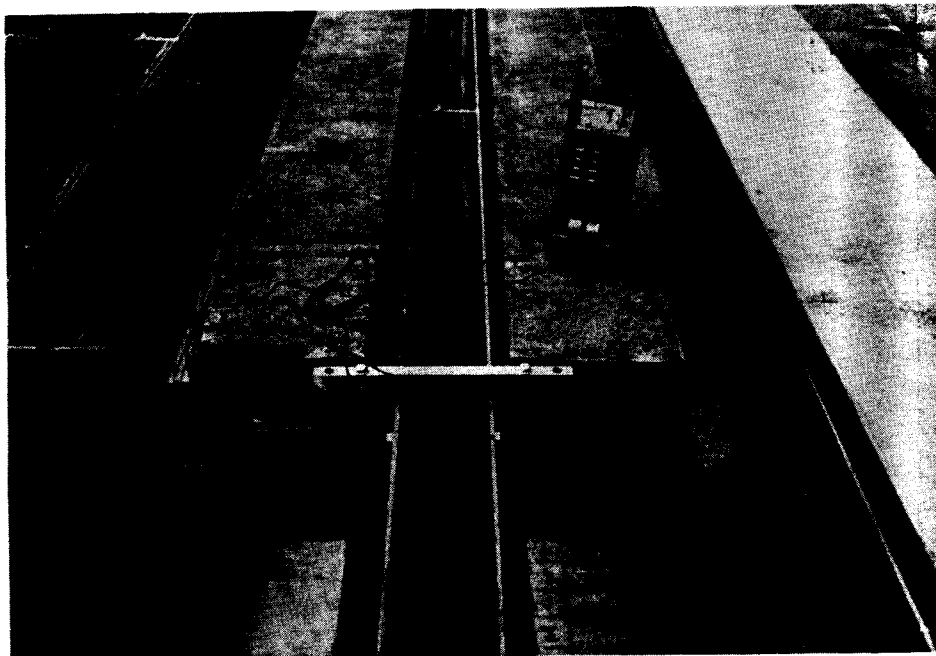
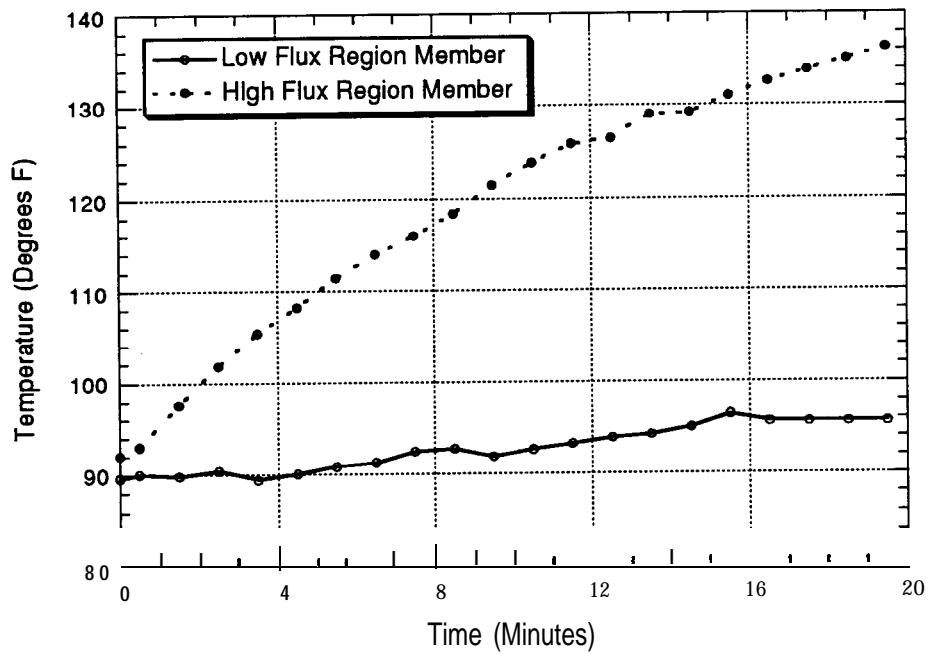
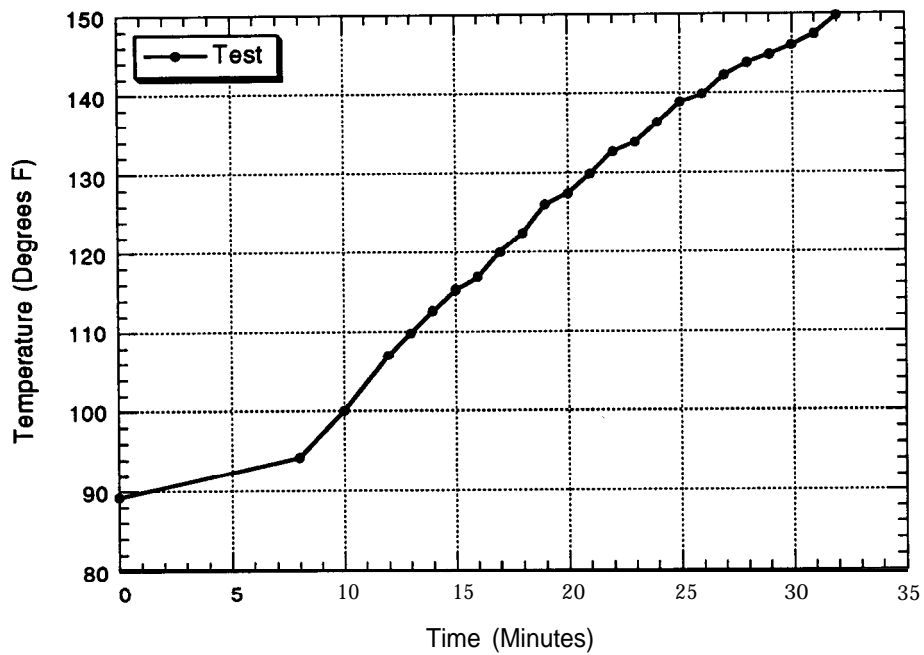


Figure 5.38 Setup for testing pickup frame heating



RFS0-091

Figure 5.39 Heating of aluminum bars when insulated from each other



RFS0-050

Figure 5.40 Heating of aluminum bars when bolted to each other

pickup core, with induced voltage increasing by over 50% as longitudinal separation is changed from zero to infinity. Similarly, magnetic field measurements several feet from the roadway will not be accurate if the roadway section is only ten feet long. Acoustic noise measurements have analogous characteristics. Acoustic testing of the pickup cores is valuable because it identifies performance of various types of cores and sound treatments, but it is difficult to extrapolate from measurements of a single core to an accurate prediction of the acoustic noise generated by the entire pickup. Measurement of current equalization in roadway, pickup, or power distribution conductors is possible only when the entire subsystem is assembled. Testing of current equalization with a single pickup core—or even a single roadway module—would yield inaccurate results as the inductances in the turnaround portion of the loops would be very significant and perturb results.

### **5.2.1 Pickup Inductor**

The pickup inductor was assembled and initially tested in Building 167 although acoustic testing of the entire pickup was performed over the test track (outdoors). Test data were used in some of the design effort, such as selection of the roadway conductor transposition pattern.

#### **5.2.1.1 Current Equalization**

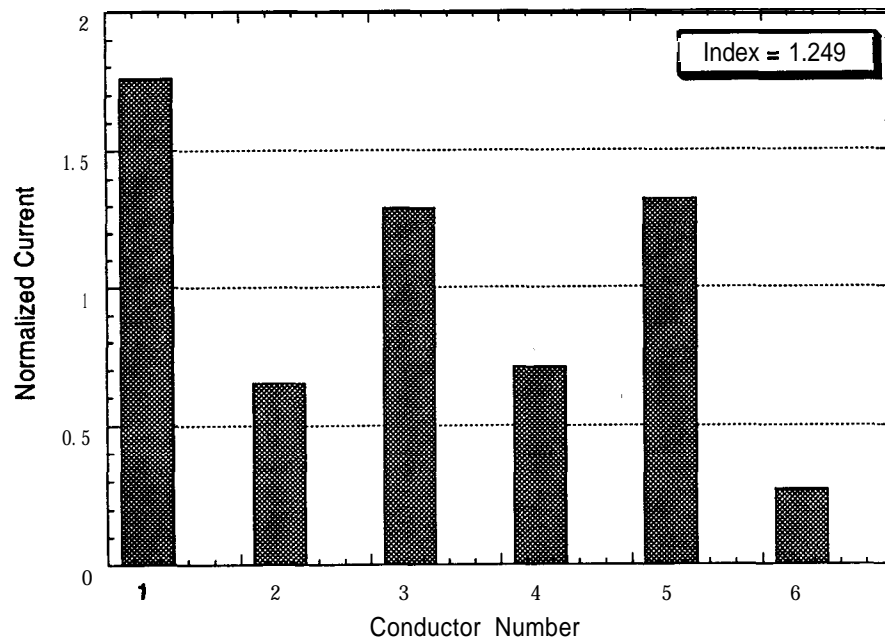
Large, high-frequency currents are required for the RPEV technology to create adequate magnetic fields in a large airgap to transfer the desired power. Due to skin effect (the tendency of current to flow near the surface of a conductor at higher frequencies), it is desirable to keep conductor sizes moderate, which requires several parallel conductors to keep resistive losses within acceptable limits. For the circuits in the inductive coupling system much of the impedance is reactive so equal resistive components in the various parallel paths do not ensure equal current distribution. In both the roadway and pickup inductors, the presence of the cores causes the total inductance (both self inductance and mutual inductance with all other cables) of the conductors to vary, depending on their positions within the conductor slot. Slight mismatches in inductance can result in large inequalities in the current distribution through the mutual inductance terms. For instance, even if the sums of all inductances for two paths are equal, if the currents in the other paths are unequal, the two paths in question will have different induced voltages (and unequal currents) because all mutual inductances must be multiplied by the current in the respective cables before being summed to determine the induced voltage.

If all turns in the pickup winding were in series, the current would automatically be equal in all conductors. With two parallel paths, the currents can be effectively equalized through symmetry considerations. The pickup has twelve conductors on each side. They are grouped into six parallel paths with two conductors (two turns) in each path. Symmetry arguments cannot be used to solve this problem.

The simplest approach to solving the crisscross problem experimentally is

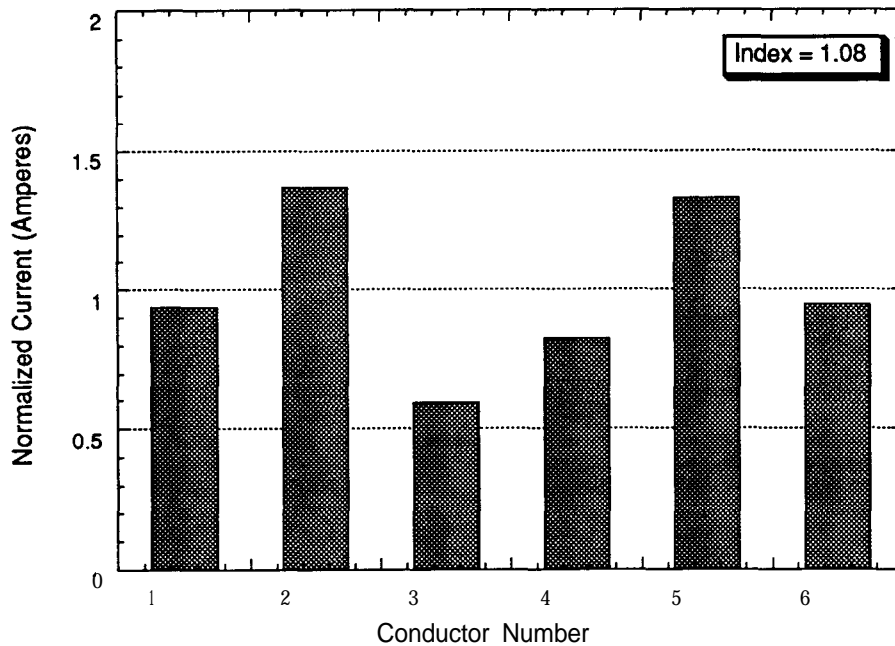
1. Attach all conductors in series, with a symmetric crisscross at one end.
2. Connect the pickup to a resistive load and power up the roadway.  
Measure the voltage on each turn.
3. List the various conductors in ascending order of voltage. Pair the highest and lowest voltage conductors together, second highest with second lowest, and so on. This gives the first crisscross, resulting in twelve paths (each with a single turn) that do not have a symmetric crisscross but have induced voltages much more equal than they would be with a symmetric crisscross.
4. List these new loops in order of ascending voltage and again pair highest with lowest, second highest with second lowest, and so on. This gives six parallel paths with two turns each.

This approach gave mediocre results as shown in Figure 5.41. The measured currents are normalized so 1.0 represents the average of all six measurements. The index (1.25) is equal to the ratio of the resistive losses with the actual current distribution to the resistive losses if all currents were equal to the average of the actual distribution. Sometimes the sum of the individually measured currents is greater than a single measurement of the total current, which may be due to instrument calibration, but is more likely caused by slight phase differences within the individual conductors. The sum is occasionally less than a single measurement of the total, which is definitely due to instrumentation error. For the case shown in Figure 5.41, the losses are 25% higher than ideal and currents deviate from the average by 75%. This index can definitely be improved and values of 1.05 or better are generally achievable. The more turns (choices for crisscrossing of conductor paths), the better the achievable index value. A trial-and-error approach (backed up by considerable engineering judgment) was used to determine other crisscross patterns that would result in more uniform current distribution. One day and approximately twenty attempts later, the index had been lowered to 1.08 as shown in Figure 5.42. Previous experience indicated that a better solution was likely although it **would** require a combination of experimental and analytic efforts.



RFS3-013

Figure 5.41 Current equalization

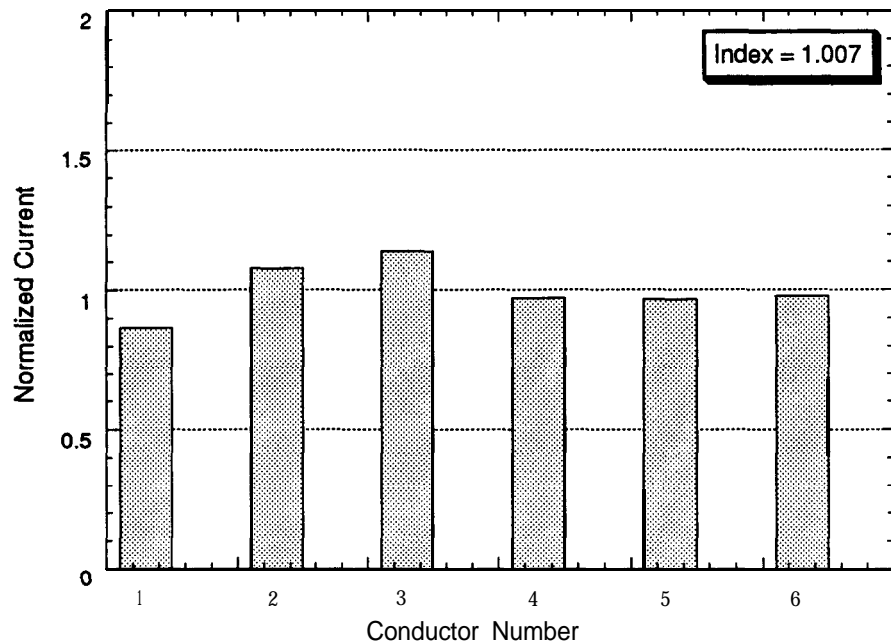


RFS3-019

Figure 5.42 Current equalization

The next method for solving the crisscross problem is much more rigorous. The inductance matrix (all self and mutual inductances) is determined experimentally, which is done by exciting each conductor separately and measuring the induced voltages in every other conductor. The mutual inductance with the roadway inductor is also determined through the same procedure. Different crisscross schemes can be analyzed with a computer using the experimentally determined inductance matrices and the most promising ones wired up and tried in the lab.

The crisscross method determined analytically was tried as shown in Figure 5.43. The initial attempt yielded an index of 1.007, an excellent value, concluding the work on the pickup crisscross.



RFS3-024

Figure 5.43 Analytically determined crisscross method

#### 5.2.1.2 Pickup Inductances and losses

Four important inductance values relate to the design of the roadway and pickup inductors. The first-open roadway inductance—deals only with the roadway. The other three—mutual inductance, pickup leakage, and roadway leakage inductance—deal with the coupled condition.

Mutual inductance measures the magnetic flux that links the roadway and the pickup. This is the flux that couples power to the vehicle and is the most important of the three inductances in the coupled condition. The pickup leakage flux is detrimental to power coupling and results in a reduction of voltage at the pickup terminals. The smaller this is, especially in comparison to the size of the mutual inductance, the better. Pickup leakage does not represent an actual loss of energy as it is a reactive, not resistive, component.

Coupled condition roadway leakage and open roadway inductance have a similar effect on the system because they both contribute to the roadway terminal voltage. The higher these terms, the larger the required voltage for the power conditioner and power distribution system. As with the pickup leakage inductance, these are reactive, not resistive, terms and do not contribute directly to system losses. They do, however, decrease the system power factor, indicating that the flux in the roadway cores is higher and roadway core losses increase as flux increases.

The three inductances relating to the coupled condition (mutual, pickup leakage, and roadway leakage) can be calculated based on open and short circuit tests. Table 5.2 shows the measured and predicted values of all three terms, showing reasonably close agreement. The open and short circuit tests also give an estimate of the experimental error-on the order of 5% for this test. Two calculations are possible for one of the inductors, and the difference between these two gives an estimate of the errors involved in these tests.

**Table 5.2**  
**Measured and Predicted Inductance**

<b>Inductance (mH)</b>			
	<b>Mutual</b>	<b>Pickup Leakage</b>	<b>Roadway Leakage</b>
Predicted	13.56	4.29	4.18
Measured	15.80	5.4	6.75

#### **5.2.1.3 Acoustic Noise**

Acoustic noise testing of the entire pickup is not as repeatable or accurate as pickup core testing since the entire pickup cannot be tested in the anechoic chamber. The

entire pickup was moved outdoors over the test track for the measurements. Ambient noise due to variable noise sources such as wind, airplanes, and traffic on I-580 along the edge of the Richmond Field Station was a problem. Measurements were taken to both the side and the end of the pickup as it was supported on the wooden test frame. The pickup was tested at several power levels. The OBC was placed in Building 167, and it is believed that noise from the OBC was not a significant factor in the pickup acoustic noise measurements shown in Figures 5.44 (side) and 5.45 (end). Data for distances less than ten feet (characteristic dimension of the noise source) are in the near field and should probably be ignored as shown in Figure 5.44 where the sound pressure level at 7.5 feet is 5 to 10 dBA lower than at 10–15 feet. The sound pressure levels are in the range of 50 – 60 dBA within the free field, approximately 10 dBA higher than free field measurements for a single pickup core at the same distance. This level is acceptable as pickup noise in the passenger compartment will be reduced due to the attenuation and shielding of the vehicle

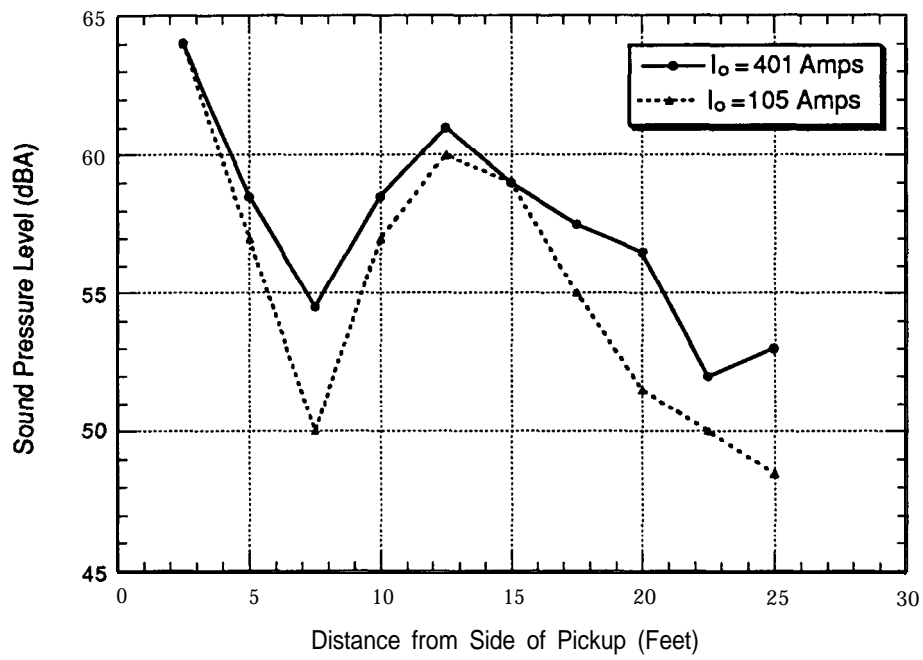
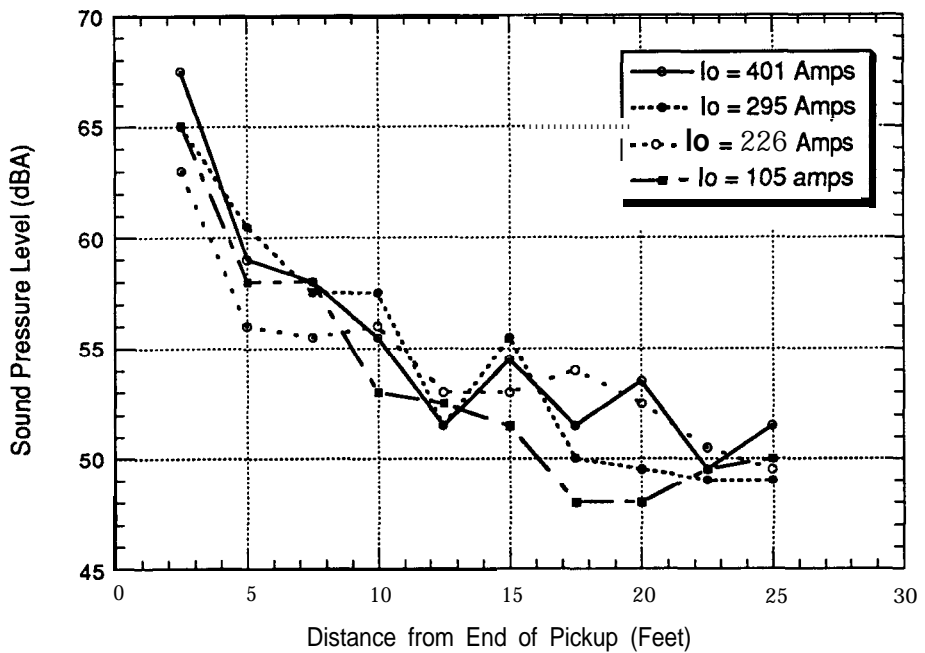


Figure 5.44 Pickup acoustic noise measurements (side)

RFS3-073

body. These data were taken without the sound treatment that was developed during acoustic testing, but it could have been added. Sound pressure levels drop off with distance as one would expect. No more the 5 dBA separates the measurements at low

output power (100 amps) and maximum output power (400 amps). Measurements from the end are shown for two intermediate power levels, and the data are tightly bunched because pickup voltage and flux levels in the cores vary weakly with power level. Noise levels would be expected to change more if the output voltage were changed (by charging a higher voltage battery pack such as the G-Van battery that has a nominal voltage of 216 as compared with 128 for the bus).



RFS3-073

Figure 5.45 Pickup acoustic noise measurements (end)

Some data taken from the first-generation pickup support this assertion. These data were taken in the breezeway at Translab, which is a poor acoustic environment. The readings tend to be higher and less repeatable than the data from Richmond Field Station, but some trends are clear nonetheless. Figure 5.46 shows data at two frequencies as pickup voltage is varied. At a given frequency, the acoustic noise increases with voltage. Higher flux levels are required at lower frequencies to get the same output voltage, which explains why the 160 Hz curve is 5 to 10 dBA higher than the 285 Hz curve. For voltages between 150 and 200, the measurements are between

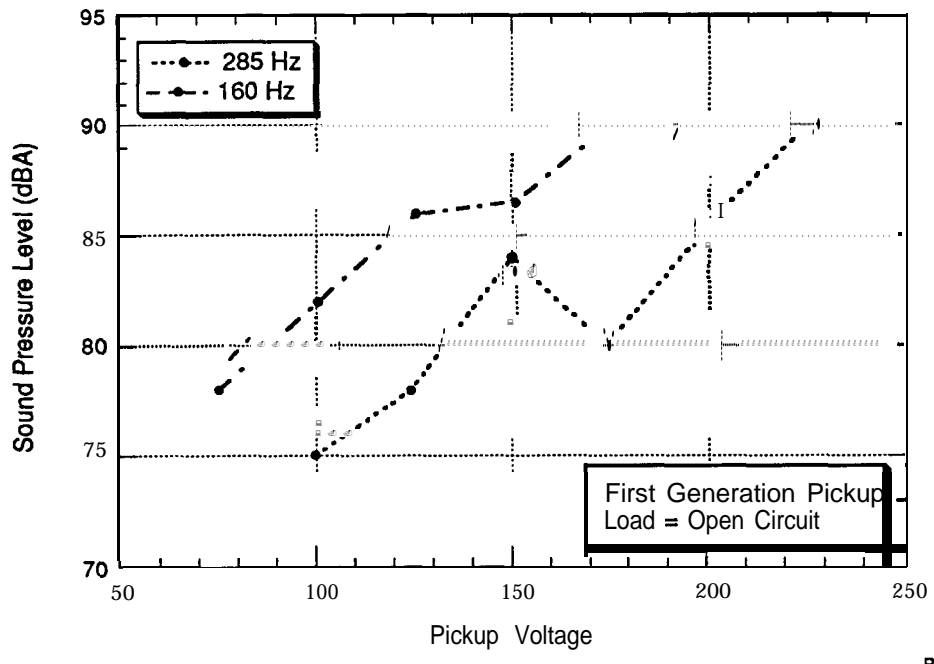


Figure 5.46 First-generation pickup acoustic noise

80 and 90 dBA, approximately 30 dBA higher than with the second-generation pickup. The acoustic environment of the breezeway may have added up to 10 dBA to the measurements. Also these data were taken at lower frequencies and therefore higher flux levels than the Richmond Field Station data, which probably account for 5 dBA. Regardless, the second-generation pickup is substantially quieter (15 -20 dBA) than the first-generation. Figure 5.47 shows acoustic noise at various frequencies with a constant roadway current, implying constant flux within the pickup for the open-circuit condition tested. The acoustic noise varies considerably although most readings lie between 70 and 80 dBA. The voltages range from 50 to 150, which is the reason that these noise levels are somewhat lower than for the previous plot.

#### 5.2.1.4 Heating

We checked pickup heating numerous times during testing and was never found any heating beyond mildly warm to the touch. Considering only temperature rise, the pickup is somewhat over-designed. The size and weight of pickup components (both cores and conductors) could be reduced, but care would have to be taken to avoid creating excessive acoustic noise or energy loss.

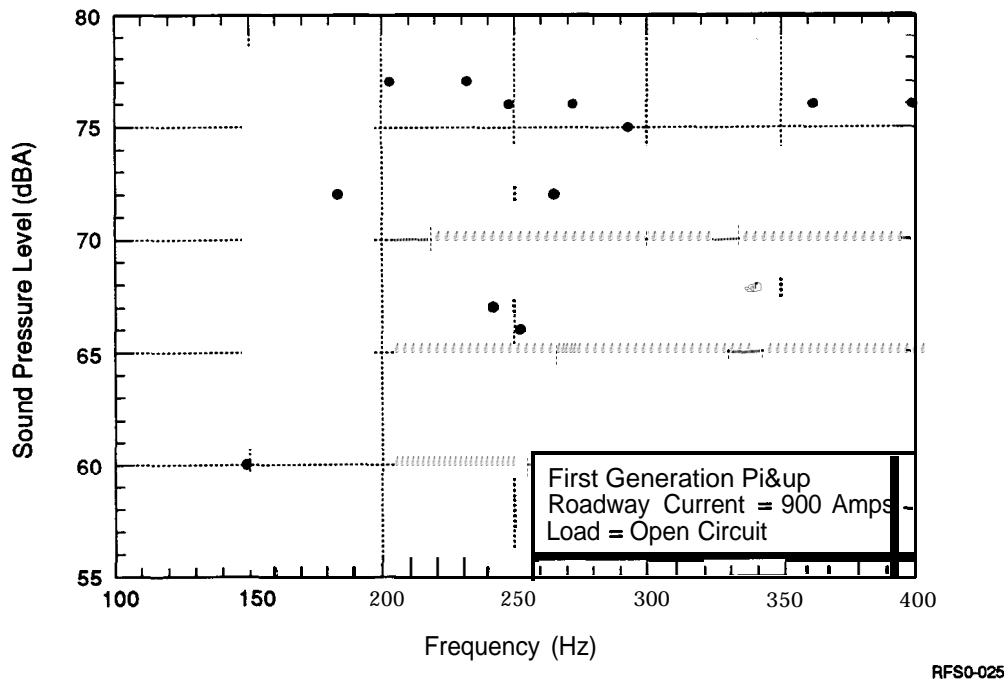


Figure 5.47 Acoustic noise at various frequencies with constant roadway current

### 5.2.2 Roadway Inductor

The roadway inductor is the element of the system that is most likely to cause adverse environmental impact. It represents one of the largest sources of losses in the system and the highest capital cost item for most possible systems, especially during the early years of deployment. The roadway inductor also presents a significant challenge to ensuring mechanical integrity. Some of these items present conflicting objectives, such as reducing costs while minimizing losses and ensuring mechanical integrity. The designs developed attempt to form reasonable compromises, and testing helped validate or disprove the design assumptions.

#### 5.2.2.1 Current Equalization

Roadway current distribution is slightly affected by the presence of the pickup and its currents, but this effect can be ignored, which makes the current equalization easier than for the pickup. On the other hand, the roadway has only one turn, which complicates the problem. If there were no junctions in a single powered segment, the current equalization would be poor, due to the limited number of choices available

to the designer. The test track was designed to have several possible transposition locations. The segment using aluminum bars as conductors has five sections (plus the bus stop) simply because forty feet was the longest length available for the bars. The cable segment was split into two sections of 120 feet and 80 feet. This split allowed the bus stop to be located near the center of the segment, permitting lane change experiments both entering and leaving the bus stop and it provides extra crisscross points, allowing much more effective equalization of the currents.

Section lengths had to be determined early in the project, long before construction began, which meant that an effective crisscross had to be determined without the benefit of experimental data. In reality, it was sufficient to determine that an effective crisscross pattern was possible with 120- and 80-foot sections, which could only be done by determining the inductance matrix analytically and then examining various section lengths to determine which had high likelihood of yielding effective crisscross patterns. The POISSON magnetic analysis program was used to determine the inductance matrix one element at a time. This effort was well rewarded as the crisscross pattern determined using POISSON's inductance matrix worked well. Figure 5.48 shows the current distribution for the cable section using this approach. The index is 1.017-a very good value-and no further work was required on current equalization in the cable segment.

With five sections on the main line plus the bus stop, eleven crisscross points are available in the bus bar segment. So many choices makes the design more difficult. To cut down on the order of the problem, we decided to wire three sections into one block, effectively forming a 120-foot section. In the vaults joining these three sections, each conductor was connected to the corresponding conductor in the next section, with no transposition. The same was done between the other two sections of the mainline, forming an 80-foot section. This makes the analysis similar to that for the cable sections.

The inductance matrix was determined experimentally rather than using POISSON. A crisscross pattern was determined and tried. In two locations, the bus bars have shorted against each other due to inadequate vertical separation caused by installation errors (discussed in Section 5.2.2.5). We determined that a new crisscross pattern could be developed in which the impact of the short circuits could be minimized by establishing equal potential on the two shorting conductors at the point of contact, in effect creating a pattern that had equal current distribution before the short and another with equal currents beyond the short. A new transposition

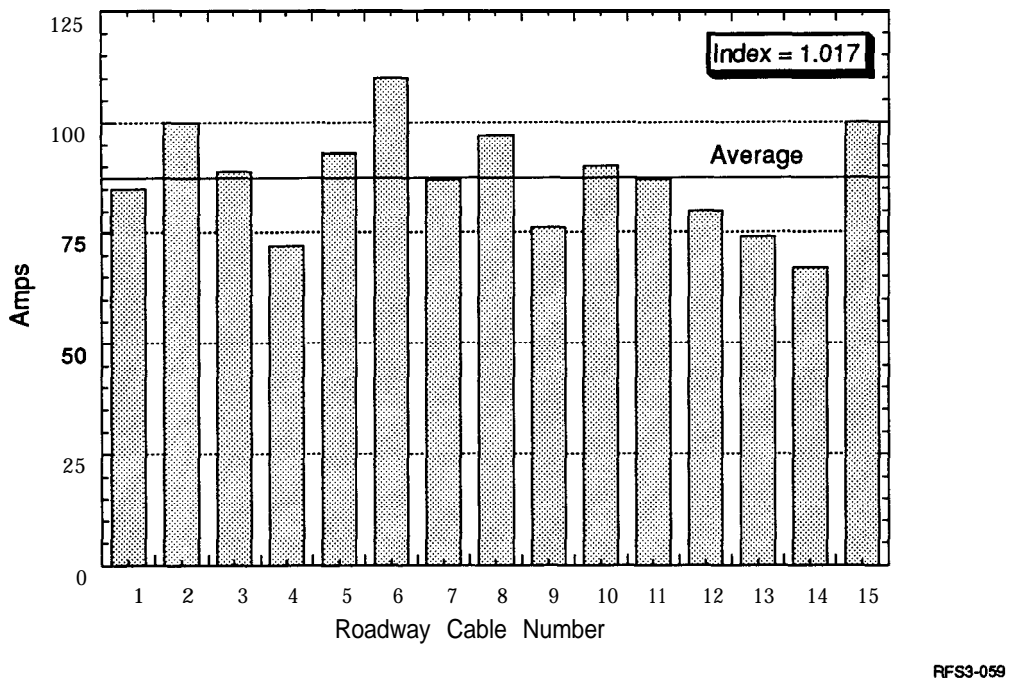


Figure 5.48 Current distribution for the cable section using POISSON

pattern was not developed in the interest of moving on to testing of the bus and conserving resources for areas where no certain solution was known. The current distribution in the **busbar** section due to the shorting caused a slightly higher (~10%) open roadway loss in this section compared to the cable section.

#### 5.2.2.2 Inductance and losses

The open roadway inductance is equal to the voltage divided by the product of the current and the frequency (in radians per second). Our test results were 182 microhenries for 220 feet of track, or 0.83 microhenries per foot, compared to the POISSON prediction of 0.73 microhenries per foot. The POISSON results are based on a calculation of the energy stored in the magnetic field generated by the roadway. Because POISSON only calculates the magnetic field out to a finite distance (5 or 10 feet from the centerline), the predicted value is smaller than the measured one.

Losses in one section of the open roadway operating at nominal conditions were measured at 18 kilowatts, compared to the calculated 7.2 kW or 12 kW based on the tests of the prototype roadway modules. Measured losses in cores are generally larger

two is often encountered. Since this is a new type of core, larger losses are not unexpected. Large core losses are most likely the cause of the losses rather than the conductor losses. This phenomenon needs to be investigated further.

#### 5.2.2.3 Acoustic Noise

Two sources of noise must be considered-the roadway inductor itself and other objects that may be excited by the magnetic flux emitted by the roadway. Previous tests had shown that neither of these would generate substantial acoustic noise. The tests of a one-foot roadway section (described in Section 5.1.2.4) gave reasonably solid evidence about the roadway. Tests done in Phase 3C of the project showed no perceptible noise in a conventional car parked above the roadway. The only acoustic noise observed was from heating samples placed directly on the pole surface and especially across the conductor slot of the roadway inductor. The first assertion proved to be well founded, but the second was not and exposed one of the most significant adverse findings of the project.

The roadway inductor itself proved to be quiet and was usually inaudible even in the usually quiet environment of the Richmond Field Station. The only audible noise was from the vault lids, and it could not be measured relative to the ambient noise levels.

A humming at twice the roadway frequency is noticeable both inside and outside conventional automobiles parked or driving over the roadway inductor. The humming was more noticeable inside cars and was objectionable when vehicles were stopped. At moderate and high speeds, the various sources of road noise (engine, tires, wind) masked the hum as did a radio played at moderate levels. We observed variations from one car to another as well as changes with roadway current and frequency. These acoustic emissions must have been present during Phase 3C testing, but were masked by the loud ambient conditions in the Translab breezeway caused by the power conditioner and series coil.

Noise measurements were taken for several cars. Lighter, less expensive cars tended to exhibit more noise. Figures 5.49 and 5.50 show sound pressure level measurements for the exterior and interior of two cars as a function of roadway current. The Tracer was louder than the LTD both inside and outside, in general by 5 to 10 dBA. Ambient exterior noise was 48 dBA. At 200 amps in the roadway, there was no perceptible hum. At 400 amps, humming was barely noticeable but the noise measurements had not yet started to climb. At 600 amps and above, the noise was

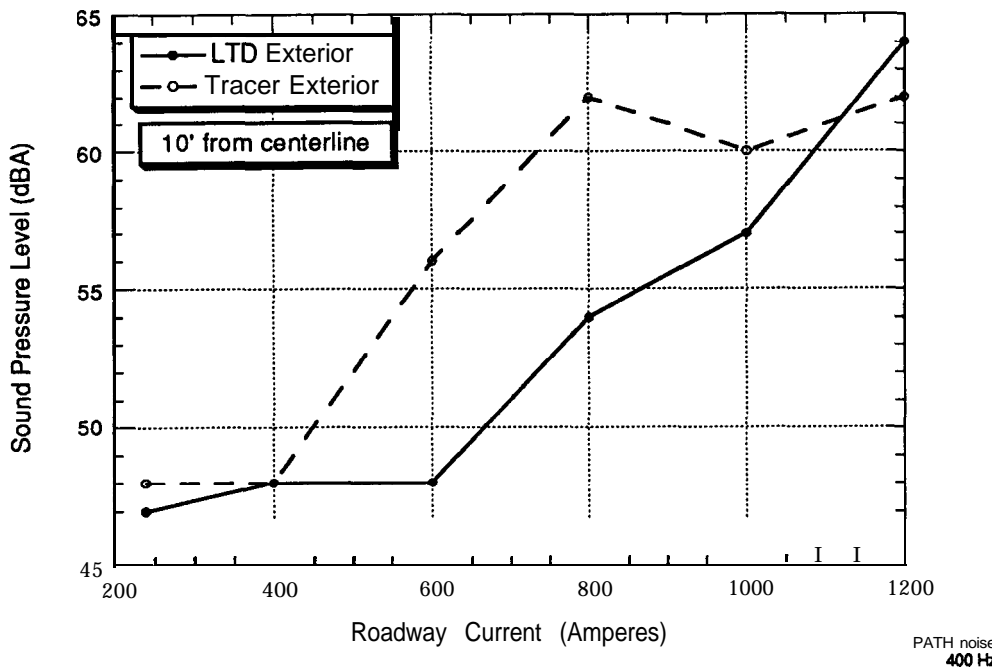


Figure 5.49 Sound pressure measurements outside automobiles

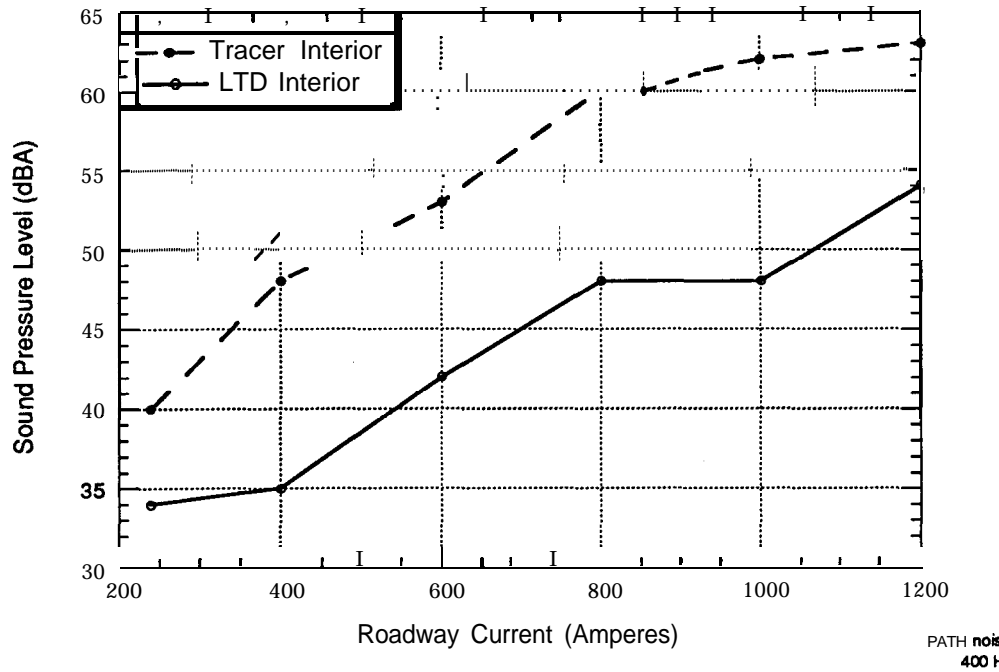


Figure 5.50 Sound pressure measurements inside automobiles

distinct and most people would be aware of it, especially in a quiet environment. The interior noise was similar to the exterior noise, but was more noticeable due to the lower ambient noise inside the cars. Figure 5.51 shows that the interior and exterior noise levels for the Tracer are similar. The LTD interior noise level is generally somewhat lower than exterior levels (between 5 and 10 dBA), presumably due to soundproofing in the more luxurious LTD.

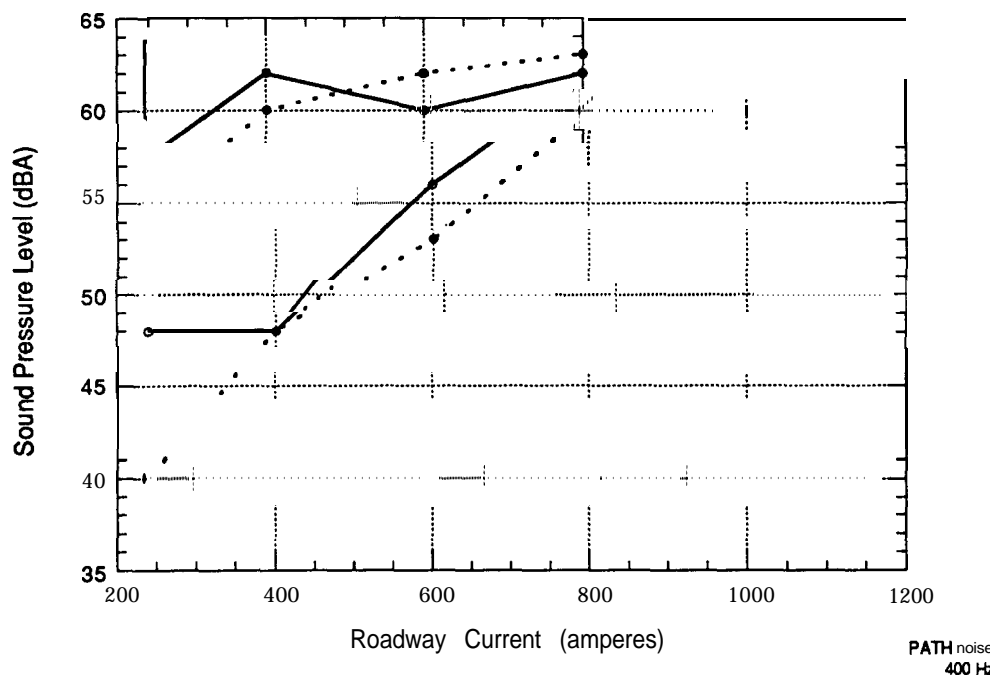


Figure 5.51 Interior and exterior Tracer noise levels

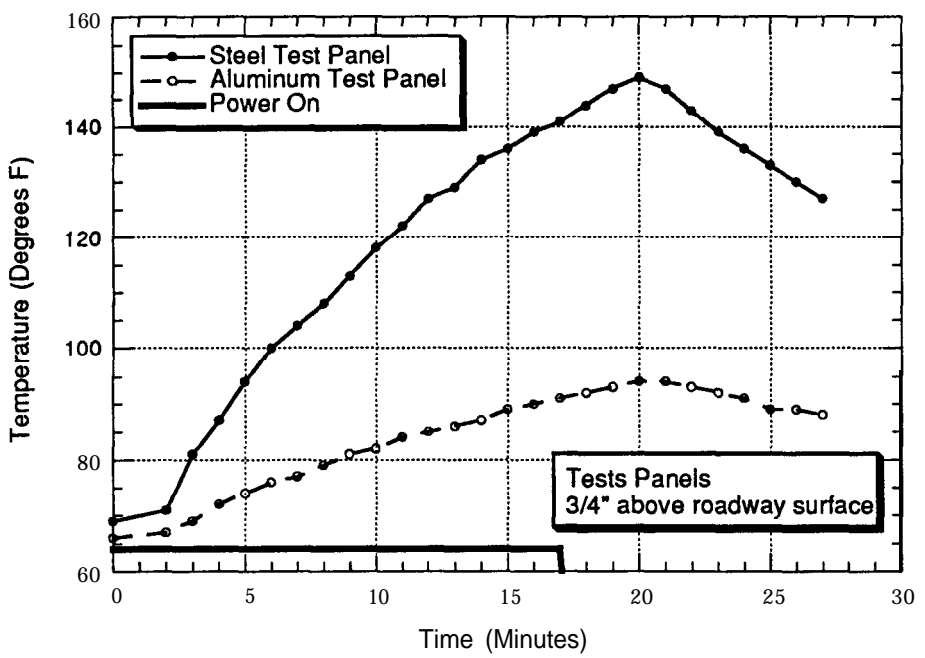
Acoustic noise in non-RPEVs is an important issue. Testing indicated that the threshold for perception at 400 Hz is above 200 amps, with roadway currents above 400 amps likely to cause objections by some segments of the population. Contrary to previous belief, acoustic noise in non-RPEVs is a significant issue and must be thoroughly investigated for any contemplated system. There is likely to be a frequency effect, but that was not investigated to any substantial degree.

#### 5.2.2.4 Heating

The roadway inductor itself heats up very little during operation of the inductive coupling system in either the coupled or uncoupled condition. The ground acts as a large heatsink and the roadway inductor's energy losses are small compared to its heat capacity. Even after five hours of operation at 125% normal rated current, the

roadway inductor was barely warm to the touch. As will be discussed thoroughly in the next section, solar loading generates more temperature rise in the roadway inductor than does normal operation.

Vault lid heating was a concern because metal placed on or near the roadway inductor can heat up significantly. Aluminum and steel were considered as material for the lids and several quick tests were performed to determine the relative parasitic heating of these two materials. In the first test, plates of each material were placed directly over the roadway inductor at a height of 0.75 inches. A 0.25-inch steel and 0.50-inch aluminum panel were used. The roadway was energized for 17 minutes. The resulting temperatures are shown in Figure 5.52. The temperature of the steel plate rose 80°F compared with 25°F for the aluminum due to the higher flux levels in the steel when it is placed near the roadway inductor.



RFS0-030

Figure 5.52 Relative parasitic heating of steel and aluminum under unrealistically severe test conditions

The test conditions were unrealistically severe as the roadway cores stop six inches from the vault lids and the conductors dive down as they enter the vaults for the cable segment of the roadway. More realistic test conditions are presented in Figure 5.53. The aluminum is as close to the cores and conductors as is reasonable while the steel is as far from the cores and conductors as is reasonable. Despite the distance, the

steel still heats up twice as quickly as the aluminum. Based on these tests, aluminum was chosen for the vault lid material.

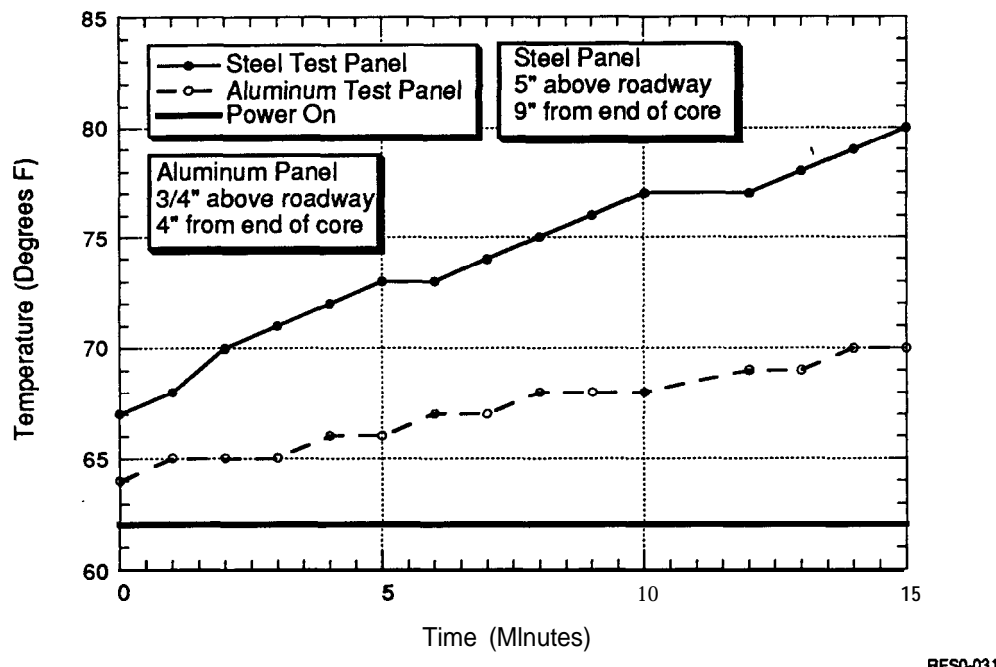


Figure 5.53 Relative parasitic heating of steel and aluminum under realistic test conditions

#### 5.2.2.5 Mechanical Integrity

The roadway inductor need to have an effective life of thirty years. If it is substantially less, the technology may not be practical or economical. The installation at Richmond Field Station is the first designed to carry street-legal tire loading. Both the cores and conductors must be able to withstand these loads effectively. The integrity of the entire pavement after the installation of the roadway inductor needs to be assured.

There has been neither sufficient time nor repetitive loading to prove anything substantive about the pavement integrity, especially considering that the Richmond Field Station inductor is in an asphalt roadway and installations in concrete roadways are likely to be more challenging.

The roadway core modules are holding up exceptionally well to the best of our knowledge nearly two years after installation. No problems of any kind have been

discovered. They are all solidly in place, with no visible cracks. The slurry seal has been worn or gouged away in a few places, but the core modules themselves have not been damaged.

Two types of conductors were used in the track at Richmond (0.25 x 1.5 rectangular aluminum bus bars and 350 MCM insulated aluminum cable) to determine how well each kind would handle road loads and thermal expansion.

The conductors are potted in place with a mixture of sand and polyester, a method that was inexpensive and had a reasonably good chance of success. Two places (one each in the cable and bus bar segments) had inadequate mixing of the catalyst and the polyester never hardened. The offending material was removed and replaced with properly mixed material. In the cable section, the material that did not harden was at the surface of the slot, making detection and replacement straightforward. In the bus bar section, the soft material was near the bottom of the slot and the upper surface had adequate catalyst to harden properly so we did not discover it until the bus bars started to buckle due to thermal loads. The soft material was removed and replaced with properly mixed material. One of the shorts mentioned in Section 5.2.2.1 was introduced during this repair operation. When properly repaired, the bus bar buckling disappeared.

During installation we attempted to seal the conductor slots with clay where they entered the vaults. In many locations, the seal was inadequate. Although the sand remained in place, the polyester leaked through the seal into the vault, leaving sand with a thin film of polyester coating the individual grains and air-rather than polyester-filling the remaining volume. These areas were very weak and developed cracks shortly after being exposed to traffic. Some broke up completely as shown in Figure 5.54 and have not been repaired.

Two cost-minimization choices in the roadway have proved troubling. One is the use of polyester rather than epoxy as the resin mixed with sand for potting the conductors in place. The thermal expansion coefficient of epoxy matches that of concrete and steel while polyester, like aluminum, has a higher one. The core modules, made of epoxy and steel, match the thermal expansion of the underlying concrete leveling course. The polyester and aluminum in the slot, however, expand much more upon heating (primarily solar loading), which has caused cracking along both edges of the conductor slots. Cracking is less pronounced in the shaded areas that have smaller temperature changes. This cracking has not caused problems yet, but is clearly an undesirable feature of the roadway as installed. Polyester may be replaced with epoxy or some other material in future applications.

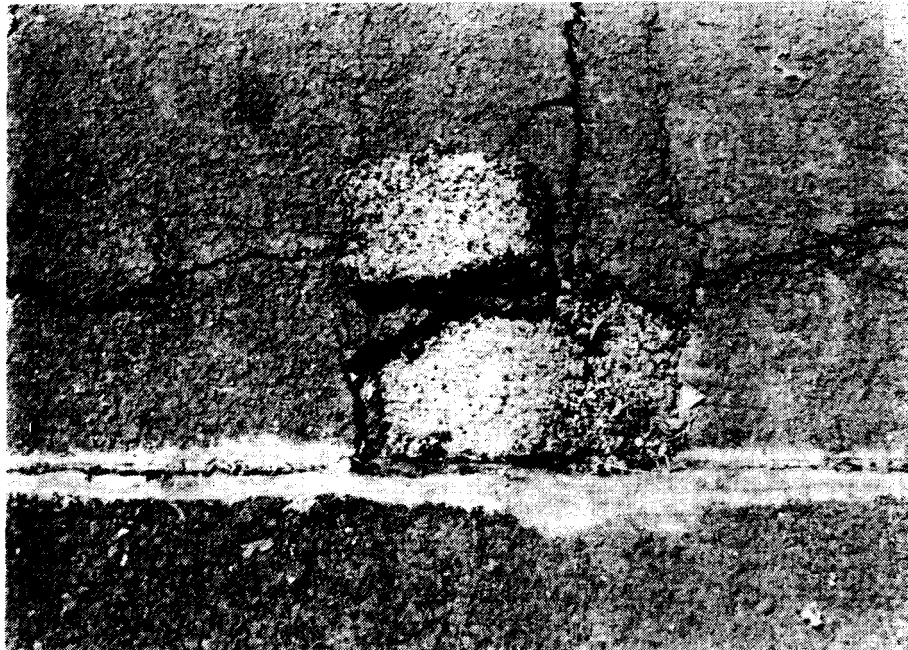


Figure 5.54 Cracks in conductor slots

The second troubling cost-minimization choice was the decision to put the 350 MCM cables used in one section of the roadway directly in the potting compound, which caused the most severe failure of the mechanical integrity of the roadway: the buckling of the cables in the 120-foot section of the roadway. Unlike the buckling in the bus bar section or the cracks at the vault entry points, there are no signs of inadequate catalyst or voids in the material that is breaking. The buckling is caused by the cables' thermal expansion. Placing cables in conduits to allow for thermal expansion was considered during the original design process. In addition to being more costly, conduits would have required the slot to be enlarged, and this was undesirable. Due to the spiraling of the aluminum strands in the cable, some of the increase in size is manifested as an increase in cable diameter rather than in cable length. We were unable to determine if the entire volume change could be taken up by the compliance of the insulation and decided to pot the cables and see what happened. The conductor slots on both sides of the 120-foot section have buckled as shown in Figure 5.55. Neither side of the 80-foot section has buckled.

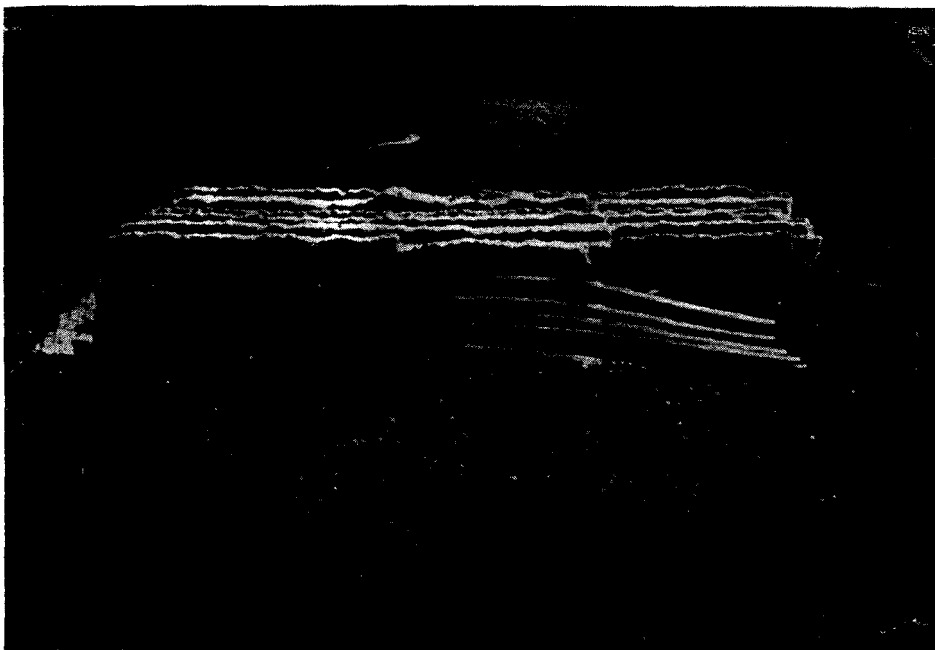


Figure 5.55 Conductor slot buckling

The conductors in the 120-foot section have been removed, and conduits (of approximately the same diameter as the original cables) have been placed in the slot and grouted in place. The conductor size has been reduced to allow them to fit into the new conduits.

#### 5.2.2.6 Magnetic Fields

Without magnetic fields to transfer power to the vehicle, the RPEV technology would not exist, but any adverse environmental impact of the RPEV technology is due to the magnetic fields. Direct effects include biological effects or interference with communications or automotive electronics. Acoustic noise and parasitic heating are two of the more obvious indirect effects.

Matching predicted magnetic fields with test measurements helps validate the analysis procedures. Test data are more useful than model results in convincing ourselves and others that the basic physics of the technology is well understood. Test data are also valuable for the environmental review process.

Figure 5.56 shows the predicted magnetic flux lines for the open roadway. These are the same fields shown in Figure 5.3 but only half of the roadway inductor is shown

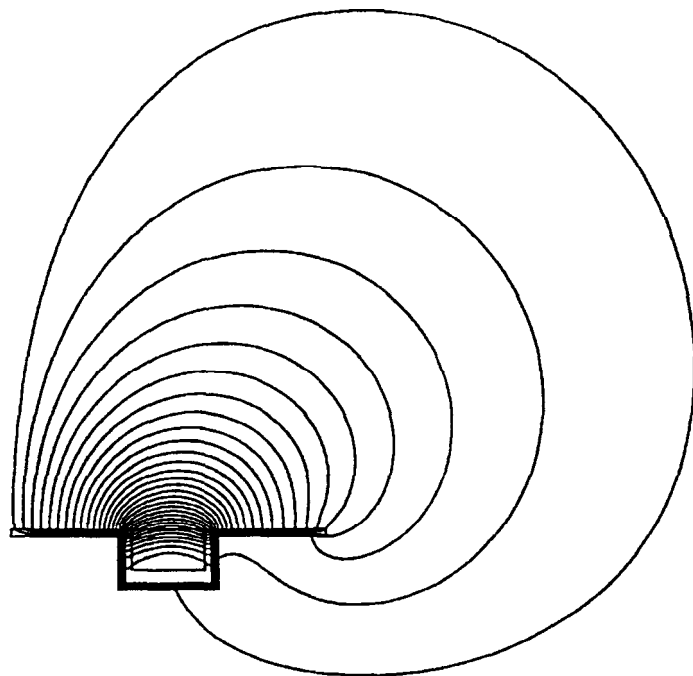


Figure 5.56 Open roadway lines of flux

as the other half is symmetric. Figure 5.57 shows the predicted magnetic flux levels 10 inches above the road surface. The solid line shows the total flux density, and the dashed and dotted lines give the lateral and vertical components. As shown in Figure 5.56, the flux lines are vertical at the inductor centerline, but become horizontal over the conductor slot, at a distance of about 12 inches from the roadway centerline. In Figure 5.57 the vertical component is at a maximum at zero lateral offset (the center of the inductor). It drops to zero at 12 inches offset and then reverses sign. The lateral component starts at zero, builds to a maximum over the conductor slot, and reverses beyond the edge of the inductor. The flux levels drop off quickly beyond the edge of the roadway. Figure 5.58 shows the predicted (solid) and measured (dashed) values for the total flux density at a 10-inch height, which match well. Figures 5.59 and 5.60 show the predicted and measured flux densities at 2- and 40-inch heights. The curves in Figure 5.59 match closely but those in Figure 5.61 do not. The error in Figure 5.61 can be attributed to the instrument used to measure the fields, which proved to be inaccurate at field levels below 3 gauss. (A more accurate gauss meter was used for the measurements reported on later.) The curve of the predicted flux levels oscillates up and down directly over the conductor slot due to the discrete size of the elements in the POISSON analysis mesh. In reality, the curves

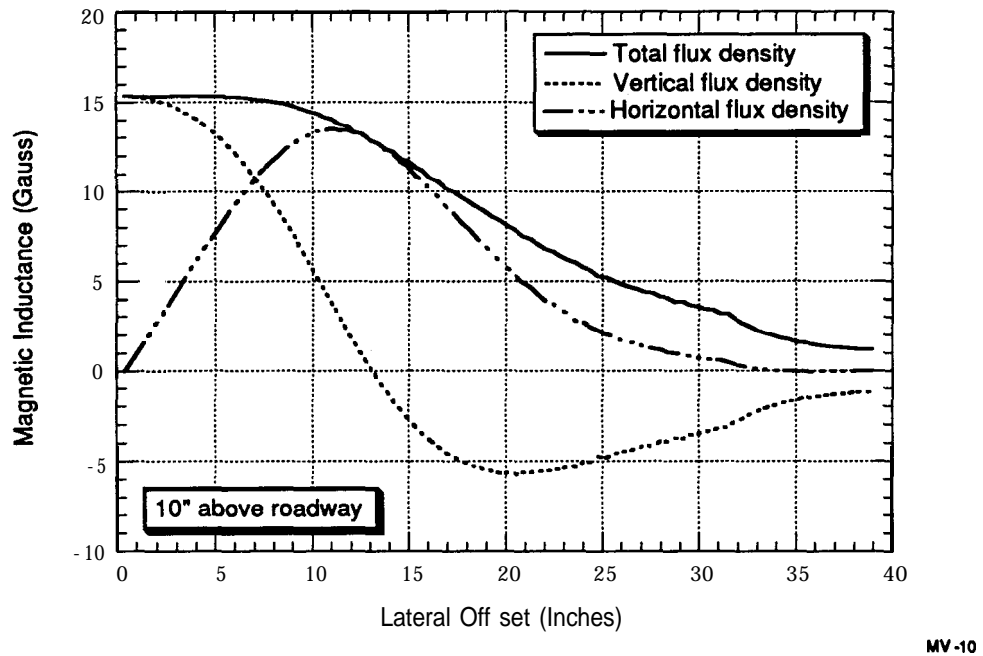


Figure 5.57 Predicted total magnetic flux ten inches above roadway

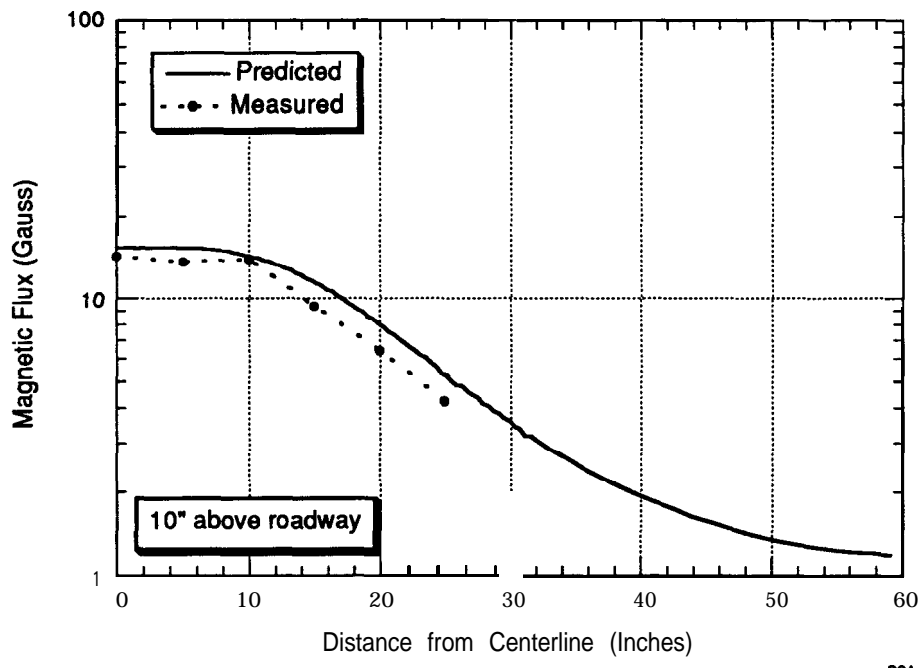
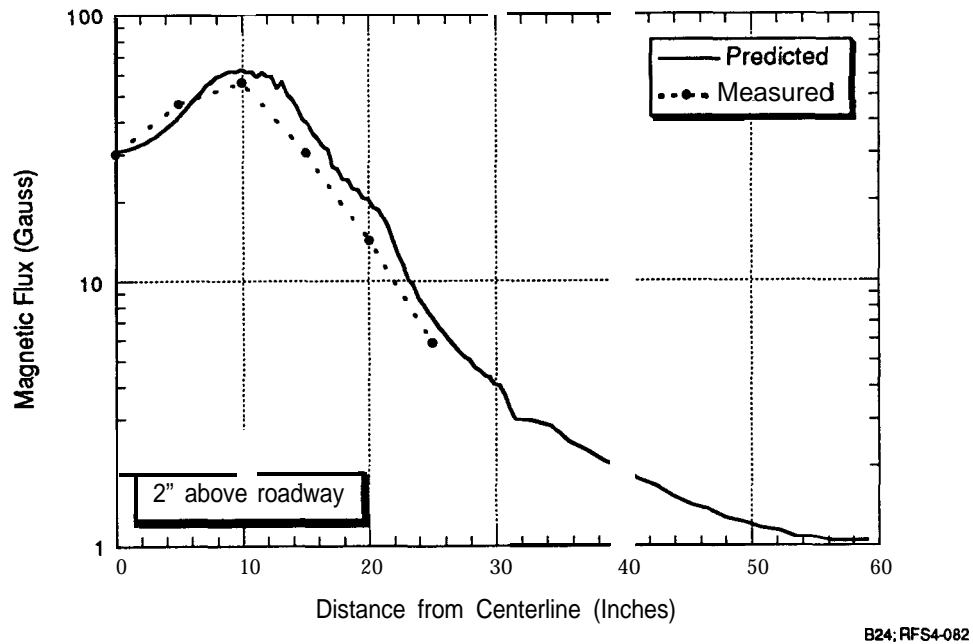
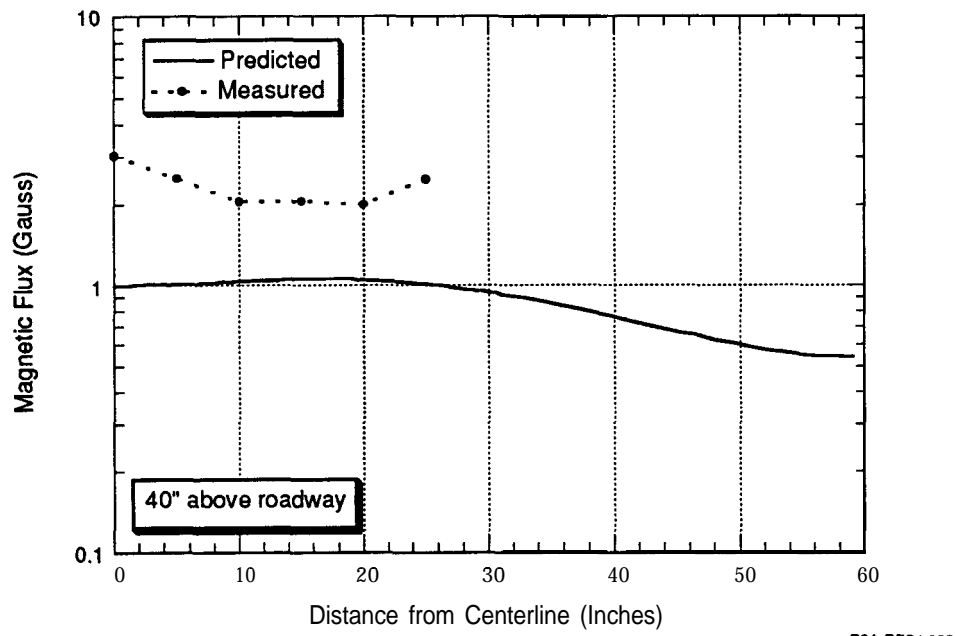


Figure 5.58 Predicted and measured magnetic flux ten inches above roadway



B24; RFS4-082

Figure 5.59 Predicted and measured total magnetic flux two inches above roadway



B24; RFS4-082

Figure 5.60 Predicted and measured total magnetic flux forty inches above roadway

are smooth although they do change rapidly near the corners of the cores: Figure 5.61 shows the predicted flux densities at larger lateral offsets.

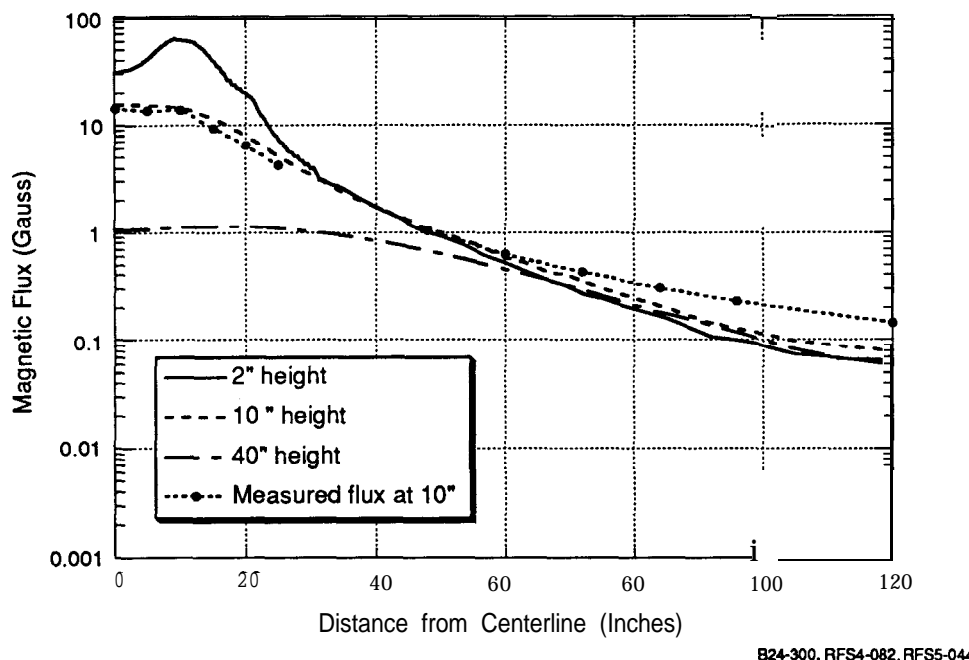


Figure 5.61 Predicted flux densities at larger lateral offsets

Magnetic flux levels were also measured inside a conventional car. These data are shown in Table 5.3, along with the data for the same 40-inch height when the car is not present. Fields inside the car are much lower because flux tends to follow the path of least resistance (lowest reluctance), which happens to be through the steel in the car's doors and floor.

**Table 5.3**  
**Magnetic Flux levels**

Height	In Car	Open Roadway
10 inches	- 400 mg	~ 15,000 mg
40 inches	-25mg	~ 1,000 mg

During the past decade, the possibility of adverse health effects of extremely low frequency (ELF) electric and magnetic fields has been raised. Interference with existing electronic apparatus, such as radio communications and electronic systems on internal combustion engine (ICE) vehicles, is also an area that needs to be examined. It is beyond the scope of this project to interpret the effects of the magnetic field that will be generated when the RPEV technology is deployed. A report prepared by the Office of Technology Assessment [8] provides an interesting and objective discussion of the issues as well as a summary and critique of work in the field.

Parasitic heating of metallic objects near the roadway was investigated during Phase 3C. The question of parasitic heating of a conventional automobile was not resolved as the power loss was too small to be measured with the existing instrumentation.

#### **5.2.2.7 Electromagnetic Interference**

Many common devices rely on magnetic or electromagnetic fields for their operation. The powered roadway creates and uses magnetic fields of an amplitude and frequency not commonly encountered so some devices may be susceptible to interference from the roadway inductor. Devices for which interference has been observed include AM radios, watches, television monitors, automotive speed sensors, and engine controls. The mechanisms for these interferences are known, and it should be possible to eliminate any interference with proper design of the RPEV system.

Due to the acoustic noise described in Section 5.2.2.3, the RPEV system has been redesigned, and operates at lower roadway currents and higher frequencies than the 1200 amps and 400 Hz used for the bus. Reducing the roadway current reduces the magnetic flux densities and any interference they might cause. The effects of the frequency change have yet to be determined.

During Phase 3C, we noticed AM radio interference on some radios that we believe was caused by the harmonics in the input waveform drawn by the power conditioner. The existing power conditioner has no input filtering, although such filtering is being considered for future installations, which is expected to eliminate AM radio interference.

Certain electronic analog watches have been observed to run quickly (either forward or reverse) within a few inches of the roadway inductor or in the **airgap** between pickup and roadway. All worked properly when reset.

Several television crews have visited the Richmond Field Station to report on the RPEV technology development. Magnetic fields from the roadway inductor have caused displays on some TV camera monitors to jitter and bounce around, but have not affected the image recorded on videotape. The monitor on the personal computer used for data acquisition has demonstrated the same phenomenon. It is not clear how much of the phenomenon is due to the power conditioner input and how much is due to the output waveform. This may be a moot point as the new designs mentioned previously address both issues.

We have noticed that some electronic speed sensors, including the speedometer on the bus, are affected by the roadway inductor magnetic fields. These sensors have a magnetic probe that senses the passing of gear teeth or some similar metallic objects. This type of sensor is often used to determine engine speed for electronic engine controls. It is also used to detect wheel speed for anti-lock brake systems. Preliminary tests indicate that these effects disappear at lower roadway currents, and no problems are expected if roadway current is reduced below 300 amps as dictated by acoustic noise concerns.

#### **5.2.3 Power Distribution System**

The power distribution system consists of all the equipment and cables used to get the proper current to the roadway inductor. As a minimum, a power conditioner and a transmission line to distribute power to the roadway segments are required. When more than one roadway segment is used, there are generally switching provisions, such as jumper bus bars, mechanical **contactors**, or solid-state switches, and power factor correction capacitance or other reactive components may be required.

The power distribution system used at the Richmond Field Station was a forced-fit solution to a challenging problem. The power conditioner specified and used during Phase 3C was designed to power two segments in either parallel or series, but was not designed for switching under load. Because the Phase 3D budget was insufficient to buy a new power conditioner, we devised a plan that had the possibility of providing segment switching capability with the existing power conditioner. The plan was to continuously power a load inductance equal to a single segment. The load could be one of the track segments or it could be the furnace coil inside Building 167, which has an inductance approximately equal to one segment's. A roadway segment would be wired in parallel with a capacitance that would offset the entire reactive component of the segment at the driven frequency. This arrangement had several

favorable consequences. First, the combination of a roadway segment and capacitor could be added in parallel to the circuit as a unit as they represented a purely resistive load at 400 Hz and would not affect the tuning of the power conditioner. Second, this load would draw power at unity power factor, reducing the current in both the transmission line and the switch. Unfortunately, due to our power conditioner's limitations, this scheme could not be implemented. This approach may work with a different power conditioner and has positive implications for a large-scale system as any transmission lines from the power conditioner to individual segments could run at unity power factor with lower currents and lower losses.

#### **5.2.3.1 Current Equalization in Transmission line**

The transmission line at Richmond Field Station consists of four quadruplex cables with 2/0 copper conductors. Two of the four conductors are used for each phase, minimizing the circuit inductance and stray magnetic fields. Since the conductors spiral within the overall jacket, a symmetry argument can be made that current should be equally divided among the conductors within each cable. Furthermore, since the phases are intermixed within a cable, there is approximately zero net current within each cable, and the proximity to other cables is of no consequence as equal currents should flow in the four cables. This arrangement is distinct from the conductor arrangement in the roadway and pickup inductors where the phases are separated. The measured current distribution within the transmission line is shown in Figure 5.62. The raw values of current are shown, not the normalized as in the current distribution analysis for the pickup and roadway inductors. The current distribution is excellent, with an index of 1.001. This approach works well for locations such as the transmission lines where phase intermixing is possible.

#### **5.2.3.2 Switching and Power Factor Correction Hardware**

The power factor correction and switching scheme, described previously and depicted in Figure 5.63, did not work as planned due, in part, to the output waveform of the power conditioner. It is nearly sinusoidal, but does have a small step (several volts) on the voltage waveform. This step input excites any resonant frequency within the driven circuit. The roadway/capacitor unit has a resonant frequency of 400 Hz. If it is added in parallel to another inductor, however, the resonant frequency of the entire circuit changes. When the two inductors were added in parallel, their combined inductance resonated with the capacitor, not just the

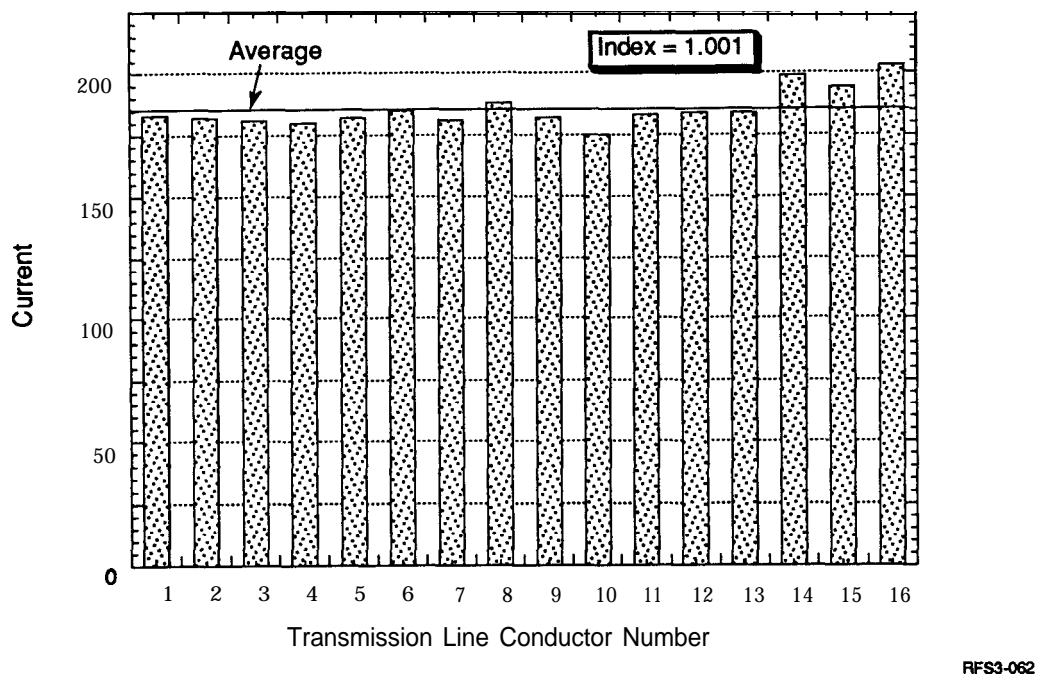


Figure 5.62 Measured current distribution within the transmission line

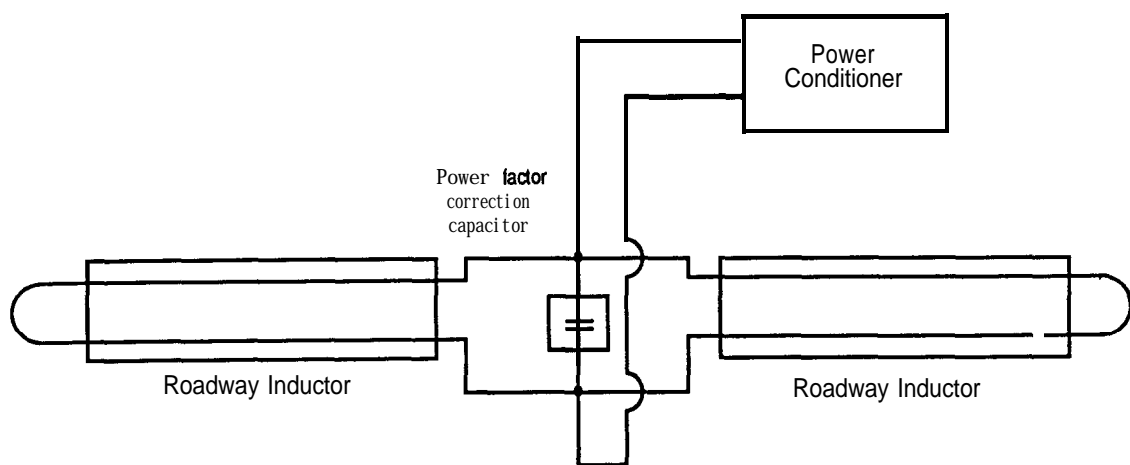


Figure 5.63 Schematic with parallel power factor correction

inductance of the roadway segment, resulting in some interesting waveforms as shown in Figure 5.64, but was of no use for powering the roadway inductor. This approach was dropped, ending our hope of being able to switch roadway segments into and out of the circuit under load in the experimental setup at Richmond Field Station.

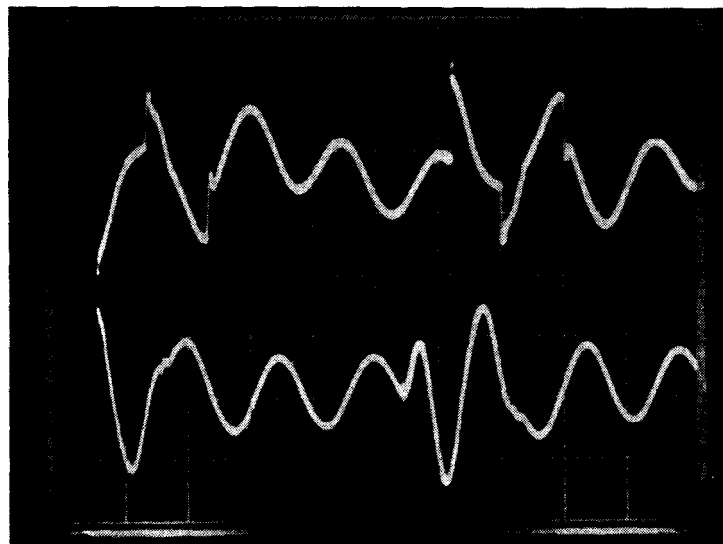
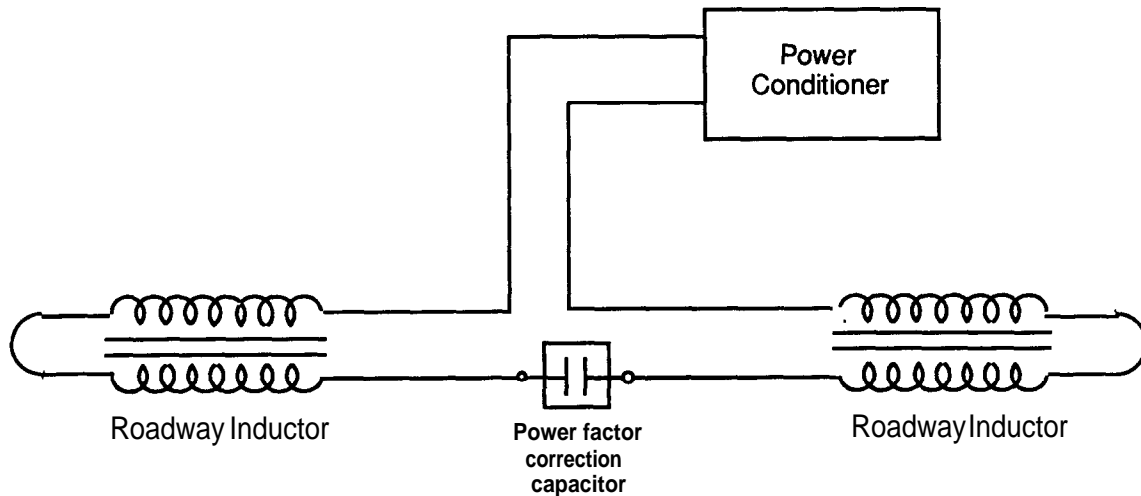


Figure 5.64 Waveform with unsuccessful parallel power factor correction

Instead we used series power factor correction, and it worked well. The roadway segments run at about 550 volts each. The cable in the transmission line is rated for 600 volts, so running the two segments in series would have driven it over-voltage. Running both segments in parallel without power factor correction capacitance would require 2400 amps rather than 1200 amps in the transmission line, again over its nominal rating. Running both roadway segments in series with a capacitor between them was the solution. The voltage and current in the transmission line remain the same as required for a single segment. The power factor of either roadway segment taken in series with the power factor correction capacitor is near unity, allowing power loss measurements to be made more easily and accurately. Figure 5.65 is the schematic of the power circuit used during nearly all testing of the vehicle. Although switching segments under load was not possible, this approach was adequate for range and acceleration tests as well as demonstrating power coupling with the vehicle in motion.



5544 05/19/93

Figure 5.65 Schematic of power distribution system-series power factor correction

#### 5.2.4 Operation of the Onboard Controller

The onboard controller was built but not tested during Phase 3C. This is a second-generation design, incorporating liquid-cooled (rather than air-cooled) capacitors and solid-state switches. Using liquid-cooled components resulted in a substantial saving in OBC volume, with the second-generation OBC having about half the volume of the original.

##### 5.2.4.1 Initial Checkout

Normal continuity checks were performed before the OBC was connected to power circuits. Initial testing was done at low power into a resistive load. As we gained confidence that everything worked properly, power levels were gradually increased. After the inductive coupling system had been run up to rated current and voltage into a resistive load, the original (Exide) bus battery was connected to the OBC output. Again testing was first performed at low current and then increased to the maximum. The inductive coupling system was run at full power for extended

periods to check the operation of both the forced-air and liquid-cooling systems. All connections and components were checked for excessive temperature rise that would indicate large losses, due to poor design or poor fabrication of the components (such as the  $di/dt$  inductors) or a poor connection, resulting in a large resistive drop and consequent heating. We determined that the onboard controller operated properly at the macro level and more detailed work could begin.

#### 5.2.4.2 Capacitance Steps

As originally built, the onboard controller had five steps of capacitance of equal size, allowing six discrete steps of output current (or nearly 100 amps of output current per capacitor step). There was a fixed (non-switchable) capacitance consisting of up to four taps of 150 microfarads. The second capacitor has six taps of 383 microfarads each. Five of these were switchable through the solid-state switches and the sixth was unused, but could be added to the fixed capacitance if necessary (if the pickup mutual inductance were considerably lower than projected). We replaced one of the 383 microfarad capacitance steps with a 150 microfarad step, in effect creating a half step and ten discrete steps of capacitance and output current, adding the slight complication that on half of the changes to a higher control state (more capacitance) the half step would be switched out while a full step was being added. If the switching was not done simultaneously, a large switching transient could occur. (See Section 5.4.2.) After testing the ten-step capacitance switching scheme, we decided to go a step further by placing several of the 150 microfarad taps of capacitance on switches, which increased the number of control states to twenty and reduced the minimum step in output current to about 25 amps, allowing any desired output current to be achieved within  $\pm 15$  amps. The upper part of Table 5.4 shows the capacitance wired to every switch for each of the wiring methods discussed. The lower part of the table lists all achievable values of switched capacitance and the switches activated to obtain that capacitance. If there is no listing, then that capacitance could not be obtained with that particular wiring method. With the final wiring method, almost every possible capacitance is achievable. The much finer control achieved with the final method allowed the actual current drawn by the vehicle to be much closer to the desired current and increases the average current coupled to the vehicle by approximately 20 amps.

We also decided to add capacitor discharge (bleed) resistors on each branch of capacitance as a safety feature to keep the capacitors from retaining a deadly electrical charge even when the ICS is turned off, allowing the OBC to be worked on safely off the powered roadway.

**Table 5.4****Capacitance Wired to Every Switch for Each of the Wiring Methods**

Switch Number	Capacitance Value Associated with that Switch		
	Initial Design	Intermediate Design	Final Design
1	383	150	150
2	383	383	150
3	383	383	300
4	383	383	383
5	383	383	766
Capacitance Value	Switches Energized* to activate desired capacitance		
0	—	—	—
150		1	1
300			1, 2
383	1	2	4
450			1, 3
533		1, 2	1, 2, 4
600			1, 2, 3
683			3, 4
766	1, 2	2, 3	5
833			1, 3, 4
916		1, 2, 3	1, 5
983			1, 2, 3, 4
1066			3, 5
1149	1, 2, 3	2, 3, 4	4, 5
1216			1, 3, 5
1299		1, 2, 3, 4,	1, 4, 5
1366			1, 2, 3, 5
1449			3, 4, 5
1532	1, 2, 3, 4	2, 3, 4, 5	
1599			1, 3, 4, 5
1682		1, 2, 3, 4, 5	
1749			1, 2, 3, 4, 5
1915	1, 2, 3, 4, 5		

\*Several capacitance values can be obtained with multiple combinations/permutations of switches

#### 5.2.4.3 Waveforms

During initial OBC checkout, we determined that the capacitance current waveforms were often highly distorted. Since the capacitor current is the derivative of the voltage across it, even slight glitches in the voltage were amplified into significant disturbances in the capacitor current. During the wiring changes described in the previous section, it became obvious that the inductance of the current limiting inductors (actually these inductors limit the rate of rise of current and are called  $di/dt$  inductors) has a strong effect on the waveforms. These inductors were originally placed in the circuit to protect the SCRs in the switches if a trigger circuit failed and fired at the wrong portion of the waveform. If fired at the peak rather than the zero-crossing of the voltage waveform, a large current would develop almost instantaneously. This rapid rise in current could destroy the SCRs.

These inductors in series with capacitor branches are also essential for limiting higher harmonics and distorted waveforms. They are important for all branches, even the fixed capacitance, that has no switch. Figures 5.66 and 5.67 display this rather clearly. In both oscilloscope photographs, a switched capacitor branch current is shown in the upper trace, and the rectifier current is shown on the lower curve. In Figure 5.66, the fixed capacitance has an inappropriate value of  $di/dt$  inductance, and the waveforms of all capacitor branch currents have a large third harmonic, nearly the same amplitude as the fundamental. In Figure 5.67, the inductor has been replaced with one with a more appropriate value, and the third harmonic has disappeared. A small glitch occurs when the rectifier input current reverses sign.

#### 5.2.4.4 Heating/Cooling

During static testing, the OBC was equipped with an automobile radiator that kept temperatures in the cooling system moderate. The radiator used on the bus was also from an automobile but is a different size to fit in the space available. The air used to cool all components (except the solid-state switches and ac capacitor) follows a circuitous path as much of the flow is diverted to flow through the rectifier. In spite of this, the cooling systems performed their function well.

Figure 5.68 shows temperatures at several locations during one test. The cooling system reservoir (radiator) warmed up approximately 10°F after 40 minutes of operation, with a 5-minute break after 15 minutes. The  $di/dt$  limiting inductors were the hottest items, with surface temperatures approaching 200°F. These Brooks coil inductors also caused heating of the OBC box wall as previously described, and were replaced with iron core conductors that operate at a lower temperature.

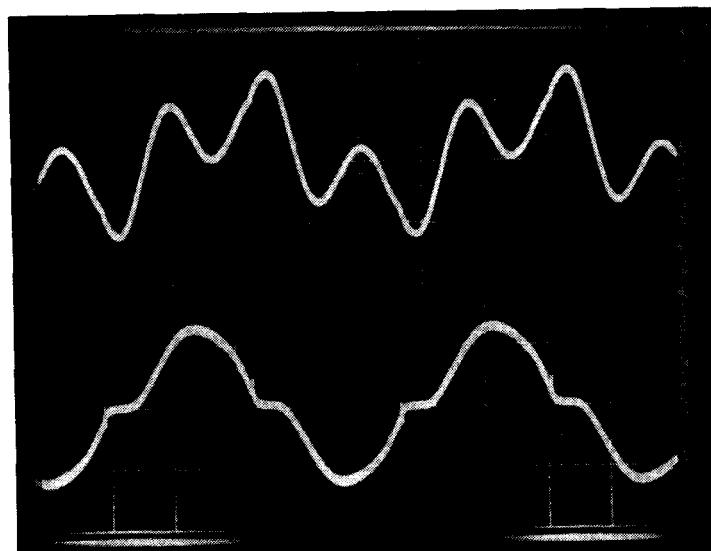


Figure 5.66 Capacitor currents with inappropriate  $di/dt$  values

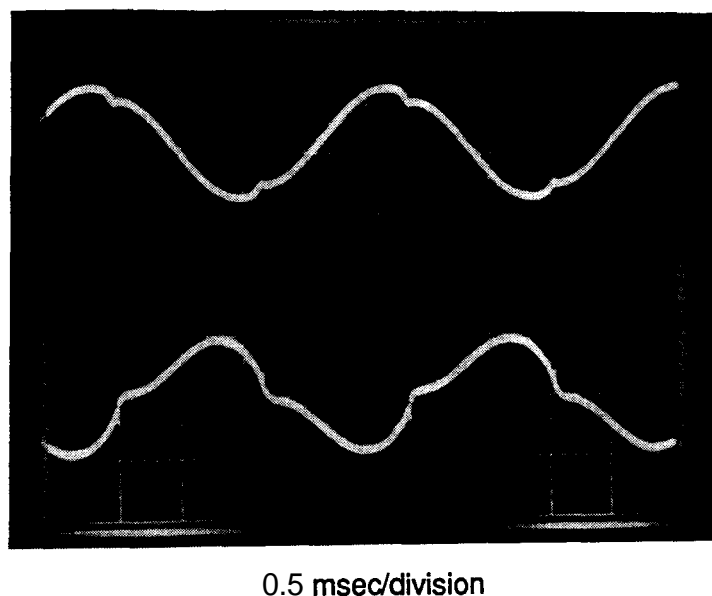
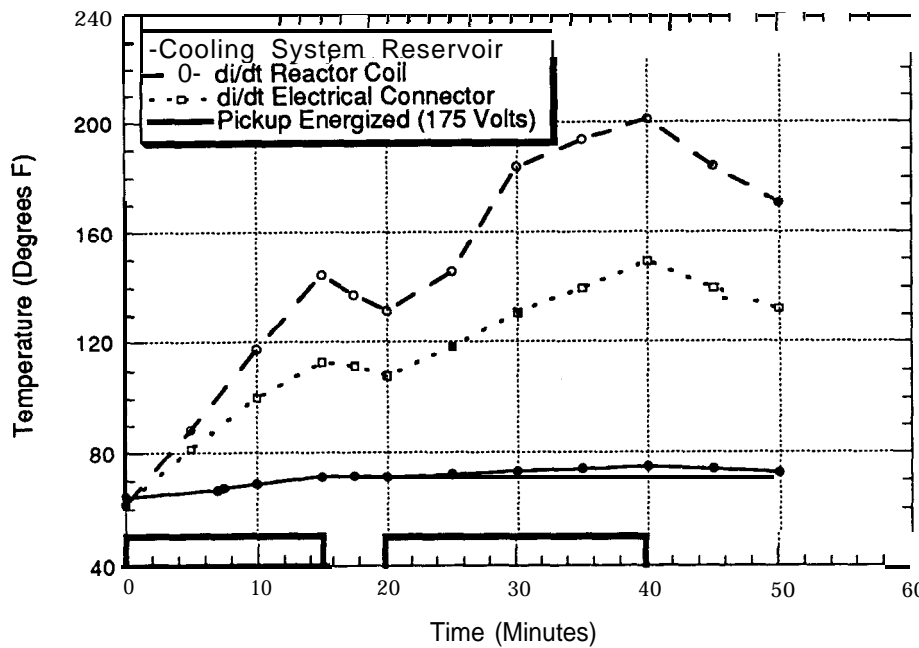


Figure 5.67 Capacitor current with good  $di/dt$  value



RFS1-022

Figure 5.68 Temperature of cooling system reservoir, reactor coil, and electrical connector during testing

#### 5.2.4.5 Acoustic Noise

The OBC emitted more acoustic noise than desired during initial testing. Due to the test area acoustics, it was virtually impossible to get accurate, repeatable readings, but our subjective judgment was that the noise must be reduced. Replacing the Brooks coil inductors helped as did sealing the boxes as much as possible. Cables, cooling lines, and air flow paths made sealing the OBC boxes more difficult during static testing than when the OBC was mounted onboard the vehicle. Even with these measures, further noise reduction was desired. The inner walls of the OBC boxes were lined with acoustic foam where possible, which provided some improvement, but installation of the OBC on the bus was required before the need for further treatments could be properly evaluated.

### 5.3 Accessory Systems

Accessory systems play an important role in inductive coupling system operation even though they do not carry power directly. Signaling systems provide vehicle-to-wayside and wayside-to-vehicle communications. The vehicle-to-wayside system

was to provide the input to the segment-switching hardware described in Section 5.2.3. The wayside-to-vehicle link provides the information needed for automatic pickup raising and lowering. The pickup suspension/retraction system provides the force that retracts the pickup. The last accessory system is the steering assistance system, which provides an **onboard** signal proportional to the vehicle's lateral offset relative to the inductor centerline. The two signaling systems will be addressed together as their operation is similar.

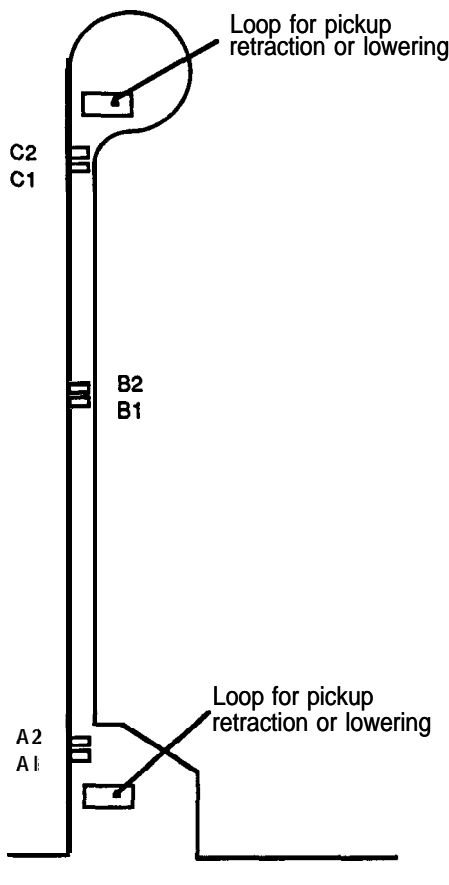
### 5.3.1 Signaling Systems

Both signaling systems operate with similar hardware: an antenna on the vehicle, an inductive loop in the roadway (which also functions as an antenna), transmitters, and receivers. The inductive loops are similar to conventional loop detectors and can perform that function as well as transmit or receive a coded identification number. The loop controllers have circuitry to receive or transmit an identification or signature code as well as perform the normal presence detection function.

The location of the loops in the roadway is shown in Figure 5.69. Unlike a conventional road, the test track is used bi-directionally, which places an additional requirement on the detector loops—they must determine the vehicle's direction of travel as well as its presence. Detector Systems supplied the loops and their controllers as well as the **onboard** antennas and their control circuitry. Detector Systems also supplied Directional Logic Units (DLUs) that are able to determine the sequence in which two loops are activated, providing information about the direction of travel. The outputs from the loop controllers (presence, direction, and identification code) were fed to a master controller unit, custom designed and built by SCT that generates the signals intended to control the switching of the power to the roadway segments.

As metal (especially a ferrous metal) approaches a coil, the coil inductance changes. The coils are excited by a small current (generally in the milliamp range and between 10 and 100 kHz). Changes in inductance (even small ones) cause a change in the resonant frequency of the circuit containing the inductive loop. Circuitry in the loop controller senses this frequency shift and signals **the** presence of a vehicle. The threshold for detection or sensitivity is generally adjustable. Given that presence detectors function through small high frequency magnetic fields, we were concerned whether the magnetic fields generated by the roadway inductor would interfere with the loop detectors' operation. A simple test performed at Translab provided encouraging results. A demonstration loop was placed on top of one of the junction

boxes for the roadway, within six inches of the cables carrying over 1000 amps. In this position, the detector worked just as well with the roadway energized as turned off. Thus, loop detectors were tentatively determined to be acceptable for use near the roadway inductor. Several loops, the controllers, **onboard** antennas, and transponders were purchased.



5544 05/03/93

Figure 5.69 Location of inductive loops in the roadway

Further testing was done at the Richmond Field Station. Operation with large loops (6 x 18 feet) raised questions not encountered with the small demonstration loop. With the near edge of the detector loop 42 inches from the end of a roadway inductor module (the nearest possible due to the size of the vaults), the amplitude of the 400 Hz voltage induced on the loop is about 2.5 volts peak to peak (or 0.85 volts rms) as shown in Figure 5.70. Since this voltage is proportional to the time rate of change of

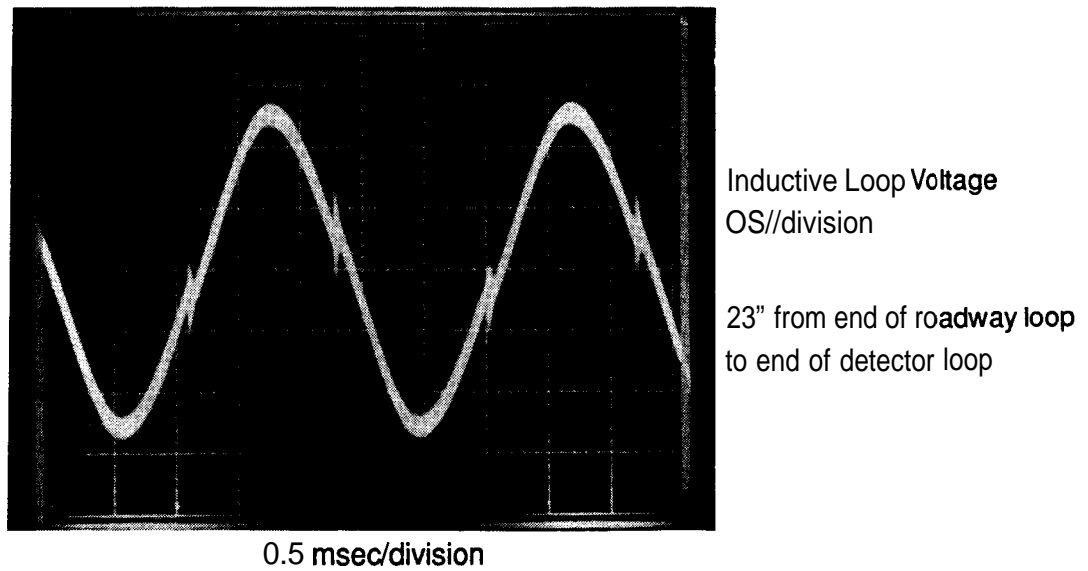


Figure 5.70 400 Hz voltage induced on presence-detector inductive loop located 3.5 feet from the roadway inductor, with loop excitation turned off

the magnetic fields through the loop, any distortions in the waveform of the roadway inductor's magnetic field appear in the voltage induced in the loop. Specifically, the glitch on power conditioner voltage is clearly visible on the induced loop voltage just before zero crossing on both the positive and negative portions of the waveform. With the loop 12 feet from the roadway inductor, the induced voltage is substantially reduced, but still clearly present as shown in Figure 5.71. The loop controllers excite the loops at 8 volts peak to peak at a frequency of about 40 kHz. Figures 5.72 and 5.73 show the loop voltage with and without the roadway current. Both traces show approximately 20 cycles of the high frequency waveform per division. The amplitude modulation of the 400 Hz signal is unmistakable in Figure 5.74 Even the glitches just before the zero crossing of the 400 Hz waveform are visible. Figure 5.74 is a repeat of Figure 5.72 with a time scale of 0.2 instead of 0.5 milliseconds per division. Here the 40 kHz waveform is distinct, but the triggering for this trace is poor so three waveforms are superimposed. Functional tests indicated that the magnetic field from the roadway was interfering with the presence detection function, although the identification code was still passed correctly.

Several high-pass filters were designed and tested in an attempt to remove the 400 Hz signal from the loop controller circuitry. These filters were installed at the input terminals of the controller. a two-stage filter was devised that worked reasonably well. Figure 5.75 shows the filtered (upper trace) and unfiltered (lower trace)

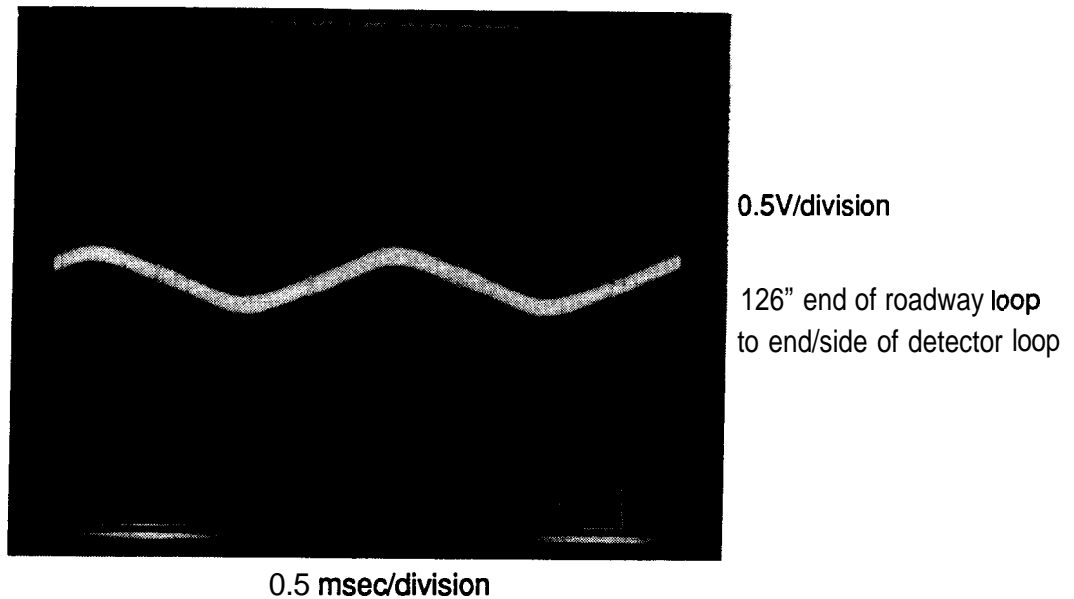


Figure 5.71 400 Hz voltage induced on presence-detector loop 12 feet from the roadway inductor, with loop excitation turned off

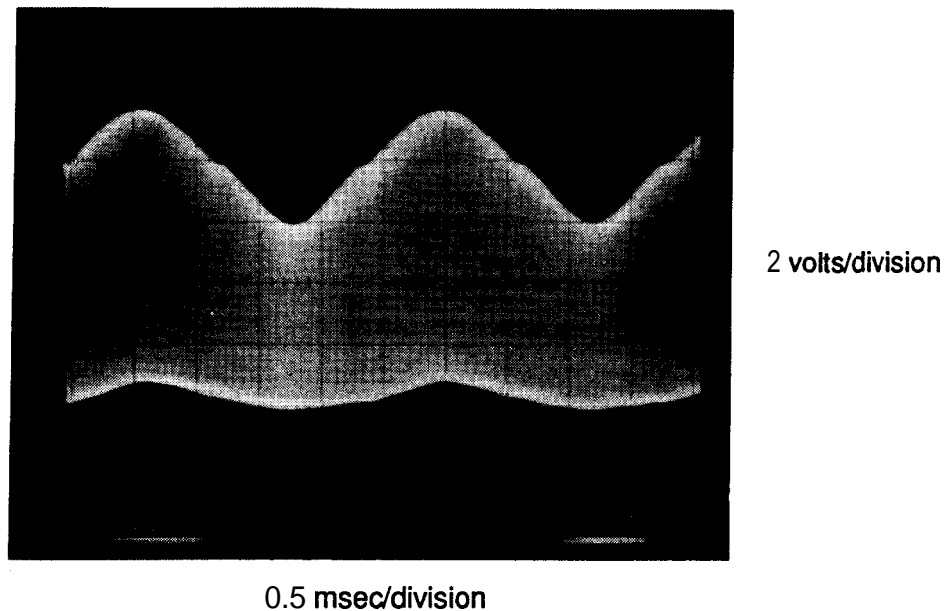


Figure 5.72 Voltage on inductive loop located 3.5 feet from roadway with roadway and loop excitation both activated

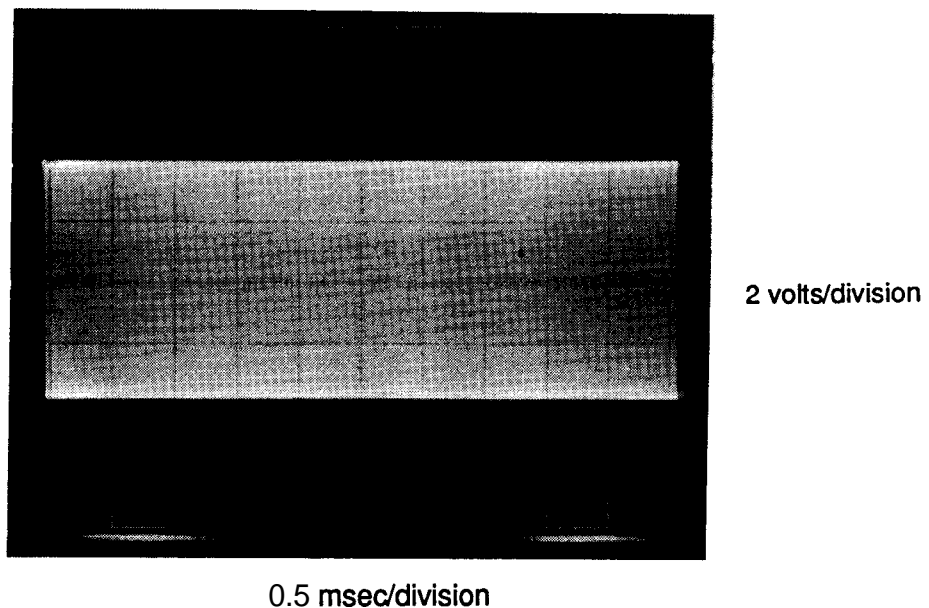


Figure 5.73 Inductive loop voltage with roadway inductor current turned off

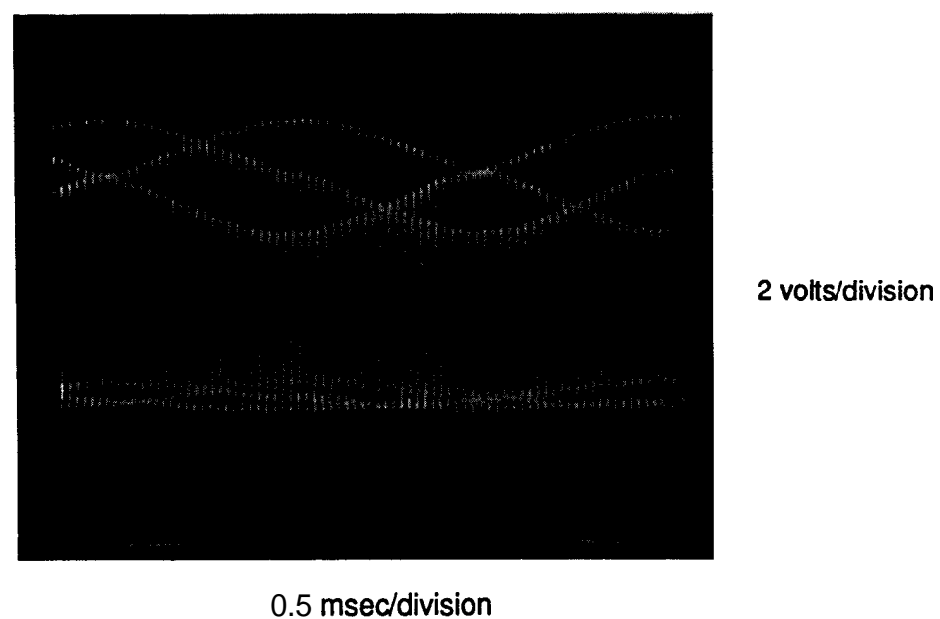


Figure 5.74 Inductive loop voltage with roadway turned on (poor scope triggering)

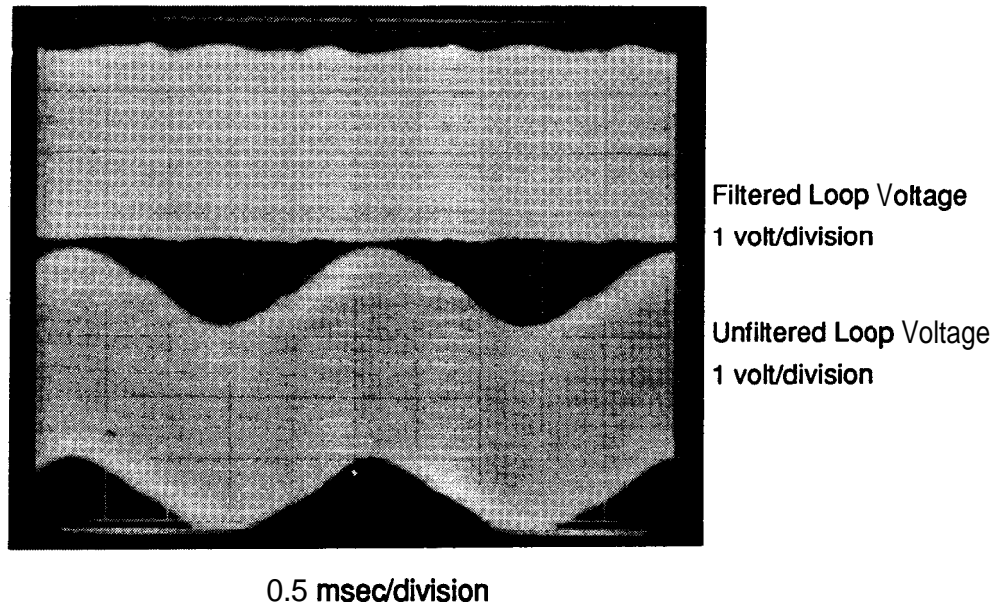


Figure 5.75 Filtered and unfiltered inductive loop voltage

waveforms. Between the two stages of the filter, the 400 Hz signal is present with an amplitude of 0.8 volts peak to peak. On the upper trace in Figure 5.75 the 400 Hz has been removed, but the glitches previously mentioned are still visible. The high-pass filter worked well and the identification function still worked properly. The presence detection function worked reliably with the power conditioner both off and on. The detection system gave an erroneous presence signal as the power conditioner was being turned off. Numerous attempts were made to solve this final conflict, including more filtering as well as adjusting the sensitivity of the detection controller. The settings range from one (least sensitive) to seven (most sensitive). At high sensitivity settings, the system gave erroneous presence signals as the power conditioner was turned off. At low sensitivities, vehicle detection was not reliable. At a setting of 2, both functions worked most of the time but there was still a 20% error rate on power conditioner shutdown, too high for an operational system. Testing of the power distribution system indicated that the power hardware would not allow switching under load, which dropped the priority of the detection system low enough so that no further work was done.

The signaling system for automatic pickup raising and lowering worked properly with or without the roadway energized. This system, like the identification code transmitted by the vehicle to the roadside segment switching control system, uses a high-frequency pulse-coded signal that is not disturbed by the 400 Hz magnetic fields of the roadway inductor.

### **5.3.2 Pickup Suspension/Retraction**

As originally designed, the system used ten pneumatic cylinders to raise and lower the pickup with cables and pulleys. The cables supporting the pickup provided no lateral or longitudinal forces to maintain the pickup in the proper position relative to the bus. Control arms would have to be provided in both directions. We were concerned that the cables might stretch and require frequent adjustment. In addition, supplying high pressure air to ten cylinders would be difficult.

The components for this system were purchased and partially assembled in Phase 3C. After attempting to complete the installation of this system, Bus Manufacturing USA, the bus subcontractor, decided that a simple mechanism was needed. Bus Manufacturing and SCT collaborated on the design of a new method.

The new system has a single hydraulic cylinder that pulls the pickup toward the rear and up. Ten swing arms at the previous cable attachment points carry the weight of the pickup. The pickup moves 8 inches toward the rear as it is retracted 4 inches vertically. The new system has two lateral control arms that transfer all lateral loads on the pickup to the bus. Lateral displacement of the pickup over its entire travel is approximately 0.25 inch. Micro-switches limit the upward travel of the pickup, turning off the dedicated hydraulic pump when the pickup reaches its raised position. The pickup is lowered by gravity. A hydraulic valve is opened for a specified time interval (adjustable, but currently set for about 5 seconds) that allows the pickup to gently travel down to the lowered position. Even with approximately 0.25 inch lateral clearance, there has never been any contact between the pickup and the bus frame.

The lowered pickup position is repeatable to within less than 0.10 inch. Raising and lowering the pickup each take about 5 seconds. Lowering the pickup is extremely quiet. The sound pressure level generated by the hydraulic pump raising the pickup, is -60 dBA in the passenger compartment.

### **5.3.3 Steering Assistance System**

The power-transfer capability of the inductive coupling system decreases when the pickup inductor is not properly aligned with the roadway inductor. Various steering assistance systems have been proposed, varying from full steering control to a simple meter that displays the vehicle's lateral position. Any steering assistance system requires a sensor to determine the vehicle's lateral offset. Others have done work using both mechanical systems, which follow a reference rail or curb, and electronic

wire-following systems, which sense the magnetic field caused by a current flowing in a wire buried beneath the surface of the road. The roadway inductor provides the ultimate magnetic field to be used for a position-sensing system. The field is strong, distinctive in shape, and very wide. The field is strong enough that simple wire coils on plywood forms provide an adequate signal without amplification.

We devised a system with two primary sensing coils mounted symmetrically about the vehicle's centerline. The difference between these two voltages provides a signal proportional to lateral offset of the vehicle up to  $\pm 2$  feet. A third coil provides a reference signal to determine the polarity of the error signal, indicating whether the vehicle is left or right of center. The control circuit performs the polarity checking and generates a signal to the meter. Using the system indicated that two meters--one more sensitive than the other--are most useful. The actual displays as seen from the driver's seat, are shown in Figure 5.76. The left meter has a scale of  $\pm 30$  inches and the right  $\pm 5$  inches.

Several sets of sensor loops were constructed and tested. The first set, shown in Figure 5.77, proved that the concept would work. Figure 5.78 shows the predicted and measured voltages as a function of lateral offset. The output voltage varies linearly with position. The computer results stop at 20 inches due to the limited lateral range of magnetic field data available to the computer. The width of the second set of loops was increased from 30 inches to 36 inches to enlarge the range over which the sensor provided a linear output. Figure 5.79 shows the (polarity) reference and the primary position signal for a second set of coils. The reference signal retains a positive value over all lateral offsets, which is in phase with the primary sensor voltage for displacements to the right (positive) and out of phase for displacements to the left. The final set of loops has a trapezoidal shape rather than rectangular as shown in Figure 5.80. This change pushed the peak measurable offset out to 30 inches and results in a plateau beyond the peak, which caused the meter to remain at full deflection for at least another 6 inches of displacement. Figure 5.81 shows test results for three sets of sensor loops. The location of the peak and the linearity of the voltage are the most important features. The amplitude can be adjusted by adding more turns to the coils. A variable gain in the control circuit calibrates the meters. Each design in Figure 5.81 expands the linear region compared to the previous design. The final design worked well, both on a test stand and while mounted on the bus as shown in Figure 5.82. The final design is shown mounted on the bus in Figure 5.83.

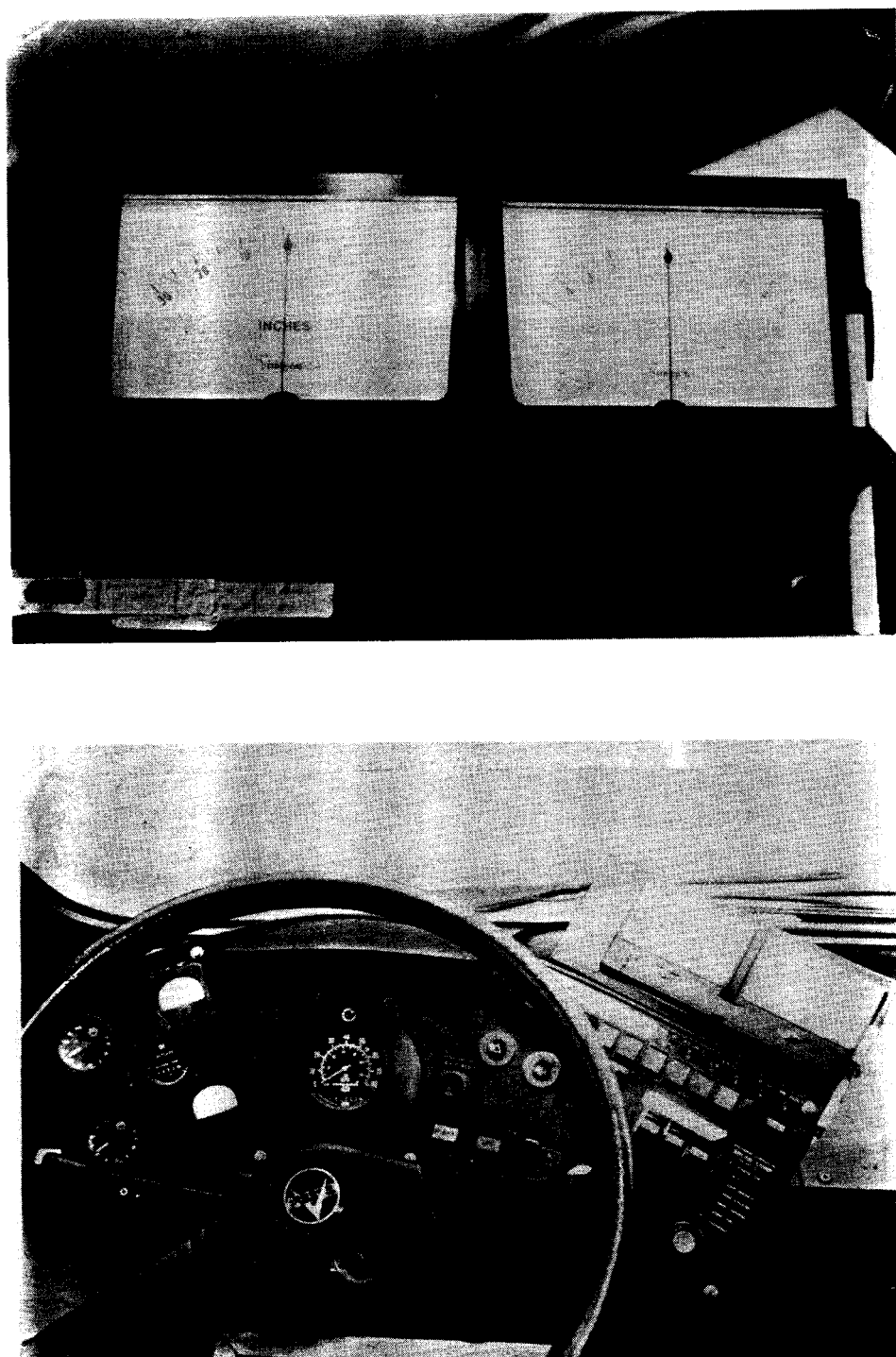
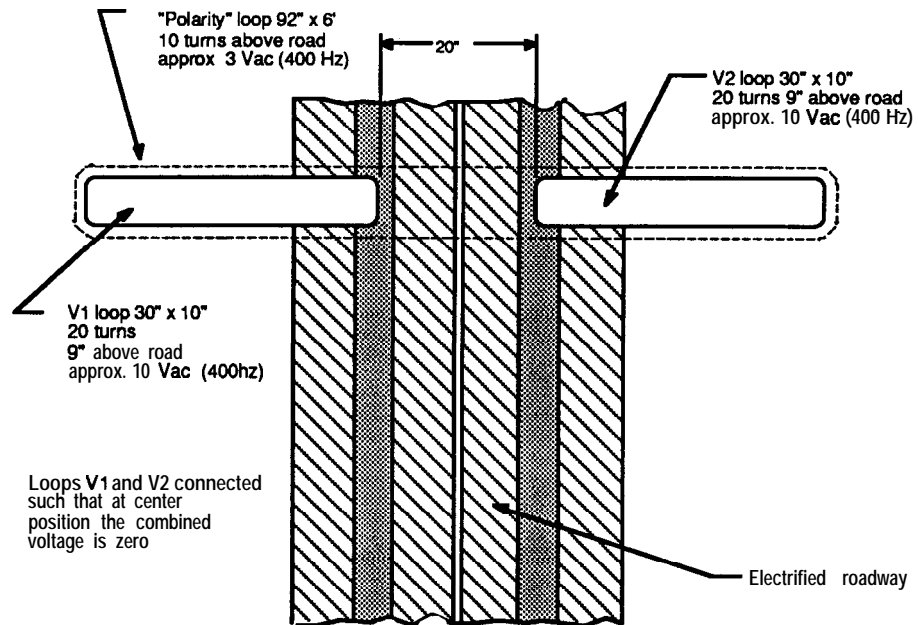


Figure 5.76 Steering assistance system-driver's view



554406115191

Figure 5.77 First set of sensor loops-10 x 30 inches

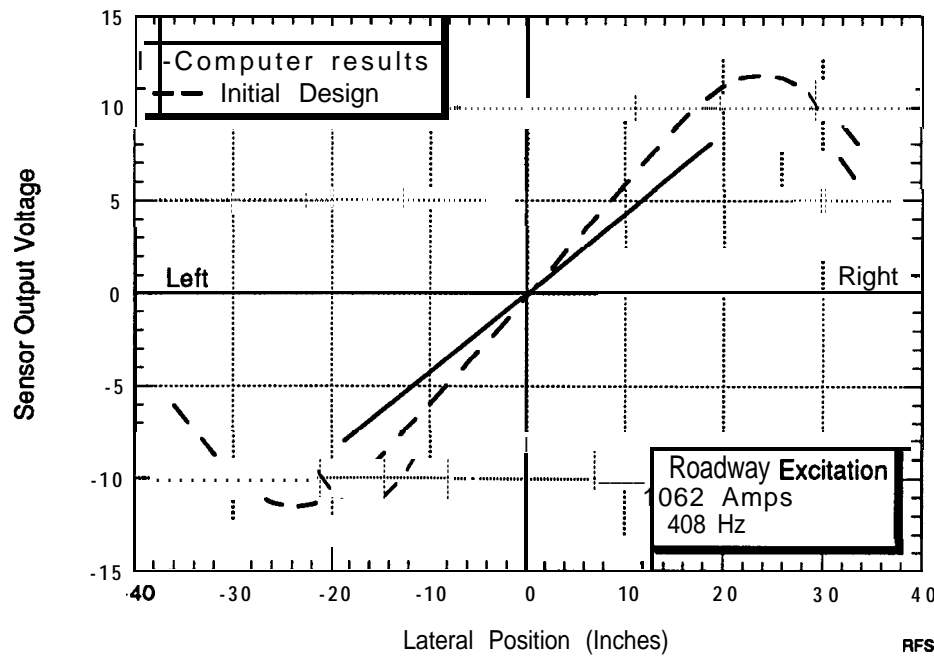
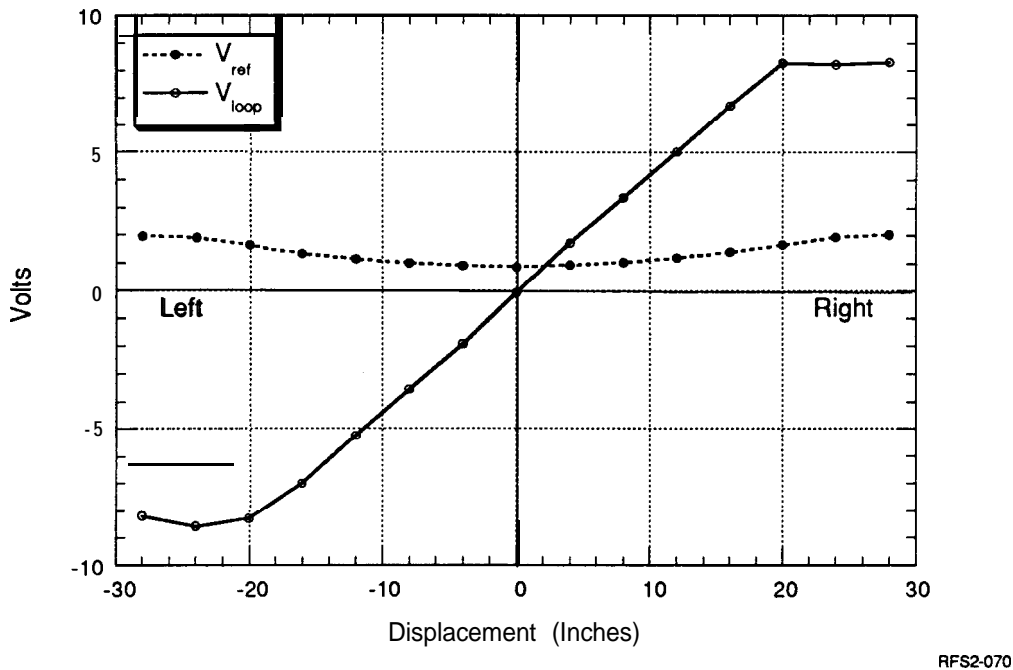


Figure 5.78 Predicted and measured voltages as a function of lateral offset



RFS2-070

Figure 5.79 Polarity reference and the primary position signal for one of the intermediate sets of coils

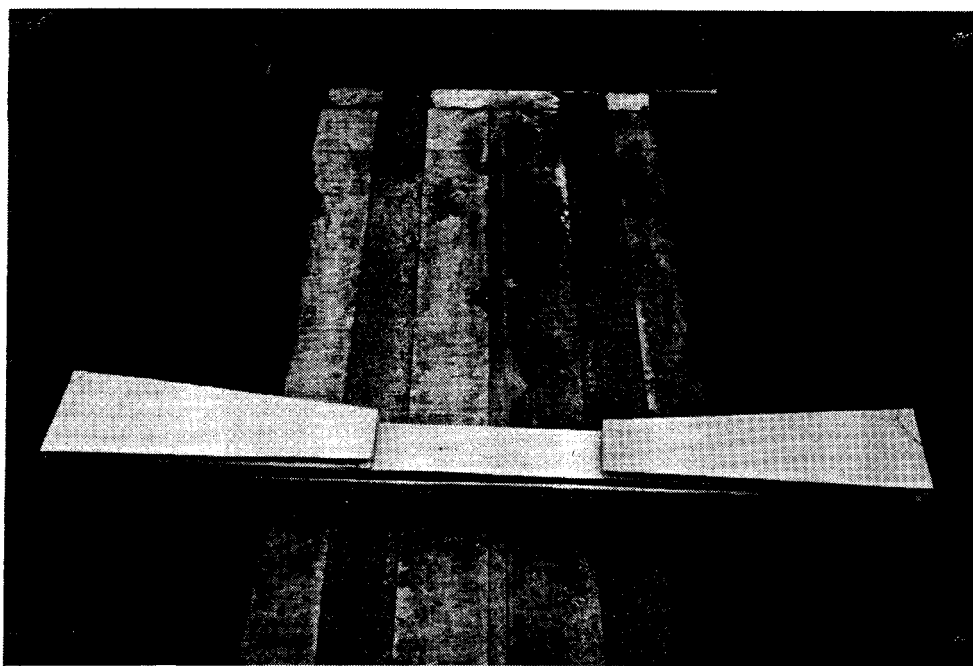


Figure 5.80 Final trapezoidal steering sensor loops

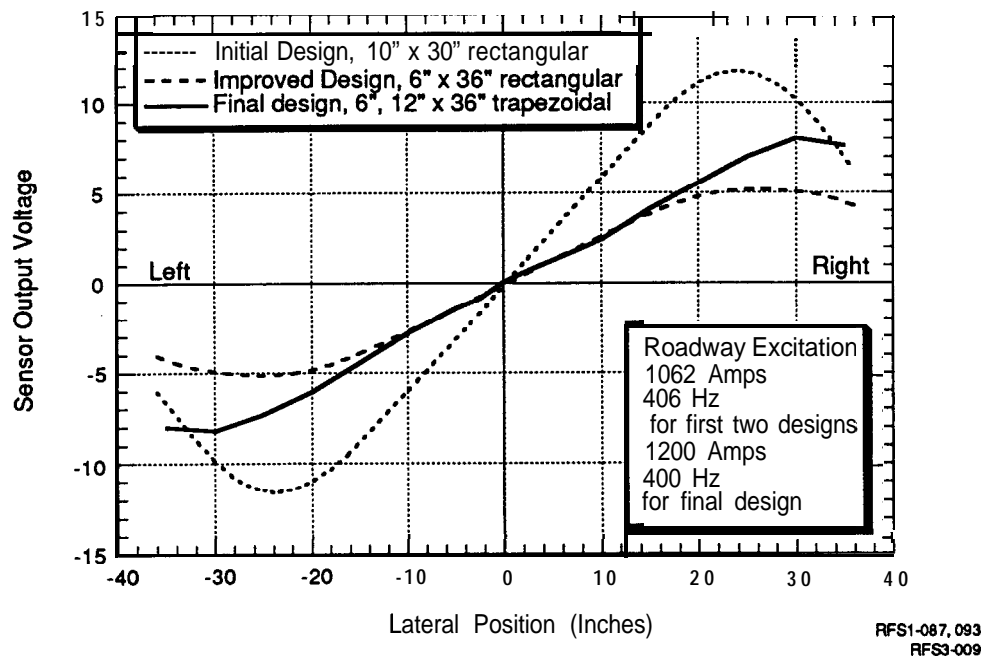


Figure 5.81 Test results for three sets of sensor loops

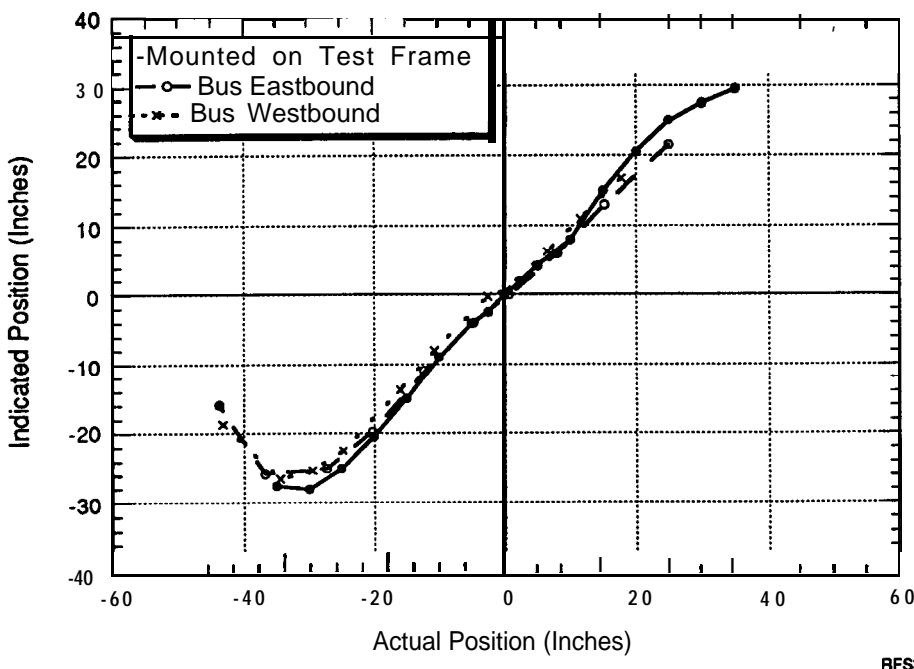


Figure 5.82 Final sensor design



Figure 5.83 Final sensor design mounted on bus

The system just described worked satisfactorily in a laboratory setting, but requires too much of the driver's attention to be practical in a public environment. SCT has started internally funded work on a system to close the steering loop automatically rather than through the driver. This low torque system would assist the driver in remaining centered on the powered roadway, but the driver could easily overpower the system to change lanes, avoid obstacles, or take emergency action.

#### **5.4 Inductive Coupling System Performance on the Static Test Stand**

The operation of the inductive coupling system on the static test stand in Building 167 provided the first and, in some ways, the most conclusive evidence of the technical viability of the RPEV hardware. On the test stand, the position of the pickup can be controlled and measured more accurately than when it is mounted on the bus. It is easier to make changes and adjustments to components as their accessibility is greatly reduced when they are mounted on the vehicle.

### 5.4.1 Power Coupling Capability

The purpose of the inductive coupling system is to transfer power to the vehicle so this was the most important test. Several items were checked including total output current, sensitivity to roadway current and pickup location, and degree of match with predicted performance.

#### 5.4.1.1 Output Current Available

Figure 5.84 shows the predicted and measured output current as a function of tuning capacitance. The measured values of many parameters, such as pickup mutual and leakage inductances, were used in the modeling. The two plots agree very well up to the last point where the power conditioner hit an internal limit that caused the roadway current to be reduced about 50 amps. During the rest of the test, output currents up to 410 amps were measured, which is about 10% lower than the design point of 450 amps. The design process assumed an average output current of about 325 amps, well below the 400 amps the ICS is capable of transferring. We did not believe that this slight shortfall in coupled current was significant as conservatism

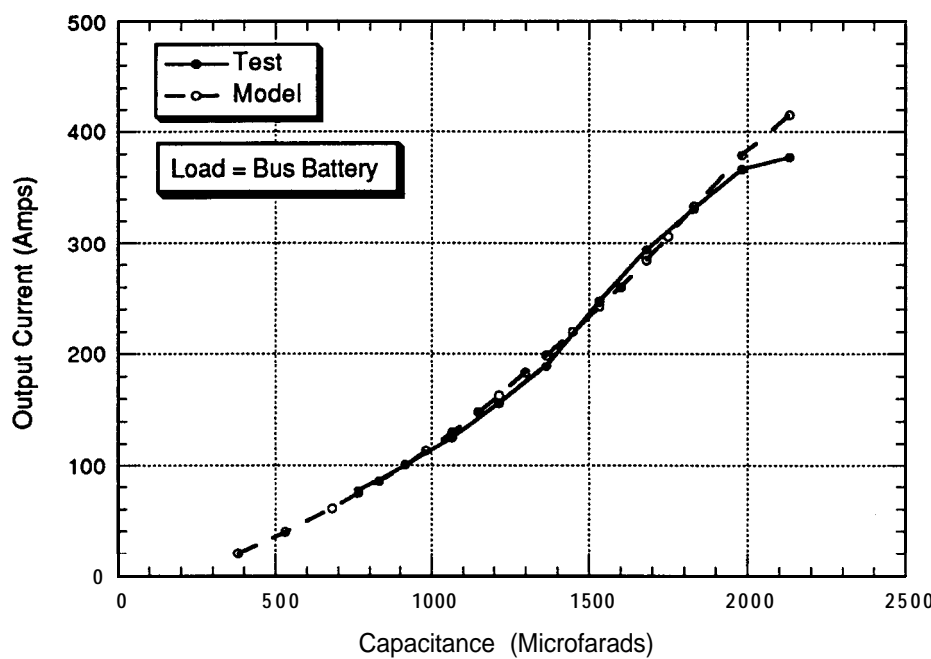


Figure 5.84 Predicted and measured output current as a function of tuning capacitance

EVS10-013

was built into the designs. Range tests have shown that the inductive coupling system is capable of coupling adequate current to the vehicle to allow all-day operation.

#### 5.4.1.2 Sensitivities to Pickup location

The test was performed with the pickup perfectly centered and at a 3-inch (magnetic) airgap height. During normal operation, there will be deviations from the design locations, both laterally and vertically. Plots of these sensitivities are shown in Figures 5.85 and 5.86.

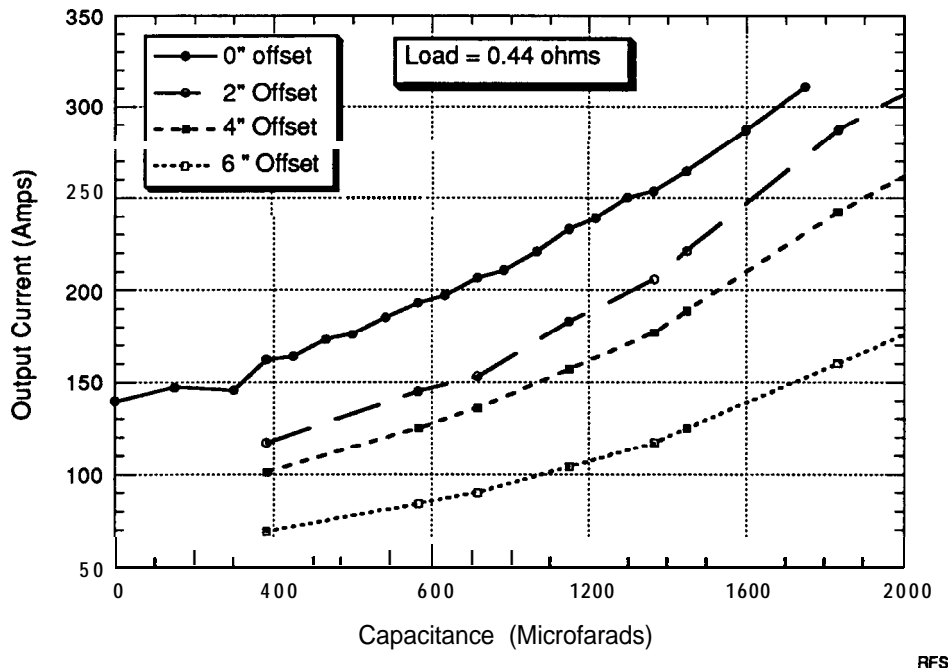


Figure 5.85 Sensitivity to lateral deviation from design location

The data for the nominal pickup position (centered with 3-inch airgap) were not recorded at the same time as the other data, and the load resistance could not be exactly repeated, causing this curve to be shifted slightly relative to the other data on both plots.

Output current drops with lateral offset, very slightly at first as the curve for 2 inches lateral offset nearly matches the centered performance.

Current decreases considerably as lateral offset increases. At 6 inches offset, output current is less than half the maximum, which is especially noteworthy as these data

were taken with the output current into a resistive load rather than the bus battery. At 190 amps output current, output voltage is about 65 volts. Output current would be greatly reduced into a load voltage of 128 volts, the nominal bus battery. Output current of this system drops nearly to zero at a 6-inch offset when run into the bus battery.

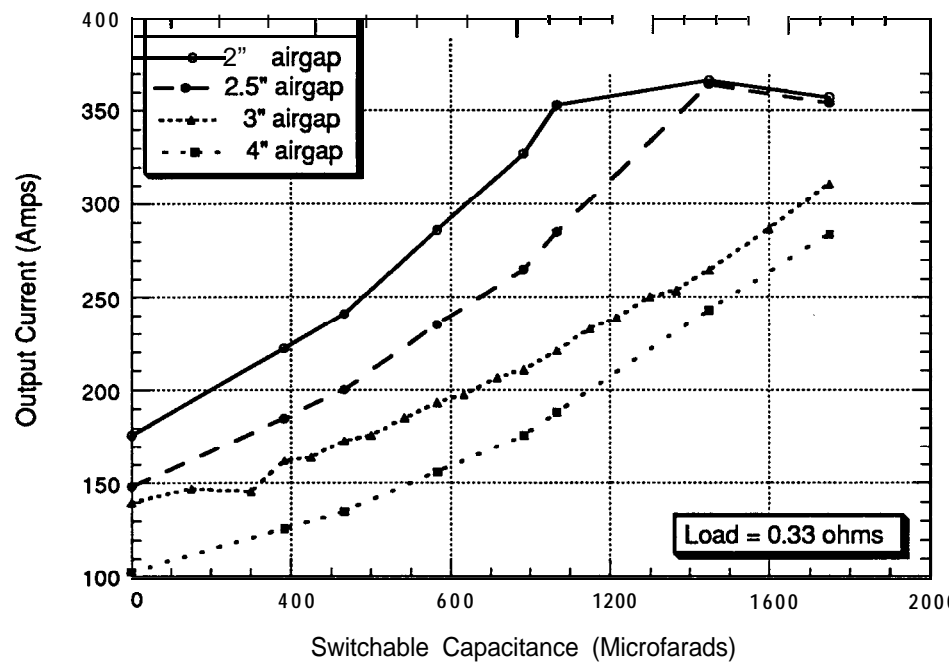


Figure 5.86 Sensitivity to vertical deviation from design location

Varying the airgap height can cause both increases and decreases in output current. For the same capacitance, output current increases if airgap height is reduced, especially below tuning capacitance values of 1200 microfarads. Similarly, increases in airgap height decrease the output current. For the 2-inch airgap, the output current peaks at about 1400 microfarads of tuning capacitance because mutual inductance increases as the airgap height decreases, requiring less capacitance to achieve full output current. For larger airgaps, output current will continue to increase beyond 1750 microfarads capacitance (the output current peak for the nominal 3-inch airgap).

#### 5.4.1.3 Sensitivity to Roadway Current

As roadway current is reduced, output current drops as shown in Figure 5.87. The capacitance required before any current is coupled increases as roadway current

decreases because onboard ac peak voltage must be greater than the battery voltage before any current is delivered to the load. The previous two figures show data taken with a resistive load. With 600 amps in the roadway, over 1000 microfarads are required before any output current flows. At this capacitance, the output current is already nearly 50% of maximum with the nominal 1200 amp roadway current.

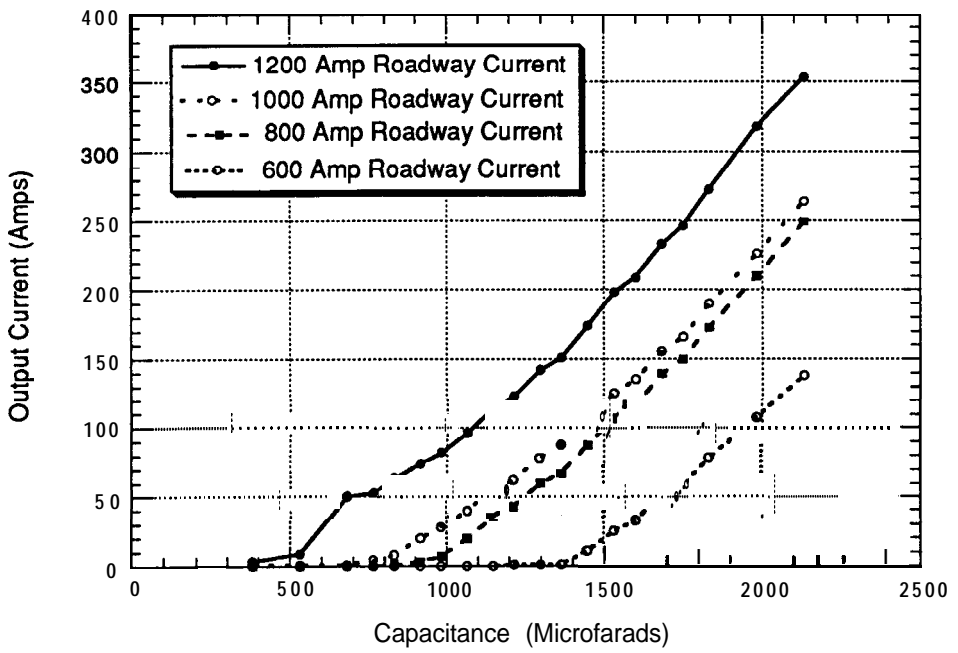


Figure 5.87 Output current as a function of roadway current

#### 5.4.2 Closed-loop Control

The inductive coupling system is designed to deliver the proper current to the vehicle regardless of changes in the pickup position or onboard dc voltage. The system is capable of tracking a time-varying input signal as would be required when the vehicle's current demand changed. For instance, if the battery were highly charged, it could accept only a low charging current. If the bus started accelerating at maximum power, however, current demand would increase, and the inductive coupling system would deliver the maximum current available. During regenerative braking, the motor (running as a generator) generates as much current as the battery can accept, so the ICS output current should drop to zero. The system's ability to track a commanded output current is demonstrated in Figure 5.88. The commanded value was varied slowly to avoid exciting power supply dynamics. The

ICS can actually change power levels much faster than shown. When operating under computer control, capacitance is switched automatically to control output current, and the actual output current tracks the command closely. The minor oscillations visible as output current passes through 260 amps are caused by dynamic interaction of the **onboard** controller with the power conditioner. The **onboard** controller is magnetically linked to the roadway (and power conditioner) and changes in the **onboard** controller occasionally excite the control circuits in the power conditioner, which has been a minor inconvenience, but warrants investigation in future systems and may require changes to the power conditioner control design.

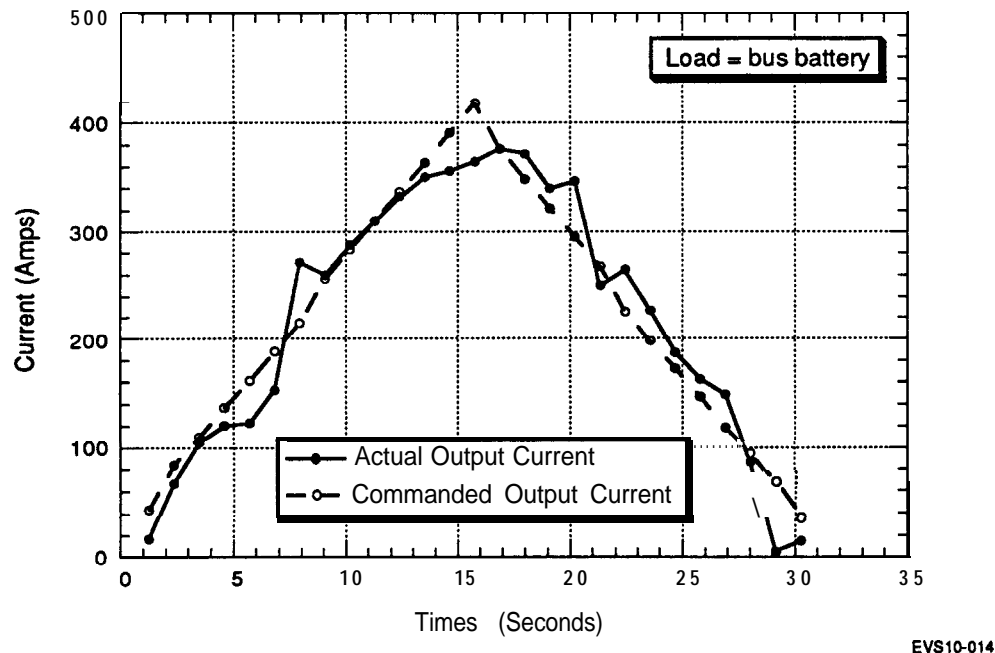


Figure 5.88 Output current tracking commanded value

The **onboard** control computer (OBCC) is programmed to control either ICS output current or battery current. Both have proved useful, and further work is required to determine the most effective control algorithms.

## 5.5 Inductive Coupling System Operation on the Bus

The inductive coupling system was mounted to the bus and tested over the outdoor test track at the Richmond Field Station. This was a complicated process because the

pickup and OBC had never been mounted on the bus and we had never operated an ICS from a moving vehicle.

### **5.5.1      Mechanical Considerations**

Most of the mechanical issues addressed during integration of the ICS into the bus involved mechanical clearance of the pickup and OBC, although acoustic noise was re-examined.

#### **5.5.1.1    Pickup Cabling**

Routing the cables from the pickup to the OBC was not completed until the pickup and OBC were mounted on the bus. The steering idler arm that ties the left and right wheels together and the cooling air exhaust from the OBC are near the cables that connect the pickup to the OBC, making routing and installation of the various elements difficult. The cable routing must allow for the pickup's motion of the (both vertical and longitudinal) as it is raised and lowered, which **was** achieved by having the cable follow a path roughly parallel to the swing arms that support the pickup. As the pickup is lowered, the swing arms and cables swing through a similar arc. A slight change in the cable path's length was taken up by a combination of bending and twisting of the cables. There are no signs of rubbing on the cable pack by the idler arm. This cable routing works well and there is apparently no need for future change, although this will be checked from time to time.

#### **5.5.1.2    OBC Installation**

Installation of the OBC proved more difficult than installation of the pickup and its cabling because the boxes as built did not fit in the appropriate space on the bus. The middle box is narrower than the other two to allow for the bulges (which accommodate the front air bags of the primary suspension) in the sidewalls of the space allowed for the OBC. Figure 5.89 shows the OBC mounted onboard the bus, with the narrow middle box and the bulges in the sidewalls clearly visible. The middle box was manufactured one inch shorter (front to back) and narrower than the space available, which resulted in the box's being too short to span the gap required for the air bag bulge. We lengthened the middle box approximately two inches, solving the mechanical interference and allowing more space for the components, primarily inductors. This box was also used to mount all the small electronic components, such as trigger circuits, bleed resistors, fuses, and terminal strips. All mechanical interfaces worked properly, including entry and exit locations for cables, liquid cooling lines, and cooling air. (See Appendix B.)

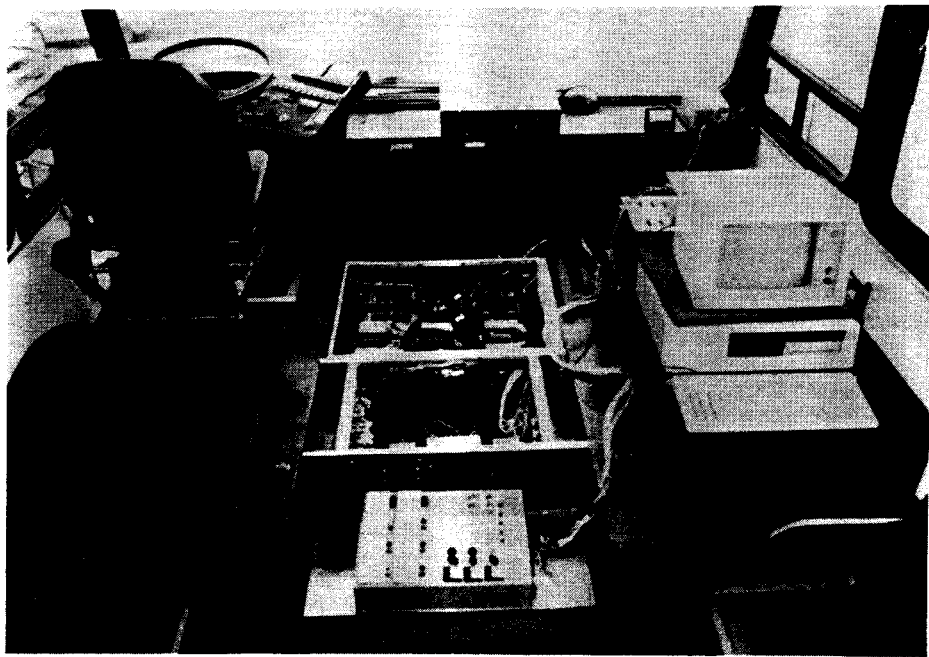


Figure 5.89 OBC mounted onboard the bus

#### 5.5.1.3 Cooling Systems

The cooling systems worked well from the outset. Adequate air flowed through the radiator and all air-cooled components. The space for the fluid-cooling lines is tight, but they fit with no kinks to hinder flow. Temperature rises within the OBC mounted on the vehicle were comparable to those observed during test stand operation.

#### 5.5.1.4 Acoustic Noise

The OBC noise inside the bus was initially very bothersome at full power, with measurements of 80 dBA at 6 feet. A sound-deadening cover spanning the top of all three OBC boxes, as shown in Figure 5.90, reduced the sound pressure level approximately 20 dBA, to about 60 dBA at full power and 55 dBA at half power. With the cover in place, the ICS noise was noticeable (but not objectionable) when coupling full power with the vehicle stopped. Even at low speeds, road noise effectively masks OBC noise.

Acoustic noise continued to be a concern as the pickup and OBC were mounted on the vehicle. Emissions from the OBC are of much greater importance as the OBC is



Figure 5.90 OBC acoustic cover being lowered into place

located in the passenger compartment, just a few feet from passengers. Passengers are shielded from pickup noise by the bus floor. Acoustic foam on the lower surface of the panels located directly above the pickup increased the floor's acoustic attenuation.

Acoustic noise from the pickup is barely noticeable either inside or outside the vehicle. The sound pressure level at the side of the roadway as the vehicle passes at 20 mph is essentially the same whether the ICS is engaged or not (62 – 66 dBA). The bus generates enough acoustic noise as it moves to mask any noise generated by the ICS. The 800 Hz hum characteristic of ICS operation could be heard by listening carefully because it is almost a pure tone. Sound pressure readings were significantly lower (56 -62 dBA) at the wayside measurement location (about 10 feet from lane center) until the rear axle of the vehicle passed. Both subjective and quantitative indications are that the rear axle and motor are noisier than the inductive coupling system. The drivetrain of the RPEV bus is 15 -20 dBA quieter than a diesel bus of the same size and weight.

### 5.5.2 Static Operation

Initial power coupling with the ICS mounted on the bus was done in the stationary mode, which results in steady-state conditions and made taking measurements both

easier and more accurate. Losses were somewhat higher than calculated, due to losses in the open roadway inductor, which were larger than expected as discussed in Section 5.2.2.2.

### 5.5.2.1 Tuning Curve

A tuning curve of output current as a function of the capacitance switched into the circuit is the mandatory first test. The cable segment was powered up with the bus stationary and centered over it. We measured both the output power and the three-phase power into the power conditioner, allowing system loss and efficiency values to be calculated. Figures 5.91 and 5.92 show the output current and power. The peak of the output current matches the data from the static test stand (see Figure 5.841, giving us confidence that the airgap with the pickup mounted onboard the vehicle was correct. Other assumptions were also verified, such as that the frame of the bus does not interfere with power coupling and that the roadway core modules in the test track perform as well as those in the indoor test stand.

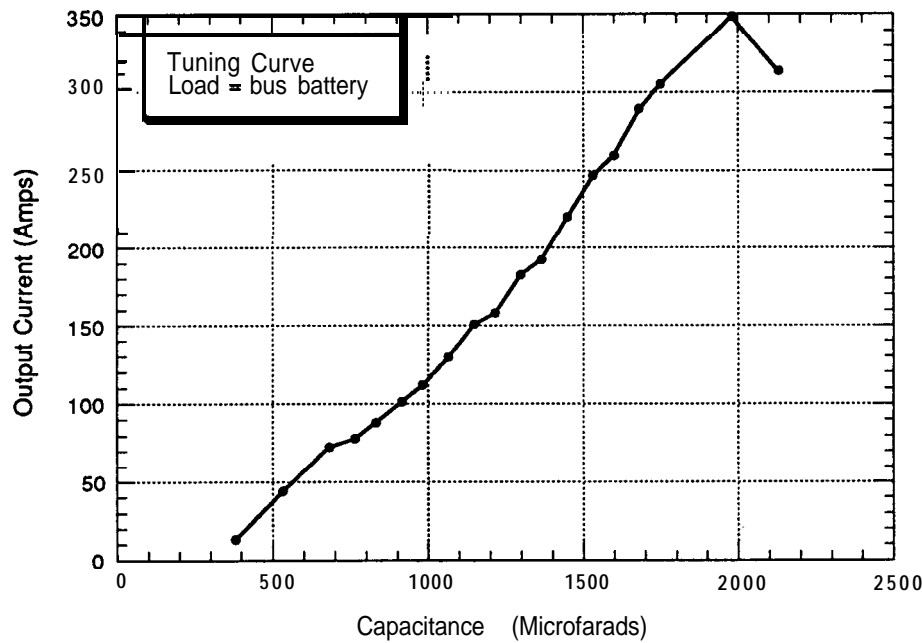


Figure 5.91 Tuning curve of output current as a function of capacitance

RFS4-045

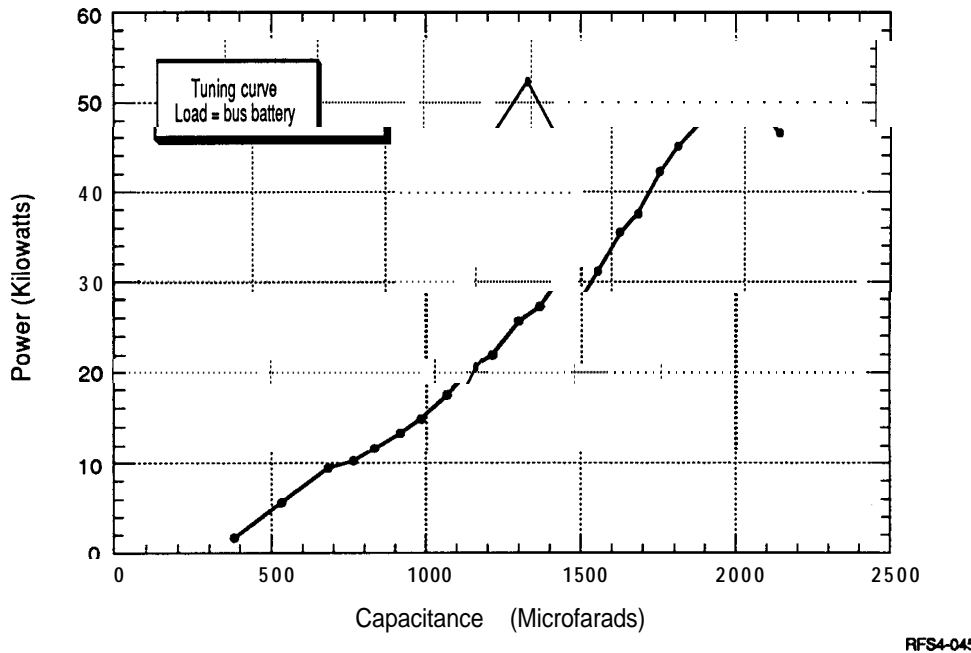


Figure 5.92 Tuning curve of output power as a function of capacitance

### 5.5.2.2 System losses and Efficiency

The input power measurement allows calculation of system losses and efficiency. The waveform of the power conditioner input current is highly distorted with high levels of odd harmonics because this current is being rectified immediately, and generally only two of the three phases are conducting at any time. Distortion makes accurate measurement of the input power more difficult and subject to larger errors than with a sinusoidal signal. A Hall effect sensor was used to measure the current rather than a current transformer because it can measure distorted waveforms more accurately.

Figure 5.93 shows output power plotted as a function of input power. In addition to the data from the previous figure (filled circles), another set of data was taken that matches that set closely. There is no output power until the input reaches 24 kilowatts, due to losses in the power conditioner, transmission line, open roadway, and coupled cores. A solid line drawn from 24 kilowatts input power with a slope of 0.8 or 80% efficiency gives the upper limit of the efficiency of this hardware if fixed roadway losses were allocated among many vehicles occupying a single segment. This efficiency is for the hardware tested and is not a fundamental limitation of the

technology. All test data fall near the solid line, indicating that losses onboard the vehicle and in the coupled roadway cores are 20% of the incremental input power. The peak output power of 60 kilowatts requires an input power of 100 kilowatts, giving an efficiency of 60% at the rated power point. The RPEV system designed for the Playa Vista project, with its greatly reduced roadway current, is projected to have a 75% system efficiency, and efficiencies above 80% appear possible.

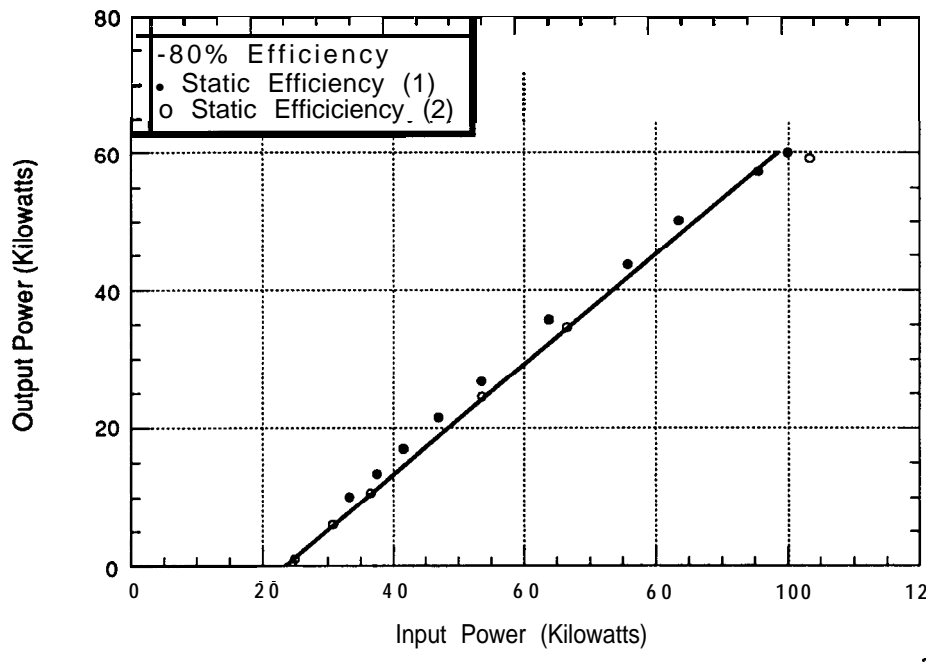


Figure 5.93 Output power as a function of input power

The efficiency of each point in the previous figure can be calculated, resulting in Figure 5.94, which gives efficiency as a function of output power. The efficiency starts at zero for zero output power, but climbs rapidly. At 10 kilowatts output power (17% of rated) the efficiency has already climbed to 30% (or 50% of peak efficiency). At 50% power, the efficiency is 87% of peak efficiency, but after that efficiency increases slowly. Most of the time, the inductive coupling system will be operating in the upper half of its power band, indicating that for the hardware tested, 55% efficiency should be expected.

Efficiency is defined as the dc power available onboard the vehicle divided by the ac power into the power conditioner. When comparing RPEV efficiencies with those of battery electric vehicles, losses in a battery vehicle that are not present (or are reduced

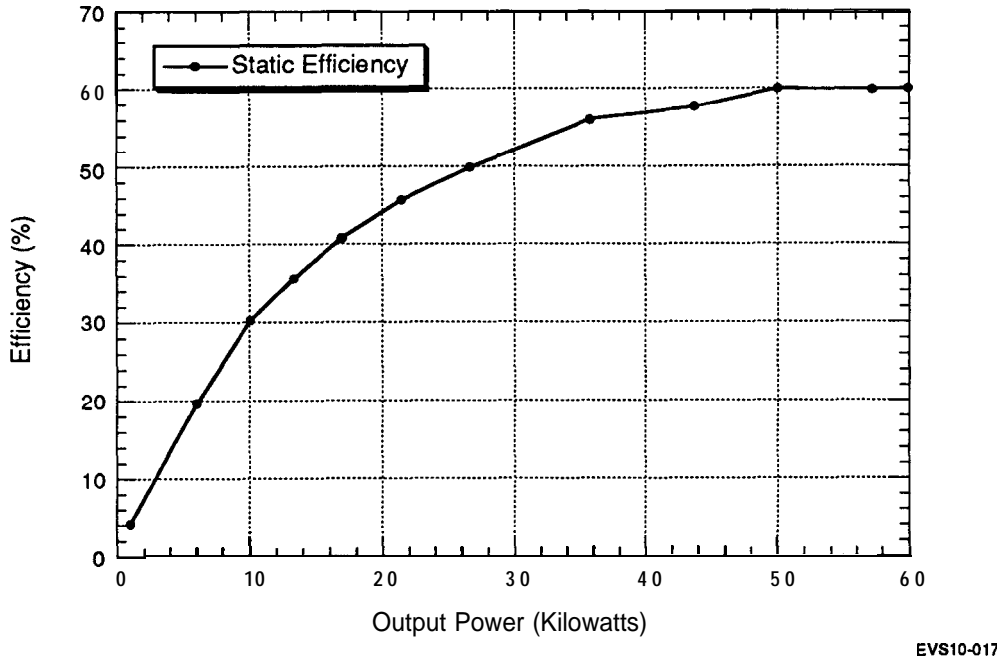


Figure 5.94 Static efficiency as a function of output power

in magnitude with RPEV) must not be ignored. These include losses in the charger and most importantly losses in the battery itself. Most of the energy transferred to the vehicle goes directly to the motor controller, saving battery losses. Depending on the driving cycle, this energy can be 50 – 95% of the ICS output current. Assuming a charger efficiency of 95% and a battery efficiency of 75%, the battery vehicle is 70% efficient in converting ac power from the utility to dc power available for input into the motor controller. These numbers are somewhat optimistic as they do not count over charging and the battery efficiency number is probably high. Many sources [9, 10, 11] indicate that a battery vehicle's dc energy consumption is 60% of the ac energy usage and values as low as 50% have been reported.

The existing hardware has an efficiency that is similar to most battery vehicles; however, the Playa Vista project indicates that improvements of at least 15% are achievable. At that point, the energy efficiency of the RPEV technology would probably be better than most battery vehicles.

### 5.5.3 Dynamic Operation

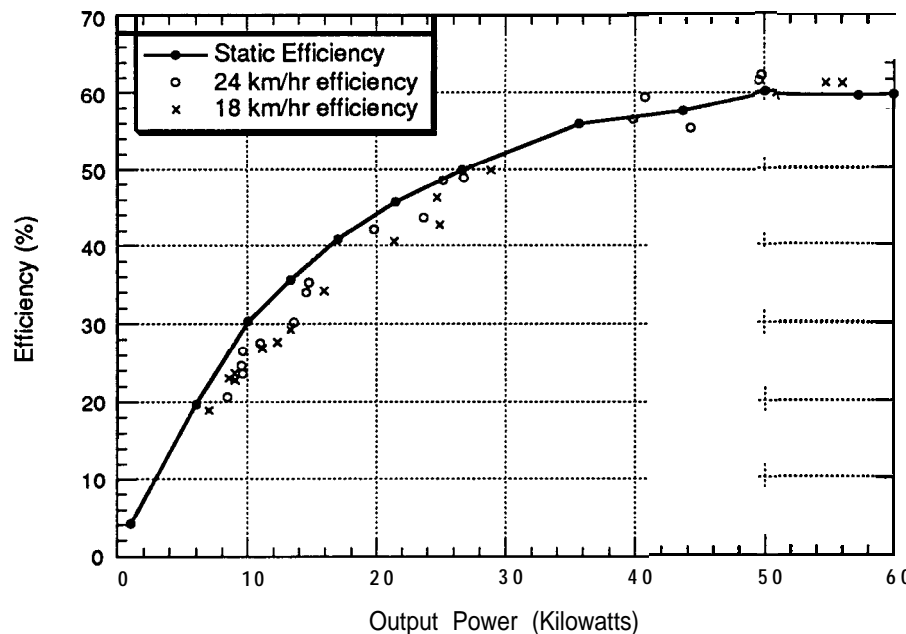
Dynamic testing of the ICS (with the vehicle in motion) represents the culmination of nearly a decade's work on the project. The dynamic results closely matched static performance. The dynamic data have more noise than static data for a number of reasons, including uncertainties in the pickup position relative to the roadway inductor (both vertically and laterally) and dynamics of the power conditioner.

#### 5.5.3.1 Power Coupling at Constant Speed

The first dynamic test was checking that power was being coupled and that there were no gross changes in any system parameters. The next tests involved driving the bus at constant speed over the roadway. Instantaneous power was recorded at the power conditioner input and the OBC output. These were integrated over time and an average value obtained. The output energy is divided by input energy to determine efficiency. As with previous efficiency tests, only the cable section of track was energized. Even 10 – 15 mph, the vehicle was over the energized roadway for approximately 10 seconds, and the first few seconds of data were unusable due to power conditioner and onboard transients. About 15 runs were done at each speed with various power transfer levels. The data are plotted in Figure 5.95. For both velocities, the data fall near the static efficiency curve. Most of it is slightly below the static curve, but several points, especially at the higher power levels, are on or above the static curve. For the data below the static efficiency curve, the extra losses may be due to poor lateral position of the bus, which slightly reduced efficiency.

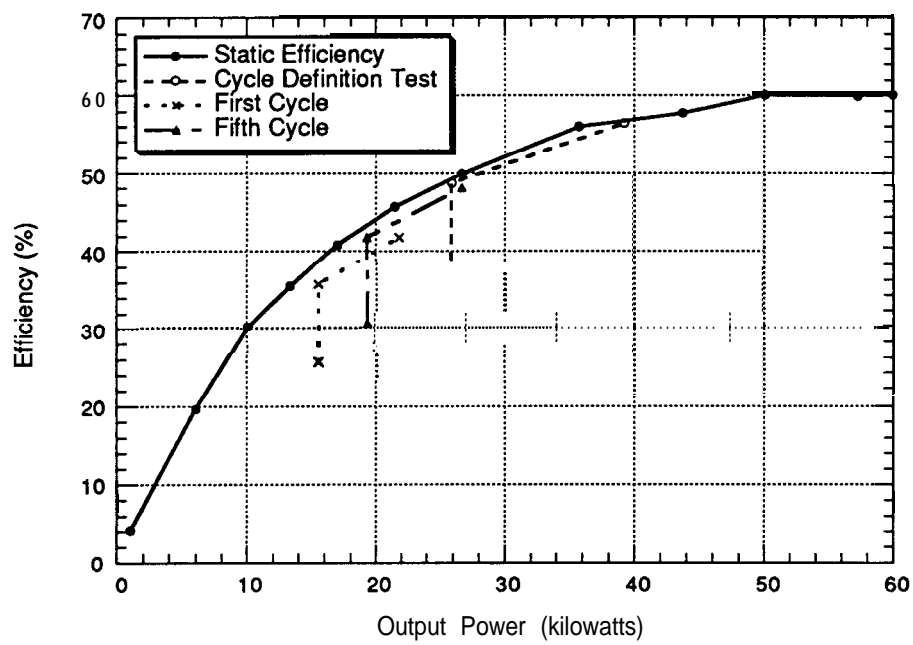
#### 5.5.3.2 Power Coupling at Variable Speed

Power and energy data were also collected during the range tests. During these tests, both segments were powered continuously because segment switching was not operational, which caused input energy to be increased considerably. Instead of having one segment powered 65% of the time and no segments powered the remaining 35% of the time, both segments were powered continuously. These extra idling losses are known and can be subtracted from the input energy. Data for three different intervals are presented in Figure 5.96, representing different battery conditions. They are conditions during which the battery was almost completely full, moderately full, and highly discharged. During the range tests, the vehicle was driven over a specific driving cycle. On the first cycle, the battery was nearly completely charged. By the fifth cycle the battery depth of discharge (DOD) was about 30%.



EVS10-017

Figure 5.95 System efficiency as a function of output power—short dynamic tests



EVS10-018

Figure 5.96 System efficiency as a function of output power—driving cycle tests

For each interval three points are plotted. The first included no corrections for extra idling losses, but was simply ac kilowatt-hours divided by dc kilowatt-hours. The power level is the average power level, calculated as total energy coupled to the vehicle divided by time. These points fall 10 – 15% below the static efficiency curve. The second point for each condition is directly above the first point. The energy lost in the second roadway segment is subtracted from the input energy. These values would have resulted if one segment had been energized continuously. These data points are much closer to the static efficiency curve, averaging 1 – 2% below it. The final adjustment involves accounting for the 35% of the time when no segments would have been energized if the segment switching hardware had been working, (the time when the vehicle was drawing no power from the roadway). The input energy corresponding to the unpowered time is subtracted from the total input energy. The average power transfer level is also adjusted as the output energy must be divided by the powered time rather than the total time. This second adjustment causes the data points for all three intervals to move up and toward the right. Again these points fall near the static energy curve, averaging 2 – 3% below the static data.

Average power coupled to the bus increases as the battery DOD increases because the battery can accept larger charging currents. Even when the battery is nearly full, the average power coupled is more than 20 kilowatts. For highly discharged conditions, the average coupled power is closer to 40 kilowatts.

The data in Figure 5.96 provide further support to the assertion that power transfer is independent of vehicle velocity. Vehicle velocities and power transfer levels from zero to 24 km/hr and 50 kw yield test data that fall near the static efficiency curve. Vehicle lateral offset and deviations in roadway current from its nominal 1200 amp value seem to have a minor effect on overall system efficiency.

#### 5.5.3.3 Controllability

Testing described in the preceding two sections was performed under both manual and computer control. The OBC operated on automatic control for the range tests. The control system performance was relatively good; the inductive coupling system was prevented from driving the **onboard** voltage above battery gassing voltage, while providing adequate energy to increase the vehicle range many fold compared with battery-only operation. One other example of computer control was tested to verify the operation of the automatic control system. The **onboard** control computer attempted to maintain a constant current of 160 amps over a large range of lateral offsets. The bus was driven down the track while gradually being steered from one

side of the track to the other. Under manual control, with fixed control state (tuning capacitance), the current dropped with lateral offset to either side. Under computer control as the current started to drop, more capacitance was switched in to maintain the desired current. In Figure 5.97 the solid circles show the data while operating under computer control. These points are between 150 and 180 amps until the vehicle offset is larger than 6 inches when this current coupling level cannot be maintained even with maximum capacitance. The open circles represent open-loop operation, and the output current drops off rapidly with lateral offset to either side.

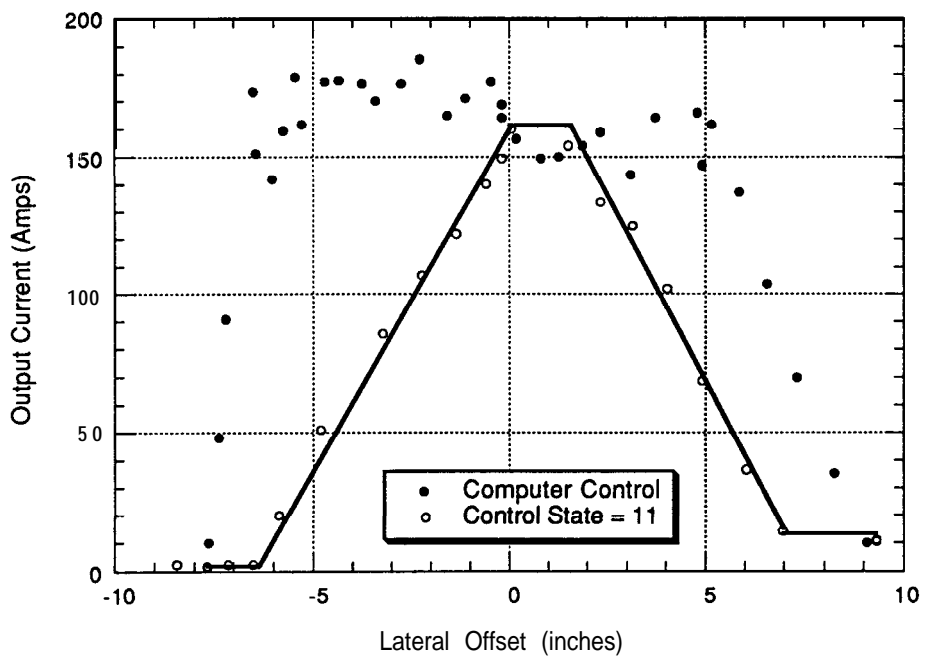


Figure 5.97 Output power as a function of lateral offset

Figure 5.98 shows capacitance as a function of lateral offset for the same test. Under computer control, capacitance is increased at larger offsets to maintain the proper output current.

The automatic control system performed its function well; it commanded the capacitor switches causing the desired current to be coupled to the vehicle. Occasionally there were dynamic interactions between the onboard control computer and the power conditioner control circuitry. Further investigation into control laws and dynamic response of the various system elements is needed.

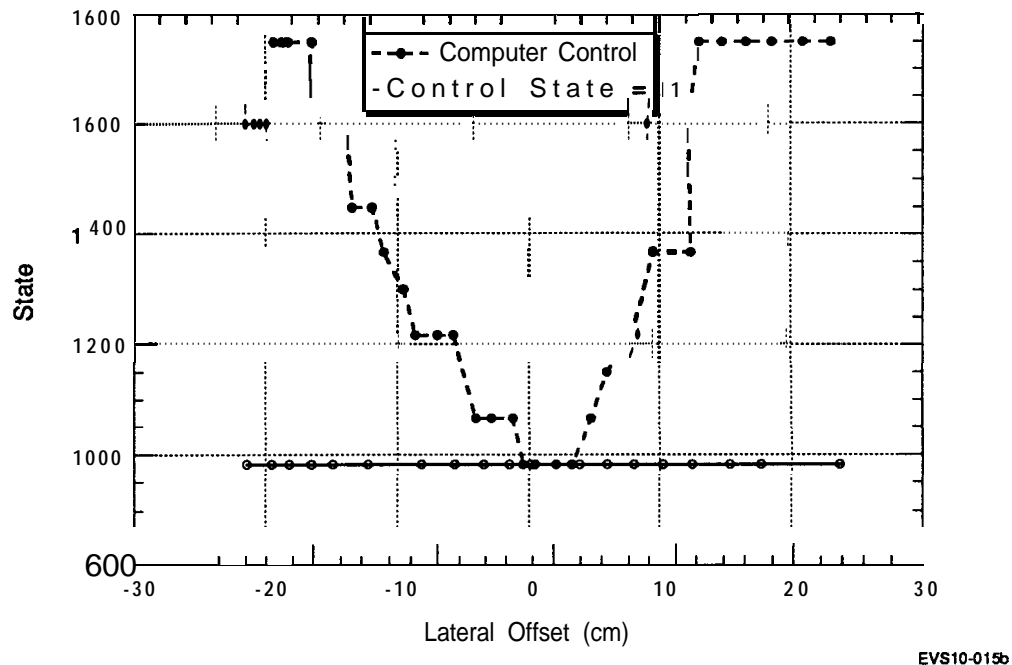


Figure 5.98 Capacitance as a function of lateral offset

## 5.6 Vehicle Operation with Inductive Coupling System

The ultimate goal of the inductive coupling system is to improve electric vehicle performance by overcoming the battery's limitations. The primary battery limitation is its inability to store adequate energy so the vehicle will have sufficient range. Other drawbacks to batteries include their weight, power limitations, and energy efficiency. If the energy storage issue were resolved, the others could be improved as well. Without having to supply the energy required for long trips, the battery could be smaller and lighter. Batteries could be engineered to maximize specific power rather than specific energy. Electric vehicles could be lighter with better acceleration. The reduction in mass would also reduce energy consumption. All these arguments return to the need for supplying energy, a function the inductive coupling system can perform better than a battery.

## 5.6.1 Range

As the test data show, RPEV technology overcomes the range limitation of battery vehicles that has been the downfall of electric vehicles since their inception a century ago.

### 5.6.1.1 Driving Cycle

The bus was designed for a specific driving cycle, characterized by a given velocity profile around a specific route, with a well-defined electrification pattern. Due to the geometry of the test track, the design driving cycle cannot be matched exactly. For instance, when the bus leaves the powered portion of the test track, it must slow and turn around on an unpowered section of pavement. Since the exact design cycle could not be duplicated, substantial effort was devoted to determining a driving cycle that could be performed at the Richmond Field Station test track and would match the design cycle closely enough to provide meaningful results. Numerous statistics of the design cycle were calculated, including average velocity, percentage of time over the powered roadway, and energy consumption per mile. Approximately a dozen driving cycles were defined and tested at Richmond Field Station to determine one that closely matched the statistics of the design cycle. The bus was driven on each of these cycles, with all data recorded for statistical analysis. One route was selected as providing an adequate match. This driving cycle consisted of ten laps of the track, nine of which were powered. On the powered laps, a 20-second stop was included just after entering the powered segment at each end of the track. On the fifth lap, one of the two stops was extended to two minutes. Table 5.5 shows the key parameters of both the design and test duty cycles. The data from the tests to determine the duty cycle represent the third set of data in Figure 5.95 showing efficiency during variable speed operation. The statistics of the test cycle are within 10% of the statistics for the design cycle, and testing on this cycle would provide excellent insight into how the bus would operate on the design cycle.

### 5.6.1.2 Range Test Results

The bus was fully charged and driven on the test cycle under battery operation only. The test was repeated with the inductive coupling system in operation. The battery in the bus is about five years old and unfortunately has not been well maintained. It was originally rated for 750 amp-hours at the 5-hour rate and about 400 amp-hours at the 30-minute rate, which is more representative of the type of loading placed on the battery while operating on the defined driving cycle. During testing, the battery was

**Table 5.5**  
**Key Parameters of the Design and Test Duty Cycles**

	Design Cycle	Test Cycle
Average Velocity, km/hr	13.1	12.5
Energy Consumption, kWh/km	1.72	1.79
Powered time, percent	62	66
Average ICS Output, amps	279	284
RMS Motor Current, amps	344	310

able to supply 280 amp-hours, indicating that it has no more than 70% of its original capacity and quite possibly less, which is consistent with test results indicating that when the battery was new, it could operate the bus for approximately 2.5 to 3 hours, but now 1.6 hours is the limit for a stop-and-go cycle. At that point, the bus could no longer meet the established end-of-test criterion. During this 1.6 hours, the bus traveled about 14 miles. The test results are summarized in Table 5.6.

**Table 5.6**  
**Summary of Test Results**

Test Mode	Range		Cycle Definition
	Test Battery Only	Range Test RPEV	
Time (hr)	1.6	6.5	0.4
Distance (mi)	14	50	3
Amp Hours supplied by battery	280	83	3
Remaining capacity (Amp-hrs)	0	201	
DOD start of test (%)	0	0	-74
DOD end of test (%)	100	30	-75
Net battery current supplied (amp-hr/mi)	20.4	1.66	1.01
Range associated with remaining battery capacity	0	169	276
Total range	14	219	326

\*Based on 201 amp-hrs at a rate of 0.63 amp-hrs/mi

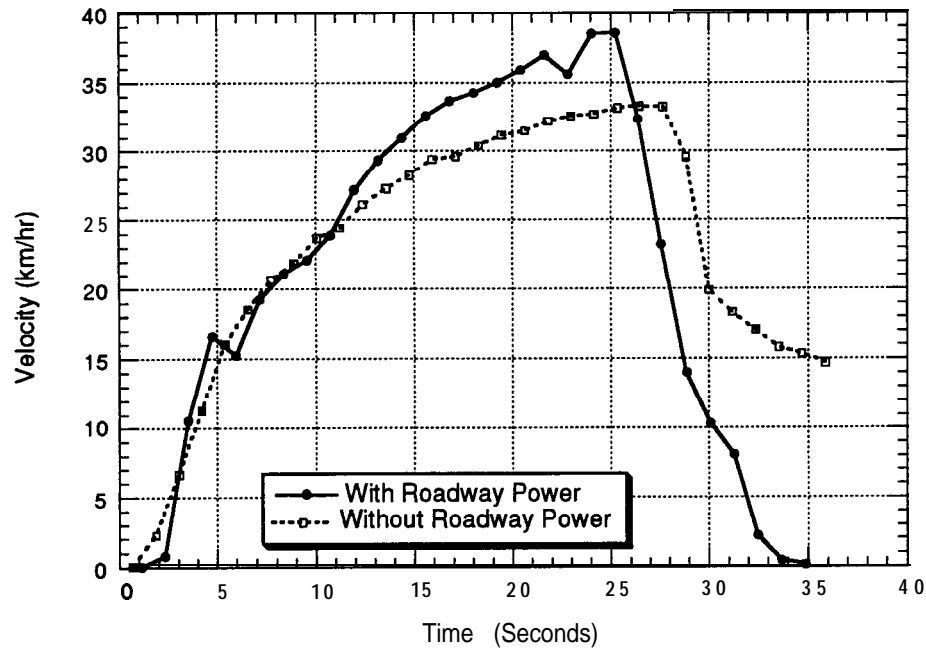
The battery discharged very slowly during testing with the inductive coupling system turned on. After 50 miles (almost 7 hours of operation), the battery had discharged 83 amp-hours (30%) or 1.67 amp-hr/mile. We changed to battery-only operation as it was clear that testing could not be completed in one day and an overnight break would allow some battery recovery. The bus operated for an hour before the end-of-test criterion was reached. During that hour, the bus traveled 10 miles and the battery supplied 201 amp-hours. At the average rate of battery discharge during the first 50 miles, the bus could have operated more than 20 hours and traveled 168 miles. As the battery becomes more highly discharged, its charge acceptance capability increases and the average coupled power increases. For instance, the inductive coupling system average output current increased 40% (from 157 to 218 amps) between the first and last 5-mile segments of coupled power testing. Notice that it was still not near the 284 amp average value listed in Table 5.5 (for the tests used to define the test cycle) that occurs when the battery is highly discharged.

During the tests used to define the test cycle, the battery was discharging 1.01 amp-hour/mile. If that battery discharge rate were achieved starting at mile 50, the vehicle's range would be approximately 250 miles. The actual range would fall between a pessimistic estimate of 168 miles and an optimistic one of 250 miles, possibly 210 miles, which is 16 times farther than the bus operated on the battery alone and about 10 times farther than the bus could have operated on a new battery.

Regardless of the exact numbers, a tremendous range increase was achieved-for all practical purposes unlimited if the vehicle operates for a significant fraction of the time over the powered roadway.

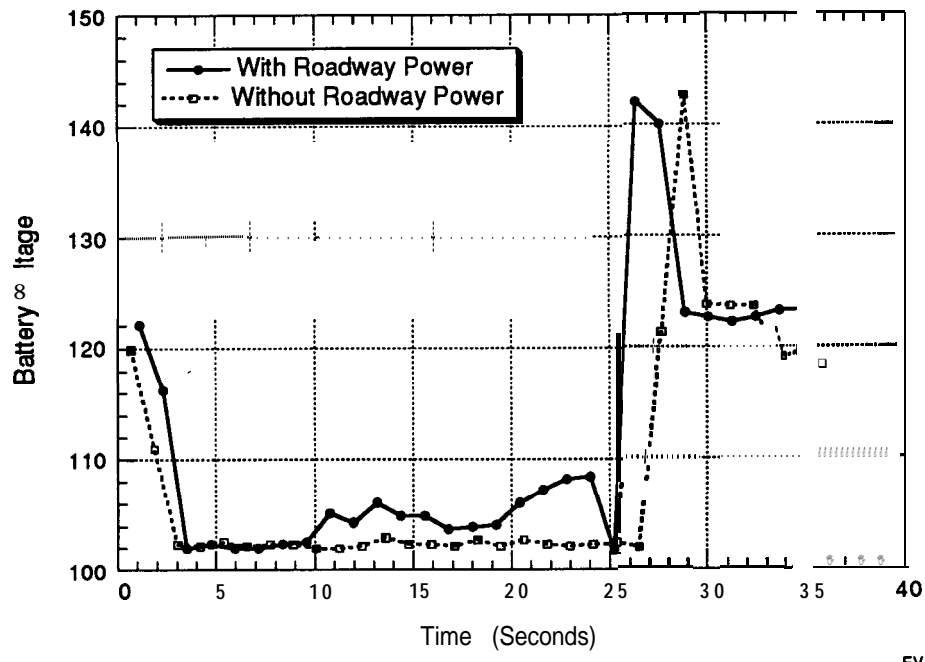
### 5.6.2 Vehicle Performance

The inductive coupling system improves the vehicle's performance in a number of ways. The most obvious is the increase in range, but the inductive coupling system provides additional power as well as energy. When the battery is moderately to severely discharged, the extra power supplied by the ICS can make a noticeable difference in acceleration, hill climbing, or top speed. Figure 5.99 shows the vehicle's acceleration with and without the roadway power. During these tests, the battery was highly discharged. At the start of these tests, the motor controller was drawing 500 amps at the motor controller minimum voltage limit of 102 volts. Figures 5.100 and 5.101 show the motor controller input voltage and current. At 10 seconds, the bus enters the powered roadway section. The output current from the



EVS10-019a

Figure 5.99 Acceleration with and without roadway power



EVS10-019b

Figure 5.100 Effects of ICS on vehicle motor controller voltage

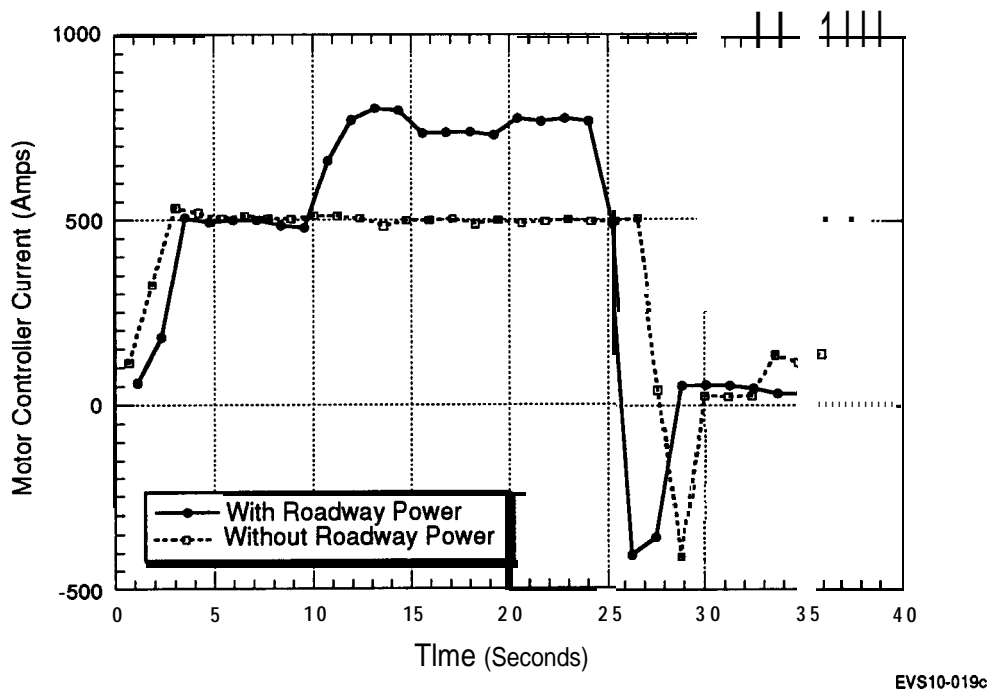


Figure 5.101 Effects of ICS on vehicle motor controller current

ICS raises the battery voltage and allows the motor controller to draw its maximum 750 amps, resulting in better acceleration. The bus accelerated from 15 to 20 mph in 4.3 seconds rather than 10.5 seconds on the battery alone.

When the battery is at a higher state of charge, the bus still performs better on the powered roadway, although the change in power may be 10 or 15% instead of 50% as in the above example. For instance, if the motor controller were drawing 750 amps at 104 volts and the ICS started providing 350 amps, the battery (discharging) current would drop from 750 to 400 amps, with a voltage increase from 104 to 120 volts and a 15% increase in power.

## 5.7 Testing Conclusions

The most important conclusion is whether the technology works: Does it accomplish the desired goals? The answer is a qualified yes. The hardware designed, built, and tested is capable of transferring power while the vehicle is stationary or moving. The power transfer is controllable in small steps over the entire range from zero to full power. This energy is sufficient to provide a dramatic range increase as high as a factor of ten or twenty, depending on the vehicle and driving cycle. In any case, for

all practical purposes, vehicles have infinite range while operating on the powered roadway. The battery size for vehicles operating most of the time on the powered roadway segments could be reduced if a smaller (lighter) battery with specific power high enough to meet the vehicle's maximum power requirements were available. Overall system efficiency is adequate, but improvements are both desirable and likely in future systems. Several tests indicate that it is desirable to move to a new operating point at higher frequency and lower roadway currents, which should increase system efficiency and reduce environmental impact.

It is difficult to make absolute statements about the environmental impact of the system as tested or as it would appear in future designs. Magnetic flux densities that people would be exposed to depend on the particular application, specifically relating to the likelihood of pedestrians being in the immediate vicinity of the open roadway while it is energized. For freeway installations or static charging applications where the roadway would be energized only when a vehicle was over it, the flux levels people would be exposed to are considered safe by most experts. The largest exposures are likely to be in arterial applications. The tested operating point resulted in unacceptably loud acoustic noise in non-RPEVs located over the powered roadway, especially while stopped or driving at low speeds where the ambient noise was low. Moving to new operating points at higher frequencies and lower roadway currents will eliminate this noise. Other phenomena related to electromagnetic interference are also expected to vanish for these new designs.

### **5.7.1 System losses and Efficiency**

The overall system efficiency is 60% at the peak power point and is expected to average about 50 – 55% over the expected operating cycle. Figure 5.102 shows the power flows and losses based on a combination of analysis and experimental data. We believe that the efficiency can be improved 10 – 20% in the next generation design.

### **5.7.2 Operating Point**

The operating point used on the bus supplies adequate power to the vehicle at a reasonable efficiency. Tests indicate that for a variety of reasons, future systems should be built with lower roadway currents, which will require higher frequencies.

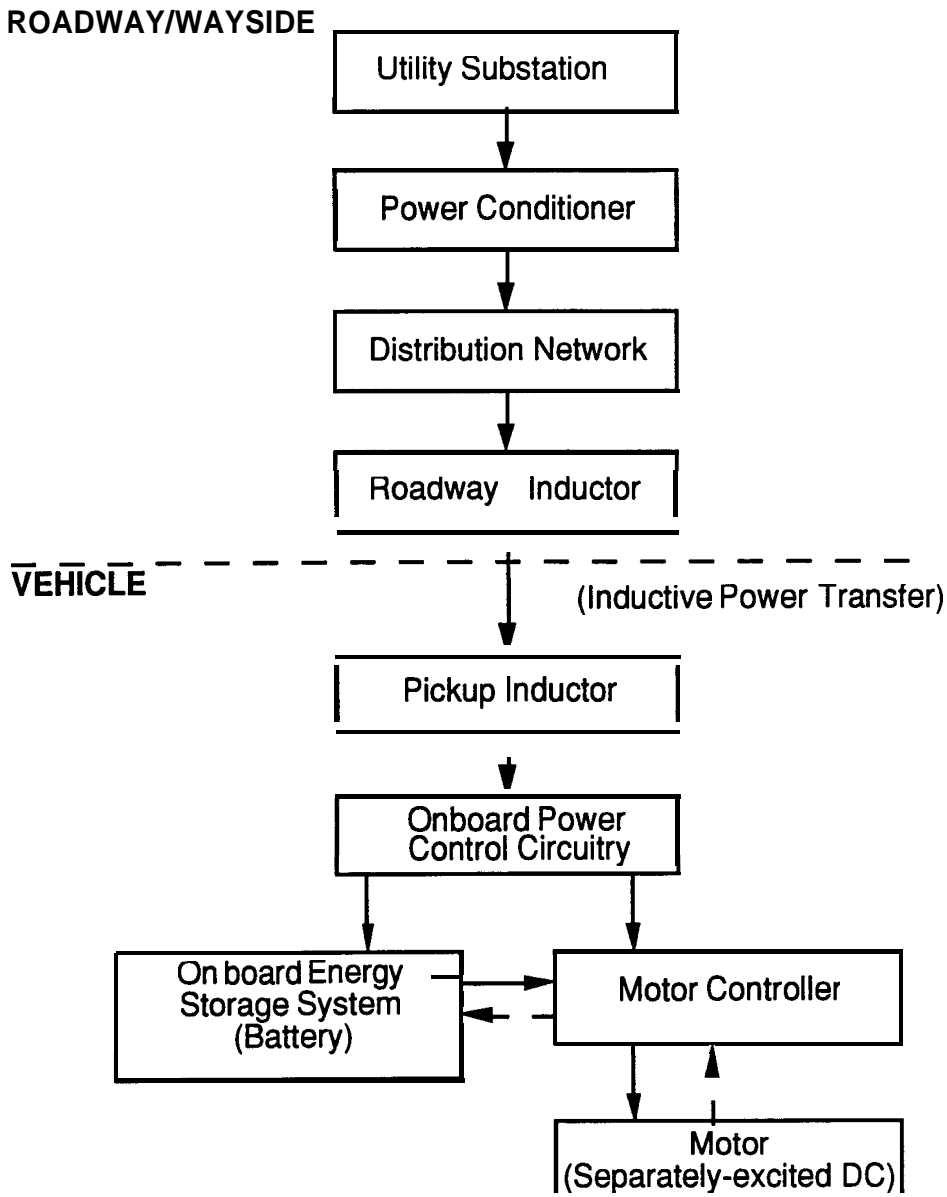


Figure 5.102 Power diagram with loss terms and efficiencies

### 5.7.3 Environmental Impact

The environmental impact of the RPEV system must be carefully studied, especially in relation to high-frequency effects. Reduced roadway current and redesigned roadway inductors in future designs will almost certainly have improved environmental characteristics compared to the hardware tested at the Richmond Field Station.

### **5.7.3.1 Acoustic Noise**

Acoustic noise in non-RPEVs is the single most surprising result discovered during the test program. Acoustic noise from the roadway and onboard equipment is acceptable with relatively simple acoustic treatments. The operating point must be changed to deal with noise in non-RPEVs.

### **5.7.3.2 Magnetic Fields**

The biological and EM1 (electromagnetic interference) effects of magnetic fields produced by an RPEV system need to be carefully studied. New RPEV design have fields strengths considered safe by most experts, but almost all tests of biological effects have been performed at 60 Hz and RPEVs operate at 400 – 10,000 Hz. EM1 effects such as interference with electromagnetic speedometers and solid state engine controls need to be investigated further; however, tests of newer designs indicate that these effects have been eliminated.

## **6. Related RPEV Research**

---

Three RPEV research projects have been conducted in addition to the Testing and Parametric Studies. One involved building and testing hardware designed to operate at higher frequencies and lower roadway currents. The other two were application studies involving a regional RPEV freeway network and near-term deployment on high-occupancy vehicle (HOV) lanes. SCT was active in all three projects and is in a good position to summarize the results.

At the completion of the PATH bus experiments, it was obvious that changes needed to be made to the bus ICS as tested. These changes involved a very significant reduction in the roadway current, which reduces acoustic noise and resistive losses in the open roadway. The operating frequency had to be increased to maintain adequate power transfer capability. These changes were incorporated into a new system when Southern California Edison (SCE) and the Los Angeles Department of Water and Power agreed to fund development of an improved RPEV system using a van-sized vehicle. This system may eventually be installed at the proposed Playa Vista development north of Los Angeles International Airport.

Southern California Association of Governments (SCAG) in collaboration with PATH, studied application of both electrification and automation technologies to the freeway system in the Greater Los Angeles region. This study defined several trial networks and analyzed impacts of these technologies on the selected networks.

UC Berkeley Institute of Transportation Studies (ITS) analyzed application of several advanced technologies, (including roadway electrification) to HOV lanes, focusing on the El Monte Busway in Los Angeles.

Final reports of both deployment studies are available, so these results will only be summarized, while a more detailed description of the Playa Vista project results are presented.

### **6.1 Playa Vista Project**

The four main objectives in the design of a new RPEV system were: lower magnetic fields, lower acoustic noise, increased efficiency, and lower cost. To meet these objectives

a major redesign of the system was needed, including a new operating point and an improved roadway geometry. Reducing onboard weight was also considered an important goal.

Because of concerns about the health effects of magnetic fields and observed interference with some automotive electronics, a new operating point with substantially lower magnetic fields had to be designed. Lower magnetic fields mean lower roadway current and higher frequency to maintain power transfer ability. The new system design converged on a 240-amp roadway current at a frequency of 8500 Hz. Consideration was also given to operating points at lower frequencies, and ICS parameters for lower frequency operation were developed.

### **6.1.1 Playa Vista System Overview**

For the initial development of the new system, SCE donated a battery electric G-Van for conversion to an RPEV. A new roadway, pickup and OBC were designed based on the G-Van power requirements and the operating point. To maintain the G-Van's performance a new battery pack weighing one-third less than the original was designed. The onboard ICS components brought the G-Van's weight back to a standard G-Van's.

Two short sections of new roadway were constructed at the Richmond Field Station. A 20-foot section was installed in the roadway adjacent to Building 167 and a 10-foot section was set up inside. The roadway was powered by a set of six power amplifiers that allowed selection of frequencies from 0 to 20,000 Hz; however, the power output was limited to about 15 kW.

The design trade-offs and requirements for this new design are detailed in the Parametric Studies report.

### **6.1.2 Performance at Nominal Operating Point**

Numerous tests were conducted on the G-Van Inductive Coupling System, including measurement of magnetic fields, tuning curves, and peak power transfer under various conditions. These test were performed at nominal and off-nominal conditions, and the results generally fell near the predicted values.

#### **6.1.2.1 Magnetic Fields**

The magnetic fields of the new roadway were measured for comparison with both predicted values and values from the old roadway. Figure 6.1 shows predicted and

measured fields for both designs 10 inches above the road surface. The measured fields track the predicted values very well, except near the Playa Vista roadway. The fields were approaching the maximum value for which the measuring equipment is rated, and

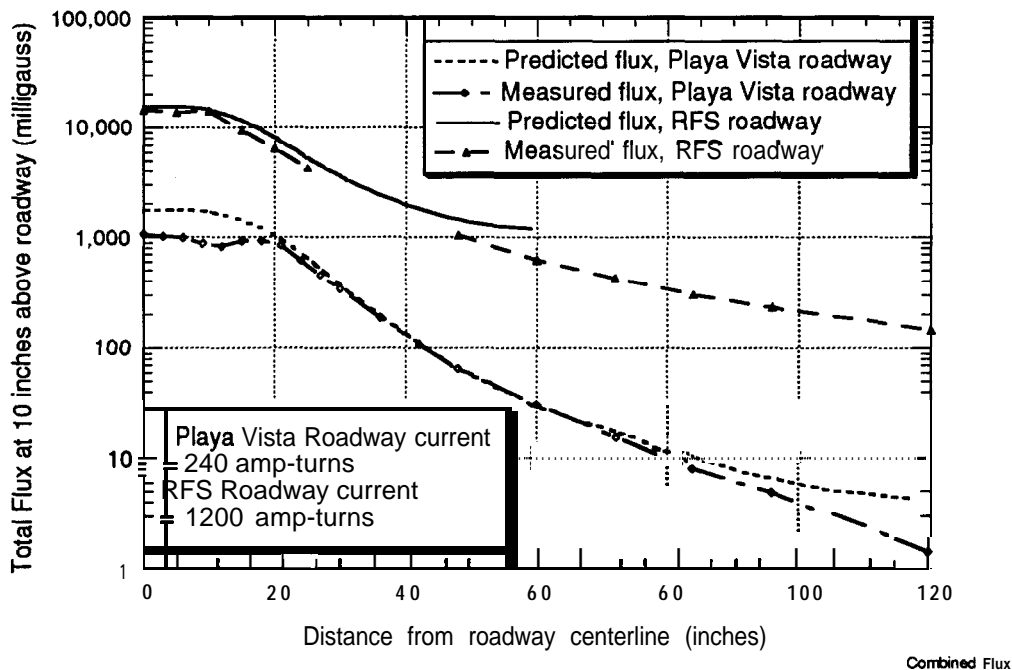


Figure 6.1 Predicted and measured fields 10 inches above roadway

the measured values are believed to be in error. Near the roadway centerline, the fields of the new design are approximately a factor of five below the old design, the ratio of the reduction in roadway current between the two cases. At a distance that is large compared to the spacing between the primary windings and the field cancellation windings (two feet), the flux levels in the new design are reduced by an order of magnitude. For both designs, the predicted fields flatten out at the edge of the universe used during the generation of the predicted flux levels, due to boundary effects experienced by the model. In reality the flux levels continue to drop off at the same rate indefinitely. This rate is approximately a factor of ten for a doubling of distance for the Playa Vista design and a factor of five for a doubling of distance with the RFS roadway. At ten feet from the roadway centerline, the magnetic fields for the Playa Vista design are down to a few milligauss, about two orders of magnitude lower than the Richmond Field Station roadway.

### 6.1.2.2 Tuning Curves and Frequency Response

The output current of the inductive coupling system is controlled by switching capacitance into and out of the secondary (onboard) circuit. This changes the resonant frequency of the system. The output of the ICS increases as the system's resonant frequency approaches the driven frequency. With no capacitance in the secondary, the resonant frequency of the pickup and onboard controller is higher than the driven frequency. As capacitance is added, the resonant frequency decreases and approaches the driven frequency. Output current is a maximum when these two frequencies are equal. If more capacitance is added, the resonant frequency of the secondary circuit drops below the driven frequency, and output current drops. Figure 6.2 shows a typical tuning curve for the system, with output current increasing with capacitance, peaking, and then dropping as too much capacitance is switched into the circuit. Figure 6.3 shows the frequency response curves of the system with three different amounts of capacitance switched into the secondary. The solid line shows response with low capacitance and shows a low output current if the system is driven at the nominal excitation and a low output current if the system is driven at the nominal excitation of 8500 Hz. The dotted curve shows the response with a moderate amount of capacitance. The secondary resonant frequency has dropped to 8500 Hz, matching the driven frequency, and the

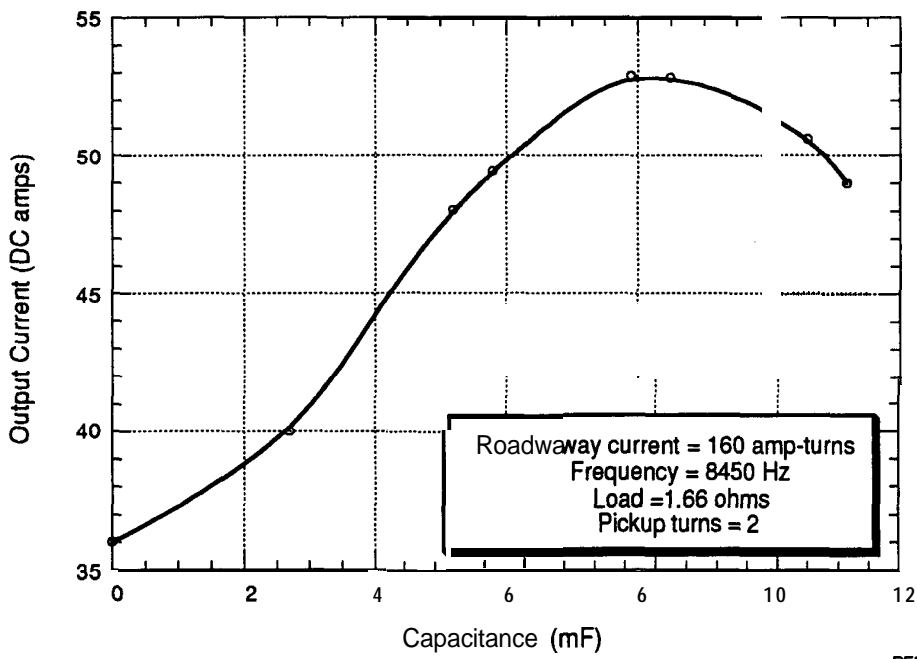


Figure 6.2 Typical measured tuning curve

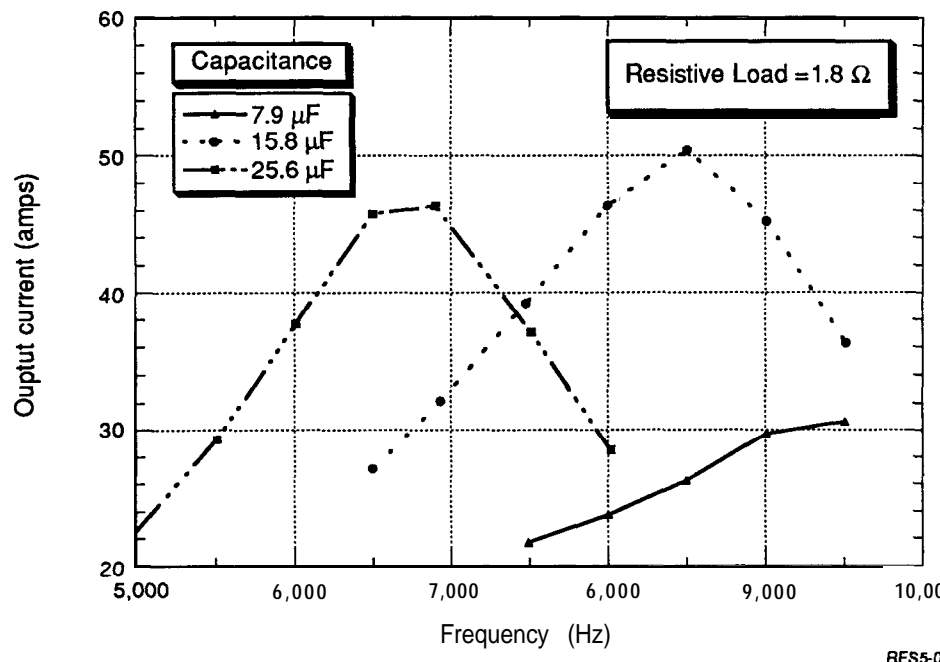


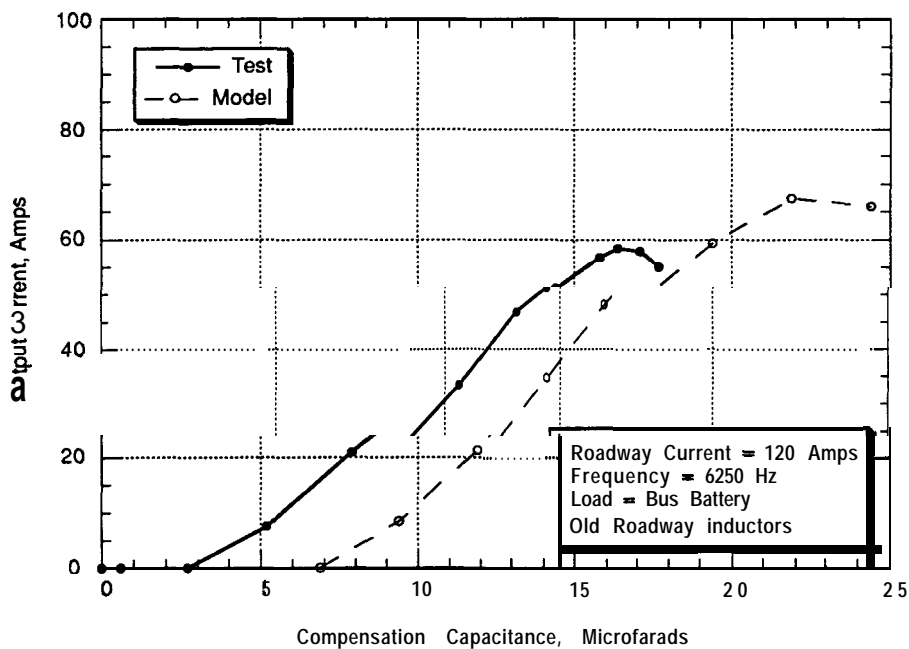
Figure 6.3 Measured frequency response with varying capacitance

output current is a maximum. As more capacitance is added, an over-tuned condition is reached, where the resonant frequency is lower than the driven frequency, and output current drops. This figure shows that at lower excitation frequencies, more tuning capacitance must be switched into the circuit to achieve a given output current.

Figure 6.4 shows model and test results of the ICS used on the RPG-Van. The curves follow the same general shape, although the curve of the test results peaks at a slightly lower output current and a noticeably lower value of capacitance. This may be due to improperly chosen resistance values in the computer model.

#### 6.1.2.3 Power Testing Methodology

The power amplifiers used as the power supply for testing were not capable of producing 40 kilowatts at 8500 Hz, so testing had to be performed at lower power levels. Unfortunately, the battery creates a huge non-linearity within the system, so it is not possible to simply scale down the roadway current by a factor of two and expect output current to be reduced by a factor of two. When testing into a resistive load, the output current and voltage are both proportional to the roadway current, allowing low power tests to easily be extrapolated. This allows results with the existing hardware to be



RFS5-026

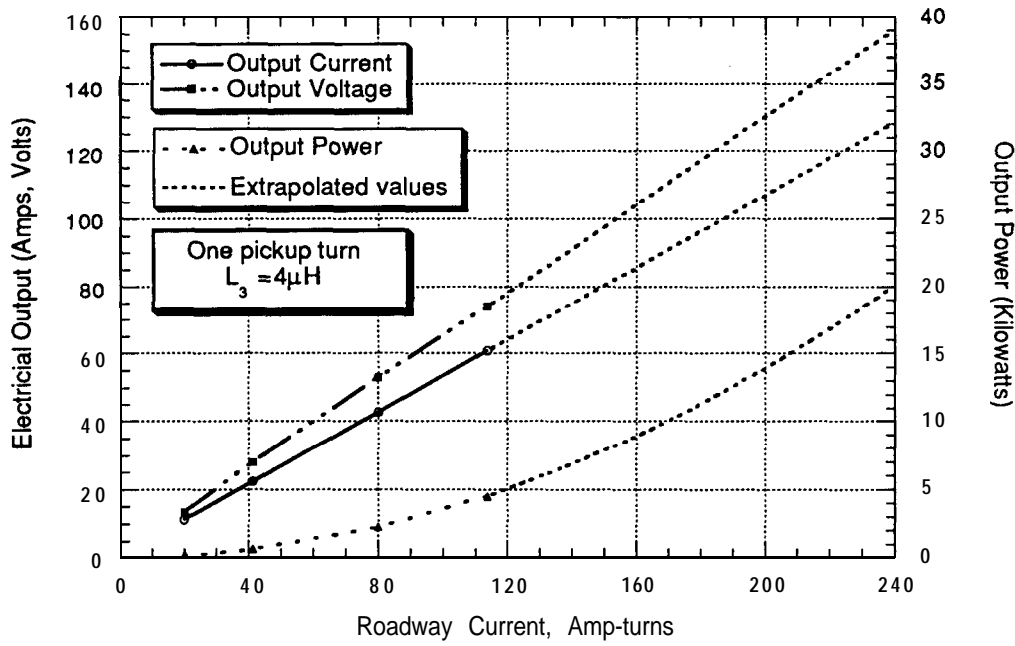
Figure 6.4 Model and test results of the ICS used in the RPG-Van

scaled up represent system performance with the rated roadway current. The only difficulty with this approach is proper selection of the value of the resistor. The initial testing was done using a resistance value of 1.2 ohms, which matches the nominal ICS output. Other values of resistance were used as well. A curve can be plotted through the results from several resistance values which represents the system performance for off-nominal conditions.

#### 6.1.2.4 Linearity of System

The design point was selected as 180 amps at 220 volts, for an effective resistance of 1.2 ohms. Figure 6.5 shows the system output into a 1.2 ohm load with various roadway currents. Data was taken for roadway currents of 24, 40, 80, and 120 amp-turns. The plots of the voltage and current are both straight lines going through the origin, indicating a linear system. Notice that the output power increases with the square of the roadway current, as both voltage and current increase with higher roadway currents. Extrapolating these curves out to a roadway current of 240 amp-turns yields an output current of 128 amps at 156 volts or about 20 kilowatts. This is below the design output voltage, current, and power. If this ICS configuration were connected to a 216-volt

battery, the output current would be slightly under 100 amps, which is not enough output to be an effective system.



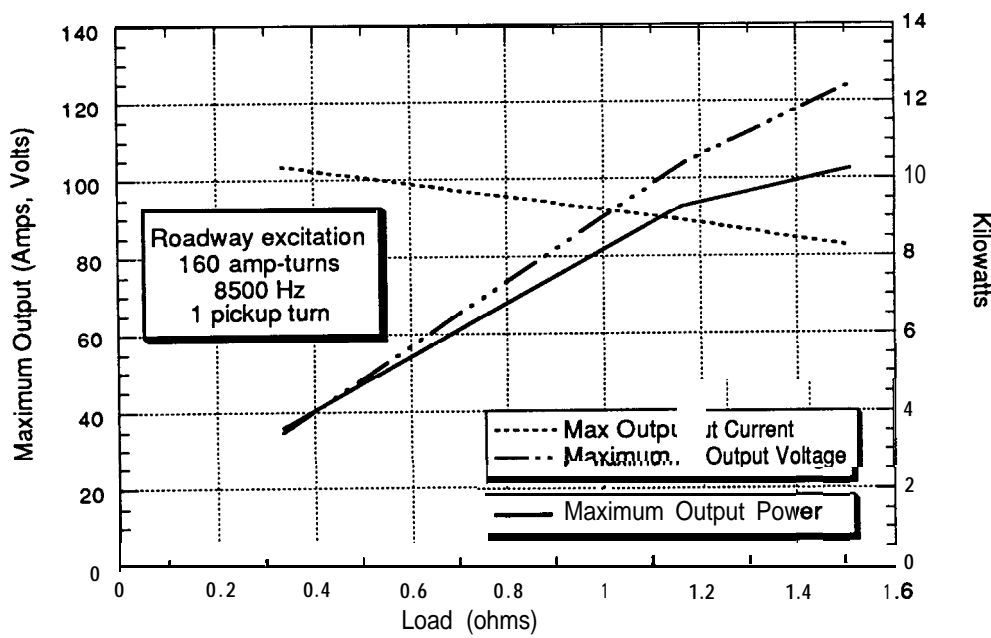
RFS5-051

Figure 6.5 System output into a 1.2 ohm load with various roadway currents

#### 6.1.2.5 Power Tests

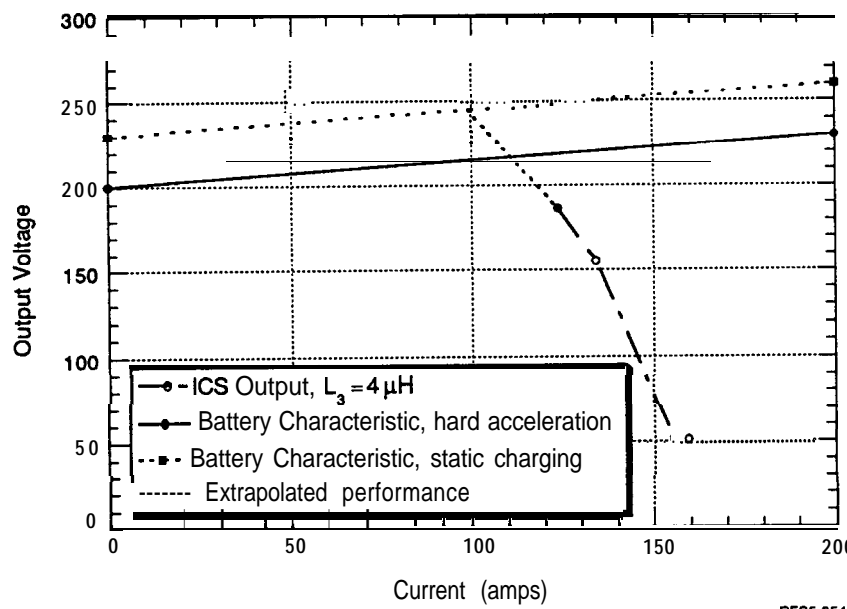
Tests into other resistance values were performed as shown in Figure 6.6, which shows that the output current decreases very slowly with increased resistance in the load. The voltage is increasing much faster than current is decreasing, as shown by the fact that the output power is rising with increased load resistance.

The data in Figure 6.6 were all taken with a roadway current of 160 amps but output values can be scaled up to correspond to a roadway current of 240 amp-turns, as shown in Figure 6.7. In addition to the output voltage and current from the ICS tests, straight lines have been added to represent the battery characteristic. The solid line starts at 200 volts and is a reasonable approximation of the battery voltage under hard acceleration (with zero ICS output). The line slopes slightly upward toward the right to represent the increased battery terminal voltage as the ICS output current increases. (This decreases the battery discharge current, resulting in a higher terminal voltage.) The intersection of



RFS5-054/055

Figure 6.6 Maximum system output into various resistive loads



RFS5-054/055/089-5

Figure 6.7 System performance scaled to roadway current of 240 amp-turns

the ICS output curve and the battery impedance line shows what the actual system output would be under these conditions. In this case, the ICS output would be about 110 amps at 216 volts, or 23.8 kilowatts. Since the G-Van requires about 25 kilowatts at its maximum cruising speed, this output is not enough to provide infinite range. An alternate battery impedance characteristic is drawn to represent static charging with 101 amps output current at approximately 245 volts.

#### **6.1.2.6 Rectifier Input Inductance Variations**

The test results in the previous section showed that the ICS output was lower than the design values. ICS output can be increased by increasing the value of the rectifier input inductor ( $L_3$ ). This inductor provides some isolation of the resonant portion of the circuit (pickup and tuning capacitance) from the load (battery or resistive load). Increasing the value of  $L_3$  decreases the effective damping in the system, causing a higher resonant peak and higher output current. The disadvantage of this approach is that the pickup voltage rises rapidly with increased rectifier input inductance, leading to higher flux levels (and losses) in the coupled roadway and pickup inductor cores, along with higher voltage and current into the tuning capacitance. These adverse factors prevent the rectifier input inductance from being increased arbitrarily high, but moderate increases can produce additional output power without increasing roadway current or frequency.

Figure 6.8 shows the output of the system for rectifier input inductance values of 4 and 16 microhenries. At the higher inductance, the output current has been increased about 45 amps or 33%, with no increase in roadway current. Using the same analysis as in Section 6.2.3.2, the output with the modified system would be 180 amps at 227 volts or a total power of 40.9 kilowatts, meeting the design goals. Figure 6.9 shows this data point being added to Figure 6.7, with curves drawn parallel to the data for the low value of  $L_3$ .

#### **6.1.2.7 System losses and Efficiency**

System losses and efficiency are an important measure of the system performance. The most useful estimates of system losses are based on published performance specifications, calorimetry tests, and electrical measurements. Table 6.1 presents our best estimate of the system losses as it would be built. Open roadway core losses are the largest component-almost half of the total system losses, making reductions in these losses a high priority in the system design. Section 6.3 discusses possible reductions in the operating frequency, and a frequency of 6000 Hz has been assumed in this table. This reduction in frequency (or possibly in roadway current) would help minimize uncoupled core losses.

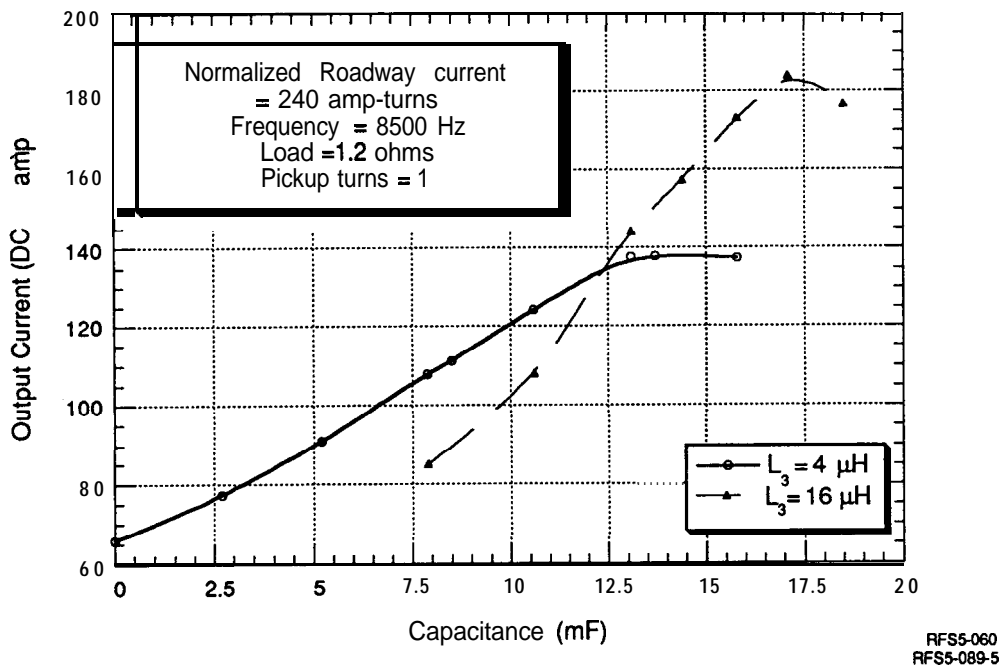


Figure 6.8 Tuning curves showing the effect of varying  $L_3$  inductance

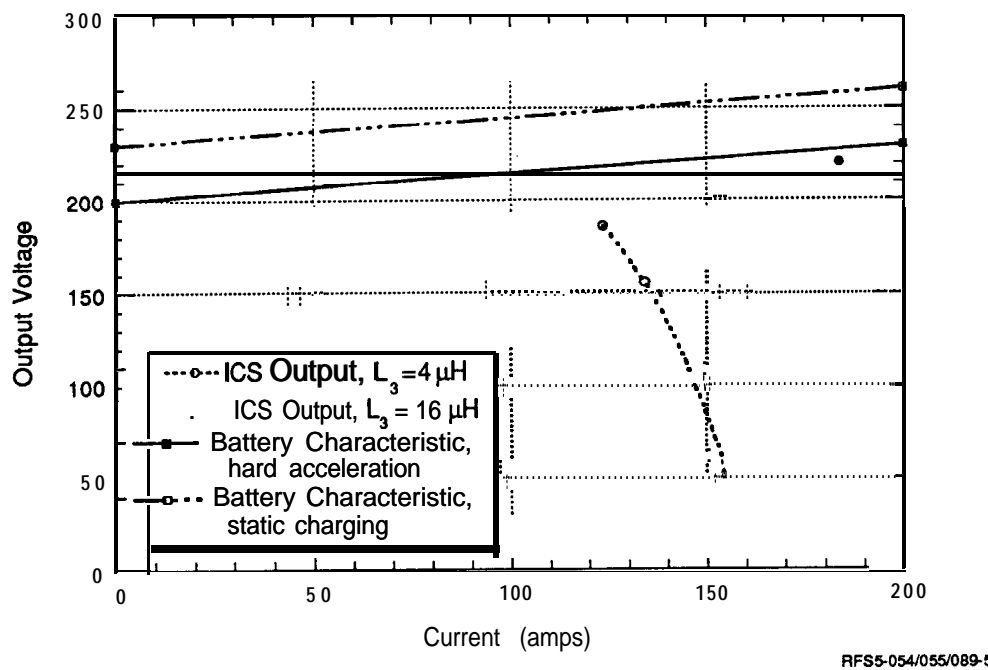


Figure 6.9 Data for  $L_3 = 16 \mu\text{H}$  added to Figure 6.7

**Table 6.1**  
**G-Van Component Losses at 6000 Hz**

	<b>Power kw</b>
output	37.5
Onboard controller	1
Pickup cores	1.6
Coupled roadway cores	3.2
Uncoupled roadway cores	11.0
Roadway conductors	1.0
Transmission line	<b>0.5</b>
Power supply	<b><u>3.0</u></b>
Total input power	59.0
Efficiency = 37.5/59.0 = 64%	
Static Charging Efficiency = 37.5/47.55 = 79	

The losses shown result in a system efficiency of about 65% for dynamic coupling of power (based on the Playa Vista segment length of 120 feet) and a static charging efficiency of about 80%. It would be possible to improve these efficiencies with more expensive materials in the cores, but that would probably increase rather than decrease life cycle costs, especially for the dynamic charging case. These efficiency numbers should be compared with conventional charging, which is 70% efficient, assuming a charger efficiency of 95% and a battery efficiency of 75%.

#### 6.1.2.8 Electra-Magnetic Interference

Electra-magnetic interference (EMI), especially with electronics aboard non-RPEVs has been raised as a potential adverse impact of the RPEV system. There has not been a comprehensive testing program with either the original 400 Hz roadway or the new high frequency system. Three specific observations are relevant, all dealing with the old 400-Hz, 1200-amp roadway. The most frequently encountered case of EMI involves the speedometer on the PATH bus. It reads properly when the bus is in motion, but when the bus is stopped over the energized roadway, the speedometer reads 45 mph. The inductive pickup for the speedometer picks up the 400 Hz field of the roadway and interprets it as the passing of “gear teeth” on the driveshaft at a frequency that

corresponds to 45 mph. Also one '89 Mazda stalled on the roadway, apparently due to the electronic engine control's being fooled about the engine speed, again due to the roadway's magnetic field being pickup up by an inductive "gear tooth" counter used to sense engine speed. A dashboard indicator light on another car indicated that the anti-lock brake system was inoperative. All examples seem to be due to the same phenomenon: an inductive (Hall effect) sensor picking up the roadway's magnetic field instead of the rotational speed it was intended to sense. On the new (8500-Hz, 240-amp-turn) roadway, the bus speedometer is not fooled. This by no means proves that the problem is solved, but it is an encouraging sign that such problems may not exist with the new design.

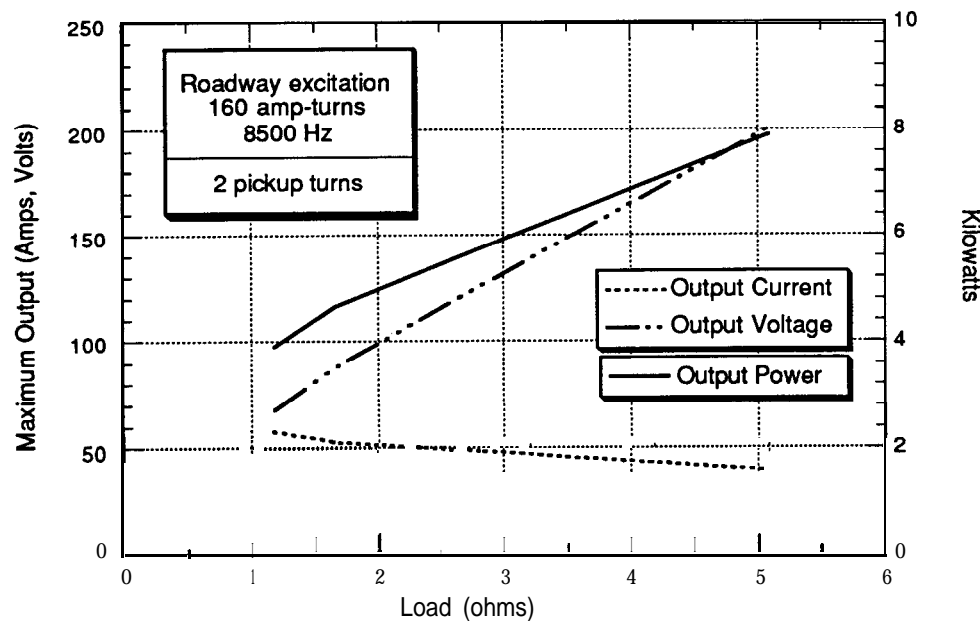
### 6.1.3 Testing at Off-Nominal Conditions

The RPG-Van will operate at both nominal and off-nominal conditions. Some off-nominal conditions, such as variations in the airgap (pickup vertical and lateral position) will certainly take place. Other variations, such as changing the number of pickup turns or changing the field cancellation windings, are choices that must be made before system fabrication. Testing off-nominal conditions follows the same procedures as testing under nominal conditions and reveals some interesting trade-offs in the system design.

#### 6.1.3.1 Pickup Turns Variations

In general, increasing the number of turns increases the output voltage that the ICS can drive into, but decreases the output current. This is analogous to changes in the turns ratio in a conventional transformer.

The first off-nominal condition tested was a change in the pickup winding from one turn to two. Figure 6.10 shows the output voltage and current into a resistive load with two turns. As with a single turn, the current decreases weakly with increased load resistance and the power increases. Figure 6.11 shows results for both one and two turns. The output current is cut approximately in half by changing from one turn to two into loads of approximately 1.5 ohms, resulting in considerably higher power at these lower output impedances. For a vehicle such as the Impact, with higher voltage and lower current requirements than a G-Van, a higher number of turns allows the same power to be transferred at higher voltage. The powers are much lower in Figure 6.11 than some of the proceeding plots, as these are raw test results and have not been normalized to a roadway current of 240 amps. The rectifier input inductance ( $L_3$ ) was at the lower value of 4 microhenries.



RFS5-061/063/066

Figure 6.10 Measured output voltage, current, and power into a resistive load

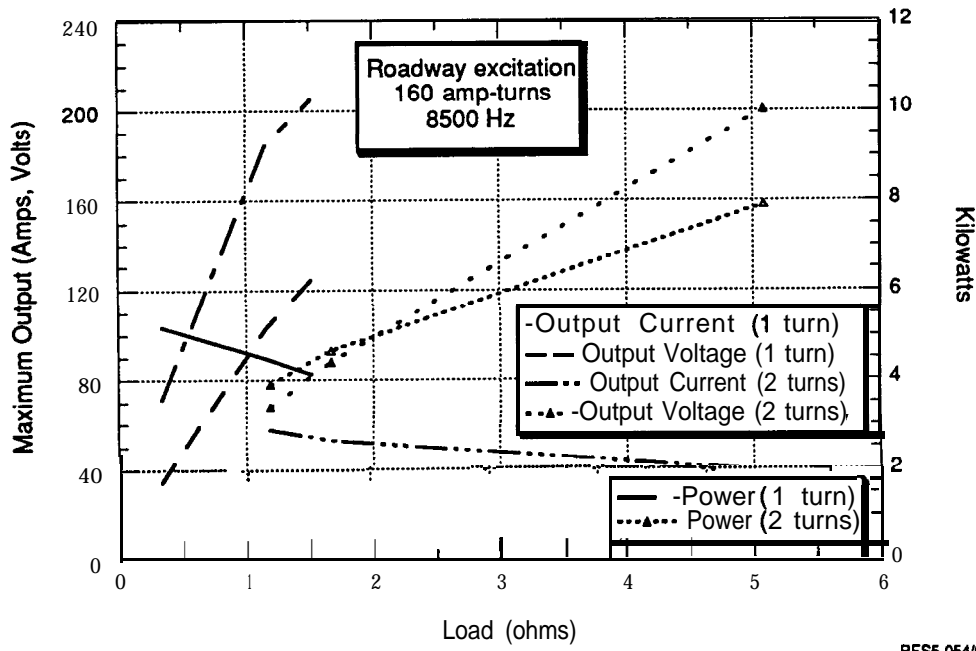
RFS5-054/055  
RFS5-061/063/066

Figure 6.11 Measured results for one and two turns

### 6.1.3.2 Airgap Variations

Variations in the airgap are certain to occur in the real world. Figure 6.12 shows predicted tuning curves as a function of lateral offset. These computer results indicate that the output power drops very little at a two-inch offset, but then drops rapidly. At a 6-inch offset, the predicted power is about half of the power when centered, and test results indicate that the roll-off with lateral offset is probably more severe than indicated in Figure 6.12.

Power decreases as the airgap height or lateral offset increases because the mutual and leakage inductances change. Mutual inductance is a measure of the magnetic flux that links the roadway inductor and pickup inductors. The larger it is, the easier it is to couple power. Leakage inductance appears as a drop in pickup output voltage and hinders coupling of energy from the roadway to the pickup.

Measured mutual inductance is shown as a function of both lateral offset and airgap height in Figure 6.13. Mutual inductance with the pickup centered varies inversely with airgap height. It decreases with lateral offset, slightly at first and then more rapidly for offsets larger than three inches.

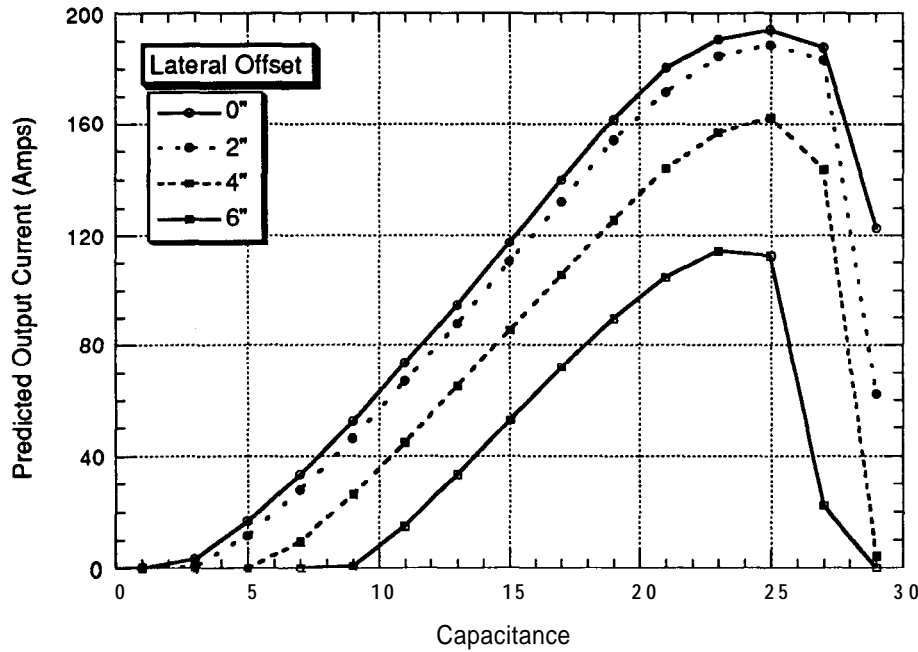


Figure 6.12 Predicted tuning curves as a function of lateral offset

RPGVLO-1

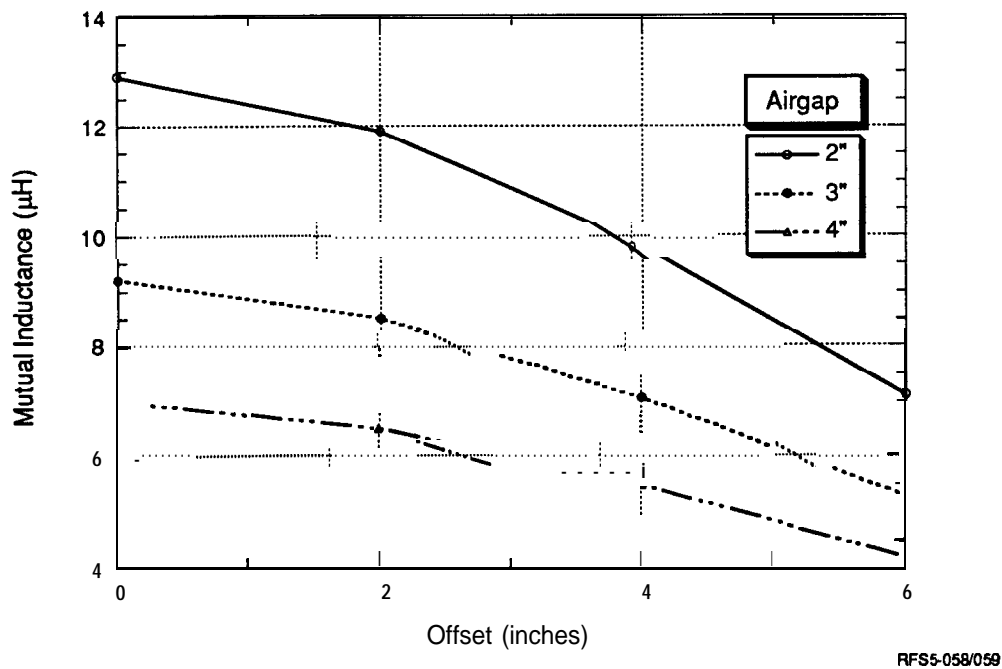


Figure 6.13 Measured mutual inductance as a function of lateral offset and airgap

The analogous data for leakage inductance is shown in Figure 6.14. When centered, leakage inductance is nearly independent of airgap height. At large offsets, the leakage is greater for small airgaps. Figure 6.15 shows the mutual and leakage inductances at a two-inch airgap height for lateral offsets up to 6 inches. The leakage inductance is nearly as large as the mutual inductance when the pickup is centered and becomes greater than the mutual inductance for offsets of three inches or more. This high ratio of leakage to mutual inductance decreases the effectiveness of the power coupling. Figure 6.16 shows the same variables, but with a three-inch airgap height. Leakage inductance is virtually unchanged, but the decrease in mutual inductance causes it to drop below leakage inductance even when the pickup is centered.

The ratio of leakage to mutual inductance for the PATH bus was under 0.50 at nominal conditions. The increased leakage inductance of the new design is believed to be caused by two factors: the geometry of the pickup conductor slot and the presence of field cancellation windings. The pickup slot for the bus was more than twice as wide as it was high. The aspect ratio for the G-Van is approximately 1:1, allowing more leakage across

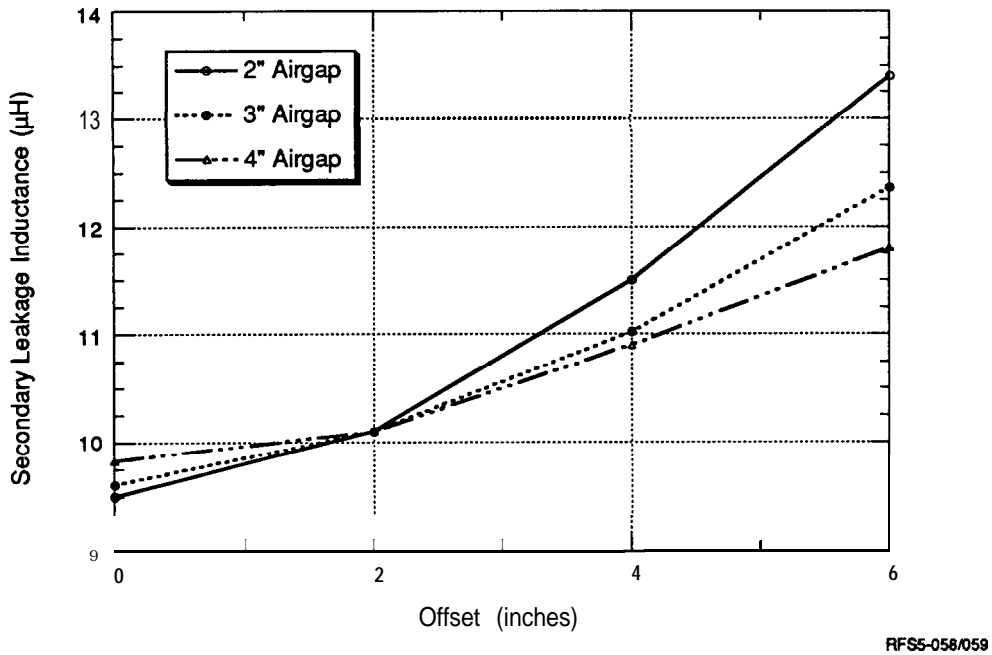


Figure 6.14 Measured leakage inductance as a function of lateral offset and airgap

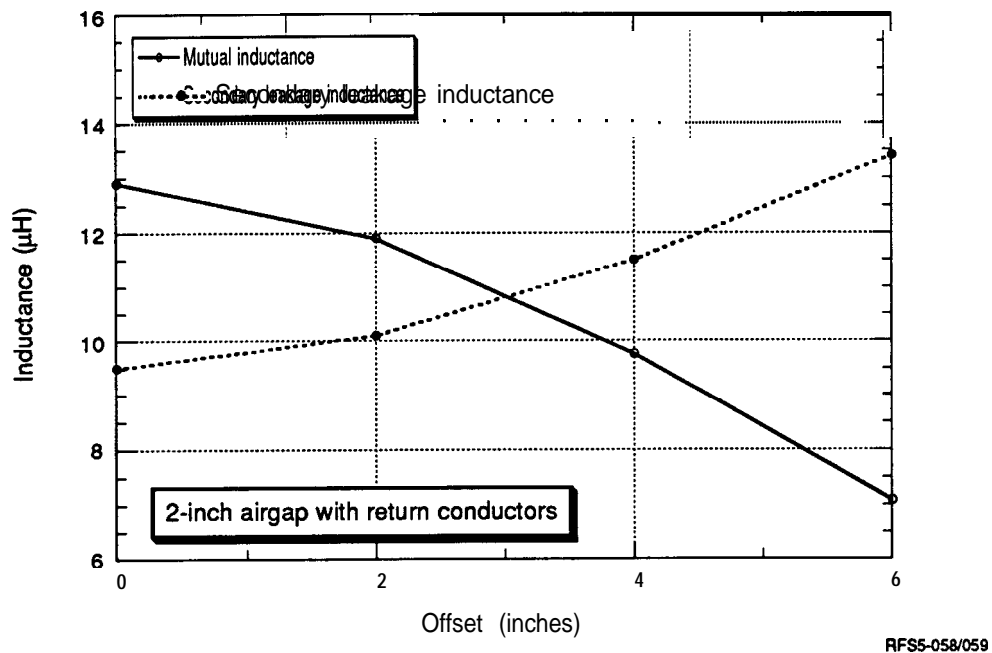


Figure 6.15 Measured mutual and leakage inductances at a two-inch airgap

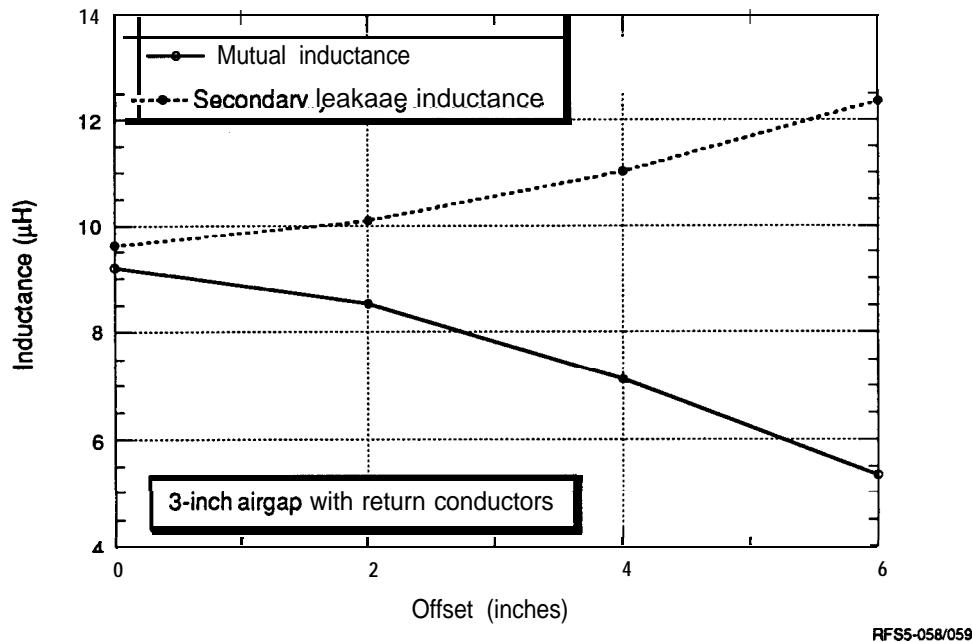


Figure 6.16 Measured mutual and leakage inductances at a three-inch airgap

the slot. Design improvements could reduce the depth of the pickup slot, which would not only reduce leakage inductance, but also reduce the pickup weight and even cause a slight decrease in coupled core losses.

#### 6.1.3.3 Field Cancellation Windings

Field cancellation windings are very effective in reducing magnetic flux levels at distances of several feet or more from the centerline of the roadway. They also cause a 15% decrease in mutual inductance, as seen in Figure 6.17. Overlooked in the earlier analysis is the fact that the field cancellation windings also cause a significant increase in the leakage inductance. With the pickup centered and with field cancellation windings, the leakage inductance crosses the mutual inductance at an airgap height of just under three inches. Without field cancellation windings, this crossover point occurs at 4 inches. Figure 6.18 illustrates the ratio of mutual to leakage inductance, making the differences with and without field cancellation windings more clear.

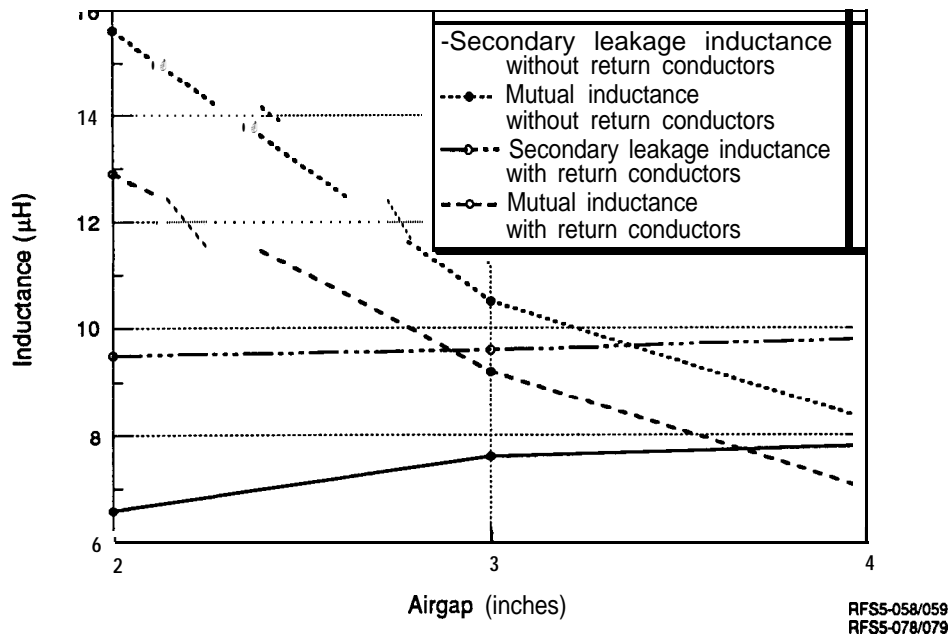


Figure 6.17 Effects of field cancellation windings on measured mutual and leakage inductance

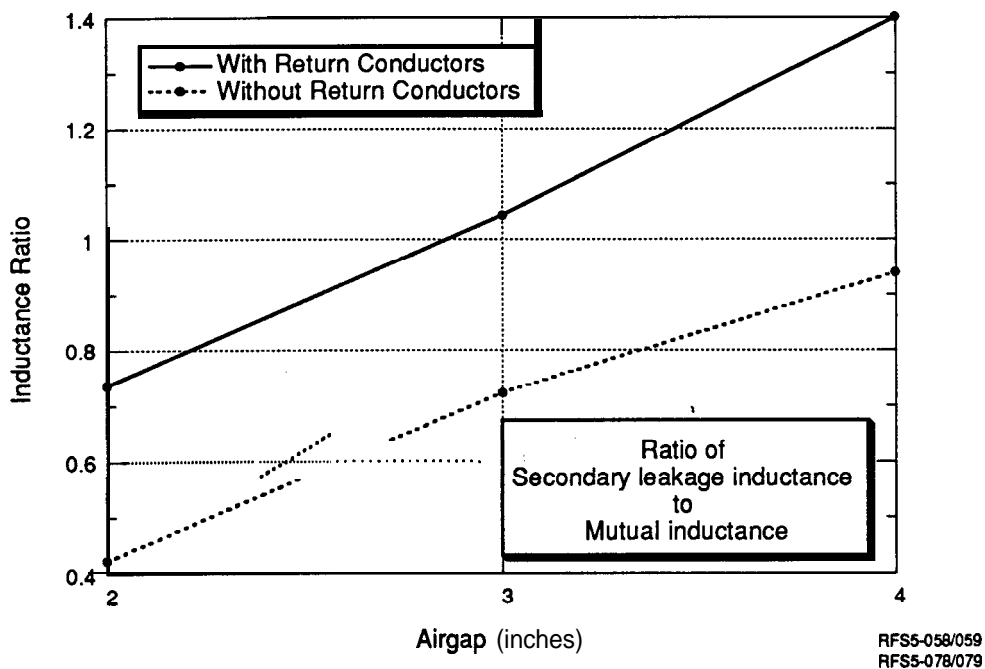


Figure 6.18 Ratio of measured mutual to leakage inductance

### 6.1.4 Alternate Frequency Tests

Testing at alternate frequencies showed that acoustic noise is very low (35 – 40 dB) and has very little frequency dependence. Both output power and open roadway losses decrease at lower frequencies. Tests performed at 4000 Hz show that 27.5 to 33 kw output power can be obtained. The original output power goal of 40 kilowatts is conservative for the G-Van (which uses 25 kilowatts when cruising at top speed), suggesting a better design with a somewhat lower output power and operating frequency, perhaps 30 – 35 kilowatts output at an operating frequency of 5000 – 6000 Hz, which would reduce open roadway losses by approximately 35–45%, and increase overall system efficiency.

Selection of the operating frequency has been an issue in the design of inductive coupling systems from their inception. In general, higher frequencies can induce larger voltages **onboard** the vehicle at any particular roadway current. On the other hand, open roadway core losses increase with increased frequency. The ICS designed for the PATH bus operated at 400 Hz with a roadway current of 1200 amps, which proved undesirable due to acoustic noise in **non-RPEVs** driving on the powered roadway. The original design for the RPG-Van uses 240 amp-turns in the roadway at 8500 Hz. Test results described in Section 6.2 indicate that the baseline design could couple 40 kilowatts into the vehicle with that operating point.

The purpose of the alternate frequency tests is to identify the frequency that is most appropriate for the RPG-Van when all factors, including power coupling, losses, and acoustic noise are considered.

Many tests were performed at alternate frequencies, including measurement of acoustic noise, power coupling, and system losses and efficiency. Some tests were performed over a wide range of frequencies, such as measurement of acoustic noise, open roadway losses, and parasitic losses. In each of these cases, changing frequency is a very simple process. For other tests, such as coupled power tests, retuning the system is a major undertaking for each new frequency, as many internal variables must be scaled with frequency. These variables include all inductors and the tuning capacitor ( $C_2$ ) in the **onboard** controller as well as the roadway power factor correction capacitor.

#### 6.1.4.1 Acoustic Noise

The first test examined acoustic noise in a passenger car parked over the roadway inductor. Tests were performed at 120 and 200 amp-turns in the roadway inductor, with

the results shown in Figure 6.19. The noise levels were 1-5 dB higher at 200 amp-turns than at 120. The acoustic noise levels were between 35 and 40 dB for all measurements taken for roadway excitations between 2000 and 13,000 Hz, which is about the same magnitude as the sound level in a library. For comparison, the same readings with 1200 amps at 400 Hz were in the 50 – 60 dB range. Although the noise levels were low, they were distinguishable in a car parked in a quiet location (30 – 40 dB). The acoustic noise was most noticeable as the power was turned on or as the car coasted onto the powered segment at low speed. When driven at moderate or high speed, car, road, and aerodynamic noise completely masked any noise caused by the powered roadway, even in the quiet environment of the Richmond Field Station. If the system is installed on freeways or urban arterials, acoustic noise should not be a problem.

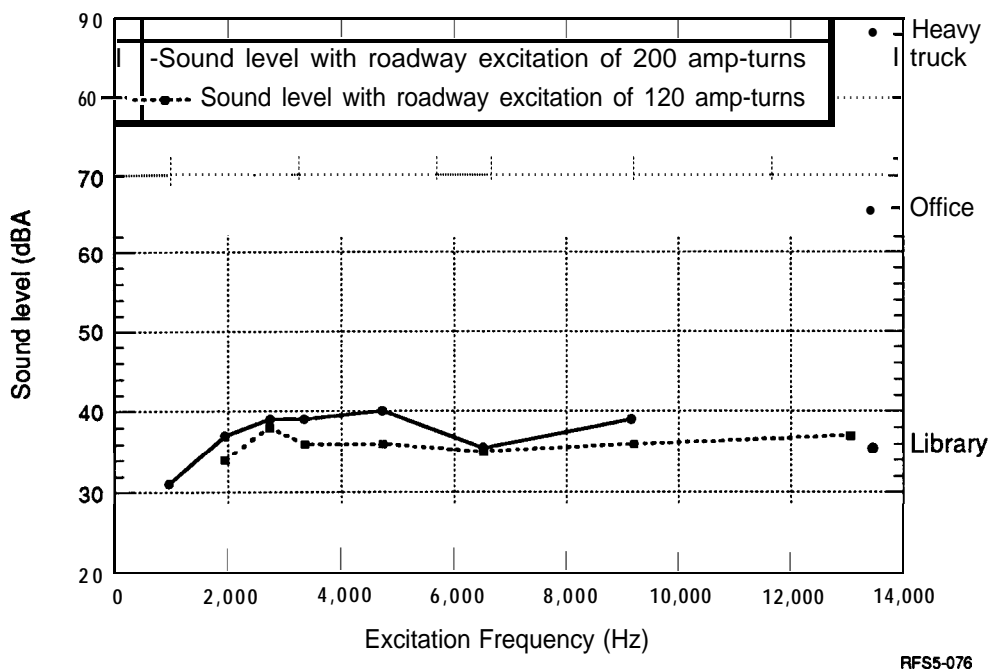


Figure 6.19 Acoustic noise in a passenger car

#### 6.1.4.2 Power Coupling into Resistive load

Several coupled power tests were performed. Tests at 1000 – 2500 Hz with two turns and 1.7 ohm resistive load indicated that output power was not close to the desired 40 kilowatts. The pickup was reconfigured to a single turn, giving increased output current and power. The final tests, measuring performance at 4000 and 8500 Hz showed that

reducing the operating frequency from 8500 Hz to 4000 Hz would still provide an acceptable output power.

**Resistive load of 1.7 Ohms.** The ICS performance into 1.7 ohms with two pickup turns at 1000-2500 Hz was tested initially. This resistance corresponds to 130 amps and 28.5 kilowatts into a 220 volt dc load (battery), which was considered the minimum acceptable output power. This output would be adequate to supply all the power required by the G-Van to cruise at maximum power, assuming the vehicle remained perfectly centered and 85 – 90% of the route length was powered. There would be no extra power for battery charging.

The tests were conducted at reduced roadway current due to limitations of the power amplifiers and were scaled up to a 240 amp-turn roadway current using the scaling method described in Section 6.2. The results were disappointing as seen in Figure 6.20. The output power starts at 44 amps and 3 kilowatts at 1000 Hz and levels out at 8 kilowatts by 2000 Hz. It became clear that the number of pickup turns would have to be decreased to increase the output current.

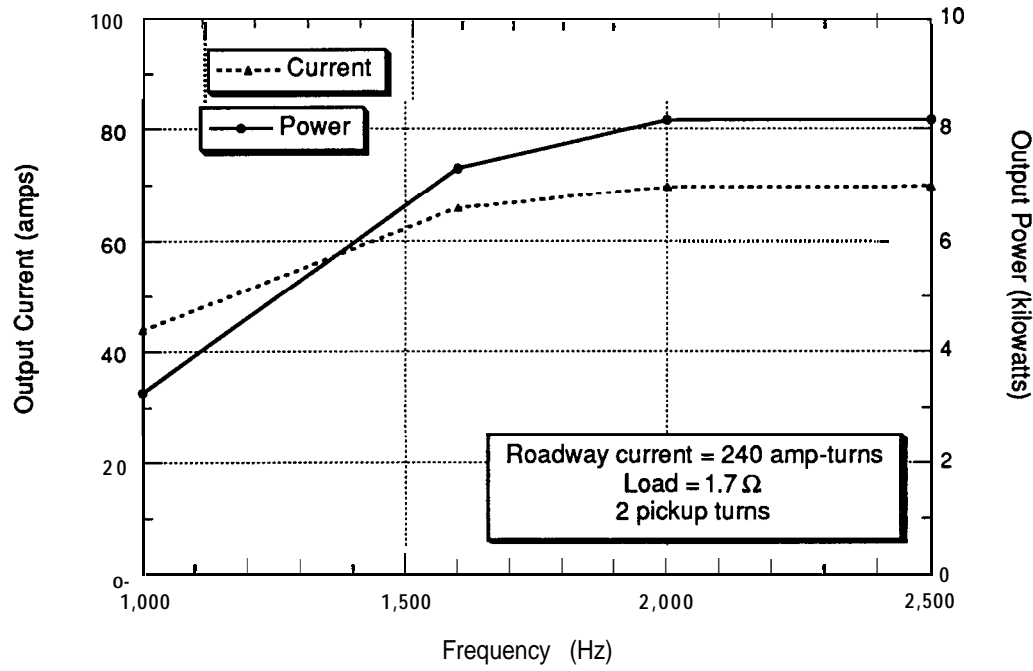


Figure 6.20 Output current and power as a function of frequency

**Resistive load of 1.2 Ohms.** The number of pickup turns was decreased to one, which raised the output current, and the excitation frequency was varied from 1400 Hz to 8600

Hz with a resistive load of 1.2 ohms. During these tests, the tuning capacitance in the onboard controller was adjusted to produce the peak output current at each frequency; however, the inductance values in the OBC were not adjusted for frequency, but were maintained at their nominal (8500 Hz) values. The desired result was 180 amps at 220 volts or 39.8 kilowatts. For cases with output current lower than 180 amps, output voltage is also lower than nominal, indicating that if the G-Van battery were used as a load, the output current would be even lower than the measured value. In fact, based on tests presented in Section 6.2, the maximum output achievable with the present design at 8500 Hz is 150 amps if the rectifier input inductance is maintained at its nominal value. By adjusting the rectifier input inductance, we were able to raise the output to 180 amps. Figure 6.21 shows how the peak output current is approximately constant at 140 – 150 amps above 5500 Hz, but drops with frequency below this breakpoint in the curve. The fact that the OBC inductance values were not adjusted from their nominal (8500 Hz) values accounts for some of the decrease in output current at lower frequencies; however, it is unlikely that the output current would be adequate at low frequencies even with proper inductance values in the OBC.

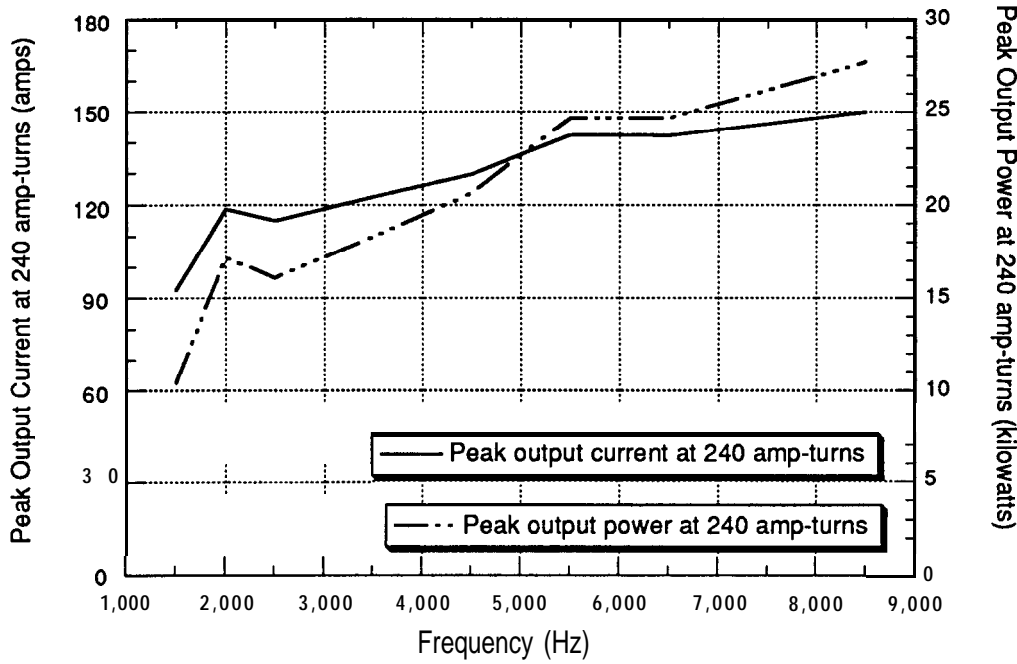


Figure 6.21 Peak output current and power as a function of frequency

The tuning capacitance required to obtain the peak output current for these tests is shown in Figure 6.22. At lower frequencies, much higher values of capacitance are

required. This data is replotted on a semi-log scale in Figure 6.23 and can be approximated by a straight line with a slope of about -0.5, indicating that the required capacitance varies inversely with frequency squared as expected. The physical size of the capacitor increases with capacitance. A 25  $\mu\text{F}$ , 8500 Hz capacitor weighs 25 pounds and occupies 0.3 cubic feet, and a 300  $\mu\text{F}$ , 1500 Hz capacitor is about 79 pounds and 0.9 cubic feet.

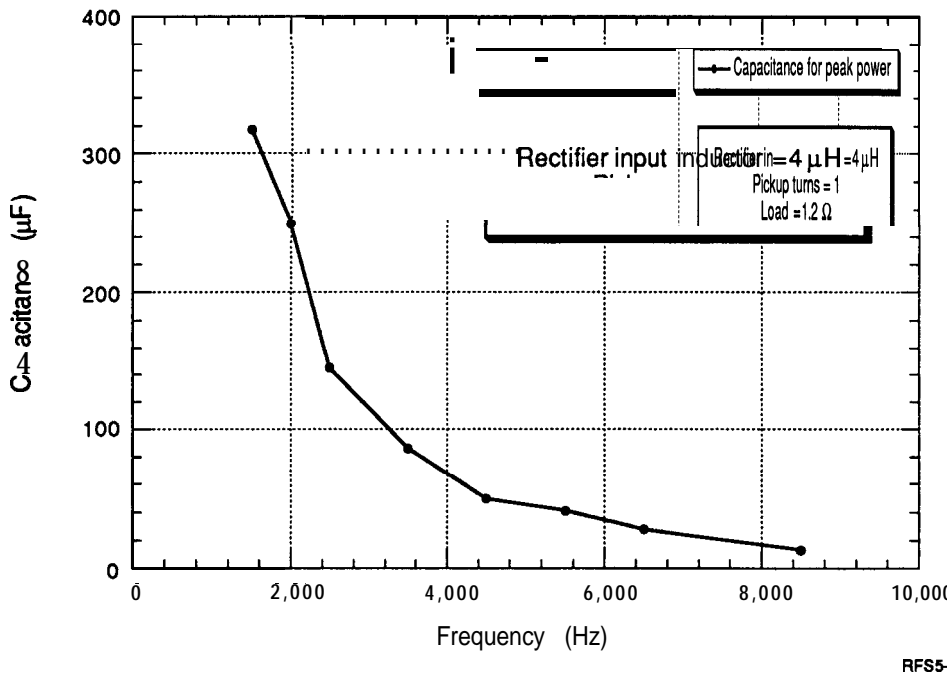
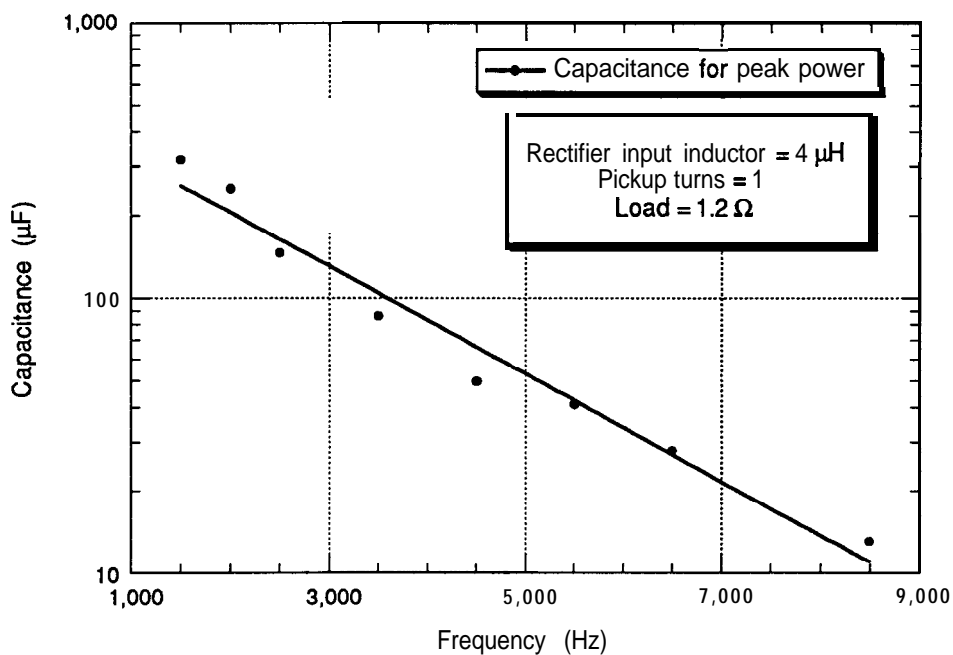


Figure 6.22 Capacitance for peak power as a function of frequency

#### 6.1.4.3 Comparison of Power Coupling at 4000 and 8500 Hz

The tests described in the previous section indicated that adjusting inductance and capacitance values is required to achieve good results at alternate frequencies. This is unfortunate as there are six inductors but only a single tuning capacitor. Due to the time required to change inductance values, tests were performed at only two frequencies (8500 and 4000 Hz) with these optimized inductance values. We selected 4000 Hz because previous results showed it was the minimum frequency at which an output current close to the design value of 180 amps could be obtained. Tuning curves for these two frequencies are shown in Figure 6.24 An output current of 180 amps (40 kilowatts) is achievable at 8500 Hz with adjusted inductance values. At 4000 Hz, the peak output is



RFS5-083//086

Figure 6.23 Data for Figure 6.22 plotted using a semi-log scale

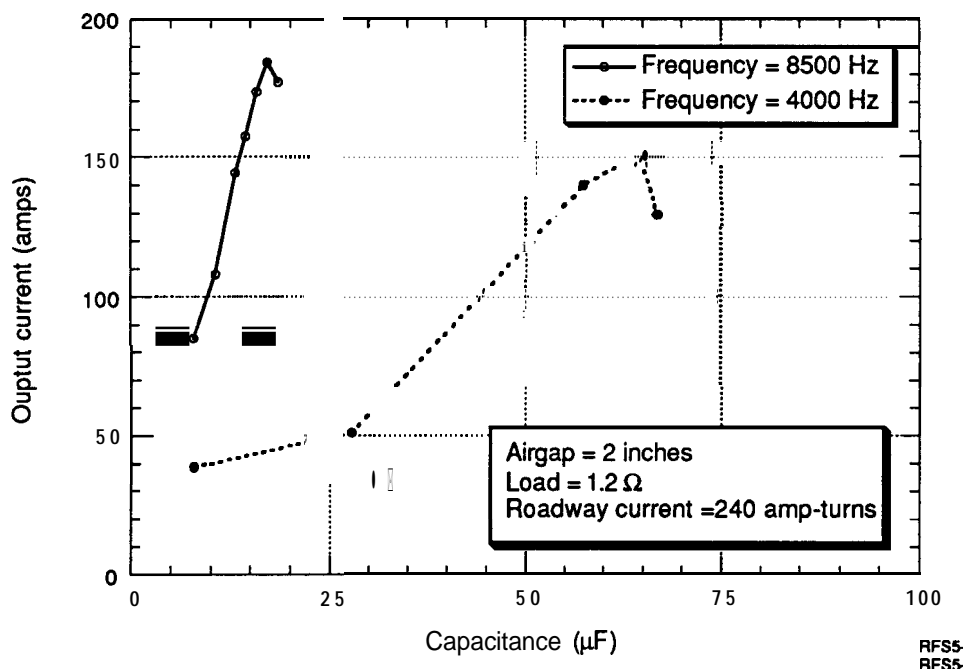
RFS5-089-5  
RFS5-091-1

Figure 6.24 Tuning curves for 4000 and 8500 Hz with a two-inch airgap

150 amps (27.5 kilowatts). An output current of 150 amps corresponds to 33 kilowatts, if it could be achieved at 220 volts and would almost certainly be acceptable. If the output current drops in proportion to the increase in output voltage, the power would remain at 27.5 kilowatts, the power required for the G-Van to cruise at its maximum speed, leaving no power available for charging the battery. This would give infinite range on the powered roadway, but autonomous trips would be limited because no net battery recharging is taking place.

Based on observations of the pickup while mounted on the vehicle at a two-inch airgap, it seemed advisable to increase the airgap. Tests were performed with a three-inch air gap and all other parameters fixed. These results are shown in Figure 6.25. The output current at 8500 Hz drops 30 amps to 150, while at 4000 Hz, the output drops nearly 50 amps to just over 100. An output current of 100 amps is too low, but several changes could be made to increase the output current. First, the inductances in the OBC could be re-optimized for the larger air gap. Second, the airgap could be increased only half an inch to 2.5 inches. Finally, the operating frequency could be selected at some value between 4000 and 8500 Hz. With properly selected inductance values, a system operating at 5000 – 6000 Hz with a 2.5 inch air gap may well prove desirable, resulting in an output current in the range of 150 amps.

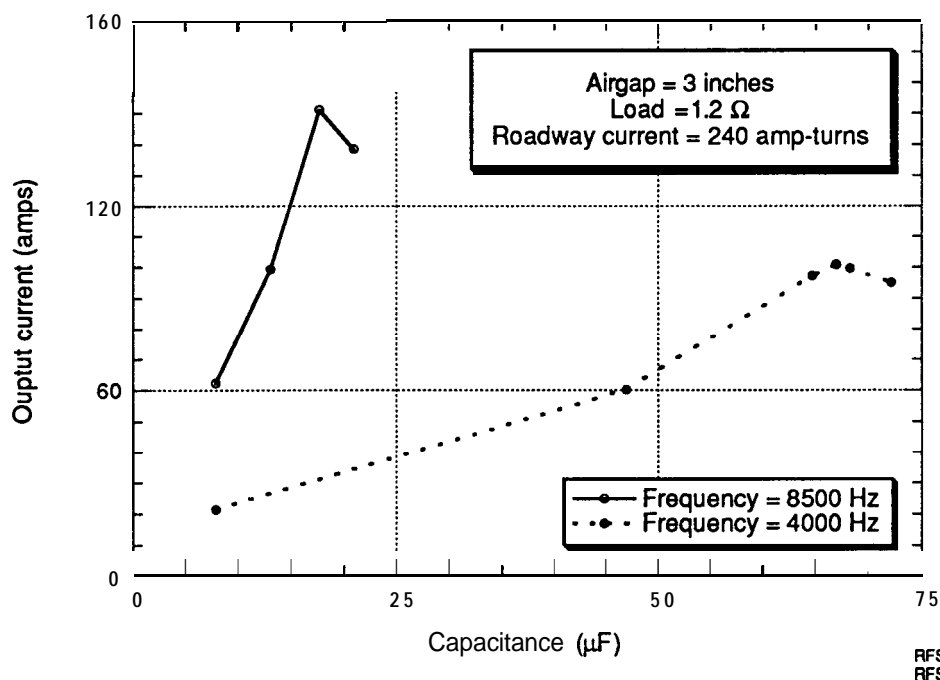


Figure 6.25 Tuning curve for 4000 and 8500 Hz with three-inch airgap

#### 6.1.4.4    losses

Losses in a twenty-foot static charging section were measured for a number of conditions. Open roadway losses were measured as a function of frequency and roadway current. The parasitic losses in a car parked over the roadway were also measured.

Open roadway losses were measured for seven frequencies at a variety of roadway currents from 60 amp-turns to 240 amp-turns. At the highest frequencies, it was not possible to drive the roadway current beyond 200 amp-turns with the power supply being used. Figure 6.26 shows total open roadway losses for several frequencies as a function of roadway current. Losses increase with roadway current squared. Losses also

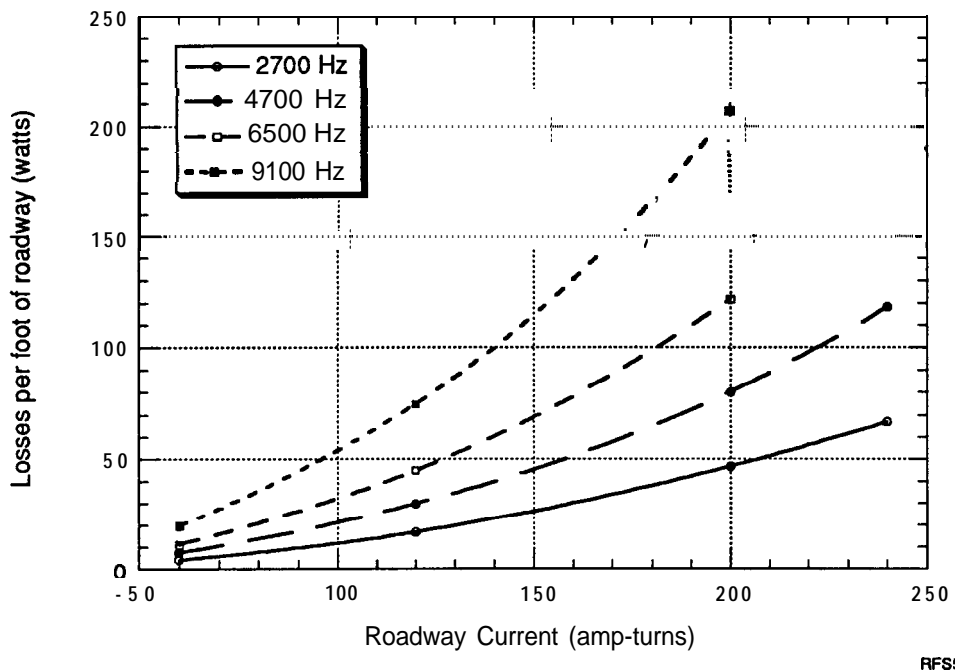
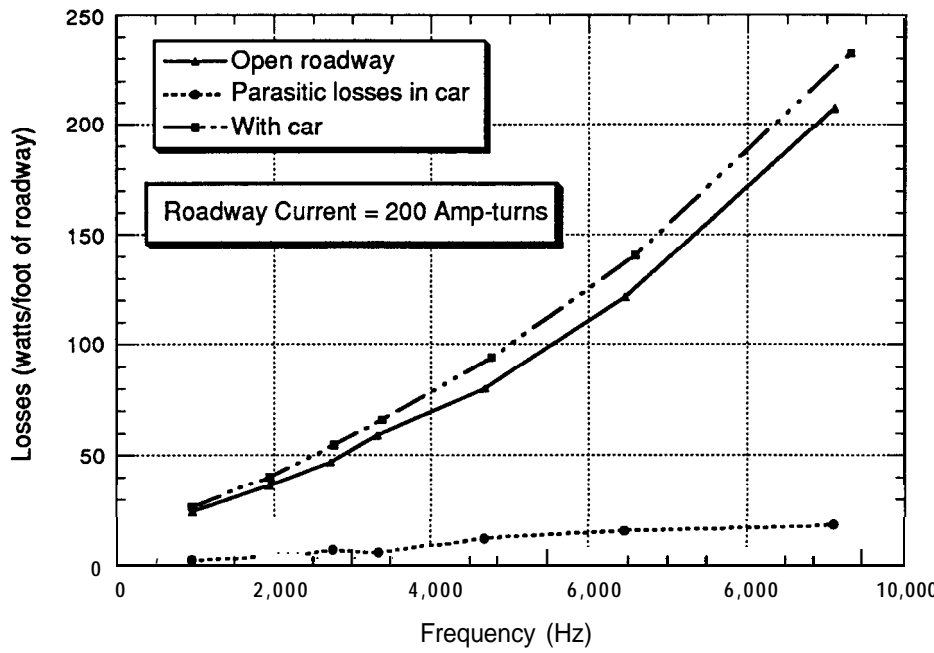


Figure 6.26 Open roadway losses at various excitation levels

increase with frequency, but since the selected frequencies are not uniformly spaced, it is difficult to draw conclusions about the exact nature of this dependence from this figure. Open roadway losses for 200 amp-turns are shown as a function of frequency by the solid curve in Figure 6.27. (Losses at 240 amp-turns would be expected to be approximately 40% higher.) The dot-dash curve shows losses with a car parked over the



RFS5-074/075/076

Figure 6.27 Parasitic losses caused by car parked over the roadway

roadway, and the dotted curve shows the losses attributable to the car only. All of these functions increase with frequency raised to a power between one and two. The exponent for core losses is often taken to be 1.6, while conductor losses increase more slowly. Open roadway losses can become quite significant at higher frequencies, which provides strong motivation to keep the frequency and roadway current as low as possible.

### 6.1.5 Conclusions

With some simple design changes, such as increasing the rectifier input impedance and changing the pickup inductor geometry to reduce leakage inductance, the 8500 Hz 240 amp-turn system should perform well and supply the G-Van with 40 kw of power.

An operating frequency reduction of several thousand Hz from the nominal 8500 Hz is likely to improve the overall system. Open roadway losses should be significantly lower and efficiency higher. Acoustic noise is very low at all frequencies and is likely to be well masked by ambient noise in any operational setting. The power coupled to the vehicle decreases at lower frequencies, which can be minimized by adjusting the inductance values in the OBC for the actual operating frequency. The original output power goal of 40 kilowatts is rather conservative for a vehicle using 25 kilowatts at the maximum

cruise speed. If this requirement is relaxed to 30 – 35 kilowatts, the operating frequency can be reduced to perhaps 6000 Hz, even if the airgap is increased from two inches to 2.5 or 3.0 inches. The system operating at 6000 Hz and 35 kw would need a lateral guidance system to keep the vehicle centered and maintain the average power close to the maximum power available. Including a lateral guidance system would be desirable in any RPEV installation. In early deployments, this is likely to be a low-power steering assistance system that tends to make the vehicle drift toward lane center rather than a system that takes over complete lateral control from the driver. Performance at large lateral offsets is unimportant when using a steering assistance system.

Open roadway losses are large and increase rapidly with frequency, especially above 4000 Hz. Reductions in frequency are nearly as effective as reductions in roadway current in the pursuit of lower open roadway losses.

## 6.2 Regional Deployment Study

The Southern California Association of governments (SCAG), in collaboration with PATH studied the application of both electrification and automation technologies to the freeway system in the Greater Los Angeles region. The project analyzed many factors, including emissions reductions, impacts on use of various forms of energy, system economics, and changes in congestion. The study timeframe was set at 2025, which is sufficiently far in the future that the technologies could be fully developed and deployed and the population of users grown to a steady-state value.

The electrification scenario was defined including 1,035 lane-miles of electrified roadway and a 15% market penetration. The trips using the electrified roadway are longer than average, as short trips can be made using the battery alone. The 15% of the vehicle miles traveled (VMT) are accumulated on only 3.3% of the trips. The effects of the battery-only trips were ignored when impacts were quantified. The economic analysis assumed that the RPEV system users paid all costs of the system, including construction costs, interest, energy costs, maintenance, operations, and administration. The key study results include:

1. Emissions reductions of 5 – 12%, depending on pollutant type
2. Increase of 1% in peak utility demand
3. Decrease of 15% in daily petroleum consumption
4. Increase of 7.2% in average natural gas consumption (used to generate electricity)

5. Very similar life cycle costs for RPEV and gasoline vehicles
6. Little impact on congestion (freeways or arterials)

More detailed information is available in the SCAG Phase I, II, and III reports[12, 13, 14] or the Executive Summary report, as well as technical papers.

### **6.3 Near-Term Deployment on HOV Facility**

The University of California, Berkeley, Institute of Transportation Studies analyzed near-term deployment of several advanced technologies on High-Occupancy Vehicle (HOV) lanes. Roadway electrification was one of the selected technologies. The El Monte Busway and all bus routes that traverse it were used for this case study.

It was determined that all lines currently using the El Monte Busway could be converted to electric operation. A three-phase deployment plan was developed. The first phase consisted of a downtown shuttle, with vehicles charging exclusively during layovers. In the second phase, the electric buses served the El Monte terminal as well as the downtown shuttle loop. Depending on the frequency of service to El Monte, static charging may be required at all bus stops as well as the layover points. In the third phase, dynamic charging is added on the El Monte Busway, amounting to approximately 22 lane-miles of electrified roadway as well as at the layover points. This would support the nine bus lines that currently use the El Monte Busway. Roundtrip lengths vary from 44 to 96 miles, with round trip times between two and five hours. Approximately 70 buses would be needed to provide 30-minute headways on these routes.

Additional information is available in the HOV project final report and technical papers.

## **7. Summary of Project Results**

---

Phase 3D of Roadway Powered Electric Vehicle development was the design and construction of an RPEV test facility at the University of California Richmond Field Station. The facility has a 700-foot test track and an operational 35-passenger RPEV. This chapter summarizes the important results of this project and the related research described in Chapter 6. The project was very successful with all of the major project goals being met and the system performing almost flawlessly.

### **7.1 Systems Engineering**

**System Parameters.** In this task the design of the inductive coupling system was refined with the roadway excitation, roadway and pickup geometry, and onboard controller configuration all being determined. The system configuration for this project was a roadway with a 1200 amp, 400 Hz excitation, a 40-inch wide roadway with a 39-inch wide and 14-foot long pickup. The OBC was redesigned to allow output power to be controlled in 20- to 30-amp steps instead of the 75- to 100-amp steps of the original (Phase 3C) design.

The operating point was chosen because it had low losses and would allow the power supply from the previous phase to be used. The roadway and pickup inductor design assumed that the vehicle would have a steering assistance system and not be subject to large lateral offsets. The resulting design has higher peak performance (when the vehicle is perfectly centered over the roadway inductor) but more rapid roll-off with lateral offsets. The pickup length was near the maximum that would fit under the bus.

### **7.2 Vehicle**

The 35-passenger battery electric bus designed and built in an earlier phase of the project was outfitted with a complete Inductive Coupling System.

**Pickup Suspension.** The suspension system to allow the pickup to be lowered within 3 inches of the road surface or raised to provide maximum ground clearance was redesigned and installed. A system with a single hydraulic cylinder and ten

swing arms replaced the original design that consisted of ten pneumatic actuators connected to the pickup via a cable and pulley system. The new pickup suspension was simple and effective.

**Onboard Controller.** The Onboard Controller was installed including both air and liquid cooling for the various components. The housing for the OBC was rebuilt to fit the space available and improve the sound isolation qualities of the enclosure. A plywood cover with additional sound insulation was placed over the OBC, which also serves as the floor for the area to the right of the driver. A control panel for the OBC with complete controls and instrumentation was fabricated.

**Motor Controller.** The bus's traction motor controller was removed and returned to the manufacturer to be upgraded to handle larger motor currents. Larger cables were installed between the motor controller and the motor.

**Instrumentation.** An extensive array of instrumentation was installed, including sensors for speed, motor current, battery current, battery voltage, and ICS output current. Additionally a lateral offset position measuring and indicating system was designed and installed. The output of the sensors was recorded on a PC-based data acquisition system powered by an inverter from the bus's 24 Vdc accessory system. Six meters display key variables to vehicle occupants, which is a desirable feature during demonstrations. Lateral offset meters are provided for the driver.

**Bus Operation.** The electric bus worked well throughout the project and has proven surprisingly durable and easy to operate. Several improvements should be included in future vehicles. The air compressor needs to be redesigned to reduce acoustic noise and improve reliability. A compressor that turned on only when air pressure went below a preset limit would be a big improvement. The traction battery mounting was tenuous at best and a stronger battery retaining system was developed.

### 7.3 Facility

The RPEV test track was built at the U.C. Berkeley Richmond Field Station and has two 200-foot inductive roadway segments two 20-foot static chargers and unpowered turnaround loops at both ends. The track was designed by Sverdrup in conjunction with SCT.

A great deal was learned about the installation of RPEV roadway during track construction. The inductor modules for the roadway were more expensive to

manufacture than anticipated, and improvement in this area has already been addressed. The track performed exceptionally well with two exceptions: conductor buckling and water in the connection vaults. Conductor buckling was solved by removing the buckled conductors and replacing them with conductors in conduits that can expand and contract without constraint alleviating the buckling forces. Water that filled the connection vaults during rain storms did not drain because the bottoms of the vaults were sealed. Putting drains in the vaults is necessary as it seems unlikely that perfect sealing of the vault lids can be guaranteed.

#### 7.4 Testing

Although much important information was gained in the preceding, three tasks, testing an operational RPEV was the main purpose of this project. The major results of the testing and their consequences are presented here.

**Roadway.** Power losses in the roadway segments were higher than anticipated and a better understanding of the roadway losses is necessary before the system can be deployed. The higher roadway losses (and lower system efficiency) are annoying but did not affect system operation. We initially planned to implement segment switching, but this proved to be impossible with the existing power supply so for most testing both segments were energized simultaneously, doubling the idling losses. Idling losses for each segment were approximately 15 kW, about twice the amount we expected.

**Magnetic Fields.** Two phenomena manifested themselves when the powered roadway was in operation, both related to the magnetic fields associated with the roadway inductor. Non-RPEVs driving over the energized road produced acoustic noise and-more importantly-in some instances the engines ran poorly or quit. The large magnetic fields generated by the roadway were apparently causing metal in the car to vibrate and in some cases interfered with the electronic engine controls. Lowering the roadway current below 300 amps eliminated the problem in the admittedly limited tests conducted. The consequences of lower roadway currents are mentioned in the section on additional RPEV research.

**Communication.** Vehicle-to-wayside and wayside-to-vehicle communications system were tested with mixed results. All aspects of the system worked when the roadway was not energized, but the presence detection system was not reliable with the roadway energized. Because segment switching was not feasible with the existing power conditioner, we did not investigate the communication system extensively.

Inductive loop sensors as tested were not completely reliable in the presence of large roadway currents and different technology should be investigated. Loops were used for this project because they were easily available, relatively inexpensive, and worked in our initial investigations.

**ICS Performance.** The ICS worked extremely well transferring 60 kW (400 A at 150 Vdc) at full power. The transfer was not affected by longitudinal motion of the vehicle and fell off as expected as lateral offset increased.

## 7.5 Related RPEV Research

A significant amount of research advancing the state of RPEV and Inductive Coupling Systems was conducted in other projects concurrent with or directly following this project.

**C-Van Inductive Coupling System.** Southern California Edison and the Los Angeles Department of Water and Power funded research to equip a G-Van with an inductive coupling system. This research showed that much lower roadway currents at higher frequency could be used to couple power to the vehicle. Power frequencies from 4000 to 6000 Hz seem to offer the best overall performance, and new designs using these frequencies are being considered. The G-Van research indicated that 35 to 40 kW of power can be coupled across a 3-inch airgap with a 240 amp-turn 4000 Hz roadway excitation.

**Regional Deployment Study.** The Southern California Association of Governments, in collaboration with PATH studied the application of both electrification and automation technologies to the freeway system in the greater Los Angeles region. The electrification scenario was defined including 1035 lane-miles of electrified roadway and a 15% market penetration. The study concluded that the life cycle costs of RPEV travel was very similar to gasoline vehicles, even when all construction, financing, and operating costs of the roadway are passed on to the users. Petroleum demand decreased 15%, while the peak utility demand increased about 1%. Emissions reductions varied between 5 and 12%, depending on emission type, counting only the trips made on the RPEV system [12, 13, 14].

**High-Occupancy Vehicle lane Deployment Study.** The University of California, Berkeley, Institute of Transportation Studies analyzed near-term deployment opportunities of several advanced technologies on High-Occupancy Vehicle lanes. The study examined all bus routes which use the El Monte Busway. Analysis indicated that all lines could be converted to electric propulsion, and a three phase

implementation plan was formed. The first phase consisted of a downtown shuttle, using opportunity charging at layover points exclusively. In the second phase, buses electric buses served El Monte. In the third phase, the *busway* was electrified, as well as the layover points at the end of each existing route, allowing all routes to be electrified.

## **Appendices**

---

- A. Metric Conversions
- B. POISSON Input
- C. Control Circuit

## **A. Metric Conversions**

---

This appendix contains tables showing the metric equivalents of the important system variables used in this report. Table A.1 lists the most common dimensions and weights and shows both the U.S. Standard and metric values. The remaining tables are repeated from the text with the metric equivalents in place of the U.S. Standard units used in the body of the text.

**Table A.1**  
**Metric Conversions**

Description	U.S. Standard Units	Metric Units
<b>Bus</b>		
length	<b>28.5</b> feet	<b>7.66</b> m
top speed	40 mph	<b>64</b> kph
weight (empty)	25,400 pounds	11,500 kg
weight (fully loaded)	31,200 pounds	14,000 kg
regenerative braking base speed	12 mph	<b>19</b> kph
battery weight	6,000 pounds	<b>2,700</b> kg
<b>Inductive Coupling System</b>		
airgap height (nominal)	3 inches	8cm
onboard controller weight	870 pounds	395 kg
<b>Pickup</b>		
length	172 inches	<b>4.36</b> m
width	39 inches	1.0 m
weight	1200 pounds	<b>545</b> kg
core length	6 inches	15cm
core width	19.5 inches	<b>50</b> cm
weight per core	15 pounds	<b>7</b> kg
total pickup core weight	780 pounds	<b>354</b> kg
<b>Roadway inductor core modules</b>		
width	20 inches	51 cm
length	112 inches	<b>2.8</b> m
thickness	4.5 inches	11 cm
weight	900 pounds	409 kg
lamination weight	420 pounds	191 kg
epoxy-sand mixture weight	480 pounds	218 kg
<b>Roadway conductors</b>		
aluminum cable conductor	0.7 inch diameter	1.8 cm diameter
aluminum <b>busbar</b> conductor	0.25 x 1.5 inches	<b>0.64 x 3.81</b> cm

length of busbar sections	<b>37.5</b> feet	<b>11.4</b> m
<b>Test track</b>		
total length	<b>700</b> feet	<b>210</b> m
electrified segments (2)	<b>200</b> feet	<b>60</b> m
length of bus stops (2)	<b>20</b> feet	<b>6.0</b> m
<b>Accessory Systems and Miscellaneous</b>		
<i>Hydraulic pickup suspension system</i>		
arms, length	9 inches	<b>23</b> cm
lateral motion	8 inches	<b>20</b> cm
vertical motion	4 inches	<b>10</b> cm
position repeatable to within	0.1 inch	<b>25</b> mm
<i>Detector loops</i>		
first set, rectangular	10 x 30 inches	<b>25 x 75</b> cm
second set, rectangular	6 x 36 inches	<b>23 x 91</b> cm
third set, trapezoidal	12 x 36 x 6 inches	<b>46 x 91 x 23</b> cm
<i>Vehicle-mounted transmitter</i>		
mounting height, above pavement	10 inches	<b>25</b> cm
<i>Anechoic chamber</i>		
height	<b>8</b> feet	<b>2.4</b> m
width	10 feet	<b>3</b> m
length	12 feet	<b>3.6</b> m

**Table 3.1**  
**Onboard Controller Weights**

Box	Weight (kg)	Components
1 (Front)	172	ac Capacitors Rectifier Solid State Switch One Inductor
2 (Middle)	122	Inductors 1 @ 41.8 = 41.8 2 @ 16.8 = 33.6 1 @ 11.8 = 11.8 2 @ 3.2 = 6.4 Box, Misc = <u>28.1</u> 121.7
3 (Rear)	27	Filter Capacitor Transducers
Total	321	

**Table 2.2**  
**Core Losses**

Lamination		Roadway C-Cores-Open Roadway Losses				Tapered Pickup Cores-Coupled Losses			
	Thickness	Thick (0.18.5 mm)		Thin (13 mm)		Thick(13 mm)		Thin (9.6 mm)	
Material	(mm)	Watts/kg	Watts/m	Watts/kg	Watts/m	Watts/kg	Watts/m	Watts/kg	Watts/m
M6	.35	.02*	.94	.04	1.0	.03	9.3	.44	13.2
M4	.28	.016	.67	.029	8.2	.21	8.6	.36	11.0
M3	.23	.014	.58	.029	.76	.17	6.9	.28	8.5
M2	.18	.011	.49	.018	.06	.15	6.0	.26	8.0

Thick Roadway C-cores	1.8cm build	700 gauss	93.5 kg/m of roadway (C-core only)
Thin Roadway C-cores	1.3-cm build	1000 gauss	61.7 kg/m of roadway (C-core only)
Thick Pickup Cores	1.3-cm build	3000 gauss	89 kg/m of pickup
Thin Pickup Cores	0.96-cm build	4000 gauss	67 kg/m of pickup

\* Extrapolated value

**Table 5.3**  
**Magnetic Flux Levels**

Height	In Car	Open Roadway
25 cm	~ 400 mg	~ 15,000 mg
1 m	-25mg	~ 1,000 mg

**Table 5.5**  
**Key Parameters of the Design and Test Duty Cycles**

	Design Cycle	Test Cycle
Average Velocity,kph	13.1	7.8
Energy Consumption, kwh/km	1.72	1.79
Powered time, percent	<b>62</b>	<b>66</b>
Average ICS Output, amps	279	<b>284</b>
RMS Motor Current, amps	<b>344</b>	310

**Table 5.6**  
**Summary of Test Results**

Test Mode	Range Test Battery Only	Range Test RPEV	Cycle Definition RPEV
Time (hr)	1.6	6.5	0.4
Distance (km)	22.5	80.4	4.8
Amp Hours supplied by battery	280	83	3
Remaining capacity (Amp-hrs)	0	201	
DOD start of test (%)	0	0	-74
DOD end of test (%)	100	30	-75
Net battery current supplied ( <b>amp-hr/km</b> )	32.8	2.67	1.62
Range associated with remaining battery capacity (km)	0	272	<b>444</b>
Total range (km)	22.5	352	525

\*Based on 201 amp-hrs at a rate of 1 .01 amp-hrs/mi

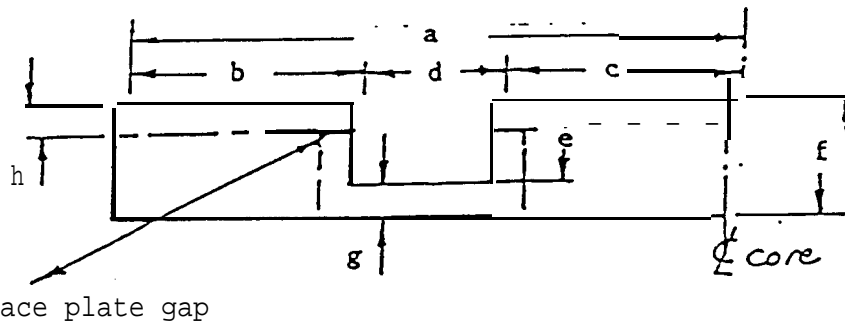
## **B. POISSON Input**

---

The following tables present input parameters for roadway and pickup cores that have been studied. The roadway geometries are identified by a single letter, and the pickup geometries are labeled as 'P' followed by a number, such as P1. There is redundant information in the tables, such as the total height of the roadway core is labeled 'f', and equals the sum of 'e' plus 'g'.

The roadway cores were examined in free space to determine the open roadway inductance and magnetic flux density in the vicinity of the roadway. Pickup geometries were generally studied with a roadway core present to determine the mutual and leakage inductances. Various combinations of roadway and pickup core geometry were examined. In addition to investigating various geometries, other parameters, such as core permeability were studied.

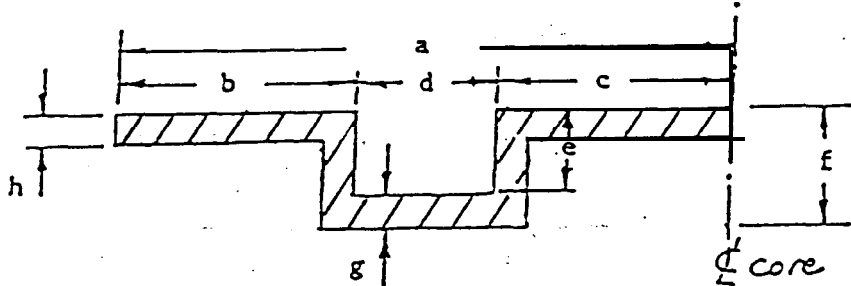
ROADWAY CORE DIHENSIONS  
 (VAX file: [FLUX.UCB]CORE.DIMS)



CORE LETTER	POISSON FILE	DIHENSIONS (cms.)								
		a	pole-faces		d	X	e	f	g	h
A	B1P762	54	22	22	10	X	10	13	3	-
B	B8, B2P762	54	20.75	20.75	12.5	X	8	11	3	-
C	B6P762	54	23	23	8	X	12.5	15.5	3	-
D	B7P762	54	19.5	19.5	15	X	6.67	9.67	3	-
E	B9, B9P762	44.46	15.88	15.88	12.7	X	8.13	11.18	3.05	-
F	B10, B11P762	54.1	20.7	20.7	12.7	X	8.13	11.18	3.05	3.05
G	B12P762	54.1	* 20.7	20.7	12.7	X*8.38	*11.43	3.05	3.05	
			including core-surface plate gap = .25cm							
H	B14, B14P762	48.26	17.78	17.78	12.7	X	8.13	8.76	.64	.64
I	B16P762	48.26	17.78	17.78	12.7	X	8.13	11.18	3.05	-
J	B17P762	48.26	17.78	17.78	12.7	X	8.13	11.18	3.05	3.05
K	B18P762	54.1	20.7	20.7	12.7	X	8.13	8.76	.64	.64
L	B19, B19P762	52.07	17.78	19.05	15.24	X	10.16	11.43	1.27	-
		(split-core with 2.54 cms. center split)								
M	B24, B24P762	52.07	18.41	19.69	13.97	X	8.89	10.16	1.27	1.27
	B25P762	(split-core with 2.54 cms. center split)					(with PD pickup design)			



PICKUP CORE DIMENSIONS  
 (VAX file: [FLUX.UCB]PICKUP.DIMS)



PICKUP CORE LETTER	POISSON FILE	DIMENSIONS (cms.)							
		pole-faces			slot size		f	g	h
a	b	c	d	X	e				

Beginning July, 1990 .....

N.B. Unless noted, pickup is centered.

P1	B50P508	67.31	31.11	31.11	5.08	X	12.70	13.97	1.27	1.27
P2	B51P508	67.31	31.11	31.11	5.08	X	6.35	7.62	1.27	1.27
P3	B52P508 B54P508	59.69	24.77	24.77	10.16	X	6.35	7.62	1.27	1.27
P4	B53P508	59.69	24.77	24.77	10.16	X	6.35	8.89	2.54	2.54
P5	B58P508 B59P508 B61P508	62.39	27.23	27.23	6.51	X	6.98	7.74	0.76	0.76
		(P5 pickup offset = 10 cms.)								

\* The P6 design is a 'U' design with a single,center slot and outer return conductor.

P6	B60P508	60.96	57.78	-	6.35	X	6.35	7.11	0.76	0.76
----	---------	-------	-------	---	------	---	------	------	------	------

## C. Control Circuit

---

The OBC “contactors” are solid-state (SCR-operated) switches. In each contactor two SCRs (SCR1 and SCR2 in Figure C.I) are placed in parallel so that the cathode of one is connected to the anode of the other. The contactor can be turned on by applying a 5 Vdc command input to its electronic triggering circuit. The command signal may be applied automatically by the Onboard Control Computer (OBCC) or manually by flipping a switch. In either case, a thermal switch mounted on the heat sink of the contactor may interrupt the command input once the thermal limit of the contactor is reached. This can happen due to insufficient coolant fluid flow or excessive current flow into the contactor. A Current (rate of change) Limiting Reactor (referred to as  $di/dt$  reactor) is placed in series with the contactor in each branch to protect the SCRs and also the branch capacitor against high rate of rise of current that could be created if the SCRs fire at a wrong time within the cycle of the pickup voltage.

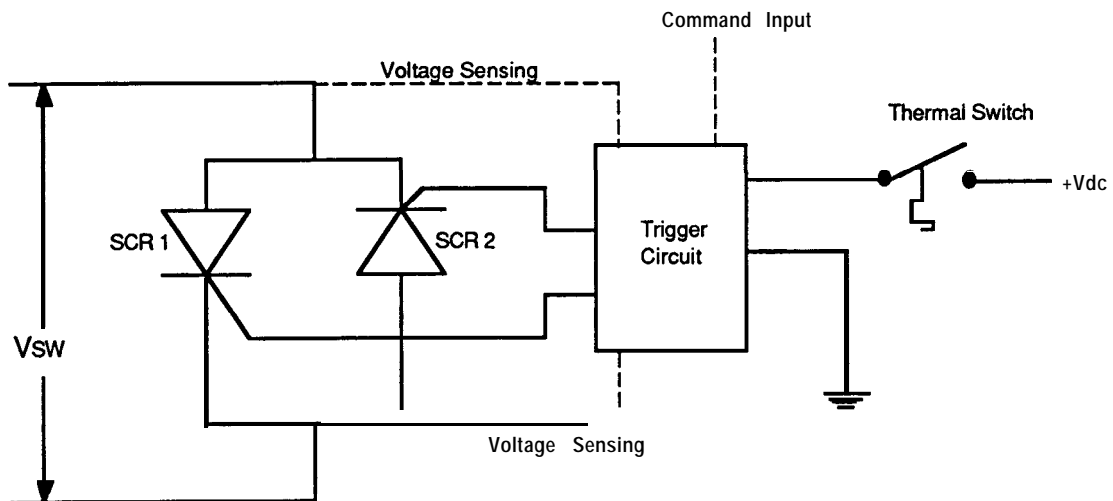


Figure C.I Solid state switch

Upon receiving the command input, the trigger circuit monitors the voltage across the switch ( $V_{sw}$ ) for zero crossing and provides gate input to one of the two SCRs immediately after  $V_{sw}(t)$  passes through zero. If the first zero-crossing after the command input is received is in the positive direction (negative half-cycle being

completed), SCR1 is triggered. Otherwise,  $V_{sw}(t)$  passes through zero after completing a positive half-cycle, and SCR2 is triggered. In either case, after a SCR is triggered, the voltage across the contactor will drop to the level required to keep the SCR forward biased; that is, slightly over 1 volt.

Bleed resistors are connected across the branch capacitors to discharge them rapidly after they are switched out of the circuit, as shown in Figure C.2. When no current is flowing, the voltage across the  $di/dt$  reactor ( $V_L$ ) equals zero, so

$$V_{sw} = V_2 - V_2$$

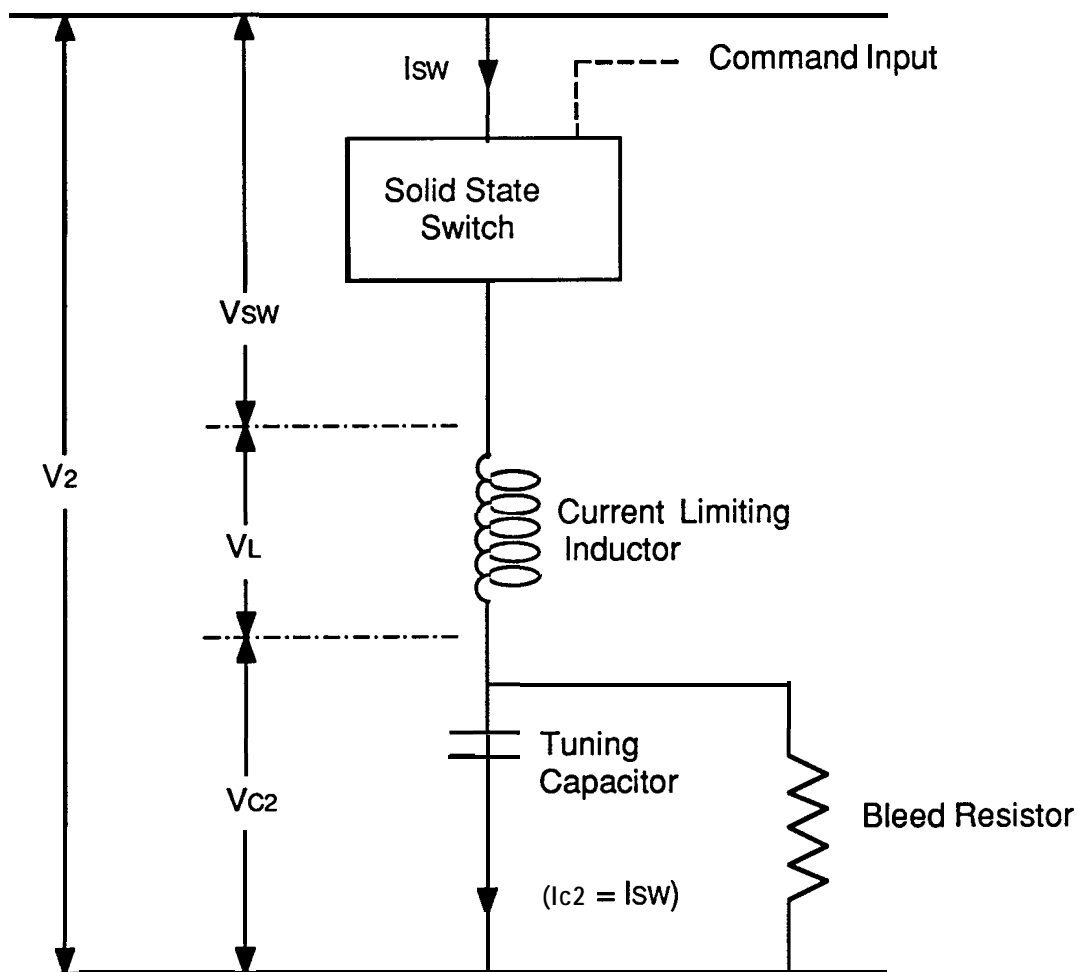


Figure C.2 Capacitor branch circuit

Assume that a branch of capacitance is activated, and the system operating with the pickup voltage ( $V_2$ ) at 200 volts zero-to-peak (141 volts rms). If this particular branch

of capacitance is switched out,  $V_2$  would drop, say to 190 volts zero-to-peak (134 rms). Without the bleed resistors, the capacitor voltage would remain at 200 volts (higher than the peak pickup voltage), and the voltage across the switch would never equal zero, as is required to activate the switch (as seen in Figure C.3). The bleed resistor causes the capacitor voltage to drop quickly when a branch of capacitance is switched out of the circuit, causing the branch voltage to drop below the (new, lower) pickup voltage, and allowing that branch to be reactivated upon request. The bleed resistor is sized small enough to allow the capacitor charge to drain off quickly, yet large enough to keep losses during normal operation modest, (typically ten watts).

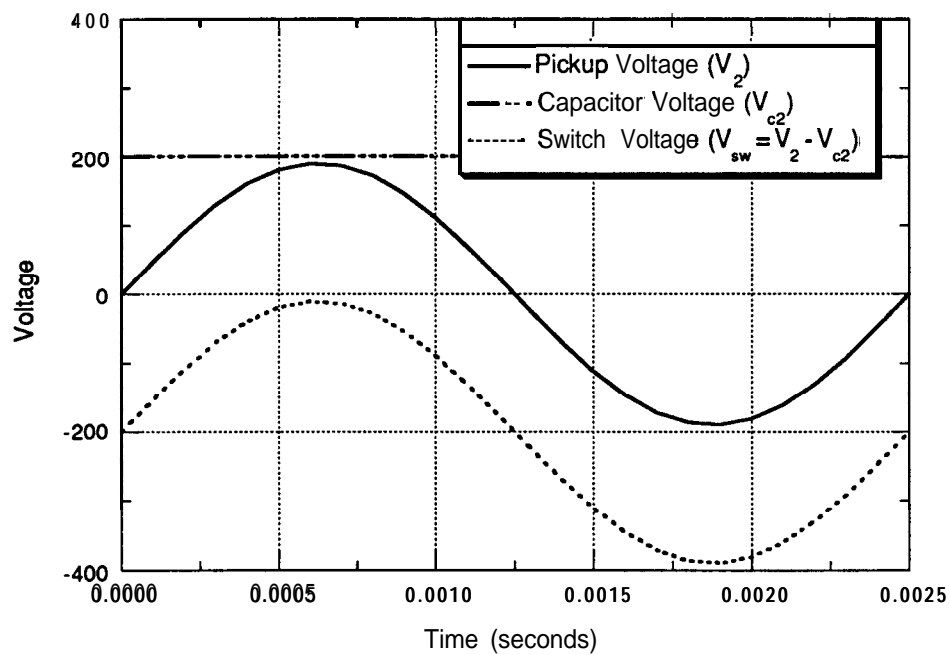


Figure C.3

Figure C.3 Voltage across switch without bleed resistors

Figure C.4 shows the waveforms of the branch current and the voltage across a contactor in operation. As shown the two wave forms are in phase; that is, they pass through zero at the same time. Once an SCR is turned on by a gate command it will only turn ‘off’ when the current through it goes to zero. Since the contactor is controlling a capacitive load, the current drops to zero when the voltage is at a maximum, as seen in Figure C.5. (This figure actually presents  $V_2$ , not  $V_{C2}$ , but when the contactor is closed, these two voltages are approximately equal as  $V_{sw}$  and  $V_L$  are both small in comparison to  $V_2$ .) Thus when the contactor opens, it leaves the

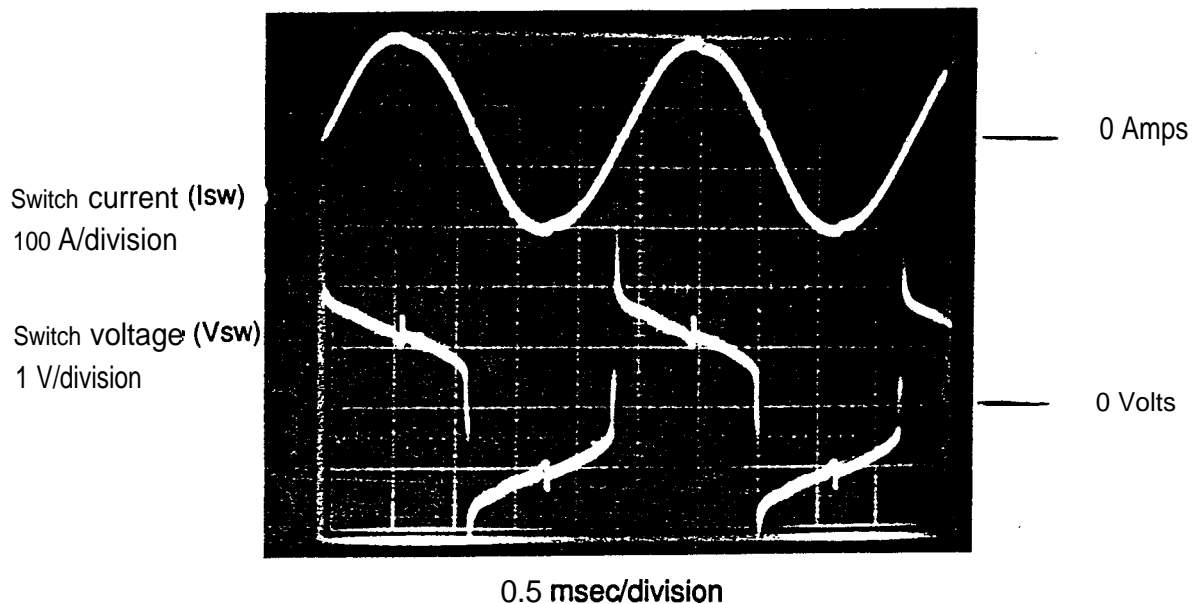


Figure 8.4 Oscilloscope traces of switch h current and voltage

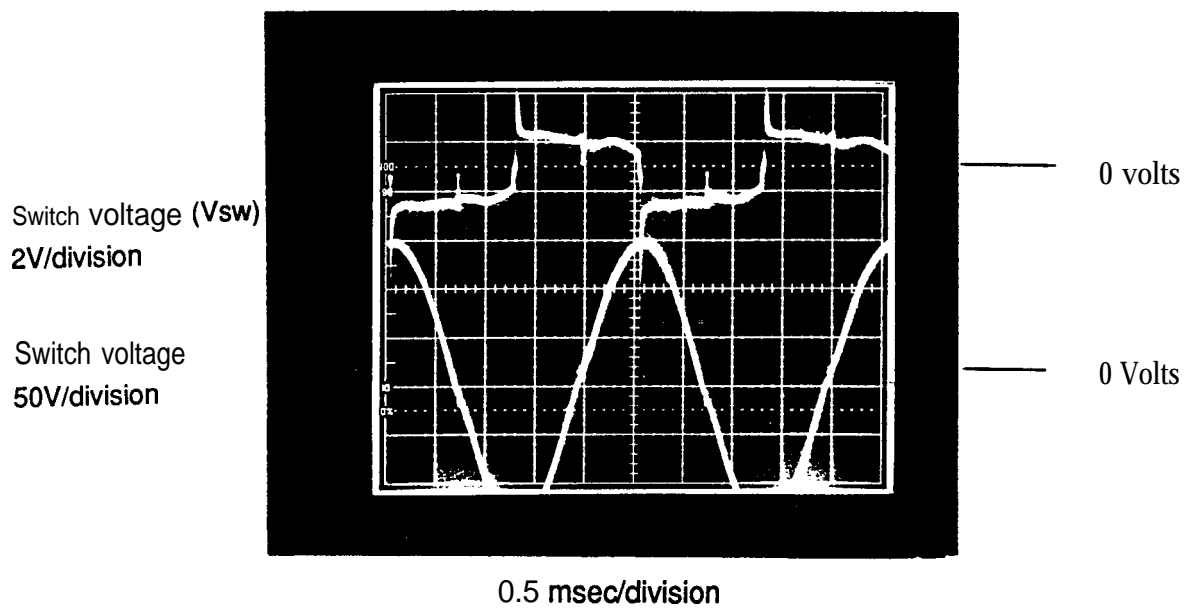


Figure B.5 Oscilloscope traces of switch voltage and pickup voltage

capacitor at its maximum state of charge, which generates the requirement for the bleed resistors. If the command input has not been removed as the current through the contactor goes to zero, the other SCR starts conducting almost instantaneously, as can be seen in both Figures C.4 and C.5. The time interval during which the contactor is open is just the time required for the voltage across the contactor to reach the level required to forward-bias the other SCR, which is less than a micro-second.

The SCRs perform ideally if the gate inputs are applied at precisely the right time in the periodical cycle of the pickup voltage  $V_2(t)$ . When the contactor is open, the right time for triggering an SCR is when  $V_{sw}$  (which is equal to the pickup voltage if the capacitor voltage has bled down to zero) passes through zero. While the contactor is in operation, the right time for triggering an SCR is still when the  $V_{sw}(t)$  crosses zero, but this now occurs when  $V_2(t)$  is near its peak value, due to the capacitive nature of the load.

### The Triggering Scheme

The triggering circuits were obtained from a commercial source, where they are used for many purposes, including switching of resistive heaters. Although the design is proprietary, the manufacturer was willing to provide SCT with the circuit diagram and assisted in making changes as required for the circuits to work properly in the RPEV application. The trigger circuits sense the voltage across the switch and provide gate signals to the SCRs upon zero-crossing of the switch voltage, whenever the input command is present.

The trigger circuits consist of a triac, an opto-coupler (opto-isolator), and assorted diodes and resistors. The opto-coupler isolates the input command from the power circuit, so a failure in the power circuit will not propagate to the computer which is generally the source of the input command. The triac actually controls the gate signal out of the trigger circuit. The resistors and diodes are used to create the proper voltages within the trigger circuit, eliminating the need for an external DC power supply.

When the OBC was first tested, the capacitor branch currents were distorted with high frequency, damped oscillations (ringing), in every half-cycle of 400 Hz. In some instances, the amplitude of the ringing was much more pronounced in one half-cycle than in the other. It was apparent that while a contactor was in operation, the branch LC circuit (the tuning capacitance  $C_2$  and the  $di/dt$  limiting inductance  $L$ ) was

exposed to a step voltage in the beginning of most half cycles of current. In other words, due to the incorrect operation of the trigger circuit, the SCRs were firing too late after the zero crossing of the voltage across the contactor. The second problem was that at a pickup voltage higher than 180 Volts the contactors would not consistently turn off. The trigger circuits continued producing a gate signal in the absence of the dc command input.

The late triggering of the SCRs is clearly visible on the negative half cycle of the capacitor branch current in Figure C.6. The duration of the zero-current interval is 0.15 – 0.20 milliseconds, corresponding to 20 – 30 electrical degrees. This results in a 50 volt step into the branch circuit, resulting in significant ringing. This propagates into the other parallel branches through the pickup voltage. This is visible as ripples in pickup voltage as it is declining as opposed to its relatively smooth nature as the pickup voltage is rising. The problem occurred because the trigger circuit was designed to operate at a constant (and relatively high) external ac voltage, as opposed to the variable magnitude of the pickup voltage in the RPEV system. Additionally, with a resistive load, a slight delay in gating the SCRs does not cause significant ringing as it does when controlling an LC circuit. The late triggering was overcome by changing some of the resistance values in the trigger circuit, causing the circuit to trigger by the time the voltage across the switch rises to 3 volts.

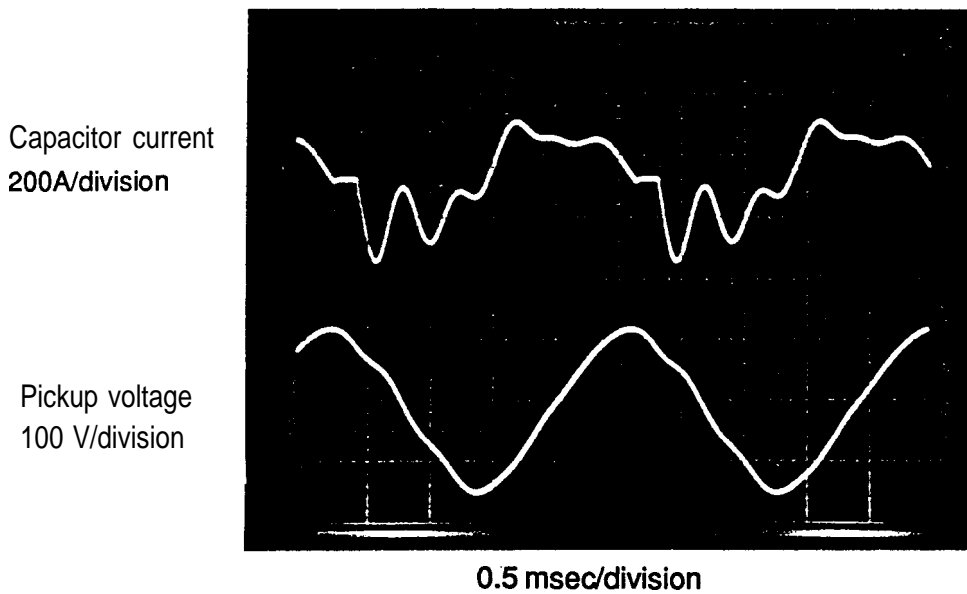


Figure C.6 Oscilloscope traces of capacitor current and pickup voltage

The second problem involved the contactor's "latching-up" or failing to de-energize when the input command was removed when operating with a high pickup voltage (above approximately 180 volts rms). This was traced to the output triac of the optocouplers, which was unable to block the flow of current at the higher ac voltages. Using opto-isolators with a higher voltage rating did not solve the problem. Using two optocouplers, with their input diodes connected in parallel and their output triacs connected in series worked effectively to prevent high voltage latch-up.

## Glossary

---

**acoustic noise** -audible sound as contrasted to electrical or signal noise

**airgap** — distance between the supply (roadway) inductor poleface and the pickup inductor poleface, usually the magnetic gap (i.e., low permeability); due to non-magnetic materials (generally fiberglass or plastic) that cover the cores, the mechanical airgap is always equal to or smaller than the magnetic airgap.

**anechoic chamber** — a chamber (approximately) free of echoes or reverberations, used for acoustic measurements; all interior surfaces of such a chamber are designed to absorb the maximum amount of acoustic energy

**AWG** -American Wire Gauge

**Brooks coil** -a short coil with windings placed concentrically

**calorimetry** — determining energy loss (as in an energized core by measuring temperature rise of the device and surrounding media (water, air), which are usually contained in an insulated vessel

**capacitive load** — an electrical load with capacitive reactance, that is, voltage follows current

**crisscross** -the transposition of parallel conductors in the pickup or roadway winding to maintain equal conductor currents

**di/dt inductors** -current rise limiting inductors

**dynamic testing** -testing with the vehicle in motion

**eddy currents** -electrical currents induced in a conductive material by a magnetic field

**extremely low frequency (ELF)** — electric and magnetic fields

**flux-usually** magnetic flux

**free field** -where sound is not affected by either the source or surfaces (compare with near field and reverberant field)

**fringing** — or fringe flux is magnetic flux that enters or leaves a magnetic core through the edge or side rather than the pole face. This fringing effectively increases the pole face area, but also increases the flux density near the sides or edges.

**gate signal** — bw voltage used to turn on an SCR or transistor

**inductive coupling system (ICS)** — a system to transmit power across a large airgap with magnetic fields

**isolation inductor** — an inductor used in the **onboard controller** to decrease the damping ratio (increase Q) in the inductive coupling system. This increases the magnitude of the response of the vehicle portions of the ICS, increasing the output current. The isolation inductors also help maintain low harmonic content in the various system waveforms.

**magnetic induction -flux level**

**mutual inductance** — measures the magnetic field that links the roadway and the pickup. This is the flux that couples power to the vehicle and is the most important of the three inductances in the coupled condition.

**near field** -within a foot of the sound source (compare with free field and reverberant field)

**nominal values** — 400 Hz frequency, roadway current of 1200 amps, coupled excitation of 3.0 volts per foot of core

**normalize** — rescaling of a variable, generally accomplished by dividing by the nominal or design value

**onboard controller** -the electronic components on the vehicle that regulate the power received by the vehicle from the ICS

**open roadway inductance**— the inductance of a segment of RPEV roadway with no vehicle present

**pickup core** — individual laminated iron pieces of which the pickup inductor is composed

**pickup inductor** -the cores and conductors formed into a large inductor

**pickup leakage flux** — detrimental to power coupling and results in a reduction of voltage at the pickup terminals. The smaller this is, especially in comparison to the

mutual inductance, the better. This leakage does not represent an actual loss of energy as it is a reactive, not resistive component.

**POISSON** — magnetic analysis program used to predict coupled and open roadway magnetic properties

**pole piece** — “I” laminations of silicon-iron used as the pole faces in the ICS roadway inductor

**power conditioner** — a large power supply that converts 3-phase 60 Hz power to single phase high-frequency power

**power distribution hardware** — switch, busbars, and cables that route power from the power conditioner to the roadway

**power factor** — the cosine of the angle between the current and voltage from the power condition to the roadway

**reactive load** — an electrical load that has no (or very little) reactive component (i.e., a large resistor)

**reluctance** — magnetic resistance

**resistive load** -a resistor (usually water cooled) into which power from a battery or inductive coupling system can be dissipated as heat

**reverberant field** -sound bouncing off a surface (compare to free field)

**roadway core modules** -roadway cores assembled into a larger unit and held together with epoxy resin or concrete for; for the Richmond Field Station track they are 9 feet 4 inches long and 20 inches wide

**roadway cores** -the individual laminated iron pieces of which the roadway inductor is constructed

**roadway inductor** — the roadway core modules and conductor installed in the road surface to make a single large inductor to supply power to an RPEV

**roadway leakage inductance** — the perceived inductance caused by flux that does not couple with the pickup inductor

**section (of roadway inductor)** — a length of roadway inductor with essentially continuous cores; the conductors are not transposed within a section

**segment (of roadway inductor)** -a length of roadway inductor, generally composed of several sections that is energized or de-energized as a unit

**segment switching** — the switching of segments on and off to ensure that the segment occupied by an RPEV is energized, while the others are de-energized to avoid open roadway losses

**Silicon Controlled Rectifiers** (SCR) — a solid-state device that conducts in one direction (similar to a diode) but must be turned on by a gate signal before conduction can begin. Two SCRs connected in parallel with a positive conduction direction can be used as a switch for ac current.

**skin effect** — the tendency of current to flow near the surface of a conductor at higher frequencies

**solid-state switches** — sometime referred to as contactors, a reference to the mechanical switches they often replace

**static testing** — test while the inductive coupling system is stationary

**steering assistance system** -a device that indicates to the driver of an RPEV the centerline of the roadway to allow the driver to better center the pickup inductor over the roadway inductor

**thermal time constant** — the characteristic time associated with thermal transients (dynamics) in an object or system

**triac** -a small integrated device that is essentially two SCRs in parallel; see SCR.

**turn** — a winding of wire or cable through an inductor or transformer core that starts and ends in the same location

## References

---

1. Santa Barbara Electric Bus Project, Phase 3A-Final Report, Systems Control Technology, Inc., September 1983.
2. Santa Barbara Electric Bus Project, Prototype Development and Testing Program, Phase 3B-Final Report, Systems Control Technology, Inc., September 1984.
3. Santa Barbara Electric Bus Project, Test Facilities Development and Testing Program-Static Test Report, Systems Control Technology, Inc., June 1985.
4. Santa Barbara Electric Bus Project, Prototype Development and Testing Program, Phase 3C-Final Report, Systems Control Technology, Inc., May 1986.
5. E. H. Lechner and S. E. Shladover, 'The Roadway Powered Electric Vehicle-An All-Electric Hybrid System,' *Proceedings of Eighth International Electric Vehicle Symposium*, Washington, DC, October 1986.
6. K. Lashkari, SE. Shladover, and E.H. Lechner, "Inductive Power Transfer to an Electric Vehicle," *Proceedings of Eighth International Electric Vehicle Symposium*, Washington, DC., October 1986.
7. S. E. Shladover, "Systems Engineering of the Roadway Powered Electric Vehicle Technology," *Proceedings of Ninth International Electric Vehicle Symposium*, Toronto, Ontario, 1988.
8. U.S. Congress, Office of Technology Assessment, *Biological Effects of Power Frequency Electric and Magnetic Fields--Background Paper*, OTA-BP-E-53. U.S. Government Printing Office, Washington, DC, May 1989.
9. Kevala, R.J., K.E. Derr, and K.F. Barber, "Maintenance of Electric Vehicles at DOE Sites," *Proceedings of Eighth International Electric Vehicle Symposium*, Washington, D.C., 1986.
10. J. Jensen, P.M. Julian, and P.M. Schutz, 'Technico-Economic Evaluation of Future Advanced EV Batteries: A European Study,' *Eighth International Electric Vehicle Symposium*, Washington, DC., 1986.
11. M. Conte, M. Romanazzo, "ENEA's (Italian Commission for Nuclear and Alternative Energy Sources) Field Testing on EV Public Fleets," *Proceedings of Tenth International Electric Vehicle Symposium*, Hong Kong, December 1990.

12. Southern California Association of Governments. *Highway Electrification and Automation Technologies. Regional Impacts Analysis Project: Phase I Report*. Los Angeles, August 1990.
13. Southern California Association of Governments. *Highway Electrification and Automation Technologies. Regional Impacts Analysis Project: Phase II Report*. Los Angeles, September 1991.
14. Southern California Association of Governments. *Highway Electrification and Automation Technologies. Regional Impacts Analysis Project: Phase III Report*. Los Angeles, April 1993.